ADVERTIMENT. La consulta d'aquesta tesi queda condicionada a l'acceptació de les següents condicions d'ús: La difusió d'aquesta tesi per mitjà del servei TDX (www.tesisenxarxa.net) ha estat autoritzada pels titulars dels drets de propietat intel·lectual únicament per a usos privats emmarcats en activitats d'investigació i docència. No s'autoritza la seva reproducció amb finalitats de lucre ni la seva difusió i posada a disposició des d'un lloc aliè al servei TDX. No s'autoritza la presentació del seu contingut en una finestra o marc aliè a TDX (framing). Aquesta reserva de drets afecta tant al resum de presentació de la tesi com als seus continguts. En la utilització o cita de parts de la tesi és obligat indicar el nom de la persona autora.

ADVERTENCIA. La consulta de esta tesis queda condicionada a la aceptación de las siguientes condiciones de uso: La difusión de esta tesis por medio del servicio TDR (www.tesisenred.net) ha sido autorizada por los titulares de los derechos de propiedad intelectual únicamente para usos privados enmarcados en actividades de investigación y docencia. No se autoriza su reproducción con finalidades de lucro ni su difusión y puesta a disposición desde un sitio ajeno al servicio TDR. No se autoriza la presentación de su contenido en una ventana o marco ajeno a TDR (framing). Esta reserva de derechos afecta tanto al resumen de presentación de la tesis como a sus contenidos. En la utilización o cita de partes de la tesis es obligado indicar el nombre de la persona autora.

WARNING. On having consulted this thesis you're accepting the following use conditions: Spreading this thesis by the TDX (www.tesisenxarxa.net) service has been authorized by the titular of the intellectual property rights only for private uses placed in investigation and teaching activities. Reproduction with lucrative aims is not authorized neither its spreading and availability from a site foreign to the TDX service. Introducing its content in a window or frame foreign to the TDX service is not authorized (framing). This rights affect to the presentation summary of the thesis as well as to its contents. In the using or citation of parts of the thesis it's obliged to indicate the name of the author

Nueva metodología para el diseño de tubos de hormigón estructural

TESIS DOCTORAL

tesis doctoral realizada por:
Albert de la Fuente Antequera

dirigida por:
Antonio Aguado de Cea
Climent Molins Borrell

Barcelona, octubre de 2011

Universitat Politècnica de Catalunya
Departament d´Enginyeria de la Construcció

Mi implicación en este trabajo se reduce sólo

a tiempo y dedicación, el resto se lo debo todo a mi

padre Miguel Àngel y a mi madre Mª Dolores, que junto

con el apoyo silencioso de mis hermanos Marcos y Carlos,

los cuatro han hecho posible que superara todas las barreras

y que alcanzara todos los objetivos plantedos a

a lo largo de mi vida

AGRADECIMIENTOS

Sin excepción a la mayoría de tesis, la mía también se planteaba inicialmente de forma difusa, con muchas ideas y objetivos, tal es así, que tanta dispersión llegó incluso a inquietarme a causa de mi carácter nervioso y activo. No obstante, esto nunca me quitó nunca el sueño, al contrario, pues siempre he sabido que estaba bien apoyado en todos los niveles (académico, personal, humano y espiritual); hecho que se ha demostrado con creces con el paso del tiempo. En este reto he puesto dedicación pero el conjunto responde a un trabajo colectivo con aportaciones de todos quienes me rodeáis, o lo habéis hecho en algún momento, y que han conducido a forjar esta tesis doctoral.

Asimismo, todo esto no hubiera sido posible sin un apoyo económico firme. En este sentido, quiero agradecer a la empresa PRECON, S.A. por su respaldo vía el convenio de colaboración CTT 6512: Obtención de un hormigón con mayor capacidad de tracción que la estándar, sin armadura en barra y con bajo coste. Del mismo modo, también quiero agradecer al soporte brindado por el proyecto financiado por el Ministerio de Educación y Ciencia BIA2010-17478: Procesos constructivos mediante hormigones reforzados con fibras. Por otra parte, expreso mi gratitud hacia la empresa PREFRAGA, clara ejemplificación de grupo innovador, que pese ámbito de acción de carácter más local, ha apostado por la Universidad como organismo vehicular para alcanzar parte importante de sus retos de futuro y que, en el ámbito de esta tesis doctoral, ha puesto a disposición el soporte material, técnico y cuanta información se ha requerido para la consecución de la misma.

Mi primer agradecimiento va dirigido a mis tutores de tesis Antonio y Climent. No digo nada nuevo al afirmar que se son dos personas de carácter distinto, pero el carisma y la profesional son, entre otras virtudes, su factor común. Ello ha hecho que me sintiera a gusto trabajando con ellos y disfrutar, en todo momento, de un gran clima de confianza. El conjunto, sumando además la paciencia y la plena disposición que siempre me han brindado, ha ayudado a integrar en un mismo trabajo aspectos que van desde el ámbito del material y la experimentación, hasta otros que conciernen la vertiente más numérica. Ambos han sabido como guiarme en todo momento y despertar en mi un interés y pasión que ha hecho que el desarrollo de esta tarea fuese una diversión, ¡incluso un lujo!

Esta misma pasión también ha sido alimentada por otras personas que, con su conocimiento y saber hacer en el arte de la enseñanza, han suscitado en mí el interés hacia el análisis no lineal de estructuras de hormigón o mixtas. Los cursos de grado y post-grado, las conversaciones y charlas informales así como toda la información que me han brindado; en definitiva, todo el conjunto me ha dado las bases y proporcionado los métodos necesarios para desarrollar gran parte de este trabajo de investigación. Toni, Quique y Jesús, vosotros sois estas personas a quienes me refería y a las que os considero parte implicada en este reto que me plantee.

Sin embargo, mi gratitud aún va mucho más lejos: Antonio, y sin ser partícipe directo en este trabajo, extiendo lo mismo a Lluís. A los dos os reservo mis mayores elogios y un aprecio ya de carácter prácticamente familiar. Me permito la osadía de no sólo apropiarme de lo aprendido en estos casi cuatro años, sino que voy más allá y me apropio también de una línea de pensamiento, de trato con las personas y de saber hacer que, en silencio, siempre he admirado. Todo esto hace que me enorgullezca enormemente sentirme discípulo vuestro y me gratifica inconmensurablemente que hayáis depositado confianza en mí.

Dentro del mismo departamento, ha habido más personas que han hecho que el levantarme cada mañana para venir a la universidad y pasar el día sea otro lujo más. Entre éstas, las primeras que se reflejan en mi mente son Montse, Carmeta, Mercè, Carme y Rachel. Vosotras, con paciencia y cariño, habéis resuelto de forma diligente todas mis dudas y problemas que han ido surgiendo. Con ellas toma sentido el dicho: ¡A veces no se valora lo que uno tiene en casa hasta que no se sale a la calle!

Asimismo, aún habiéndome librado, por esta vez, de enfundarme en el mono de azul y dedicarme a sólo orbitar como un mero espectador alrededor de las prensas del LTE y de mis otros compañeros, que sí trabajaban; sí que he tenido las ocasiones suficientes para darme cuenta del gran equipo profesional, formado por Camilo, Robert, Jordi y Carlos y excelentemente capitaneado por Tomás, que tenemos en el departamento y que nos da soporte en las tareas experimentales. Espero que en un futuro nuestras relaciones no se queden sólo en los partidos de baloncesto (que no estaría mal

recuperar) o en las charlas en la entrada del edificio hablando, en palabras de Lluís, de lo divino y de lo humano; eso sí, con una gran predominancia de lo humano.

Ahora sí, me toca acordarme de vosotros, de todos con quiénes he compartido despacho, juergas o noches de vela ante el ordenador esperando que algún algoritmo convergiera, o, al menos, dese señales de vida. Me tomaré la libertad de dirigirme a vosotros como amigos. Mis primeros descubrimientos iniciales: Filipe, Sergio, Jussara (indudablemente con el pack Adam, Carlos y Rosa), Oriol, Sandra, Virginia, Rolando, Cristian, Betty, Noé, Ana Carolina y Edison; los que os he ido conociendo más en la última etapa: Juliana, Nayara, Izelman, André y Luís, y, mención aparte: los sucesivos fichajes de nueva temporada (con todo el cariño) y que compartimos, entre otras cosas, la misma carga y responsabilidad de ser Ingenieros de Caminos (ya me sale la vena corporativista): Bernat, las dos piezas fundamentales en todos los sentidos del *team*, Pablo y Ana, el futuro Conseller de la Generalitat, oriundo de Reus, Francesc e Isaac.

En todo este mismo contexto: Juan Carlos, Mar y Marta, también me venís al primer plano, pues desde los inicios de nuestra vida universitaria hasta en estos momentos, acabando en una dirección muy paralela, hemos compartido momentos y experiencias de todos los colores.

Una mención especial en este trabajo se la hago al profesor Figueiredo. Si bien, nos conocimos hace relativamente poco en Barcelona, durante este corto periodo hemos compartido muy buenos momentos que para nada se quedan sólo en el terreno profesional, sino que se ha abierto un vínculo de amistad que valoro enormemente y que, pese a la distancia y al ajetreo del día a día, no tengo la menor duda que vamos a mantener.

¡Y cómo no! también os dedico esta tesis a vosotros, Pep y Roger, que, a años luz, sois con los quienes más me he reído y más me he enfadado; en definitiva, un cóctel explosivo que hace que os tenga siempre presentes y os admire profundamente; para vosotros sólo tengo y tendré buenas palabras y muestras de afecto. Por otra parte, doctores de la vida Ramón y Aiman: os conocí por culpa de las "servesitas" de Pep; entre los tres me liasteis más de un jueves por la noche a sumarme a vuestras escaramuzas en el Sutton hasta que echaban el pestillo de la puerta de entrada y retiraban al resto de maleantes; aún así, no contentos, me acababais convenciendo para invertir el viernes, incluso el sábado, para seguir haciendo diabluras. ¡Vaya fin de semanas de 3 días non-stop que hubo que padecer!, ¡Suerte que se puso cabeza!, sino aún estaría buscando bibliografía para escribir el primer artículo. Pues sí, a vosotros dos también os quiero dedicar estas líneas y agradeceros los buenos ratos que pasamos juntos. Asimismo, aprovecho el canal abierto para reconocer que la mitad se cayó de camino al servicio, de forma inocente, debido a un ligero traspié.

A todo esto, se merecen una alusión enérgica a quienes en cierta medida me han domado y han forjado parte de la forma que tengo de plantear mi vida. Alberto, Gaizka, Msn. Emili, Marc, Iñigo y Xavi os agradezco la paciencia, comprensión, consejos y formación que me habéis dado, en todos los planos, durante los 5 años que he convivido con vosotros en el Colegio Mayor Pedralbes.

De forma particular, expreso una gratitud preferente al que fue mi primer mentor profesional y quien me motivó a hacer el doctorado. Jaime: ¡siempre me he sentido apoyado y respaldado por ti!

Papa, Mama, Marcos y Carlos, por vosotros y para vosotros es TODO, no puedo entender nada de esto sin vuestro amor y soporte incondicional.

Y por último, y no menos, a ti: Yen, por la paciencia y el cariño que me has ofrecido durante este tiempo.

¡GRACIAS A TODOS!

RESUMEN

El hormigón reforzado con fibras ha demostrado ser una alternativa atractiva frente al hormigón armado tradicional en numerosas tipologías estructurales. En los últimos diez años, los avances técnicos llevados a cabo en relación con este material han sido muy importantes, prueba de ello es que varios códigos normativos nacionales a nivel europeo ya han aceptado las fibras estructurales como material de refuerzo del hormigón, entre ellos la instrucción española EHE-08 "Instrucción de Hormigón Estructural" en su Anejo 14.

A pesar del escenario aparentemente positivo, la consideración de aporte resistente asociado al uso de las fibras es todavía anecdótica, lo cual no responde en la mayoría de las ocasiones a razones técnicas, sino a la gran inercia al cambio existente en el sector general de la construcción.

Este es el caso de las tuberías de hormigón armado para redes de saneamiento. Se trata de una tipología estructural para la cual la idoneidad técnica y económica del uso de fibras ya se ha demostrado. Asimismo, también ha sido regulado por varias normativas nacionales específicas de tubos, entre éstas, la UNE-EN 1916:2008 "Tubos y piezas complementarias de hormigón en masa, hormigón armado y hormigón con fibra de acero". Sin embargo, el empleo de forma natural de fibras en tubos de hormigón está siendo lento, por una parte, debido a la inercia al cambio anteriormente citada, a lo que debe sumarse el hecho que pocas de las varias experiencias llevadas a cabo se han plasmado en la literatura técnica, y, por otra, a que no existe un método de diseño estandarizado, ágil y fiable al alcance de los proyectistas que permita tener en cuenta la incorporación de las fibras como material resistente.

En esta dirección, la presente Tesis Doctoral tiene como objetivo cubrir estos aspectos asociados con los tubos de hormigón armado. Para ello, los trabajos llevados a cabo han permitido lograr distintos avances en relación con los tubos de hormigón armado tradicionales y los tubos de hormigón armado con fibras. Respecto a estos últimos, se propone el primer método para el diseño conocido hasta la fecha y que permite considerar la contribución resistente de las fibras. Además, de cara a maximizar la difusión de los resultados tanto hacia la comunidad científica como hacia la industrial, el documento de Tesis se plantea como un compendio de artículos aceptados y/o en estado de revisión en revistas científicas en los que se recogen los resultados específicos de cada una de las partes, cuya unión, ha permitido alcanzar el objetivo principal de esta Tesis Doctoral.

Primeramente, se ha expone la herramienta numérica Analysis of Evolutionary Sections (AES) desarrollada para abordar el análisis de la respuesta resistente de secciones de hormigón armado. La herramienta es general y permite simular distintas estrategias de armado (barras de acero pasivo y/o activo con la posibilidad de incorporar fibras) e, incluso, la construcción evolutiva de la sección teniendo en cuenta el comportamiento reológico de los materiales. El modelo AES se emplea posteriormente como herramienta de cálculo de secciones con el fin de abordar estudios paramétricos así como motor de cálculo en los otros dos modelos desarrollados en el ámbito de esta Tesis Doctoral.

La segunda línea de trabajo se centra en el estudio de tubos de hormigón armado convencionales. Para abordar el diseño óptimo de éstos y con la finalidad de mejorar los sistemas tradicionales de diseño indirecto, se ha desarrollado el modelo Análisis de Tubos de Hormigón (ATH). El modelo permite simular su respuesta resistente bajo el ensayo de tres aristas considerando distintas geometrías y configuraciones de armado. Para ello, se ha implementado como subrutina de cálculo el modelo AES. El interés práctico del modelo radica en que se pueden obtener las cuantías óptimas de refuerzo para alcanzar los requerimientos resistentes especificados en proyecto. Estas cuantías deducidas con el modelo son, en la mayoría de las ocasiones, inferiores a las recogidas en las tablas de diseño que se emplean tradicionalmente.

En esta misma línea, con el fin de corroborar la idoneidad del modelo ATH para el diseño óptimo de tubos de hormigón armado convencionales, se ha llevado a cabo una campaña experimental con tubos de 2800 mm de diámetro y de clases resistentes elevadas. Mediante el modelo, se han logrado reducciones del armado de hasta el 30.0% respecto a las empleadas para este diámetro junto con diferencias en el comportamiento resistente que no superan el 10% respecto al alcanzado en el ensayo de tres aristas realizado en laboratorio. Los diseños obtenidos mediante el modelo ATH se

emplearon posteriormente para confeccionar el armado de todos los tubos de 2800 mm y clases resistentes C-135 y C-180 fabricados para ejecutar los 2270 m que amida el colector perteneciente a la Zona Residencial Arco Sur de Zaragoza.

La tercera y última línea de trabajo ahonda en la vertiente técnica e industrial de los tubos de hormigón con fibras. Por una parte, se llevan a cabo una amplia campaña experimental (parte de ésta desarrollada en la Universidade de São Paulo) en la que se aborda aspectos asociados con el hormigón con fibras así como otros relacionados con el ensayo de tres aristas y la respuesta resistente de tubos de distinto diámetro y armados con cuantías de fibras variables. Por otra parte, paralelamente se desarrolla el Model for the Analysis of Pipes (MAP) para la simulación de la respuesta resistente de tubos de hormigón reforzado con fibras.

Los resultados de la respuesta resistente de los tubos de hasta 1000 mm de diámetro ensayados se han contrastado con las simulaciones realizadas con el modelo MAP, obteniéndose correlaciones excelentes y sin superarse, en ningún caso, el 5.5% de error relativo entre las cargas de diseño que se han comparado. A raíz de los buenos resultados obtenidos, se concluye que la metodología de diseño que se presenta, basada en el empleo del modelo MAP, garantiza resultados que se ajustan a la realidad y que las cuantías de armadura que se deducen son muy próximas a las óptimas necesarias para alcanzar los requisitos resistentes fijados en cada caso.

SUMMARY

Fiber reinforced concrete has proved to be an attractive alternative to traditional reinforced concrete in many structural applications. In the past ten years, the important technical advances carried out regarding this material have led to appearance of different International Building Codes and Recommendations, including the Annex 14 in the Spanish Instruction EHE-08: "Instrucción de Hormigón Estructural".

Despite the apparently positive panorama, the consideration of structural contribution of fibers is still anecdotal, which in most cases does not correspond to technical reasons, but to the strong inertia to change in the construction sector.

This is the case of reinforced concrete pipes for sewage. This is a type of structure for which the technical and economic suitability of using fibers has been proved. It has also been regulated by several codes and recommendations specifically for concrete pipes, among these, UNE-EN 1916:2008 " Tubos y piezas complementarias de hormigón en masa, hormigón armado y hormigón con fibra de acero". However, the use of fibers in concrete pipe is slow, on the one hand due to the aforementioned inertia to change, to which the publication of only few of the many experimental campaigns performed must be added, and on the other hand due to the lack of a standardized, agile and reliable design method that accounts for the structural contribution of fibers.

In this sense, this Doctoral Thesis aims to cover these aspects with regard to reinforced concrete pipes. For this purpose, the work carried out has led to various advances concerning the traditional reinforced concrete pipes and the fiber reinforced concrete pipes. Regarding the latter, the first design method known to date is proposed which allows considering the strength contribution of the fibers. Furthermore, in order to favour the spread of the results both to the scientific and the industrial community, the document of the Doctoral Thesis is presented as a compendium of articles accepted and / or in review status in scientific journals. Each of these articles presents the results of each of the lines of work and whose union has helped to achieve the main objective of this Doctoral Thesis.

Firstly, the numerical tool Analysis of Evolutionary Sections (AES) developed to deal with the analysis of the strength response of reinforced concrete sections is presented. The tool is general and can simulate different reinforcement configurations (passive and/or active reinforcement with the possibility of incorporating fibers) and even the evolutionary construction of the section taking into account the rheological behaviour of materials. The model AES was subsequently used as a calculation tool of sections with the aim of addressing parametric studies as well as the calculation engine in the other two models developed in the scope of this Doctoral Thesis.

The second line of work focuses on the study of conventional reinforced concrete pipes. To address their optimal design and in order to improve the traditional systems of indirect design, the model Análisis de Tubos de Hormigón (ATH) has been developed. The model allows simulating the response of concrete pipes under the three edges test considering different geometries and reinforcement configurations. For this, the model AES has been implemented as a subroutine. The practical interest of the model lies in the possibility of obtaining the optimal amount of reinforcement which meets the requirements in terms of bearing capacity specified in project. These reinforcements obtained from the models are, in most of the cases, inferior to the amounts in the design tables that are used traditionally.

In this line, with the purpose of confirming the suitability of the ATH model for optimal design of conventional reinforced concrete pipes, an experimental campaign with tubes of 2800 mm of diameter and high strength classes has been carried out. By using the model, reductions up to 30% of the reinforcement have been obtained for pipes with the aforementioned diameter, while the differences in the bearing capacity do not exceed 10% when compared to the results of the three edge bearing tests performed in the laboratory. The designs provided by the ATH model were used later to prepare the reinforcement of all the pipes (of 2800 mm and strength classes C-135 and C-180) manufactured to build the collector of 2270 m in the residential area Arco Sur in Zaragoza.

The third and final line of work deepens into the technical and industrial side of the fiber reinforced concrete pipes. On the one hand, an extensive experimental campaign (some of it developed at the

Universidade de São Paulo) is conducted, addressing issues associated with fiber reinforced concrete as well as others regarding the three edges test and the structural response of tubes of different diameters and with different amounts of fibers. On the other hand, the model for the Analysis of Pipes (MAP) was developed simultaneously for simulating the structural response of the fiber reinforced concrete pipes.

The results of the bearing capacity of tubes up to 1000 mm of diameter tested have been compared with simulations performed with the MAP model, obtaining excellent correlations and not exceeding, in any case, the 5.5% relative error between the design loads. In view of the good results, it can be concluded that the design methodology herein presented, based on the use of the MAP model, ensures results that fit real behaviour and that the amounts of reinforcement provided are very close to the optimum necessary to meet the strength requirements established in each case.

CAPÍTULO 1

Introducción

1.1. Introducción

El Hormigón Reforzado con Fibras (HRF) es un material compuesto, mayoritariamente utilizado hasta la fecha en pavimentos y revestimientos en túneles y laderas, si bien su uso se está extendiendo hacia otras aplicaciones y tipologías, dando a las fibras una mayor responsabilidad estructural. Ello se debe en gran medida a los frutos derivados de la investigación llevada a cabo durante las últimas dos décadas. Durante este periodo, deben destacarse importantes mejoras asociadas a su respuesta mecánica, a los sistemas de producción, al control de calidad, a la metodología de ensayo (tanto destructiva como no destructiva), a los métodos y sistemas de cálculo, entre otros. Asimismo, la aparición y el desarrollo de distintos tipos de fibras (variedad en material y geometría) ha sido también uno de los factores motriz que ha permitido aumentar el rango de aplicación de este material.

Desde la vertiente económica, el desarrollo de nuevas tendencias de construcción y el incremento tanto del coste de los materiales como los recursos humanos, han obligado a la industria a buscar alternativas y soluciones innovadoras. En esta línea, las empresas de prefabricados muestran un interés creciente hacia nuevas aplicaciones del HRF. La respuesta a este fenómeno radica principalmente en las posibilidades que este material ofrece en relación a la reducción de costes, vistos desde una perspectiva integradora, y a la mejora de las propiedades globales del producto final.

Hoy en día el HRF ya se emplea, de forma prácticamente sistemática, en:

1. Pavimentos industriales y soleras.
2. En algunos elementos prefabricados de baja o moderada responsabilidad estructural (acequias, losas, paneles, tuberías y arcos enterrados a poca profundidad y con solicitaciones externas nulas o de baja intensidad, mobiliario urbano, entre otros).
3. En el ámbito de la construcción subterránea, en forma de revestimiento primario y/o secundario mediante la técnica de la proyección (vía seca y/o húmeda) o en anillos de dovelas prefabricadas.
4. Algunas aplicaciones de carácter arquitectónico en las que se recurre al trabajo por forma para resistir las tracciones producidas por la flexión.

Así pues, de forma natural, el uso del HRF se ha ido extendiendo a otros campos en los que la armadura activa y/o pasiva en forma de barras ha sido la solución tradicional hasta la fecha. Esta tendencia responde a que, con el tiempo y en virtud de los avances llevados a cabo, al HRF se le está confiando una misión que no se reduce a un mero reemplazamiento de las cuantías mínimas, sino que se le asigna una tarea estructural más intensa para hacer frente a los estados límite de servicio y de rotura. En este sentido, y avanzando varios de los resultados de interés alcanzados en esta Tesis, se ha visto que en varios casos la configuración de refuerzo óptima tanto en términos de eficiencia estructural como económicos consiste en el uso de una cuantía moderada de fibras como alternativa al refuerzo tradicional e, incluso, en una solución mixta entre ambas tipologías de refuerzo.

Sin embargo, de cara a generalizar el uso del HRF a un mayor número de tipologías estructurales, y, en cualquier caso asentarlo en aquéllas en las que ya está prácticamente consolidado, es necesario superar varias barreras. Por una parte estaría la *barrera técnica* entre los proyectistas y la aplicación de este material a causa de la falta de experiencia y/o el desconocimiento de los métodos ya disponibles para la fabricación, diseño y control de calidad del HRF por parte éstos. Si bien, en no pocas situaciones esta barrera técnica responde a la falta de un método sistemático, en forma de ecuaciones o tablas como los existentes para estructuras de hormigón armado, que facilite el diseño de secciones de HRF. Por otra parte, debe sumarse la *barrera psicológica*, la cual viene motivada en gran medida por la gran inercia al cambio hacia las nuevas estrategias de refuerzo que ofrece el uso de fibras como alternativa a las soluciones tradicionales. Esta barrera se debe, en parte, a la falta de difusión hacia la comunidad técnica e industrial de aplicaciones del HRF que sean referentes y que pongan de manifiesto el correcto desempeño de este material.

Dentro de este marco planteado, y de los diversos casos que podrían citarse, es paradigmático el caso del empleo de fibras en tubos de hormigón para conducción de aguas pluviales y/o de saneamiento. Se trata de una aplicación conocida y que ha demostrado ser competente frente a la solución tradicional con barras de acero (ver Fig. 1.1a) desde el punto de vista técnico y económico. No obstante, aun habiendo quedado demostrada su idoneidad e incluso existiendo códigos normativos[1] que ya incorporan la posibilidad del uso de fibras como refuerzo del hormigón (ver Fig. 1.1b) en el campo específico de los tubos, su implementación a escala industrial está siendo lenta.

Los principales motivos que dan pie a esta situación en el campo de los tubos de hormigón son:

1. La *necesidad de un método de diseño sistemático para el dimensionamiento de tubos de HRF* orientado a las gamas de diámetro y clases resistentes comerciales para las que el uso de fibras es una solución competente. En este sentido, en la actualidad existen métodos sistemáticos y fiables (tablas) para el diseño de tubos de hormigón armado tradicionales que permiten fijar las cuantías mínimas de refuerzo en función de la geometría y clase resistente del tubo, sin embargo los resultados no son extrapolables a tubos de HRF. Además, las normativas específicas de tubos que ya regulan el uso de fibras como elemento de refuerzo, no fijan cuantías mínimas de fibras debido al hecho de que existe un amplio espectro de fibras en el mercado y con comportamientos estructurales muy distintos. En definitiva, se requiere de una metodología de apoyo a los técnicos proyectistas que

[1] A nivel europeo sería la EN 1916:2002 “Concrete pipes and fittings, unreinforced, steel fibre and reinforced” y a nivel nacional español sería el complemento nacional UNE-EN 1916:2008 “Tubos y piezas complementarias de hormigón en masa, hormigón armado y hormigón con fibra de acero”.

permita el diseño de tubos de HRF y así superar la única *barrera técnica* importante aún existente entre el HRF y su consolidación definitiva dentro del marco de los tubos de hormigón.

2. *Falta de experiencias reales* a gran escala publicadas en la literatura técnica en la que se recojan: sistemas de fabricación y patrones de dosificación específicos de HRF para la confección de tubos, métodos para el control mecánico de los tubos (ver Fig. 1.1c) así como un análisis crítico de los mismos, estudios paramétricos que permitan fijar las fronteras de la aplicabilidad de las fibras, entre otros aspectos. En definitiva, se requiere que el sector industrial perciba el uso del HRF en tubos de hormigón como una alternativa desarrollada y apta para poder ser implementada, sin mayores dificultades, en la misma cadena de producción que se emplea para los tubos estándar. De este modo se proporcionarían argumentos sólidos desde el punto de vista técnico y económico que a la postre conduzcan a prevalecer sobre la *barrera psicológica*.

Fig. 1.1. (a) Jaula de armadura para un tubo de hormigón armado convencional, (b) vertido de fibras para la fabricación de un tubo de HRF y (c) ensayo de aplastamiento de un tubo de HRF.

Ambos aspectos son de suma importancia y es necesario abordarlos profundamente con el fin de garantizar tanto el desarrollo tecnológico del HRF como el impulso definitivo para asentar su uso de forma sistemática en el campo de los tubos de hormigón. Así pues, la presente Tesis se ha desarrollado con la intención de dar respuestas y soluciones que permitan superar las *barreras tecnológicas y psicológicas*, anteriormente citadas, genuinas del uso de HRF en tubos de hormigón.

Complementariamente, y aprovechando los avances y herramientas desarrolladas que han conducido a dar respuesta a las necesidades planteadas en el ámbito de tubos de HRF, se ha abordado el estudio del empleo de fibras para el refuerzo del hormigón en otras tipologías estructurales: dovelas de hormigón prefabricado para el revestimiento de túneles, escamas para muros de tierra armada y forjados de edificación. Si bien, con el fin de independizar el trabajo llevado a cabo en el marco de las tuberías de hormigón y el resto de tipologías estructurales, se ha dedicado el grueso del cuerpo a los avances asociados a los tubos, mientras que en cada uno de los anejos del documento se presentan las investigaciones relacionadas con el resto de tipologías tratadas.

Finalmente, se destaca que el formato del presente documento responde al deseo de garantizar la máxima difusión de los trabajos y avances alcanzados en cada uno de los distintos aspectos tratados en esta Tesis Doctoral. Por esta razón, y bajo el amparo del marco reglamentario específico, cada uno de los capítulos y anejos que componen el documento son artículos científicos que ya han sido publicados, aceptados para su publicación o en proceso de revisión en revistas científicas de ámbito nacional y/o internacional.

1.2. Objetivos

El *objetivo general* consiste en desarrollar una metodología de diseño de tubos de HRF en base a la experiencia ya existente para tubos de hormigón armado y apoyada en los avances y herramientas que permiten la consideración resistente de las fibras en la misión estructural. Asimismo, dicha metodología debe ir respaldada y contrastada con los resultados de una amplia campaña experimental asociada a la fabricación y el ensayo de tubos de HRF para los cuáles el empleo de fibras es viable.

Además, para garantizar la consecución del objetivo general es necesario fijar los siguientes *objetivos específicos*:

1. Desarrollar una herramienta numérica para el análisis general de secciones de hormigón armado y con la posibilidad de incorporar fibras como elemento resistente.
2. Diseñar y ejecutar una campaña experimental asociada a tubos de hormigón armado convencionales y tubos de HRF.
3. Desarrollar modelos que permitan la simulación de la respuesta mecánica de tubos de hormigón.

Todos estos puntos son tratados de forma secuencial en los distintos capítulos que forman el cuerpo de la Tesis y que dan pie a los diversos artículos redactados con el objetivo optimizar la difusión de los trabajos.

1.3. Metodología

Dado, por un lado, la relación contractual del candidato a doctor como profesor Ayudante del Departamento de Ingeniería de la Construcción de la UPC y, por otro lado, la necesidad de publicar en revistas de máximo nivel de cara a su consolidación como profesor de plantilla, se ha perseguido una estrategia centrada en la máxima transmisión de los resultados hacia la comunidad científica y la industrial. Ello da lugar a una Tesis Doctoral compuesta por una compilación de artículos (opción contemplada en la normativa vigente de la UPC) estructurada en capítulos y anejos (ver Fig. 1.2) correspondientes a cada uno de los artículos fruto de los trabajos desarrollados.

El *cuerpo de la Tesis* recoge los avances asociados a los tubos de hormigón y está compuesto por una introducción global (el presente Capítulo 1); el Capítulo 2 donde se presenta el modelo numérico para la simulación de secciones de hormigón y utilizado en las distintas tipologías estudiadas; los Capítulos 3, 4 y 5 en los cuales se ahonda en los avances específicos relativos a los tubos de hormigón, y, por último, el Capítulo 6 en el que se resume el trabajo realizado y se plasman unas conclusiones de carácter general y específico.

En la misma Figura 1.2 se pone de manifiesto la existencia de 4 anejos. En los Anejos A, B y C se aborda el estudio del empleo del HRF en otras tipologías estructurales, mientras que el Anejo D se hace un análisis exhaustivo de las distintas ecuaciones constitutivas recogidas en instrucciones de países europeos para la simulación del comportamiento a tracción del HRF.

A título individual, cada uno de los capítulos centrales del cuerpo de la Tesis responde a los artículos:

Numerical model for the analysis up to failure of precast concrete sections

Se trata de un artículo que se encuentra en proceso de revisión en la revista Computers and Structures. En este trabajo se estudian los temas específicos asociados al análisis no lineal de secciones de

hormigón. Concretamente, se presentan todas las bases e hipótesis adoptadas en el modelo numérico Analysis of Evolutionary Sections (AES) así como su contrastación con datos experimentales de ensayos sobre vigas compuestas. Parte de éste trabajo fue desarrollado en el marco de la Tesina de Especialidad presentada por el mismo autor de esta Tesis Doctoral para la obtención del título de Ingeniero de Caminos Canales y Puertos. Si bien, con el fin de aumentar la robustez y velocidad del modelo así como incrementar el rango de secciones que se pueden analizar con del modelo, se ha hecho una reestructuración del código y se han incluido las ecuaciones constitutivas más recientes para la simulación del comportamiento de tracción del HRF (Anejo D). Este modelo se emplea como subrutina interna para el cálculo de secciones en el resto de herramientas numéricas desarrolladas en esta Tesis para la simulación de la respuesta resistente de tubos de hormigón, tal como puede verse en la Fig. 1.2.

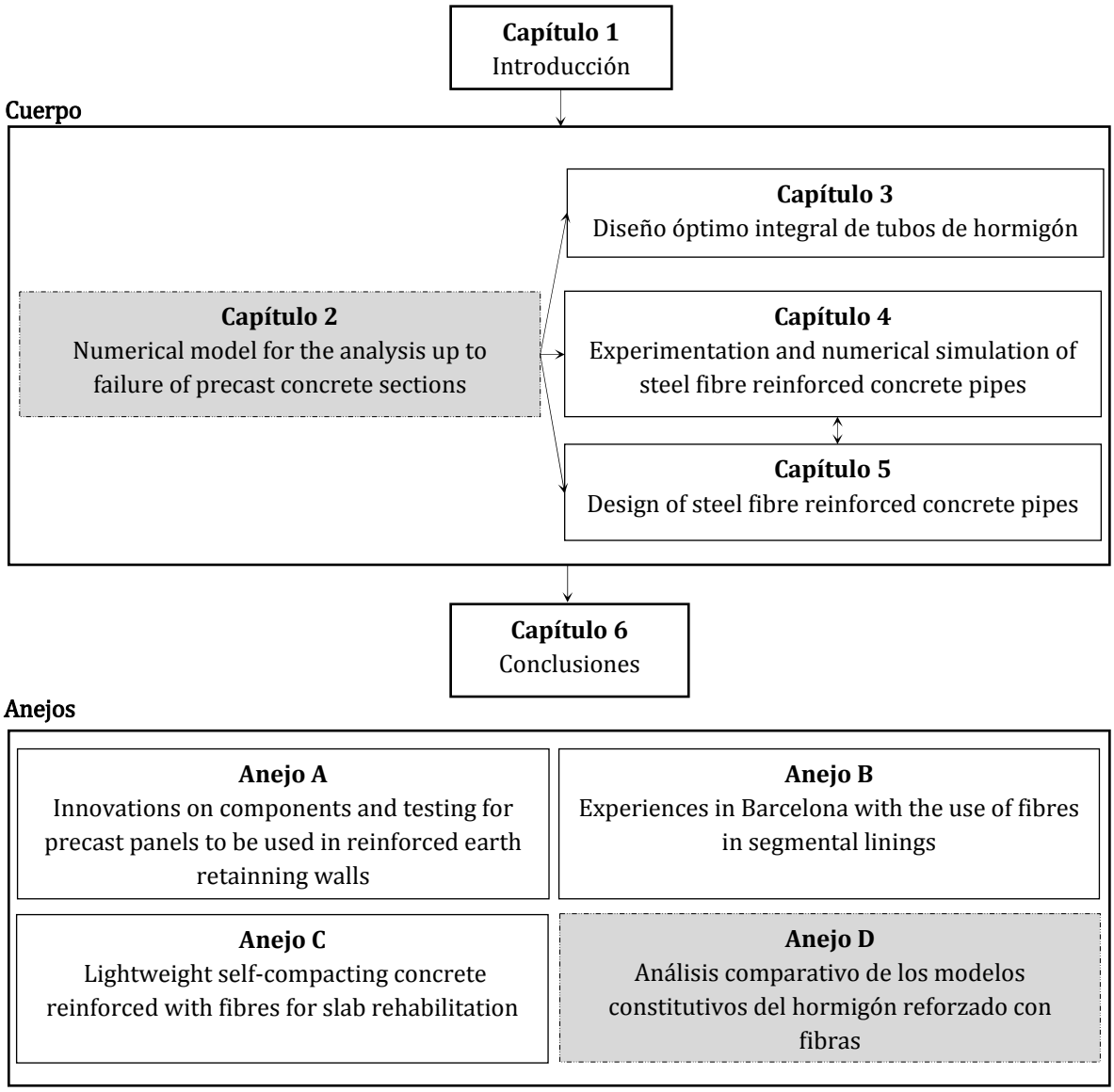

Fig. 1.2. Organización documental de la Tesis Doctoral.

Diseño óptimo integral de tubos de hormigón

Consiste en un trabajo ya publicado en la revista Hormigón y Acero, en el cual se tratan aspectos tanto de fabricación y control como de diseño asociados a los tubos de hormigón armado convencionales. Concretamente, se presenta:

- Un estudio del arte relativo a los métodos disponibles hasta la fecha para el diseño del refuerzo a flexión de dichos tubos.
- Un análisis exhaustivo y general de la respuesta mecánica de los tubos frente a las condiciones de contorno impuestas en el ensayo de tres aristas.
- Las bases y consideraciones implementadas en el modelo numérico Análisis de Tubos de Hormigón (ATH). Este modelo se ha desarrollado en el ámbito de esta Tesis para la simulación de la respuesta mecánica de tubos de hormigón con cualquier configuración de armadura.
- Una campaña experimental sobre tubos de 2800 mm, los cuales se emplearon posteriormente en una obra real de gran envergadura con el diseño propuesto. Este tipo de tubo está fuera de normativa, y se requiere de estudios específicos para su implantación, para lo cual el trabajo realizado en esta Tesis Doctoral puede ser muy interesante.
- La contrastación de los resultados experimentales con los obtenidos numéricamente así como varias propuestas de diseño para este tipo de tubos.

Experimentation and simulation of steel fibre reinforced concrete pipes

Consiste en un artículo ya publicado en la revista Materiales de Construcción. Este es el primero de los artículos específicos de tubos de HRF y, en particular, se recogen los siguientes aspectos:

- Un estado del arte referente a esta tipología de tubos.
- La presentación de la metodología llevada a cabo y los resultados obtenidos en el ensayo de tubos de HRF de 600 mm de diámetro interior.
- Las consideraciones e hipótesis aceptadas para la implementación del Model for the Analysis of Pipes (MAP). Un modelo implementado en esta Tesis para la simulación de la respuesta resistente de tubos de HRF de hasta 1000 mm de diámetro interior.
- La contrastación de los resultados experimentales con los obtenidos numéricamente con MAP.

Design of steel fibre reinforced concrete pipes

En este artículo se culminan los trabajos relacionados con los tubos de HRF desarrollados en esta Tesis. El mismo está en proceso de revisión en la revista Construction and Building Materials. Este artículo se redacta en aras de difundir avances como:

- El primer análisis detallado y general de la respuesta mecánica de los tubos de HRF sometidos al ensayo de tres aristas recogido en la bibliografía especializada.
- Los resultados obtenidos en una amplia campaña experimental sobre tubos de 1000 mm de diámetro reforzados con distintas cuantías de fibras.
- La contrastación de los resultados experimentales con los resultados obtenidos con el modelo MAP para los mismos tubos.
- La primera metodología de diseño de tubos de HRF disponible hasta la fecha. Ésta se basa en el uso del modelo MAP.

Finalmente, el cuerpo de la Tesis lo cierra el Capítulo 6. En éste se recogen unas conclusiones de carácter tanto general como específico que pretenden dar respuesta a los objetivos planteados en esta Tesis Doctoral.

Complementariamente, en los anejos se presentan otros trabajos realizados en el marco del empleo de fibras en elementos de hormigón:

Innovations on components and testing for precast panels to be used in reinforced earth retaining walls

Artículo publicado en la revista Construction and Building Materials y cuyo interés radica principalmente en que se proponen:

- Un nuevo sistema de anclaje panel-fleje que conduce a una reducción tanto de las tareas de montaje como de los riesgos de fallo en servicio.
- Un nuevo sistema de ensayo para el control mecánico de los anclajes. La particularidad es que se trata de un ensayo de fácil y rápida ejecución así como representativo del comportamiento real en servicio del sistema de anclaje.
- El uso de fibras con carácter estructural como alternativa al refuerzo en forma de barras.

La conexión de este artículo con el contenido del tronco de la tesis radica en que, igual que las tuberías de hormigón con fibras, en las escamas para muros de tierra armada se presentan casos en lo que los esfuerzos de diseño son reducidos y pueden ser resistidos con cuantías de fibras moderadas, eliminándose parte o la totalidad de la armadura en forma de barras.

Experiences in Barcelona with the use of fibres in segmental linings

Artículo aceptado en la revista Tunneling and Underground Space Construction y que se centra en el uso de fibras para el refuerzo de dovelas de hormigón prefabricado para anillos destinados al revestimiento de túneles urbanos. De este trabajo se destacan los siguientes avances:

- Un estudio exhaustivo del estado del arte relativo al uso de fibras como único refuerzo del hormigón en túneles con revestimiento a base de anillos de dovelas prefabricadas.
- Dos aplicaciones reales de las fibras como elemento de refuerzo del hormigón en combinación con armadura pasiva tradicional en 2 túneles urbanos construidos en el área metropolitana de Barcelona mediante Tunnel Boring Machine (TBM). En ambos casos, la cuantía total de armadura se ha diseñado de modo que ésta fuese la óptima, empleándose el modelo de análisis seccional AES.

La inclusión de este artículo en los anejos de esta Tesis Doctoral responde, entre otras razones, a que para el diseño de las dovelas de hormigón analizadas se utiliza una metodología basada en el empleo del modelo AES equivalente a la empleada para los tubos de hormigón. Asimismo, las dovelas de hormigón son un caso de tipología estructural en el que ya se emplean fibras, pero su contribución estructural para hacer frente a las tracciones raras veces se considera en proyecto.

Lightweight self-compacting concrete reinforced with fibres for slab rehabilitation

Se trata de un artículo publicado en la revista Materiales de Construcción y relacionado con el uso de fibras para el refuerzo de hormigón ligero y autocompactante en la rehabilitación de forjados. El estudio consta de una parte experimental y otra de diseño estructural, siendo la segunda de éstas objeto de esta Tesis Doctoral y para la cual se ha empleado también el modelo AES.

Análisis comparativo de los modelos constitutivos del hormigón reforzado con fibras

Por último, en este anejo se presenta un trabajo, publicado en la revista Hormigón y Acero, asociado con el análisis de las ecuaciones constitutivas recogidas en los distintos códigos nacionales a nivel europeo para la simulación del comportamiento post-fisuración del HRF. Para dicha tarea, se han implementado las citadas ecuaciones en el modelo de AES y se han contrastado distintos resultados obtenidos numéricamente, de interés tanto académico como práctico, con resultados experimentales.

Como puede verse, los diferentes artículos incorporados tanto en el tronco como en los anejos de la presente Tesis Doctoral, buscan un equilibrio de ámbitos: nacional-internacional, científico-profesional, materiales-estructuras-procesos. Esta estrategia responde a la creencia de que la labor del profesor de universidad debe tener una visión global e integradora de los diferentes aspectos que conforman cada temática tratada.

ÍNDICE

CHAPTER 2

Numerical model for the analysis up to failure of precast concrete sections

2.1. Abstract

This paper introduces the numerical model Analysis of Evolutionary Sections (AES) for the design of composite sections. Constitutive models including both concrete cracking and post-peak response of the materials were implemented. Likewise, the time-dependent behavior of the materials has been considered to model the sequential construction process. In order to validate the results obtained by the model, an experimental campaign (from the literature) was used. The comparison of the experimental results to those numerically obtained was satisfactory. The AES is already in use in several Spanish precast concrete factories for the optimization of bridges constructed with precast – prestressed concrete girders.

Keywords: Section; Concrete; Creep; Design; Model; Prestress.

2.2. Introduction

Usually, the construction of any kind of concrete and/or steel structure takes place in several stages which leads to changes in the structural behavior of the cross-sections. These changes can be due to [1]: addition of materials with different rheology, changes in the support configuration and variations in the environmental thermo-hygrometric conditions. All of them involve alterations in the distribution of stresses and internal forces both at a sectional and at a structural level that must be taken into account. In some cases, these redistributions involve strains and displacements which can even compromise the suitable service behavior of the structure [2]. Nevertheless, construction in several stages does not only affect the service performance of the structure but also, in certain cases, may alter its failure response [3]. Fig. 1 illustrates two composite sections in which the staged construction and the time-dependent phenomena may determine the service and the failure response.

Fig. 1a shows a section consisting of a welded steel girder and a concrete slab. The latter is prestressed prior to the connection in order to prevent its cracking (hogging moments). On the other hand, Fig. 1b illustrates a section made up of a precast – prestressed and postensioned high strength concrete (HSC) girder and composed with a reinforced cast-in-place normal strength concrete (NSC) slab. The prestressing strands are released in factory when the concrete reaches the required strength so that the microcracking and/or cracking of the slab are avoided. Then a second prestressing process by means of postensioning strands is carried out in order to increase the stiffness of the precast section and to improve its resistance to tension stresses in service. After its installation, a reinforced concrete slab is cast. The final section undergoes sagging moments.

In both cases important redistributions of stress occur between the partial sections, even when the connection is flexible [4-5]. Moreover, depending on the type of construction (propped or non-propped) the response in service as well as in failure may be completely different [3]. All this highlights that it is necessary consider the construction procedure to evaluate the sectional behavior properly. Likewise, the use of this kind of sections usually implies high global economic expenses [6]; thus, the design accounting for the real phenomena is justified.

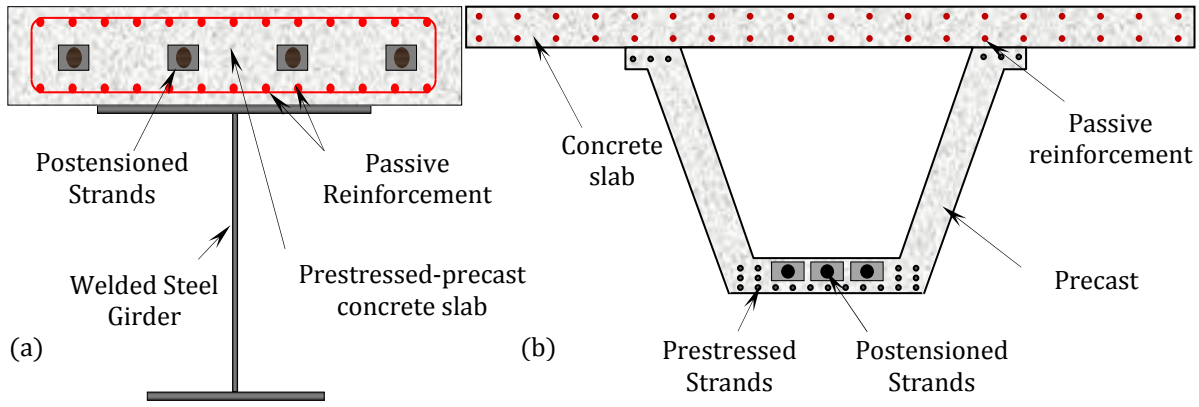

Fig. 1. Composite sections: (a) with a prestressed concrete slab; (b) precast pre and postensioned girder.

On the other hand, simultaneously with the phenomena related to the time variable, the effects of the mechanical non-linearity of the materials must also be considered. Concrete is a brittle material with a low tensile strength that cracks under relatively low load levels. This is a fact which must be dealt with at the level of analysis and design. At the former level, cracking introduces a degree of non-linearity which can be modeled with relative accuracy [7], taking into consideration the constitutive equation of tensioned concrete. At the latter level, cracking involves loss of sectional stiffness and, therefore, an increase of crack widths and displacements.

Similarly, as regards advanced states of instantaneous and/or maintained loads, another sort of non-linearities must be considered, such as: yielding, buckling of the compressed steel and non linear creep due to high compression stresses. These phenomena tend to affect strongly the sectional behavior.

Regarding the evaluation of time-dependent concrete strains, the integral of Volterra [8] is generally used to simulate the concrete visco-elastic behavior. There are two groups of approaches to the calculation of this integral. The first group consists of those approaches initially meant for manual application; they resort to an approximation of the integral by only one term (only one stage of calculation). Among these, the Effective Modulus Method [9] (EM), the Mean Stress Method [10] (MS), the Age-Adjusted Effective Modulus Method [11] (AAEMM) and the *j*'s method [12] are highlighted. These methods provide reasonably accurate results and, in some specific cases, may even lead to the exact solution. On the other hand, the second group consists of those methods exclusively aimed at a computer-assisted use. Their strategy is based on an approximation of the integral by means of a discrete summation with a finite number of calculation intervals. Among these, the more commonly used are the Dischinger Method [13] and the step-by-step methods [14], which are also the most general and accurate.

The literature presents several models for the evaluation of both the time-dependent phenomena of concrete and the mechanic non-linearity. Likewise, there are analytic formulations which allow considering the time-dependent properties of concrete, but not its cracking [15], and others which do also take cracking into consideration [16].

Thanks to the great development of computers in the past 30 years, numerical models for sectional analysis permitting to deal with both time-dependence and the non-linearity of the materials have been developed: CRACK [17], RESPONSE [18], SECSER [19], and VSEC [3], among others. Likewise, some of these models have even been included into routines aimed at the simulation of structures: CPF [20], CONS [21], ANSER [19] and PORTICO [3].

2.3. Main goals and methodology

Unlike the great majority of commercial and academic models, the one introduced in this paper aims at analyzing the behavior with time of sections subject to either low or high stress levels. Likewise, the model has been developed not only to solve specific problems (limitations on the maximum and minimum stresses, imposed geometries, pre-defined reinforcement configurations) but also to deal with any kind of geometry and combination of materials (passive and/or active reinforcement and concrete with different ages, strengths and rheological properties). The only restriction of the model lays on the existence of a straight bending condition.

This is achieved by considering the following items in the analysis: (1) the construction of the section in different stages and the time-dependence of both the mechanical and rheological parameters of the materials; (2) the suitable constitutive equations to model NSC and HSC; (3) the yielding and the post-peak behavior of the materials; (4) the effects of non-linear creep to simulate high levels of sustained stresses; (5) systematic evaluation of the pre- and post-tension losses in each strand, as well as the systematic verification of the serviceability limit state according to the parameters established beforehand by the designer or adopted by default in the model; (6) an algorithm based on an incremental-iterative strategy to solve non-linear systems. This makes it possible to achieve convergence in all cases with the highest computational efficiency, as well as to register phenomena such as snap-through and mechanical softening response.

All these considerations are implemented in AES, which is a general model for the analysis of sections implemented with the MATLAB® code. Modular architecture of the program allows further improvement of the model with new constitutive equations, as well as the addition of new subroutines.

This paper is divided in two main parts. The first one is dedicated to the introduction of the modeling strategy adopted for the materials and the hypothesis of sectional behavior. The second part consists of the comparison of several numerical results with the results obtained in an experimental campaign

published in the literature. This comparison also aims at highlighting the potential of the model to simulate the sequential construction of sections.

2.4. Modeling material behavior

In this paper, and also in similar ones [1,3,19,2 and 22], total strains (Eq. 1) are regarded as the total sum of the mechanic strains $\varepsilon^m(t_o)$ produced instantaneously in t_o and non-mechanic strains (creep, shrinkage and aging) $\varepsilon^{nm}(t,t_o)$ (Eq. 2) evaluated in an arbitrary instant of time t.

$$\varepsilon(t,t_o) = \varepsilon^m(t_o) + \varepsilon^{nm}(t,t_o) \quad (1)$$

$$\varepsilon^{nm}(t,t_o) = \varepsilon_\varphi(t,t_o) + \varepsilon_{sh}(t,t_r) + \varepsilon_a(t,t_o) \quad (2)$$

In order to characterize the instantaneous behavior of compressed concrete, several constitutive equations are implemented. Among them, it is highlighting diagrams such as TTJ [23] (see Fig. 2a), since it captures properly the whole stress – strain behavior both for NSC and HSC [3], and the Hognestad diagram [24] (see Fig. 2b), which is a worldwide normative reference.

As regards the simulation of the tensile response of a concrete layer, the contribution of the tensioned concrete between cracks is evaluated by means of a law of either Collins [25] (see Fig. 3a) or Djamic and Owen [26] (see Fig. 3b). The latter allows calibrating the parameters α_1 and α_2 according to experimental results or by means a numerical model [19]. Finally, the crack width w is evaluated by means of the formulation gathered in EUROCODE-2 [27].

Creep strains ε_φ (t,t_o) are evaluated through integral formulation (Eq. 3) imposing the superposition principle.

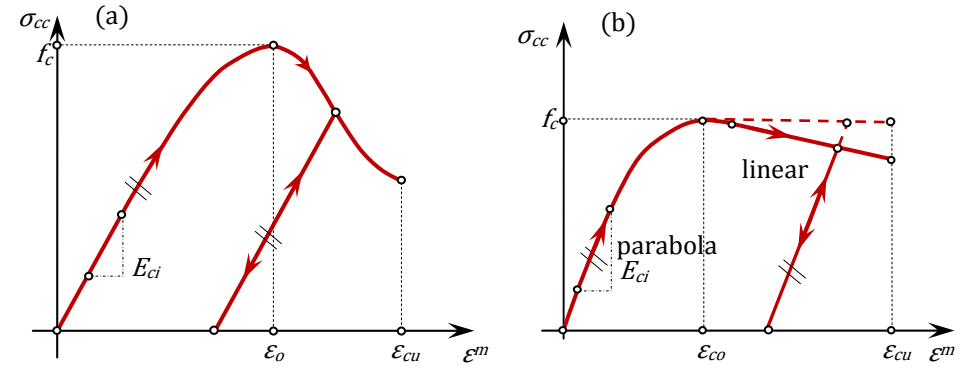

Fig. 2. Diagrams for compressed concrete: (a) TTJ; (b) Hognestad.

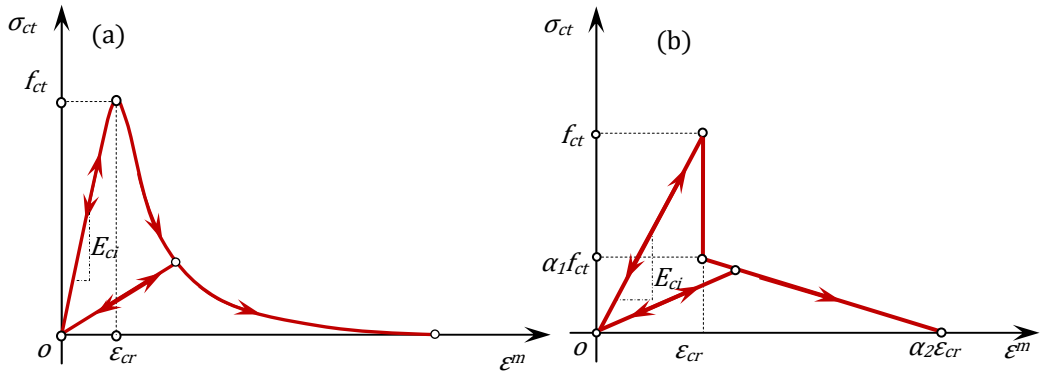

Fig. 3. Tensioned concrete diagrams: (a) Collins diagram and (b) Djamic-Owen.

$$\varepsilon_{\varphi}(t,t_o) = \sigma_c(t_o)J(t,t_o) + \int_{t_o}^{t} J(t,\tau)\frac{\partial\sigma_c(t)}{\partial\tau}d\tau \quad (3)$$

where $J(t, \tau)$ is the creep function (Eq.4).

$$J(t,\tau) = \frac{1}{E_{c,28}}\left(\frac{E_{c,28}}{E_c(\tau)} + \varphi_{28}^{*}(t,\tau)\right) \quad (4)$$

For $\sigma_c(t_o) \leq 0{,}40 f_{cm}(t_o)$, the linear creep coefficient $\varphi_{28,lin}$ is considered. Otherwise, the creep coefficient increases non-linearly and therefore must be corrected. The non-linear creep coefficient $\varphi_{28,nlin}$ (Eq. 5) is evaluated according to the loading age and the compressive strength by means the model proposed by Fernandez *et al.* [28].

$$\varphi_{28,nlin}\left(t,t_o,\frac{\sigma_{cc}}{f_c}\right) = \varphi_{28,lin}(t,t_o)\left\{1 + 2\left(\frac{\sigma_{cc}(t_o)}{f_c(t_o)}\right)^4\right\} \quad (5)$$

The linear creep coefficient $\varphi_{28,lin}$ is calculated with the formulation suggested in MC 2010 [29] which allows considering concrete with compressive strength up to 120 N/mm².

Creep might reduce the long-term bearing capacity of the concrete fibres. In order to consider this phenomenon, the modification of the concrete constitutive law proposed by Fernandez [3] has been considered in the present model. This approach allows reproducing the behavior of a concrete layer subject to a variable stress time-history (see Fig. 4).

The strategy consists of considering that a concrete layer contained into a cross section undergoes a stress redistribution (path 1-2) once an equilibrium state (point 1) is reached at t_o (law 1). This redistribution happens due to an increase of the delayed strains with time and a reduction of the stiffness of the concrete layer relatively to the rest of the materials. The elastic behavior is assumed for any reloading stage (with the elastic modulus calculated at the beginning of the reloading stage) up to the previous maximum stress level $\sigma_{cc}(t_o)$ (point 3). The reloading process continues with the instantaneous branch of the concrete (law 2*) at that particular time t. Assuming such behavior, the maximum strength $f_{c^*}(t)$ of the fiber at time t is smaller than the maximum strength $f_c(t)$ of the fiber with a unique load at time t. This happens due to the partial lose of resistant capacity of the fibre (path 1-2). The same model is applied to the concrete in tension.

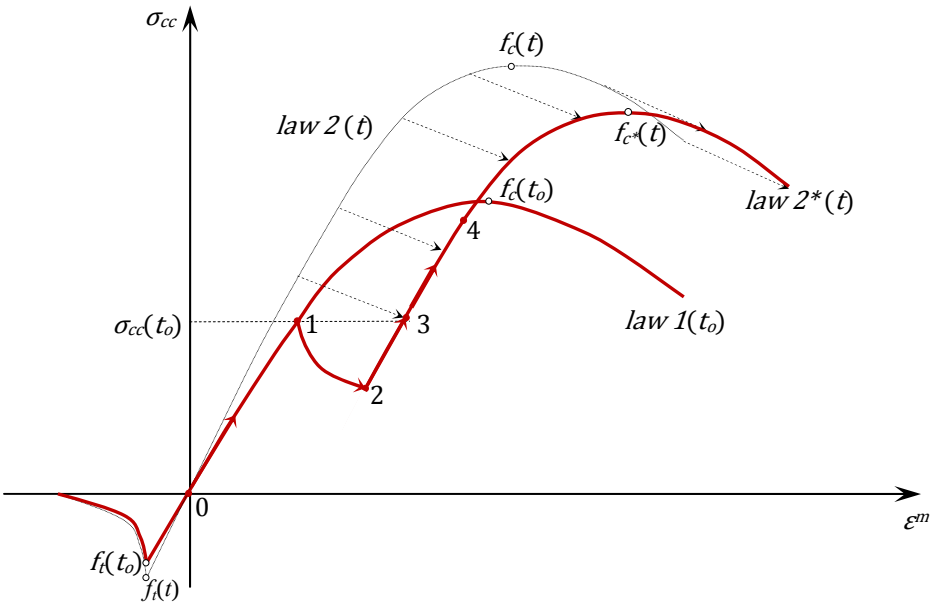

Fig. 4. Constitutive law for a concrete layer subject to a time-history stress pattern.

To evaluate the mechanical parameters of concrete (E_c, f_c, f_{ct}) and their time-evolution, the equations suggested in MC 2010. Likewise, the model admits the input of results obtained experimentally for the mechanical behavior of concrete.

Several strategies have been implemented for the numerical evaluation of the integral (Eq. 3). The project engineer can choose according to the desired type of section and accuracy: (1) the first strategy consists in a step-by-step resolution by means of a numerical integration [14]. From a numerical point of view, this is the most demanding alternative; however, it is also the most general and the most accurate. The total time interval of analysis (t_o-t) is divided into the different stages I_k, which are discretized into smaller intervals Δt_k. This discretization is carried out through a geometric series [30]; (2) the second strategy is less accurate, but less expensive from a computational point of view. It consists in the application of AAEMM [14]. In this case the discretization interval Δt_k coincides with the calculation-stage magnitude I_k.

Both the structural steel used in steel girders and the traditional passive steel rebars have been modeled through an elasto-plastic diagram [16]. In order to consider the possible buckling of compressed steel, a control of its minimum strains $\varepsilon_{s,min}$ is carried out (shortenings are taken with the negative sign).

The modelization of the stress-strain behavior of the active reinforcement is carried out by means of the law proposed by Ramberg and Osgood [31]. This law was chosen because it allows an adjustment to the experimental curve through 3 parameters (Eq. 6).

$$\sigma_p = E_p \varepsilon_p \left[A + \frac{1-A}{(1+B\varepsilon_p)^{\frac{1}{C}}} \right] \leq f_{pu} \tag{6}$$

A, B and C are the calibration parameters of the Eq. 6.

The law of relaxation of the active steel is the one proposed by Magura [32] (see Eq. 7).

$$\Delta\sigma_{p,rel} = \frac{log(24t)}{10}\left(\frac{f_{po}}{f_{py}} - 0.55\right) f_{po} \tag{7}$$

For strands subject to non constant strains, the Eq. 7 must be corrected (see Eq. 8) to account for that fact and to evaluate correctly the intrinsic relaxation. In this case, the reduced relaxation coefficient χ_r may be used. The graph proposed by Ghali and Trevino [33] to evaluate χ_r is used in the model.

$$\overline{\Delta\sigma}_{p,rel} = \chi_r \Delta\sigma_{p,rel} \tag{8}$$

2.5. Model for the analysis of sections

2.5.1. General

The following hypotheses have been assumed: (1) initially plane sections remain plane after load application or imposed strain (Navier Hypothesis); (2) strains originated by shear stress are not significant, therefore they have been rejected; (3) perfect bond among the materials that made up the section; and (4) internal forces are applied on the symmetrical axis of the section.

2.5.2. Section idealization

The section is discretized into parallel layers which are perpendicular to the symmetry axis (see Fig. 5). The layers consist exclusively of one material, even though several layers can be superimposed in order to represent different materials placed in the same ordinate. The section is analyzed by taking the bottom layer of the section as reference.

The positive signs are assigned to: (1) the bending moment compressing the upper layer; (2) the axial forces compressing the section; (3) the compression stresses; and (4) the elongations.

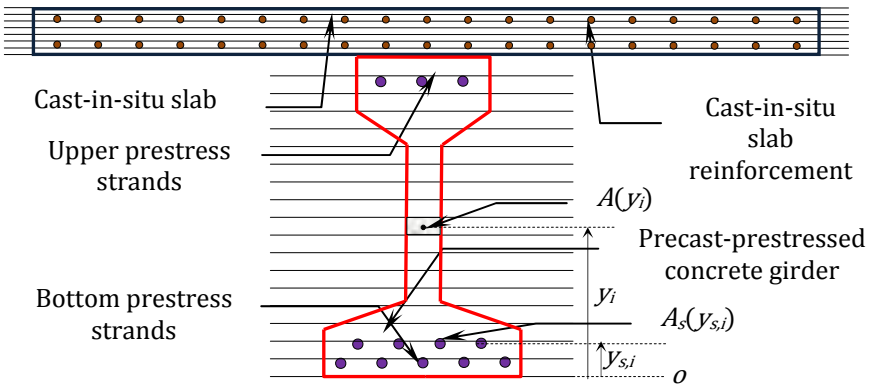

Fig. 5. Example of discretization of a composite section.

2.5.3. *Equilibrium and compatibility*

The equilibrium between sectional stresses and external forces is obtained by imposing the equations (Eqs. 9-10):

$$\Delta N(t) = \iint \Delta\sigma(t,y)dA \tag{9}$$

$$\Delta M(t) = \iint y\Delta\sigma(t,y)dA \tag{10}$$

Hypothesis of Navier (Eq. 11) and the perfect bond (Eq. 12) between the different materials forming the section are considered.

$$\Delta\varepsilon(t,y) = \Delta\varepsilon_o(t) + y\Delta\chi(t) \tag{11}$$

$$\Delta\varepsilon(t,y_i)_{y_i=y_s} = \Delta\varepsilon_s(t,y_s) \tag{12}$$

2.5.4. *Strategy adopted to solve the sectional problem*

The integrals of equations (Eqs. 9-10) are approximated through the Trapezoidal Rule [34] obtaining (Eqs. 13-14), respectively.

$$\Delta N(t) = \frac{\Delta y}{2}\left[\Delta\sigma(t,y_b)b_b + \sum_{i=1}^{n_c-1}\Delta\sigma(t,y_i)b_i + \Delta\sigma(t,y_t)b_t\right] + \sum_{i=1}^{n_s}\Delta\sigma_{s,i}(t,y_{s,i})A_{s,i} \tag{13}$$

$$\Delta M(t) = \frac{\Delta y}{2}\left[y_b\Delta\sigma(t,y_b)b_b + \sum_{i=1}^{n_c-1}y_i\Delta\sigma(t,y_i)b_i + y_t\Delta\sigma(t,y_t)b_t\right] + \sum_{i=1}^{n_s}y_{s,i}\Delta\sigma_{s,i}(t,y_{s,i})A_{s,i} \tag{14}$$

Two iterative methods have been implemented in order to find the solution ($\Delta\varepsilon$, χ) for the coupled system (Eqs. 11-14) for all load levels compatible with the section: (1) the Newton-Raphson method [35]. This is a numerically efficient method if a suitable guess is available (the solution from the previous step is used); otherwise, the number of iterations increases greatly and may even not converge. (2) The bisection method [36], is implemented to solve the system in those cases where the first method does not converge (high loading levels without a suitable guess, for instance). Numerically, this is a more demanding method but, on the other hand, it is more robust and can cover the cases for which the first method does not provide a solution.

2.6. Experimental validation

2.6.1. *Introduction*

The results measured in an experimental campaign are contrasted with those obtained with the model in order to validate the latter. The selected experimental campaign was developed by Choi [37]. In this

campaign, 9 pre-cast-prestressed HSC girders of 12 m of length, with and without NSC slab were casted and tested. They were subdivided into three groups, according to the strength of the concrete which was used in each case: 69 N/mm², 97 N/mm² and 124 N/mm². The beams were tested up to failure in a four-point bending test, aging between 120 and 232 days. Thorough information about the casting, instrumentation and the test procedure can be found in [37].

This example aims at verifying the capability of the model to reproduce the behavior up to failure of sequentially-constructed sections made of HSC. First, curvature-moment M-χ diagrams are obtained numerically, and then the cracking-bending moments M_{cr} and the failure-bending moments M_f are compared to those observed during the tests. Likewise, prestress losses are evaluated numerically and then contrasted to those measured so as to verify that the model registers the internal stress redistributions properly. Alternatively, some of the results obtained with the AES model are contrasted to those produced by RESPONSE [18].

2.6.2. Geometry, materials and test configuration

The geometry of the prestressed section as well as the prestress strands configuration is presented in Fig. 6a. The number of strands in each section corresponds to the compressive strength f_c of the concrete used. In that sense, the classification codes which had been used were: 10PS, 14PS and 18PS for strengths of 69 N/mm² (10 ksi), 97 N/mm² (14 ksi) and 124 N/mm² (18 ksi), respectively. A reinforced concrete slab with a height of 20.3 cm and variable width (1S if the width was 30.5 cm, 5S if it was 152.0 cm and N if there was no slab; see Fig. 6b) was casted.

Prestressing strands used in the girder specimens were 13 mm in diameter, 7-wire, Grade 270 (1860 N/mm²) with low relaxation.

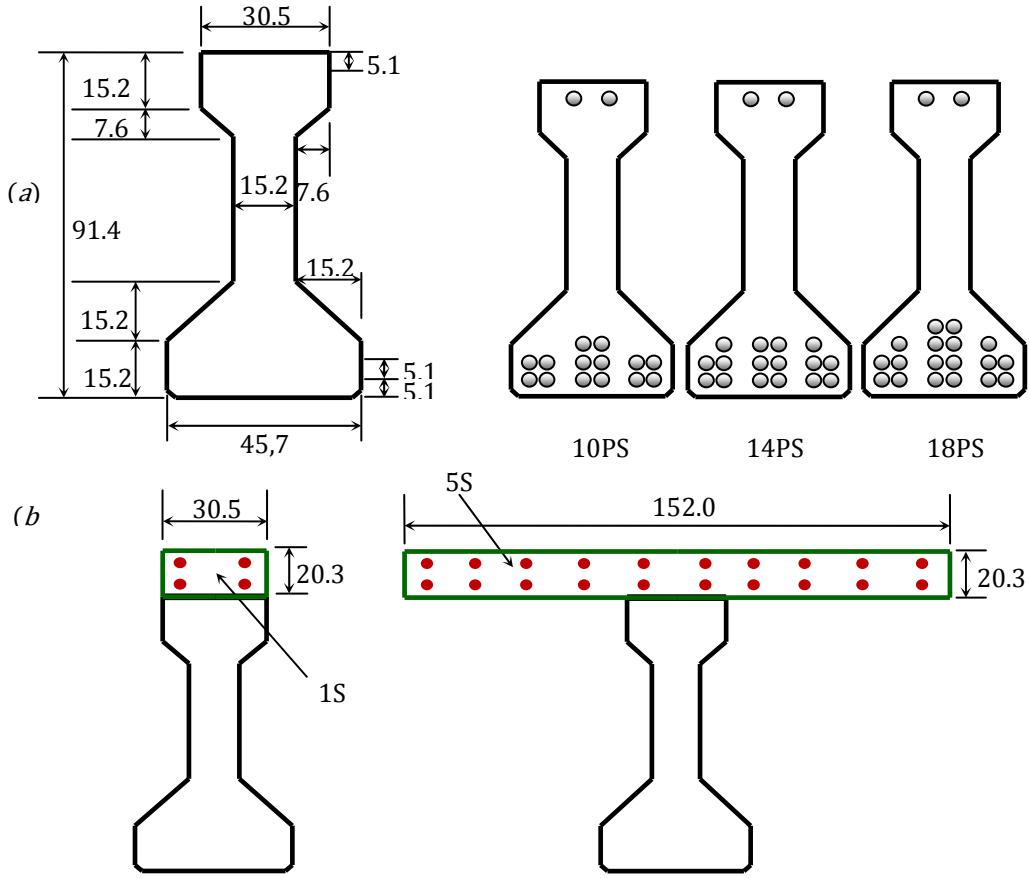

Fig. 6. (a) Cross-section and prestress strands configuration and (b) upper slab dimensions (in cm).

Fig. 7 shows the configuration of the test which had been carried out. The load was applied with a piston through a steel spread beam. This support and load configuration led to an intermediate area, length namely *s*, subjected to pure bending. The beams were loaded with a regime of 2.54 mm/min until cracking took place. Subsequently, they were reloaded at the same speed until yielding of the prestress strands was achieved. Once this state had been reached, loading speed was increased up to 6.35 mm/min and was maintained until failure of the element was detected.

Measures were taken during the processes of casting and storing as well as during the testing stage. Among these, extensometric gauges were installed at the intermediate and the extreme layers of both the beam and the slab, as well as at the most-bottom strands to measure strains. The stress of the prestressing strands was calculated considering a modulus E_p of 200000 N/mm² and the strains experimentally obtained. Besides, strand end slippage was also measured, and load cells were installed in order to control prestress force in both ends of the prestressing bed (130 m).

2.6.3. Time-dependent behavior. Prestress losses

In order to verify that the AES numerical model is capable of reproducing stress redistributions among the constitutive materials, a comparison of the evolution of stress in the bottom strands for the 10PS set of beams is carried out (see Fig. 8).

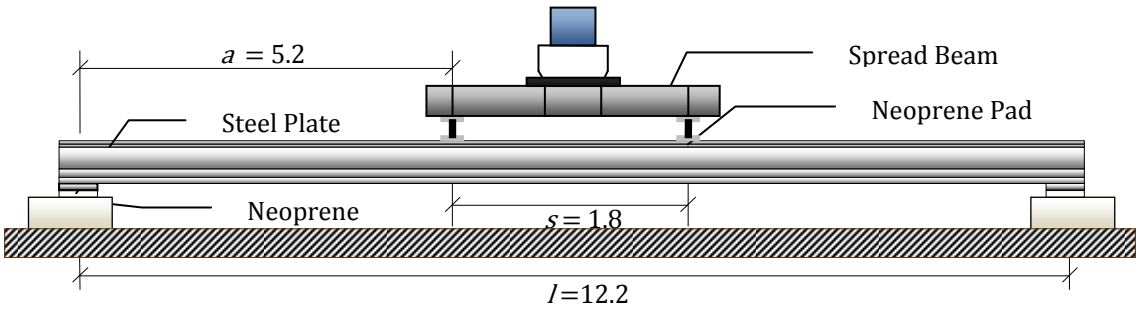

Fig. 7. Main dimensions of the test device (in m).

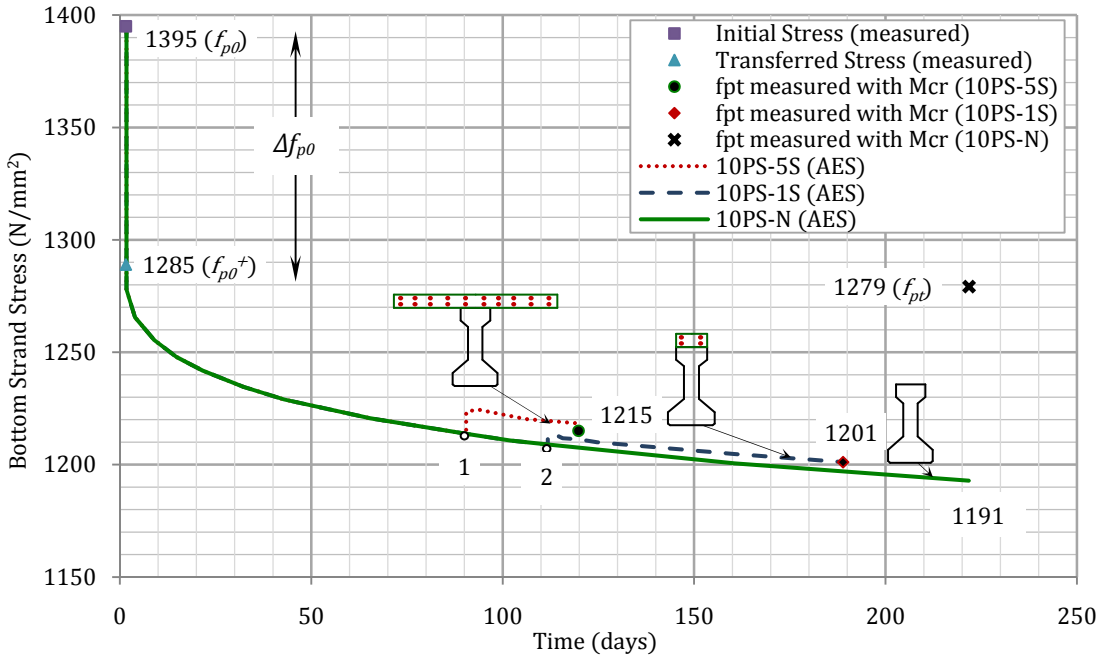

Fig. 8. Time-stress evolution of the bottom strands.

The results shown in Fig. 8 reflect that the model represents the stress drop Δf_{po} (instantaneous losses of the prestress tension) properly. In this sense, the stress after release f_{po}^{+} is 1285 N/mm², 1301 N/mm² and 1303 N/mm² according test [37], evaluated by Choi [37] and AES, respectively. This agreement between experimental results and the results obtained with the AES model (error of 1.4 %) is mainly due to knowing beforehand the measured values of the main parameters (E_c, δ_m, l_b, f_{po}) that control the instantaneous prestress losses (elastic shortening and strand-end slippage).

After the release, the stress in the strands decreases following the same tendency until the construction of each concrete slab (point 1 for type 5S and point 2 for type 1S). From those two instants onwards, the self-weight of the slab produces an instantaneous increase of stress, which causes the deviation of the initial stress evolution. Similarly, the coexistence of two concretes of different ages leads to an interaction between them which generates new stress redistributions due to creep and shrinkage.

Final stresses f_{pt} are measured before proceeding to the load test described in Fig. 7, carried out through different beam ages. In Fig. 8 the values f_{pt} measured indirectly with the value of the observed cracking moment M_{cr} are marked: 1215 N/mm² for beam 10PS-5S, 1201 N/mm² for beam 10PS-1S and 1279 N/mm² for beam 10PS-N. That is, evaluate the effective prestressing force with the cracking strength and the measured modulus of rupture. This is the strategy adopted by Choi [37] in those cases where the experimental measures obtained with gauges are inconsistent (f_{pt} is superior to f_{po}^{+}, which makes no sense physically).

The results shown in Fig. 8 confirm a good agreement between the values of f_{pt} measured experimentally in beams 10PS-5S (error of 0.2 %) and 10PS-1S (error of 0.0 %) and those calculated with AES. On the other hand, the error of 7.2% detected in beam 10PS-N may be due to, among other reasons, some variation in the parameters which are involved in the curing of the elements (humidity, for instance).

Table 1 shows the measured instantaneous and final prestress losses evaluated analytically by Choi [37] by means of the AASHTO-LRDF [38] formulation and, lastly, those obtained with the AES model for the nine tested beams.

Table 1. Instantaneous/final prestress losses as percentage of f_{po} (1395 N/mm²).

Code	Measured	Evaluated by Choi [37]	Evaluated with AES
18PS-1S	9.8/11.3	7.9/15.1	6.6/12.6
18PS-5S	5.3/12.9	7.9/14.2	6.6/11.7
18PS-N	6.9/10.1	7.7/14.3	6.6/12.8
Average	7.3/11.4	7.8/14.5	6.6/12.4
14PS-1S	8.0/10.8	7.5/15.6	6.9/13.0
14PS-5S	7.1/11.2	7.9/15.0	6.9/12.0
14PS-N	8.6/7.3	7.9/17.2	6.9/13.3
Average	7.8/9.8	7.8/15.9	6.9/12.8
10PS-1S	8.2/13.9	6.6/14.8	7.2/13.4
10PS-5S	8.4/12.9	6.6/13.7	7.2/12.3
10PS-N	7.3/8.3	6.6/14.7	7.2/8.3
Average	7.9/11.7	6.6/14.4	7.2/11.3

The results presented in Table 1 corroborate that the model provides well-adjusted values of the instantaneous prestress losses Δf_{po} in comparison with those measured experimentally. In this sense, the 14PS series shows the maximum difference with regard to the measured values (0.9 %). However, the AES model tends to underestimate the instantaneous losses of the analyzed beams. This can be caused by the fact that the real position of the strands may slightly differ from the theoretical one (see Fig. 6a). Likewise, the values proposed by AES for the final prestress losses Δf_{pt} do not differ more than 3.0 % (14PS series)

with respect to the average measured values. Thus, taking into account the uncertainties associated with the values of the parameters which are involved, this is a limited margin of error. Therefore, it is considered that the correlation is satisfactory and, consequently, the model reflects accurately the time-dependent behavior of the prestressed strands.

2.6.4. Behavior from service up to failure

In this section, the suitability of AES to deal with the analysis up to failure of the tested beams, taking into account evolutionary history, is assessed. With this aim, moment-curvature M-χ diagrams are used enabling the consideration of those aspects and providing accurate information about the sectional response.

Fig. 9 shows the M-χ diagrams of the sections of the 10PS series subjected to pure bending (sections within the length s, see Fig. 7). Cracking moments M_{cr} and failure moments M_f are marked as representative values of the global sectional response.

Fig. 9 highlights that the use of a slab leads to an increase of both bending strength and global ductility in the section. In fact, beams 10PS-1S (2361 kNm) and 10PS-5S (2693 kNm) present a bending moment increase of 23.1 % and 40.4 %, respectively, with regard to the beam without slab 10PS-N (1918 kNm). In all cases, the failure pattern obtained with AES begins with the yielding of the prestress strands and the subsequent failure by crushing due to compression at the top fiber of the section. This behavior was also observed in the specimens tested. In this sense, the neutral axis was inside the slab in the case of the girders with a 5S slab and inside the flange for both the girders without slab (N) and with a 1S slab [37].

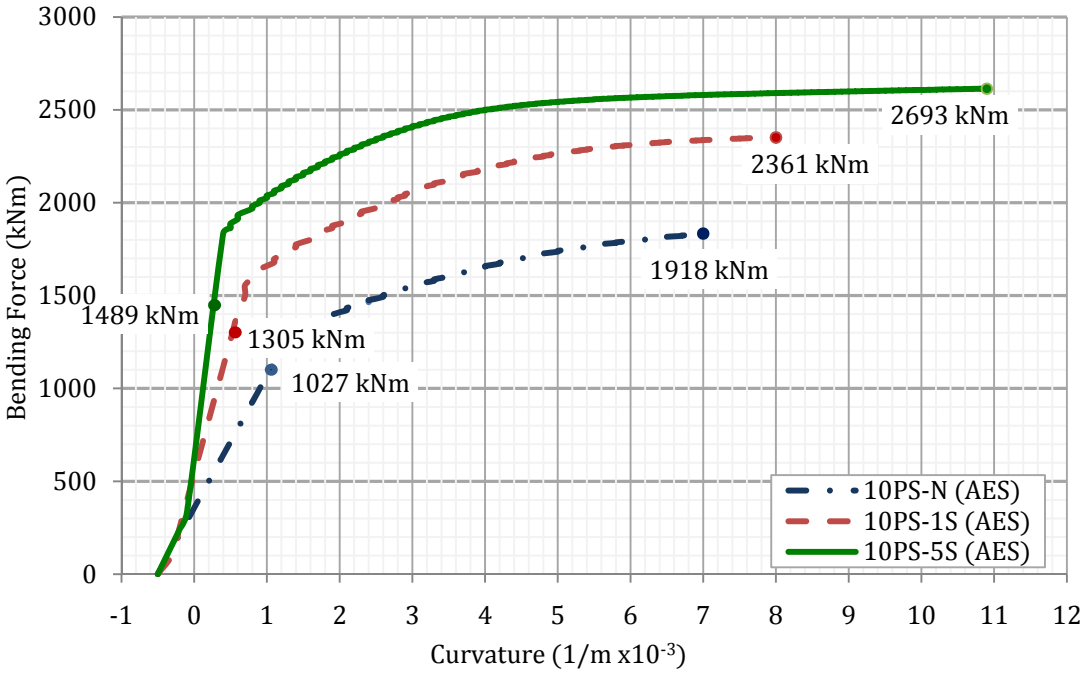

Fig. 9. M-χ diagrams of the central sections of the 10PS beams series.

Table 2 gathers the measured values for M_{cr} and M_f, those proposed by the author through analytical formulations [37] and those obtained by means of the AES model. Furthermore, the values for M_f evaluated by Choi [37] by means of RESPONSE have also been added. The coefficient ξ represents the ratio between the measured and the calculated moment.

In view of the results gathered in Table 2 it could be noticed that: (1) the cracking moment M_{cr} is evaluated satisfactorily both through the analytical formulation proposed by Choi [37] and through AES. In this respect, average values for ξ of 1.03 (Choi [37]) and 1.01 (AES) are obtained, hence both models

propose results which are on the side of safety; (2) the two numerical strategies presented here for the calculation of M_f (RESPONSE and AES) provide values which are very similar to those measured experimentally (ratios of ξ=1.03 for both model). Likewise, the analytical model produces more conservative results for M_f (average ξ of 1.11).

Table 2. Values obtained for M_{cr} and M_u.

Specimen	Cracking moment M_{cr}					Failure moment M_f						
	Measured	Proposed by Choi *et al.* [37]		AESS model		Measured	Proposed by Choi *et al.* [37]		RESPONSE [37]		AESS model	
		M_{cr}	ξ	M_{cr}	ξ		M_f	ξ	M_f	ξ	M_f	ξ
10PS-5S	1488	1439	1.03	1489	1.00	2879	2582	1.12	2681	1.07	2693	1.07
14PS-5S	1718	1687	1.02	1684	1.02	3185	2957	1.08	3046	1.05	3092	1.03
18PS-5S	1867	1862	1.00	1849	1.01	3448	3178	1.08	3315	1.04	3381	1.02
10PS-1S	1268	1250	1.01	1305	0.97	2376	2113	1.12	2353	1.01	2361	1.01
14PS-1S	1429	1402	1.02	1458	0.98	2632	2313	1.14	2614	1.01	2632	1.00
18PS-1S	1534	1532	1.00	1504	1.02	2825	2481	1.14	2857	0.99	2769	1.02
10PS-N	1083	960	1.13	1027	1.05	1987	1795	1.11	1943	1.02	1918	1.04
14PS-N	1176	1079	1.09	1164	1.01	2289	2060	1.11	2201	1.04	2222	1.03
18PS-N	1245	1231	1.01	1209	1.03	2452	2294	1.07	2458	1.00	2452	1.00

Consequently, considering the results obtained, it is concluded that the AES model is suitable for the calculation of internal bending moments M_{cr} and M_f in composite sections made of types of concrete with different resistant and rheological characteristics, even high-strength concrete. Furthermore, the model is particularly useful when dealing with analyses of composite sections where the neutral axis remains in the precast beam during the whole loading process (1S series). In these cases, a practical formulation to assess the value of M_f is not proposed in the rules due to the difficulty of derivation analytical expressions for these cases.

2.6.5. Load-deflection response

A subroutine including AES as a sectional analysis model has been implemented in order to verify its suitability for predicting the response of beams as the one presented in Fig. 7. Through this subroutine, the P-δ laws of each of the tested beams are obtained, and then compared with both the experimental results and the results generated by RESPONSE. This strategy aims at corroborating that the model is capable of reproducing the behavior up to failure of isostatic beams with a composite cross section.

The algorithm implemented to obtain the P-δ laws consists of:

1. Obtaining the M-χ (see Fig. 10a) diagram of the composite section considering the mechanical properties and prestress losses at the day of the test of each element.
2. Dividing the half span (symmetry) of the beam into segments of length Δx (see Fig. 10b).
3. Fixing an increment of the midspan displacement $\Delta\delta_B$.
4. Fixing tolerances for the values $\Delta\delta_B$ and ΔP, $\text{tol}_{\Delta\delta}$ and $\text{tol}_{\Delta P}$ respectively.
5. Assuming a trial value of the force ΔP.
6. Evaluating the increment of bending forces ΔM_i in each point x_i (Fig. 10b) by means of the Eq. 15.
7. Calculating the accumulated bending force M_i in each point x_i.
8. Finding de bending stiffness K_i of each section by means of the M-χ diagram (Fig. 10a).
9. Solving Eq. 16 in order to obtain $\Delta\delta_{ev,B}$ (see appendix B).
10. Verifying that $|\Delta\delta_{B,ev} - \Delta\delta_B| \leq \text{tol}_{\Delta\delta}$.
11. Returning to the step 5 when the condition of the step 10 is not verified. In this case, an iterative procedure based on the algorithm of Newton-Raphson [34] is used.

$$\Delta M = \begin{cases} \frac{\Delta P}{2} x & for\ 0 \le x \le a \\ \frac{\Delta P}{2} a & for\ a < x \le a + \frac{s}{2} \end{cases} \quad (15)$$

$$\Delta\delta_B = \Delta P \left[\int_0^a \frac{l-(2+l)x}{4K(x)} dx - \frac{as}{16K_a}(2l + 4a + s) \right] \quad (16)$$

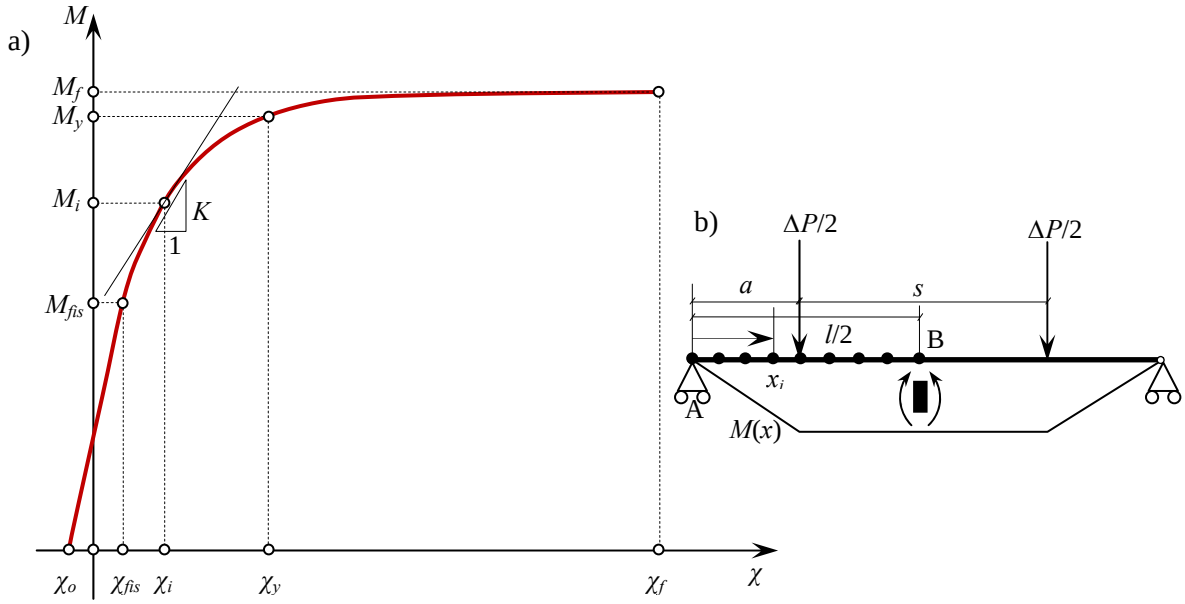

Fig. 10. (a) Generic moment-curvature diagram and (b) bending moment diagram.

Following this strategy, the *P*-δ laws of the 10PS beams tested have been obtained (see Fig. 11).

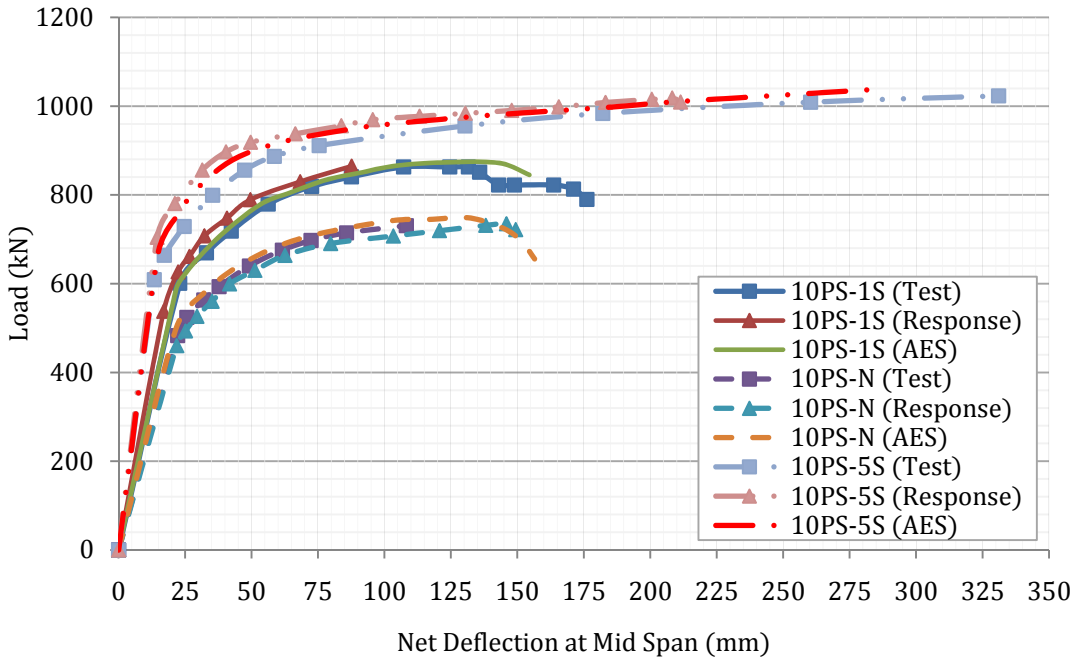

Fig. 11. *P*-δ curves measured and obtained by means of the two numerical models.

Based on the results shown in Fig. 11, it is concluded that the P-δ curves proposed by the AES model adjust satisfactorily to those obtained experimentally and to those evaluated with RESPONSE through all loading stages. Table 3 gathers maximum loads and ultimate deflections obtained for the beams of the 10PS series.

Table 3. Maximum load P_{max} and ultimate midspan displacement δ_u for the 10PS series.

Specimen	P_{max} (KN)			δ_u (mm)		
	Experimental Data	RESPONSE [37]	AES	Experimental Data	RESPONSE [37]	AES
10PS-N	731	735	749	108	149	156
10PS-1S	863	865	875	176	88	155
10PS-5S	1023	1018	1037	331	211	284

The results presented in Table 3 show that the two numerical models evaluate the maximum load P_{max} with excellent accuracy, which is in accordance with the conclusions obtained regarding the M_f values (see Table 2). In this sense, the RESPONSE model provides closer values of P_{max} (maximum error of 0.5 %) than the AES model (maximum error of 1.5 %) with respect to the experimental values. Nevertheless, these differences are not significant in terms of design. Furthermore, there is a deviation regarding the ultimate displacement δ_u. In particular, both models provide results on the safety side for beams with a slab, being the values of AES closer to the real ones. Specifically, the average and the maximum deviations are of 41.4 % and 50.0% with RESPONSE, and of 23.5 % and 44.4 % with AES. This is mostly because the value used for ε_{cu} (which controls the failure mode) is more restrictive than the real values measured in the beams with slab (5S and 1S).

2.7. Conclusions

This article presents a model for the analysis of sequentially-constructed composite sections made up of materials such as concrete and steel. The appropriate constitutive equations for simulating the instantaneous and time-dependent behavior of concrete were implemented with the aim of covering a wide range of analysis cases. In this sense, the results of an experimental campaign (from the literature) were used to validate the AES model for the analysis of composite sequentially-constructed sections. These data were contrasted with the results provided by the model AES, showing satisfactory correlation ratios and confirming the feasibility of the same for designing purposes. In this sense, the AES model is already in use in several Spanish precast concrete factories for the optimization of bridges sections constructed with precast – prestressed concrete girders

Considering the potential of AES for the analysis of sections such as the ones studied in this paper, several research lines were initiated to further develop the model. Among these, it is highlighting the consideration of biaxial bending, the inclusion of AES in a 3D finite element model and the implementation of the constitutive equations to model the post-cracking behavior of steel fiber reinforced concrete (SFRC).

2.8. Acknowledgments

The authors wish to acknowledge PRECON, S.A. for the financial support and resources. Also, the authors want to recognize the valuable technical support provided on several of the work stages by Professor Antonio Marí (Department of Construction Engineering of the Universitat Politècnica de Catalunya). Likewise, the authors of this document wish to show gratitude for the economical support received by means of the Research Project BIA2010-17478: *Constructive processes by means fibre reinforced concretes*.

2.9. References

1. Marí AR, Mirambell E, Estrada I. Effects of construction and slab prestressing on the serviceability behaviour of composite bridges. J Constr Steel Res 2002;**59**(2):135-63.

2. Roca P, Marí AR. Numerical treatment of prestressing tendons in the nonlinear analysis of prestressed concrete structures. Comp Struct 1993;**46**(5):905-16.

3. Fernández M. Evaluation of the structural non-linear effects due to the steel and concrete deferred strains, PhD thesis, Universidad Politécnica de Madrid, 2003 [in Spanish].

4. Fabbrocino G, Manfredi G, Cosenza E. Modelling of continuous steel-concrete composite beams: computational aspects. Comp Struct 2002;**80**(27-30):2241-51.

5. Ranzi G, Bradford MA. Analytical solutions for the time-dependent behaviour of composite beams with partial interaction. Int J Solids Struct 2006;**43**(13):3770-93.

6. Barakat S, Kallas N, Taha MQ. Single objective reliability-based optimization of prestressed concrete beams. Comp Struct 2003;**81**(26-27):2501-12.

7. Laurencet P, Jaccoud JP, Favre R. Cracking of Prestressed Concrete Structures: Modelization, validation and interpretation. RILEM Mater Struct 1999;**32**(32):360-69 [in French].

8. Bazant ZP. Numerical determination of long-range history from strain history in concrete. RILEM Mater Struct 1972;**5**(3):135-41.

9. McMillan FR. Discussion of the paper by AC Janni: Method and designing reinforced concrete slabs. Trans Am Soc Civ Eng 1916;**80**:1738.

10. Dezi L, Leoni G, Tarantino AM. Algebraic methods for creep analysis of continuous composite beams. ASCE J Struct Eng 1996;**122**(4):423-30.

11. Trost H. Auswirkungen des superpositionsprizips auf kriech und relaxations probleme bei beton und spannbeton. Beton und Stahlbetonbau 1967;**62**(10):230-38 [in German].

12. Martínez Calzón J, Ortiz J. Composite steel-concrete construction. Editorial Rueda, Madrid, 1978 [in Spanish].

13. Kawano A, Warner F. Model formulations for numerical creep calculations for concrete. ASCE J Struct Eng 1996;**122**(3):284-90.

14. Bazant ZP, Wittman FH, editors. Creep and shrinkage in concrete structures. New York: John Wiley & Sons, 1982.

15. Morano SG, Mannini C. Preflex beams: A method of calculation of creep and shrinkage effects. ASCE J Bridge Eng 2006;**11**(1):48-58.

16. Kwak H-J, Seo Y-G. Long-term behavior of composite girder bridges. Comp Struct 2000;**74**(5):583-599.

17. Ghali A, Elbadry M. User's manual and computer program CRACK. Research Report CE85-1 (revised 1991), Department of Civil Engineering, University of Calgary, Alberta (Canada), 1991.

18. Bentz E. Sectional analysis of reinforced concrete members. Ph.D. Thesis. Department of Civil Engineering, University of Toronto, Toronto (Ontario), 2000.

19. Torres Ll. Numerical model and experimental validation of the serviceability behaviour of concrete structures, PhD thesis, Universitat Politècnica de Catalunya, 2001 [in Spanish].

20. Ghali A, Elbadry M. User's manual and computer program CPF: Cracked Planar Frames in Prestressed Concrete. Department of Civil Engineering. Research Report CE 85-2, The University of Calgary, 1985.

21. Marí AR, Valdés M. Long-term behaviour of continuous precast concrete girder bridge model. ASCE J Bridge Eng 2000;**5**(1):22-30.

22. de la Fuente A, Aguado A, Molins C. Numerical model for the non linear analysis of precast and sequentially constructed sections. Hormig y Acero 2008;**57**:69-87 [in Spanish].

23. Thorenfeldt E, Tomaszewicz A, Jensen JJ. Mechanical properties of high–strength concrete and application in design. In: Proceedings of the symposium Utilization of High Strength Concrete, Stavanger (Norway), 1987.

24. Hognestad E, Hanson NW, McHenry D. Concrete stress distribution in ultimate strength design. ACI J 1955;**52**(4):455-79.

25. Collins MP, Mitchell D. Prestressed concrete structures. Englewood Cliffs, NJ: Prentice Hall; 1991.

26. Djamic F, Owen DRJ. Practical considerations for modelling of post-cracking concrete behaviour for finite element analysis of reinforced concrete structures. Computer Aided Analysis and Design of Concrete Structures, Pineridge Press, Swansea, 693-706, 1984.

27. EN 1992-1-1. Eurocode 2: design of concrete structures – part 1-1: general rules and rules for buildings; 2004.

28. Fernández M, Muttoni A, Gambarova PG. Relationship between nonlinear creep and cracking of concrete under uniaxial compression. J Adv Tech 2007;**5**(3):1-11.

29. Comité Euro International du Béton-Fédération International de La Précontrainte (CEB-FIP). CEB-FIB Model Code 2010 (draft version); 2010.

30. Comité Euro International du Béton (CEB). Structural effects of time-dependent behaviour of concrete. Bulletin d'information No. 142, 1984 [in French].

31. Ramberg W, Osgood WR. Description of stress-strain curves by three parameters. Technical Note No. 902, National Advisory Committe for Aeronautics, Washington DC, 1943.

32. Magura DD, Sozen MA, Siess CP. A study of stress relaxation in prestressing reinforcement. PCI J 1964;**9**(2):13-57.

33. Ghali A, Trevino J. Relaxation of steel in prestressed concrete. PCI J 1985;**30**(5):82-94.

34. Yang WY, Wenwu C, Chung TS, Morris J. Applied numerical methods using Matlab. John Wiley & Sons Inc., Hoboken, New Jersey, 2005.

35. Thanoon WA, Hamed HA, Noorzaei J, Jaafar MS, Al-Silayvani BJ. Inelastic analysis of composite sections. Comp Struct 2004;**82**(20-21):1649-1656.

36. Terro JM, Hamoush SA. Inelastic analysis of sections subjected to axial force and bending moment. Comp Struct 1996;**59**(1):13-19.

37. Choi W. Flexural Behaviour of prestressed girder with high-strength concrete, PhD thesis, North Carolina State University, 2006.

38. AASHTO LRDF. 2005. *Bridge design specifications*. 2nd ed. American Association of State Highway and Transportation Officials, Washington DC.

APPENDIX A: Notation

A: area of the analyzed material.
$A_{s,i}$: area of the analyzed steel bar/strand.
A: distance support-spread beam.
b_b: width of the bottom layer of the section.
b_i: width of the analyzed concrete layer.
b_t: width of the top layer of the section.
E_c: secant modulus of concrete.
E_{ci}: tangent modulus of concrete in the origin.
$E_{c,28}$: secant modulus of concrete at 28 days.
E_p: modulus of prestressed steel for strands.
f_c: compressive strength of concrete.
f_{cm}: average compressive strength of concrete.

f_{ct}: tensile strength of concrete.
f_{po}: initial stress of active steel.
$f_{po}+$: stress of active steel after realise.
f_{pt}: prestress tension of active steel at time t.
f_{pu}: failure stress of active steel.
f_{py}: yielding stress of active steel.
I_k: k-th interval.
J: linear creep function.
K: bending stiffness.
l: distance between the supports.
l_b: prestressing transfer length.
M: applied external bending moment.
M_{cr}: cracking bending moment.
M_f: failure bending moment.
M_i: bending moment in i-section.
M_y: bending moment of yielding of the strands.
P: applied load.
P_{max}: maximum applied load.
n_c: number of concrete layers.
n_p: number of points.
n_s: number of steel bars/strands.
s: distance subjected to pure bending.
t: arbitrary instant of evaluation.
t_r: initiation time of restrained shrinkage.
t_o: loading age
x_i: distance of the i-section the left support.
y: ordinate of the material.
y_i: ordinate of the analyzed concrete layer.
y_b: ordinate of the bottom layer of the section.
y_t: ordinate of the top layer of the section.
y_s: ordinate of the steel element.
$y_{s,i}$: ordinate of the analyzed steel bar/strand.
w: crack width.
ΔA_i: concrete area of the i-element.
$\Delta\delta_B$: midspan displacement increment.
$\Delta\delta_{ev}$: evaluated midspan displacement increment.
Δf_{pt}: total prestress losses at time t.
Δf_{po}: instantaneous prestress losses.
$\Delta\varepsilon$: strain increment in the analyzed fibre.
$\Delta\varepsilon_o$: strain increment of the reference fibre.
$\Delta\varepsilon_s$: strain increment of the steel.
$\Delta\varepsilon_{s,i}$: strain increment of the analyzed steel bar/strand.
ΔM: bending moment increment.
ΔM_i: bending moment increment in section i.
ΔN: axial load increment.
ΔP: load increment.
$\Delta\sigma$: stress increment of the analyzed material.
$\Delta\sigma_{p,rel}$: stress increment of active steel due to relaxation.
$\overline{\Delta\sigma_{p,rel}}$: corrected stress increment of active steel due to relaxation.
$\Delta\sigma_{s,i}$: stress increment of the analyzed steel bar/strand.
Δt_k: time increment of the k-th stage.
Δy: height increment.
Δx: horizontal distance increment.
$\Delta\chi$: sectional curvature increment.
α_1, α_2: parameters of calibration.
ε: total concrete strain.
ε_a: concrete strain due to aging.
ε_{cr}: concrete cracking strain.
ε_{co}: strain for maximum compressive stress.
ε_{cu}: ultimate strain of compressed concrete.
ε^m: mechanical concrete strain.
ε^{nm}: non-mechanical concrete strain.

ε_p: active steel strain.
ε_{sh}: concrete shrinkage strain.
$\varepsilon_{s,min}$: minimum strain of steel.
ε_φ: concrete creep strain.
δ: displacement.
δ_m: average strand-end slippage.
δ_{max}: midspan displacement.
ξ: measured/predicted values ratio.
σ: stress of the analyzed material.
σ_c: concrete stress.
σ_{cc}: concrete compressive stress.
σ_{ct}: concrete tensile stress.
σ_p: stress of active steel.
τ: integration instant.
$\varphi_{28,lin}$: linear-creep coefficient at 28 days.
$\varphi_{28,nlin}$: nonlinear-creep coefficient at 28 days.
χ: global sectional curvature.
χ_{cr}: sectional curvature when the concrete cracking occurs.
χ_i: curvature of the i-section.
χ_f: sectional curvature in failure.
χ_r: reduced relaxation coefficient.
χ_y: sectional curvature for strands yielding.

APPENDIX B: Derivation of the equation 16

The increment of rotation in A $\Delta\varphi_A$ as well as the increment of vertical displacement in B are evaluated by means of the first theorem (Eq. B.1) and the second (Eq. B.2) theorems of Mohr.

$$\Delta\varphi_B = \Delta\varphi_A + \int_0^{a+\frac{s}{2}} \frac{\Delta M(x)}{K(x)} dx \tag{B.1}$$

$$\Delta\delta_B = \Delta\delta_A + \Delta\varphi_A \frac{l}{2} + \int_0^{a+\frac{s}{2}} \frac{\Delta M(x)}{K(x)} \left(\frac{l}{2} - x\right) dx \tag{B.2}$$

The values of $\Delta\varphi_B$ and $\Delta\delta_A$ are zero due to the symmetry condition.

Likewise, substituting (Eq. 17) in (Eq. B.1) and in (Eq. B.**2**), and designating $K(a) = K_s$, the following Eq. B.3 and B.4 are obtained:

$$0 = \Delta\varphi_A + \int_0^a \frac{\Delta P}{2K(x)} x\, dx + + \int_a^{a+\frac{s}{2}} \frac{\Delta P a}{2K_s} dx \tag{B.3}$$

$$\Delta\delta_B = \Delta\varphi_A \frac{l}{2} + \int_0^a \frac{\Delta P}{2K(x)} x \left(\frac{l}{2} - x\right) dx + + \int_a^{a+\frac{s}{2}} \frac{\Delta P a}{2K_s} \left(\frac{l}{2} - x\right) dx \tag{B.4}$$

Integrating the Eq. B.3-B.4, the values of $\Delta\varphi_A$ and $\Delta\delta$, expressed in function of both the unknown ΔP and the bending stiffness (Eq. B.5-B.6, respectively), are obtained.

$$\Delta\varphi_A = -\frac{\Delta P}{4}\left[2\int_0^a \frac{x}{K(x)} dx + \frac{as}{K_s}\right] \tag{B.5}$$

$$\Delta\delta_B = \Delta\varphi_A \frac{l}{2} + \frac{\Delta P}{2}\left[\int_0^a \frac{\frac{l}{2}}{K(x)} dx + \frac{as}{8K_s}(2l - 4a - s)\right] \tag{B.6}$$

Then, substituting Eq. B.5 in Eq. B.6 a final relation between $\Delta\delta_B$ and ΔP is derived (Eq. B.7).

$$\Delta\delta_B = \Delta P\left[\int_0^a \frac{\xi(x)}{4K(x)} dx - \frac{as}{16K_s}(2l + 4a + s)\right] \tag{B.7}$$

where:

$$\xi(x) = l - (2 + l)x \tag{B.8}$$

Eq. B.7 is solved iteratively (Eq. B.9).

$$\Delta\delta_B^{k+1} = \Delta P^{k+1}\left\{\frac{\Delta x}{2}\left[\frac{\xi(0)}{4K(0)} + \sum_{i=1}^{n_p-1}\frac{\xi(x_i)}{4K(x_i)} + \frac{\xi(a)}{4K(a)}\right] - \frac{as}{16K_s}(2l + 4a + s)\right\} \tag{B.9}$$

CAPÍTULO 3

Diseño óptimo integral de tubos de hormigón

3.1. Resumen

En este artículo se presenta el modelo Análisis de Tubos de Hormigón (ATH), una herramienta para el diseño y la verificación de tubos de hormigón con cualquier configuración de armadura (barras y/o fibras estructurales) sometidos al ensayo de aplastamiento. El modelo permite reproducir el comportamiento hasta rotura del tubo teniendo en cuenta la fisuración y la respuesta post – pico de los materiales. Éste se ha planteado en dos partes: (1) un modelo de análisis no lineal de secciones y (2) un modelo que simula el tubo y la configuración de ensayo. Con ello se pretende, por una parte, estudiar la influencia de distintos parámetros y, por otra, facilitar al proyectista una herramienta para el diseño óptimo y la comprobación de tubos. Asimismo, se presenta un caso real de diseño de un tubo de 2.80 m de diámetro. Se verifica que los resultados propuestos por el modelo concuerdan satisfactoriamente con los experimentales.

Palabras clave: Tubos de hormigón; Hormigón con fibras; Análisis no lineal; Ensayo de aplastamiento; Fisuración.

3.2. Introducción

Los tubos de hormigón (TH) para conducciones de saneamiento, ya sean de hormigón en masa (THM) o de hormigón armado con armaduras pasivas (THA) son una solución conocida y aceptada [1].

Asimismo, las alternativas de hormigón con fibras (THF) [2-6] y mixta armaduras pasivas y hormigón con fibras (THAF) también son posibles [2-4]. Éstas proporcionan ventajas tanto desde el punto de vista técnico como económico. Desde el primero, se logra una mejora apreciable de varias propiedades mecánicas del hormigón (ductilidad, tenacidad) y, en particular, con la adición de fibras metálicas [7]. Asimismo, la combinación mixta armado + fibras conduce a una sinergia estructural positiva: las barras desarrollan la principal función resistente [8], mientras que las fibras cosen toda la superficie de las fisuras reduciendo su separación y anchura así como colaboran, junto con las barras, en la función resistente. Desde el segundo, el ahorro de armadura tradicional se traduce en una disminución de las operaciones de montaje, mano de obra, maquinaria y riesgos asociados [4].

Ahora bien, en España, estas dos alternativas se han contemplado en varias campañas experimentales [4], sin embargo, aún no se han introducido en el mercado. Esa falta de implantación puede ser fruto de la tradicional dificultad para vencer la inercia al cambio [9], que dificulta la innovación, así como a factores de riesgo de pequeños cortes en la manipulación de los tubos o bien, a la falta de métodos de cálculo para este material. Respecto a esto, hasta la entrada en vigor de la EHE-08 [10], las fibras no estaban consideradas como material resistente.

De caras a dar respuesta al problema del diseño de TH reforzados con las estrategias habituales (THM y THA) así como con las más recientes (THF y THAF), se presenta este artículo con el objetivo de dar a conocer un nuevo método de diseño óptimo de TH. Para comprobar la bondad de la propuesta en THA, se incluye un ejemplo de diseño de una tubería de 2.80 m de diámetro interior (D_i) en el que se comparan los resultados obtenidos numéricamente con los obtenidos experimentalmente, habiéndose obtenido una excelente correlación entre ambos. Este procedimiento ha permitido alcanzar un significativo ahorro de material.

El método de diseño propuesto se plantea en dos partes diferenciadas:

1. Un modelo de análisis no lineal de secciones que acepta múltiples configuraciones de armado.
2. Un modelo de análisis estructural, que incluye el modelo de análisis seccional como subrutina y que simula el tubo y la configuración del ensayo de aplastamiento (EA) o de tres aristas (E3a) (ver Fig. 1), permitiendo reproducir el comportamiento integral hasta rotura del tubo.

Fig. 1. Ensayo de tres aristas o de aplastamiento. Cortesía de PREFRAGA.

3.3. La situación actual

3.3.1. Método directo y el método indirecto de diseño

El *método directo* [11-13] se fundamenta en la definición de las leyes de esfuerzos considerando la interacción suelo–estructura mediante el método de elementos finitos (MEF) [14-16] o, alternativamente, mediante distribuciones de presión aproximadas [17 y 18]. A partir de éstas, se verifica la capacidad estructural del tubo frente a: (1) la flexión; (2) la tensión diagonal (cortante); (3) la tensión radial; (4) la deformación excesiva del hormigón comprimido y (5) frente a un ancho de fisura (w) fijado.

El uso de este método conduce, en general, a diseños estructuralmente eficientes y económicos [15], si bien con elevado esfuerzo de cálculo y tiempo. Su uso se reserva para:

1. El diseño de tuberías de gran diámetro y/o con grandes coberturas de terreno.
2. Casos en los que un diseño, considerando las condiciones reales de instalación, pueda conducir a reducciones importantes de costes económicos.
3. Estudios paramétricos.

El *método indirecto* se basa en la determinación experimental de la resistencia del tubo mediante el EA (Fig. 1). Las condiciones de este ensayo se pueden reproducir fácilmente en las plantas de prefabricados que producen TH.

La principal diferencia de este método frente al *método directo* es que no se precisa de la determinación de las leyes de esfuerzos en la configuración final del tubo. Además, se supone que el EA reproduce la condición más pésima de apoyo en situación de servicio (apoyo directo) [4]. Esto hace que sea el método más extendido, aparte de la fiabilidad y reproducibilidad del EA, viniendo todo ello apoyado por la existencia de códigos que facilitan la tarea del proyectista.

La carga que debe alcanzar el tubo en el EA está tabulada en función del: diámetro nominal D_n (D_i en TH), el tipo de verificación (servicio o rotura) y la clasificación resistente (E y A, europea y americana, respectivamente).

A nivel de cálculo, existen varias aproximaciones analíticas para reproducir el comportamiento integral hasta rotura de los THM y los THA [19] bajo la configuración del EA. Incluso, existen modelos numéricos que tienen en cuenta también la interacción suelo–estructura: el Soil Pipe Interaction Design and Analysis (SPIDA) [14-15] y el Standard Installation Direct Design (SIDD) [20], por ejemplo. A pesar de ello, éstos han sufrido cierto desfase en comparación con los modelos actuales en cuanto el tratamiento a nivel sección [21]. En este sentido, estos modelos no son operativos cuando se pretende afrontar el diseño y/o comprobación de THF y THAF.

3.3.2. Situación normativa

A nivel europeo, la UNE-EN 1916 [22] regula tanto los THM como los THA o tubos de hormigón reforzados con fibras de acero (THFA). Si bien, ésta no considera la situación mixta de fibras y armadura pasiva (THAFA). Por otro lado, dicha normativa europea recoge conceptos de las americanas ASTM C14 [23] y C76 [24] para THM y THA, respectivamente; basadas en el *método indirecto*.

La UNE-EN 1916 [22] no sugiere ni cuantías mínimas de armadura pasiva tradicional ni de fibras para alcanzar las clases resistentes A o E. Éstas se fijan en las normativas nacionales y están basadas en la ASTM C76 [24] o en algún método de diseño de THA [18 y 25]. En este sentido, en España es la UNE 127916 [26] la que fija las cuantías mínimas de acero en THA. Sin embargo, no se establecen cuantías mínimas de fibra de acero para THFA, sino que debe disponerse la reflejada en los documentos de fábrica.

3.3.3. Retos de futuro

Para THA, de lo expuesto hasta aquí se deduce, por un lado, que en ocasiones la armadura mínima sugerida por las normativas conduce a resultados del EA demasiado conservadores y, por otro, que

diámetros nominales elevados (por encima de 2.50 m), su diseño no queda contemplado en las normativas

En relación con los THFA, debido a la falta de recomendaciones y métodos de cálculo simplificados, el diseño se hace por tanteo: probar con varias dosificaciones y/o espesores hasta que se logra una cuantía óptima para alcanzar la clase resistente deseada en el EA.

De caras a dar respuesta a estos vacíos, se ha desarrollado un modelo de análisis no lineal de TH llamado Análisis de Tubos de Hormigón (ATH) para la simulación numérica del EA (Fig. 1). Con esta herramienta se puede estudiar: (1) configuraciones de armadura y clases resistentes no recogidas en normativa; (2) la inclusión de fibras, con capacidad estructural, como elemento resistente y cuantificar su aportación en todas las fases de carga; (3) la influencia de parámetros geométricos del tubo y mecánicos de los materiales y (4) la sinergia estructural derivada del empleo de fibras y armadura pasiva.

Se pretende, de este modo, que el técnico pueda emplear el modelo ATH para adecuar el diseño de los tubos a las condiciones reales de planta y optimizar el tipo y las cuantías de refuerzo. Así, se evitará recurrir al ensayo como método de prueba–error de diseño, lo que resulta antieconómico debido al gran número de diámetros comerciales, espesores y clases resistentes y, por lo tanto, frena el desarrollo tecnológico de este elemento (la aceptación de fibras estructurales, por ejemplo).

Antes de plantear el modelo, parece conveniente explicar con cierto detenimiento el EA con el fin de entender mejor comportamiento del mismo, tanto a nivel estructural y seccional como del material.

3.4. El ensayo de aplastamiento (EA) o de tres aristas (E3a)

3.4.1. Procedimiento de ensayo

La ASTM C497-05 [27] y UNE-EN 1916 [22] especifican las dimensiones, materiales, el procedimiento a seguir y la configuración para ejecutar el EA. La sección transversal y el perfil longitudinal del EA se presentan esquemáticamente en la Fig. 2.

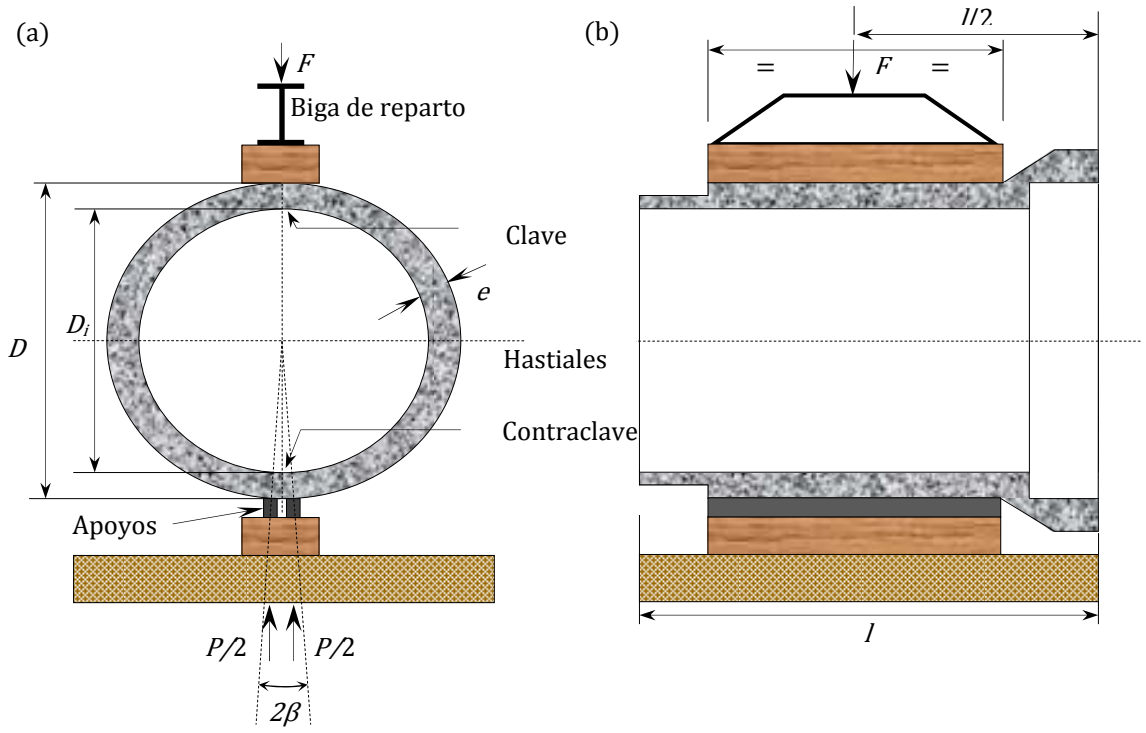

Fig. 2. (a) Sección transversal y (b) sección longitudinal del EA.

El proceso de carga y los requerimientos resistentes son función del tipo de armado [22]. Concretamente, para THA el ensayo se lleva cabo de forma continua hasta la rotura del tubo, verificándose que se alcanza la carga de fisuración controlada (F_c) para la cual se produce una fisura estabilizada de ancho 0.3 mm y longitud continua máxima de 300 mm y, también, que la carga de rotura (F_u) es superior a la carga de rotura especificada (F_n). Por otra parte, un THFA debe:

1. Resistir F_c durante un minuto sin que aparezcan fisuras, siendo F_c igual o superior al 67% de F_n.
2. Llevar el tubo hasta rotura, obteniéndose F_u la cual debe ser superior a F_n.
3. Cuando la carga ha descendido más de un 5% respecto a F_u, se procede a la descarga para posteriormente recargar. En esta segunda carga se debe alcanzar, como mínimo, el 67% de F_n. Este nivel de carga debe ser soportado durante un minuto sin que se produzca la ruina del tubo. La historia de carga completa se recoge en la Fig. 3.

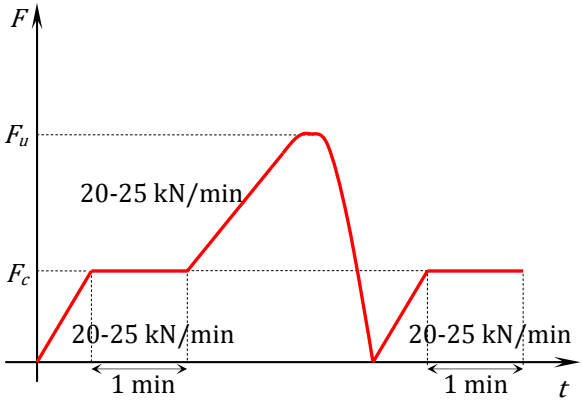

Fig. 3. Patrón de carga en el tiempo *F-t* aplicado en el EA en los THFA.

La razón de ser de este proceso de carga cíclico es verificar que el tipo y la cuantía de fibras son las adecuadas para garantizar la carga mínima post–rotura y, de forma indirecta, que el anclaje fibra–hormigón y la resistencia post–pico del hormigón reforzado con fibras de acero (HRFA) son las adecuadas [6].

3.4.2. Respuesta estructural de TH bajo el EA

La respuesta estructural se descompone en las fases reflejadas en las Fig. 4a y 4b: (1) Elástica, (2) Elástica–Fisurada, (3) Fisurada, (4) Pre–Rotura, (5) Rotura y (6) Post–Rotura.

Los TH recorren las mismas fases durante el EA independientemente del tipo de refuerzo. En estado de agotamiento, los modos de fallo de la estructura pueden ser varios: flexión, cortante y tensiones radiales [11]. Si bien, este trabajo se centra en los mecanismos de rotura por tensiones normales.

La tubería es una estructura con un grado de hiperestatismo y, consecuentemente, tiene la posibilidad de redistribuir esfuerzos de flexión en función de la capacidad de giro de las secciones críticas. En este sentido, la capacidad de redistribución no sólo depende de la geometría (D_i, e) y de las condiciones de apoyo, sino también del tipo, cuantía y configuración de armado.

Por esta razón, previo a describir el modelo ATH, se hace un análisis teórico de la respuesta de los TH frente al EA. La exposición se apoya en las curvas cualitativas carga F desplazamiento vertical en clave v (Fig. 4a) y en la evolución de los esfuerzos flectores M con F en las dos secciones críticas (Fig. 4b). En este sentido, la clave y la contraclave trabajan a flexión simple, mientras que el resto de secciones a flexión compuesta.

Fase Elástica (1)

La respuesta en esta fase está gobernada principalmente por la geometría (D_i, e y β), el módulo de elasticidad de la matriz de hormigón (E_c) y su resistencia a tracción (f_{ct}). Asimismo, ésta es prácticamente independiente del tipo y de la configuración de armadura [6]. La tubería en esta fase ofrece su máxima

rigidez frente al aplastamiento y los materiales responden elásticamente hasta que se alcanza la carga de primera fisura (F_{cr}), a partir de la cual se pasa a la fase fisurada. Para la carga F_{cr}, las secciones críticas trabajan a $M_{cr,c}$ en clave y $M_{cr,s}$ en riñones.

Fase elástico – fisurada (2)

En esta fase la sección de clave ha fisurado. Debido a la pérdida de rigidez a flexión de ésta y, en virtud del hiperestatismo del sistema, se produce una redistribución de momentos hacia los hastiales (Fig. 4b). Asimismo, la curva F–v sigue una tendencia lineal (Fig. 4a) con una ligera pérdida de rigidez respecto a la fase anterior.

La fase finaliza cuando se alcanza la fisuración de los riñones para $M_{cr^*,s}$ (superior a $M_{cr,c}$ debido a la existencia de un esfuerzo axil en esa sección de valor $F_{cr^*}/2$) y para un esfuerzo flector $M_{cr^*,c}$ en clave.

En tubos con cuantía de armadura superior a la mínima de flexión $A_{smin,f}$ [28 y 29], siendo ésta la suma de toda la armadura traccionada (barras+fibras), no se produce la ruina al alcanzar F_{cr^*} (Fig. 4a).

Contrariamente, en THM, en algunos THF y, en el caso extremo, en THA y/o THAF con cuantías inferiores a $A_{smin,f}$, la carga F_{cr}* es la de rotura (F_u) y, el modo de fallo es frágil. En este caso, no existen prácticamente fisuras adicionales aparte de las concentradas en las secciones críticas (ver Fig. 5).

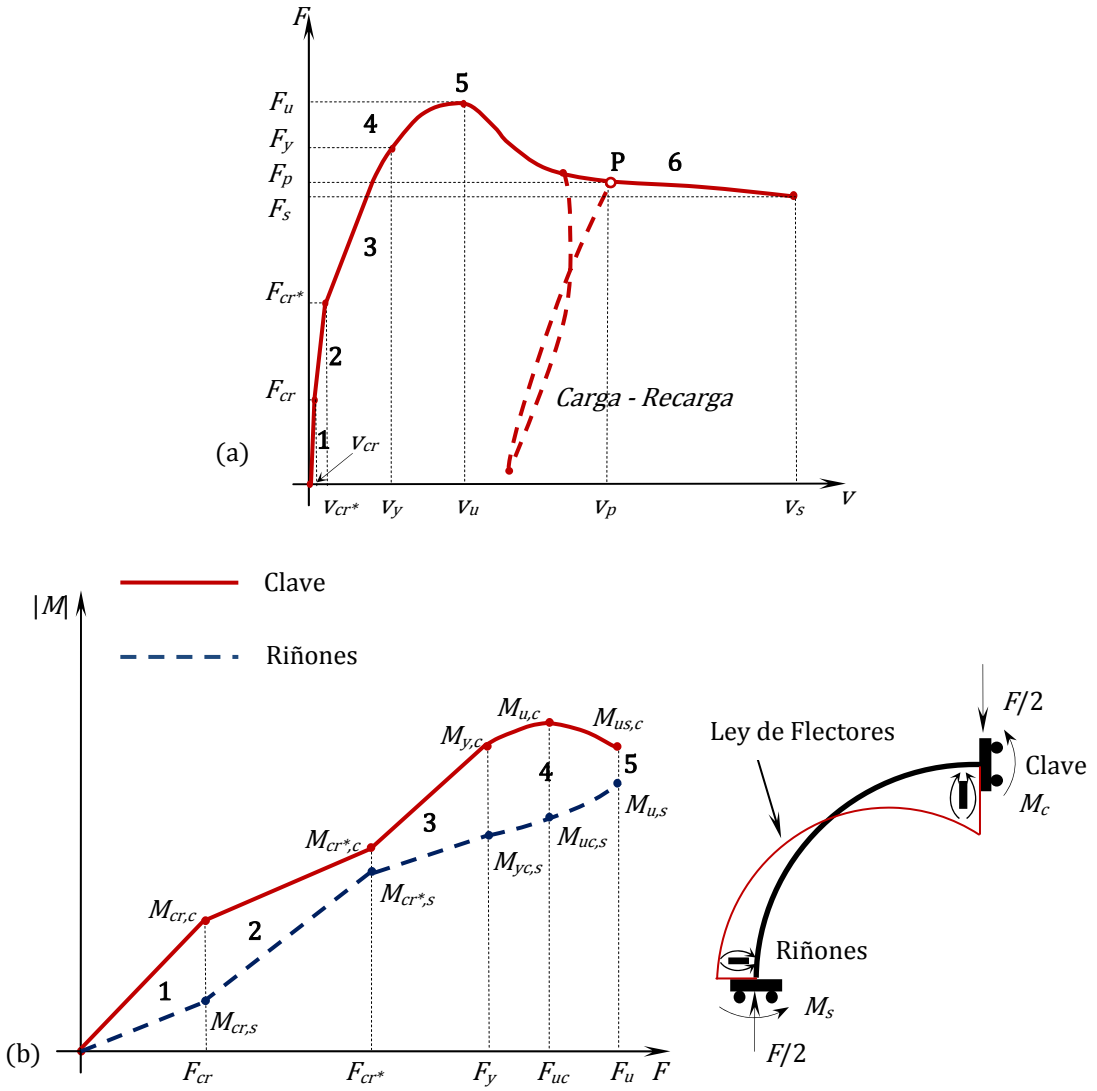

Fig. 4. Diagramas: a) F–v_A y b) M–F para una tubería con capacidad de redistribución plástica completa.

Fig. 5. Patrón de fisuración en rotura en THFA. Cortesía de PREFRAGA.

Fase fisurada (3)

En esta etapa se inicia un nuevo proceso de redistribución de momentos: la clave se rigidiza debido a la fisuración de los riñones, que han perdido parte de su rigidez inicial al final de la fase 2. En el transcurso de esta fase, el patrón de fisuración se estabiliza y el ancho de fisura (w) en las secciones extremas aumenta con F. La respuesta en el espacio F-v es lineal (ver Fig. 4a).

Los THA presentan la carga de prueba F_c [22] en el rango [F_{cr}-F_y], siendo F_y la carga para la cual la sección más crítica plastifica. En general, con las configuraciones de armadura habituales, esta sección es la de clave, siendo $M_{y,c}$ su momento de plastificación y $M_{yc,s}$ el momento en riñones cuando se alcanza $M_{y,c}$.

Fase Pre – Rotura (4)

La fase de pre-rotura consiste en un proceso de degradación progresiva de la tubería que, generalmente, activa un proceso de fisuración secundaria. Se produce una pérdida no lineal de la rigidez con el aumento de F (Fig. 4a) produciéndose una nueva redistribución de momentos hacia los riñones. No obstante, se precisa de dos requisitos para que se pueda dar esta redistribución y que la rotura se alcance primero en la sección en clave:

- Homogeneidad de la matriz de H en THM o de la matriz de HRF en THF. En tal caso, la existencia de un axil de valor axil $F/2$ en la sección de riñones tiene un efecto favorable y retrasa su rotura. Bajo esta hipótesis, se puede garantizar que los riñones no agotan cuando se alcanza F_y y que pueden absorber más energía de flexión. En la Fig. 6a se presenta un diagrama de interacción axil–flector cualitativo de una sección de un THM o un THF con las trayectorias de esfuerzos de las secciones críticas. Nótese, que se trata de una superficie simétrica respecto al eje horizontal. Esto se debe a la simetría tanto de la sección (rectangular) como a la distribución homogénea del refuerzo, en el caso de existir éste. Teniendo en cuenta este hecho y la existencia del axil ($F/2$) en los riñones, se comprueba que $|M_{u,s}| > M_{u,c}$ y, en consecuencia, la capacidad de redistribución de sistema.
- Refuerzo adecuado de la sección en riñones en THA y THAF. En referencia a esto, las cuantías de armadura empleadas para resistir las tracciones en la zona de riñones en THA oscilan entre un 60% [22] y un 75% [19] de las dispuestas en clave. En general, estos porcentajes son suficientes para que la plastificación se inicie en clave ($M_{y,c}$) y pueda desarrollarse la redistribución de esfuerzos clave–riñones de esta fase. La Fig. 6b recoge el diagrama de interacción axil–flector cualitativo de una sección de un THA o un THAF. En ésta se observa que, a diferencia del caso anterior, $|M_{u,s}|$ no es, en general, superior a $M_{u,c}$ debido a los porcentajes de armadura anteriormente mencionados.

Esta fase finaliza cuando se alcanza la carga F_u, siendo $M_{us,c}$ el momento en clave cuando se alcanza $M_{u,s}$.

Rotura (5)

La fase de rotura se concentra en el punto de coordenadas (F_u, v_u) del diagrama F–v (Fig. 4a). Se trata de un estado a partir del cual el sistema no acepta mayor carga. El modo puede ser frágil o dúctil; concretamente, los THM y tubos los THA, THF y THAF con cuantías inferiores a $A_{smin,f}$ presentan rotura frágil y se produce al final de la fase 2. Por el contrario, los tubos con cuantías superiores a $A_{smin,f}$ presentan un comportamiento más dúctil y con un patrón de fisuración con mayor número de fisuras.

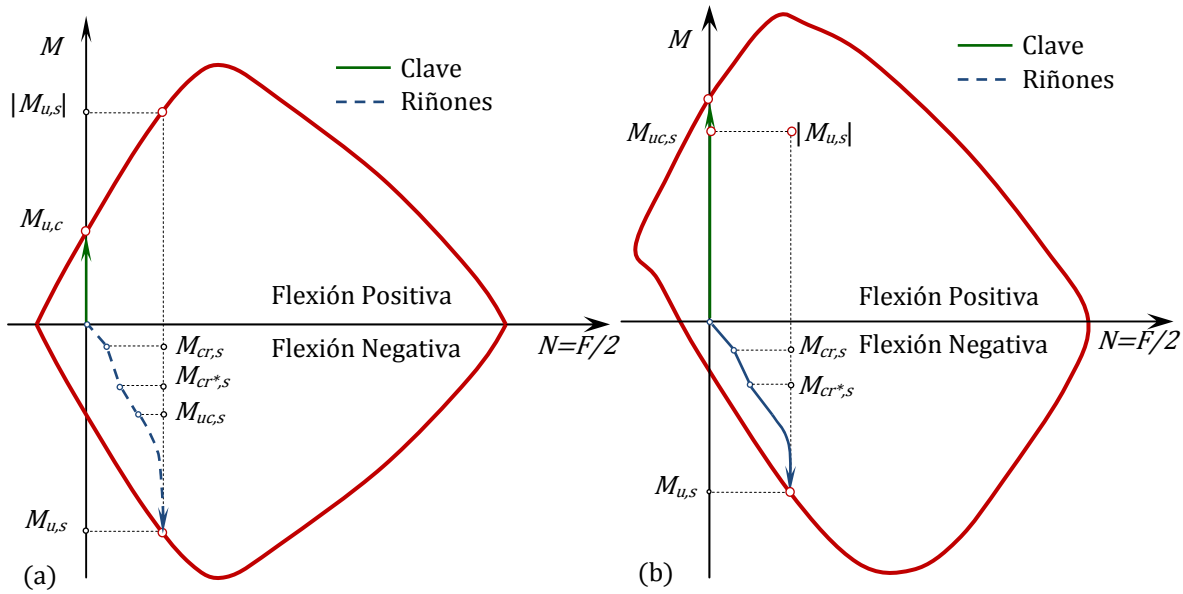

Fig. 6. Diagramas de interacción N_u-M_u y trayectorias para secciones (a) de hormigón en masa o con fibras y (b) con refuerzo asimétrico.

En tubos de clases resistentes elevadas y diámetros medios–altos (D_i>1.8 m), es habitual no someter los tubos hasta la carga F_u por varias razones: (1) falta de capacidad de carga de las prensas habituales; (2) deformaciones elevadas del sistema en pre–rotura y, por lo tanto, peligro de fallo del pistón y/o del sistema hidráulico; (3) en ocasiones sólo interesa conocer la carga F_o, en consecuencia, se detiene el ensayo cuando se alcanza dicho valor para luego reaprovechar el tubo. Habitualmente, F_c suele ser la más determinante y la que gobierna el diseño del tipo y configuración de armadura. Estas razones son las que justifican la poca disponibilidad de resultados de ensayos para este rango de diámetros y niveles de carga.

Post-Rotura (6)

En esta fase, el sistema se limita a deformarse con resistencia decreciente al aplastamiento. Las fisuras de mayor ancho se sitúan en las secciones críticas (clave, contraclave y riñones). Para éstos, el EA se detiene cuando se alcanza un desplazamiento se seguridad (v_s) con el fin de evitar fallos en el pistón (ver Fig. 4a).

Los THM sufren rotura frágil y no ofrecen prácticamente resistencia post-rotura. Del mismo modo, para la verificación de los THA sólo se requiere conocer F_c y, en algunos casos, F_u, por lo tanto, no es necesario someter al tubo hasta estos niveles de deformación. Si bien, si las cuantías de acero son las adecuadas, la rotura dúctil está garantizada.

En cambio, para THFA se precisa someter al tubo a un proceso de descarga–recarga (Fig. 3) hasta alcanzar altas deformaciones. En [6] se recogen los resultados de una campaña experimental dedicada, entre otras, a corroborar que la respuesta post–rotura es prácticamente independiente de si se ha realizado el ensayo de forma continua o de forma cíclica. En este sentido, esta respuesta depende, fundamentalmente, del tipo de fibras empleadas. Nótese, que el punto P de la Fig. 4a pertenece tanto a la curva respuesta del ensayo continuo como a la del ensayo cíclico. Este hecho facilita enormemente las operativa de ensayo, pudiéndose aplicar un ensayo continuo cuando se emplean fibras con resistencia y anclaje adecuados.

3.5. Modelo numérico para la simulación del EA

3.5.1. Introducción

Para la simulación del EA hasta altos niveles de deformación se requiere una subrutina que tenga en cuenta aspectos como: la respuesta fisurada y post–rotura de los materiales y la modelización de la respuesta del HRFA. Para ello, se ha empleado el modelo Análisis de Secciones Simétricas (AES) [30].

Por otra parte, se ha desarrollado la rutina ATH, que incluye el modelo AES. Este modelo permite evaluar la repuesta de TH con múltiples estrategias de refuerzo sometidas al EA. En lo que sigue, se exponen las bases principales del modelo AES incidiendo en las modificaciones introducidas para este trabajo y el modelo ATH.

3.5.2. Modelo de análisis seccional

Modelización de los materiales

El modelo AES considera la deformación total del hormigón $\varepsilon(t,t_0)$, evaluada en un instante t, como la suma algebraica de las deformaciones de origen mecánico y las deformaciones no mecánicas [ver 30 y 31]. En este trabajo, las segundas no se tienen en cuenta por 2 razones: (1) el esquema de cargas aplicado EA es de naturaleza instantánea y (2) que, en la mayoría de los casos, los efectos de la retracción sobre el estado tenso-deformacional de los materiales es pequeña y puede despreciarse [19].

Para simular el comportamiento a compresión del hormigón se emplea el diagrama TTJ [32] porque abarca un rango amplio de resistencias del hormigón y simula adecuadamente la rama post–pico. Por otra parte, el comportamiento a tracción y la rigidización entre fisuras se describe mediante un diagrama de Collins y Mitchell [33].

El comportamiento a compresión del HRFA se simula con la expresión propuesta en [34], mientras que su respuesta a tracción se modela mediante un modelo tipo tensión–deformación [35], implementado por ser referente internacional [36].

Por otra parte, el ancho de fisura (w) se evalúa de distintas formas según el tipo de tubos: (1) para THA se emplea la formulación recogida en el Eurocódigo 2 [37]; (2) para THAF se emplea una extensión de la formulación anterior [35] y (3) para THM y THF se ha deducido una expresión a falta de algún modelo alternativo en la bibliografía para su evaluación.

En concreto, para THM y THF se supone que la tubería se comporta como un sólido rígido bajo el EA. Esta hipótesis es razonable en este tipo de tubos, ya que se trata de tubos de diámetro pequeño-mediano (D_i<1.0 m) en los que la repuesta es rígida.

Supóngase que el sólido rígido de la Fig. 7 representa un cuarto de tubería y que el ancho de fisura (w=2 w^*) se puede evaluar descomponiendo el movimiento total en A en un giro con centro en el punto B de valor θ_B, que provoca un descenso de valor v_A y un cierre de la fisura h_A, y en un desplazamiento horizontal de los riñones de valor u_B que tiende a abrir la fisura.

Atendiendo a esta descomposición, el valor de w se deduce de la Ec. 1a, donde h_A puede suponerse aproximadamente igual a v_A (Ec. 1b) al tratarse de pequeños desplazamientos. Por lo tanto, w se puede relacionar con v_A y u_B (valores que derivan del cálculo estructural) mediante la Ec. 1c.

$$w = 2u_A - v_A \tag{1a}$$

$$h_A \approx v_A \tag{1b}$$

$$w \approx 2u_B - v_A \tag{1c}$$

El acero pasivo para armadura se modeliza con un diagrama trilineal con la posibilidad de endurecimiento.

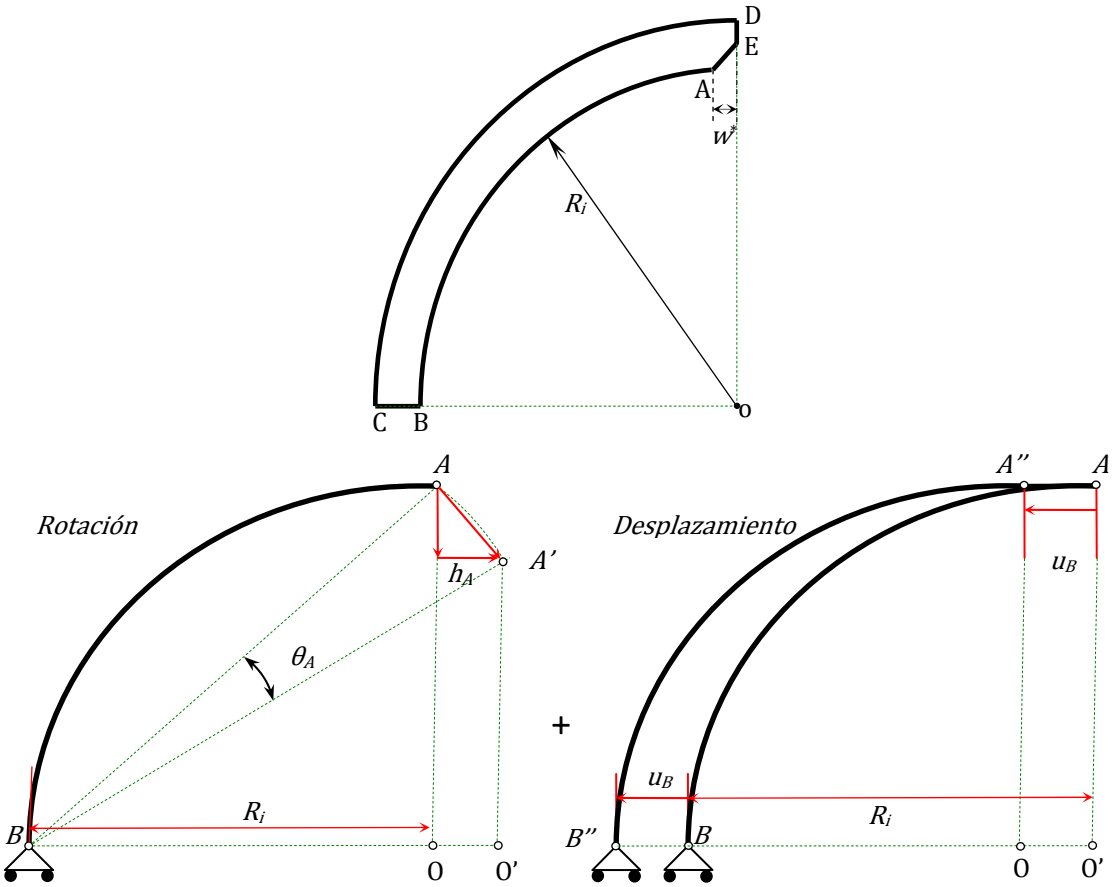

Fig. 7. Esquema de sólido rígido adoptado para el cálculo de w en THM y THFA.

Hipótesis básicas

Se han tomado las siguientes hipótesis: (1) Las secciones tienen un eje de simetría y están sometidas a estados de flexocompresión recta; (2) adherencia perfecta entre los materiales que componen la sección; (3) las secciones inicialmente planas permanecen planas tras la aplicación de las cargas o deformaciones impuestas; (4) las deformaciones de cortante son depreciables y no se consideran; y (5) se desprecian los efectos de la curvatura de la pieza (sección circular) sobre la distribución de tensiones y deformaciones de los materiales que constituyen la sección.

Idealización de la sección

La sección de hormigón se descompone en elementos área dA_c y las barras de acero se simulan con puntos que concentran el área equivalente de la barra $A_{s,i}$ en cota $y_{s,i}$. En la Fig. 8 se presenta un esquema de discretización de una sección transversal de tubería cualquiera.

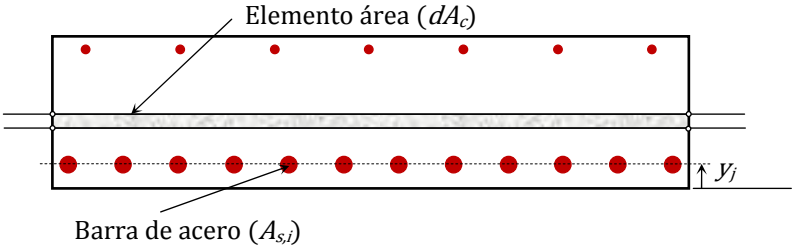

Fig. 8. Ejemplo de discretización de una sección de tubería.

Equilibrio y compatibilidad

El plano de deformaciones (definido por la deformación del centro de gravedad del elemento área de referencia ε_o y la curvatura χ) y el estado tensodeformacional de los materiales constituyentes de la sección bajo una combinación de cargas externas (N y M), se obtienen aplicando las ecuaciones de equilibrio interno (Ecs. 2a y 2b) y fijando la hipótesis de adherencia perfecta entre las fibras de hormigón y el acero adyacente a éste (Ec. 2c).

$$N = \int_{A_c} \sigma_c \, dA_c + \sum_{i=1}^{n_b} \sigma_{s,i} \, A_{s,i} \tag{2a}$$

$$M = \int_{A_c} \sigma_c \, (y_c - y_o) dA_c + \sum_{i=1}^{n_b} \sigma_{s,i} \left(y_{s,i} - y_o\right) A_{s,i} \tag{2b}$$

$$\varepsilon(y) = \varepsilon_o + \chi(y - y_o) \tag{2c}$$

donde:

- N: Axil.
- σ_c: Tensión del hormigón
- ε_c: Deformación del hormigón.
- dA_c: Diferencial de área de hormigón.
- n_b: Número de barras en la sección.
- $\sigma_{s,i}$: Tensión de la barra i-ésima de acero.
- $\varepsilon_{s,i}$: Deformación de la i-ésima barra de acero.
- M: Momento.
- y_c: Cota del centro de gravedad elemento de área de hormigón.
- y_o: Cota del centro de gravedad del elemento de área de referencia.
- $y_{s,i}$: Cota del centro de gravedad de la barra i-ésima de acero.
- $A_{s,i}$: Área de la barra i-ésima de acero.
- y: Cota del centro de gravedad del elemento analizado.

El conjunto de Ecs. 2 forma un sistema de ecuaciones no lineal que se resuelve empleando un esquema iterativo tipo Newton-Raphson [38] donde ε_o y χ son las incógnitas.

3.5.3. Modelo de análisis estructural

Hipótesis básicas

Para la simulación a nivel estructural del EA se han considerado válidas las siguientes hipótesis: (1) La estructura se puede idealizar como una pieza de plano medio de directriz curva y radio medio (R_m) constante (ver Fig. 9); (2) simetría respecto el eje vertical y, por lo tanto, la vinculación de los puntos A y D se resuelve mediante dos empotramientos deslizantes; (3) el apoyo del tubo consiste en una deslizadera que reacciona con una carga $F/2$ que forma un ángulo β respecto a la vertical; (4) la curvatura inicial de la pieza no influye ni en la distribución de esfuerzos a lo largo la directriz de la pieza ni en su configuración deformada [19], por lo tanto, se puede emplear la teoría clásica de vigas rectas; (7) se desprecian los efectos del axil y del cortante en el cálculo de los movimientos de la tubería y (8) se considera que el ensayo continuo es representativo para simular el comportamiento de THFA hasta la post–rotura [6].

Estrategia de análisis

El problema se ha planteado de modo que se pueda obtener el máximo rendimiento de la subrutina de cálculo seccional. Para ello se ha hecho uso de la ecuación de la energía (Ec. 3), escrita en términos del campo de curvaturas $\chi(\theta)$.

$$W_f = \frac{1}{2} \int_0^{\pi} \chi(\theta) M(\theta) R_m d\theta \tag{3}$$

Las leyes de esfuerzos (Ec. 4) se obtienen aplicando el equilibrio de la cara frontal de la dovela Q (Fig. 9).

$$N(\theta) = \begin{cases} 0 & si\ 0 \le \theta \le \beta \\ \frac{F}{2}\sin\theta & si\ \beta < \theta \le \pi \end{cases} \quad (4a)$$

$$M_f(\theta) = \begin{cases} M_A - \frac{F}{2}R_m \sin\beta & si\ 0 \le \theta \le \beta \\ M_A - \frac{F}{2}R_m \sin\theta & si\ \beta < \theta \le \pi \end{cases} \quad (4b)$$

El giro en el punto A (Ec. 5) se obtiene derivando la energía a flexión (Ec. 3) respecto M_A. Este giro, considerando la condición de simetría, debe ser nulo en dicho punto.

$$\varphi_A = \frac{\partial W_f}{\partial M_A} = \int_0^\pi \chi(\theta) d\theta = 0 \quad (5)$$

(5)

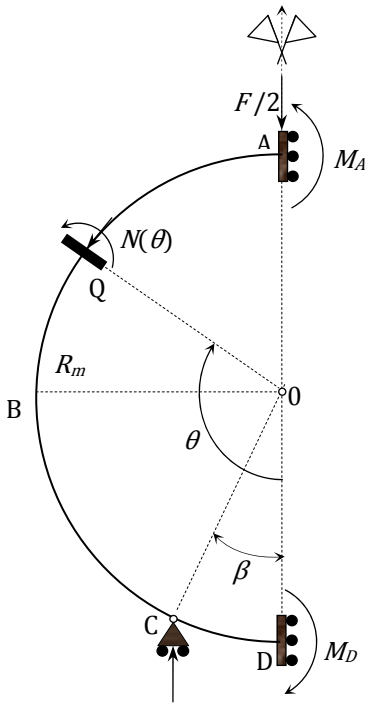

Fig. 9. Esquema estático considerado por el modelo ATH.

Por otra parte, el desplazamiento en A (Ec. 6a) se puede obtener derivando la energía de flexión (Ec. 3) respecto a la carga F.

$$v_A = \frac{\partial W_f}{\partial F} = \int_0^\pi \chi(\theta) \frac{\partial M(\theta)}{\partial F} d\theta \quad (6a)$$

La derivada parcial de M respecto F recogida bajo el símbolo integral de la Ec. 6a, se calcula mediante la Ec. 6b.

$$\frac{\partial M(\theta)}{\partial F} = \begin{cases} -\frac{1}{2}R_m \sin\beta & si\ 0 \le \theta \le \beta \\ -\frac{1}{2}R_m \sin\theta & si\ \beta \le \theta < \pi \end{cases} \quad (6b)$$

La resolución del sistema de Ecs. 4 permite deducir la incógnita del problema F. Por otra parte, éste es no lineal desde el instante en que se produce la fisuración de alguna sección.

Algoritmo para la resolución del sistema no lineal de ecuaciones

El modelo descrito anteriormente puede resolverse numéricamente siguiendo el siguiente esquema incremental a nivel estructura e iterativo a nivel sección:

1. Se discretiza la mitad de la tubería (ver Fig. 9).
2. Se fija la tolerancia para el giro φ_A (tol_φ) y para la fuerza F (tol_F).
3. Se fija un incremento de curvatura en el punto A ($\Delta\chi_A$).
4. Se calcula, mediante el modelo AES, el valor de M_A^{k+1} asociado a la curvatura $\chi_A^{k+1} = \chi_A^k + \Delta\chi_A$.
5. Se supone un valor de la fuerza aplicada F^k. Como primera aproximación se toma el valor obtenido en el paso anterior k tras el proceso iterativo.
6. Se obtienen los esfuerzos $N(\theta)^{k+1}$ y $M(\theta)^{k+1}$ mediante la Ec. 4.
7. Se calcula el campo de curvaturas $\chi_A(\theta)^{k+1}$ derivado de las leyes de esfuerzos $N(\theta)^{k+1}$ y $M(\theta)^{k+1}$.
8. Se verifica la condición de simetría corroborando que $|\varphi_A| \leq tol_\varphi$ (Ec. 5) y que $|F^{k+1} - F^k| \leq tol_F$. Para ello se integra el campo de curvaturas $\chi_A(\theta)^{k+1}$. En el caso de que no se cumpla dicha condición se retrocede al paso 5 con un valor de F corregido (F^{k+1}) mediante el método de Newton-Raphson [38].
9. Si se alcanza la convergencia en el paso k+1, se calcula v_A^{k+1} mediante las Ecs. 6.

3.6. Ejemplo de aplicación

3.6.1. Introducción

De caras a verificar la bondad de los resultados propuestos por el modelo numérico y a poner de manifiesto su potencialidad en la optimización del armado, se presenta un ejemplo real consistente en dos THA de diámetro nominal (D_n) 2.80 m C–135 (F_c=90 kN/m² y F_n=135 kN/m²) y C–180 (F_c=120 kN/m² y F_n=180 kN/m²) proyectados para el colector, de 2270 m de longitud, perteneciente a la Zona Residencial de Zaragoza Arco Sur. Del total de la longitud de éste, 1070 m se resolvieron con la clase C-135 y los 1200 m restantes con la C-180.

Ambos tubos se diseñaron mediante el modelo ATH, proponiéndose un armado optimizado para alcanzar las clases resistentes especificadas en proyecto, que posteriormente se corroboraron en el EA.

La inclusión de este ejemplo tiene interés por varios motivos:

- Se trata de un diámetro y clases resistentes que requieren de un diseño especial [26]. En estos casos, la práctica más habitual consiste en extrapolar las cuantías mínimas exigidas para los tubos sí contemplados en normativa. Esto conduce, por una parte, a un sobredimensionamiento del elemento, y, por otra, a que la fabricación sea excesivamente dificultosa a causa de la alta densidad de armadura.
- Se pone de manifiesto la influencia del procedimiento constructivo y, en especial, la necesidad de asegurar unas tolerancias en los recubrimientos. En este sentido, la carga de fisuración en el EA sufre una importante merma si éstos son excesivos a causa del movimiento de las jaulas durante el proceso de hormigonado.
- Son diámetros raramente empleados debido a varias razones: (1) requieren de maquinaria pesada para su transporte y colocación (ver Figs. 10a y 10b, respectivamente); (2) se precisa un exhaustivo control de la colocación con el fin de garantizar el sellado de las juntas; y (3) se requiere de grandes prensas para, al menos, alcanzar la carga de fisuración controlada F_c en el EA.

3.6.2. Optimización del armado mediante el modelo ATH

Se acudió al modelo ATH con el fin de optimizar el consumo de armaduras necesarias para alcanzar las clases resistentes C-135 y C-180 y simular su respuesta resistente en el EA. Como valores de tanteo iniciales, se extrapolaron las cuantías mínimas de tubos sí contemplados en la UNE 127916 [26], obteniéndose: 24.9 cm²/m y 14.9 cm²/m en la cara interna y externa, respectivamente, para la C-135 y 34.5 cm²/m y 20.7 cm²/m para la C-180. Asimismo, para ambas clases, se estableció un espesor de pared de 280 mm y se fijó el recubrimiento nominal en 40 mm. En este sentido, el recubrimiento nominal

mínimo establecido en la UNE 127916 [26] es de 30 mm para este caso. Sin embargo, teniendo en cuenta la densidad de armadura que se emplea y los posibles movimientos de ésta durante el hormigonado, se tomó un valor superior de caras a la seguridad.

Fig. 10. (a) Transporte y (b) colocación de los tubos. Cortesía de PREFRAGA.

Para la modelización, se emplearon valores característicos de las resistencias. Concretamente, para la resistencia a compresión se tomaron los valores mínimos de ($f_{ck,28}$) establecidos en la UNE 127916 [26] (35 N/mm² para la C-135 y 40 N/mm² para la C-180). Asimismo, la resistencia a tracción $f_{ctk,28}$ y el módulo $E_{c,28}$ se obtuvieron mediante las formulaciones recogidas en la EHE-08 [10]. Por otra parte, para el acero de armaduras pasivas se fijó en 500 N/mm² el límite elástico (f_{yk}) y en 200 kN/mm² su módulo elástico de deformación (E_{yk}).

Después de diversos tanteos, se obtuvieron unas cuantías mínimas de armadura para la C-135 y C-180 de: 20.3 cm²/m en la cara interna y 10.7 cm²/m en la externa para el primero, y, para el segundo, 22.5 cm²/m y 18.0 cm²/m en la cara interna y externa, respectivamente. Ello supone un ahorro total de la armadura del 29.9% para la C-135 y del 26.7% para la C-180 respecto a los valores extrapolados de la normativa.

En la Fig. 11 se presenta el diagrama F-v_A obtenido mediante el modelo ATH para cada clase resistente y con las cuantías mínimas propuestas por el mismo. Se marcan los valores de las cargas más representativas. La carga F se ha dividido por el diámetro interior (D_i) para trabajar acorde con la UNE-EN 1916 [22] y la UNE 127916 [26].

A raíz de los resultados reflejados en la Fig. 11, se pone de manifiesto que las cuantías propuestas son suficientes para alcanzar las clases C-135 y C-180. En concreto, las cargas F_c (asociadas a un w de 0.3mm) obtenidas son: 99 kN/m² y 127 kN/m² para la C-135 y la C-180, respectivamente (10.0% y 5.8% superiores a los valores correspondientes a cada clase). Del mismo modo, las cargas F_u son 143 kN/m² y 181 kN/m² (un 5.9% y un 0.6% superiores a las F_n estipuladas para cada clase). No obstante, los valores en rotura pueden ser ligeramente superiores porque la simulación se interrumpe cuando se alcanza el momento máximo en clave, quedando aún parte de la capacidad resistente de los riñones y de deformación global aún por agotar (ver Fig. 12).

Por otra parte, teniendo en cuenta los posibles movimientos de las jaulas durante las operaciones de montaje y hormigonado, se ha hecho un estudio de sensibilidad del recubrimiento nominal de las armaduras para el tubo de la clase C-135 (siendo equivalentes las conclusiones obtenidas para el tubo C-180). Con éste, se pretende enfatizar en la necesidad de disponer los elementos necesarios que garanticen un recubrimiento máximo comprendido entre los 40 y 45 mm para poder alcanzar la clase resistente deseada con la cuantía óptima de armadura propuesta.

Los resultados de este análisis se presentan mediante las curvas F-w, asociadas a cada recubrimiento, recogidas en la Fig. 13.

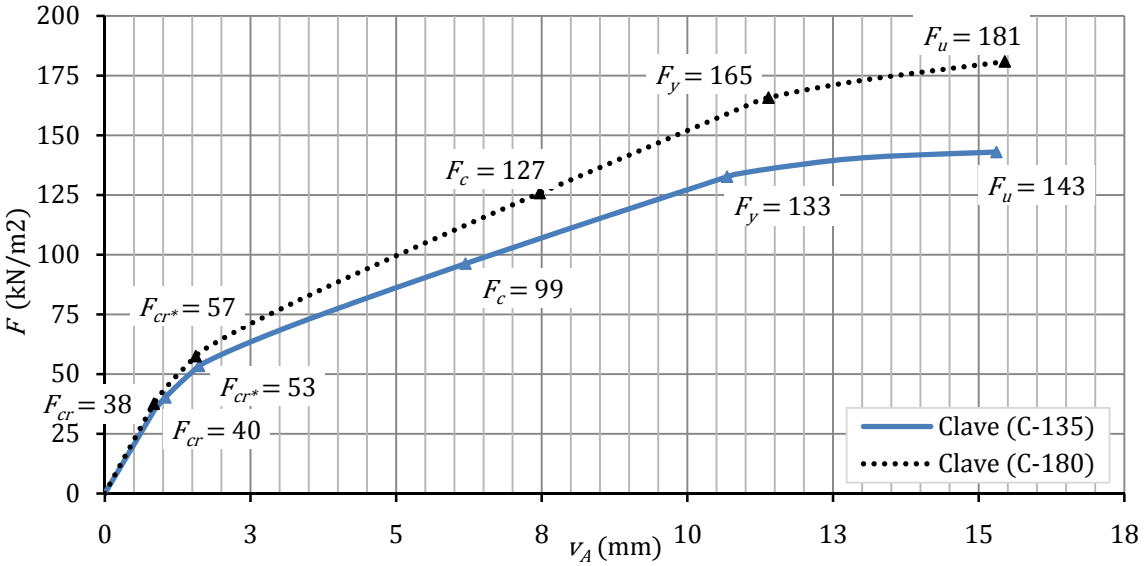

Fig. 11. Curva F–v_A para el tubo D_n 2.800mm C-135 y C-180.

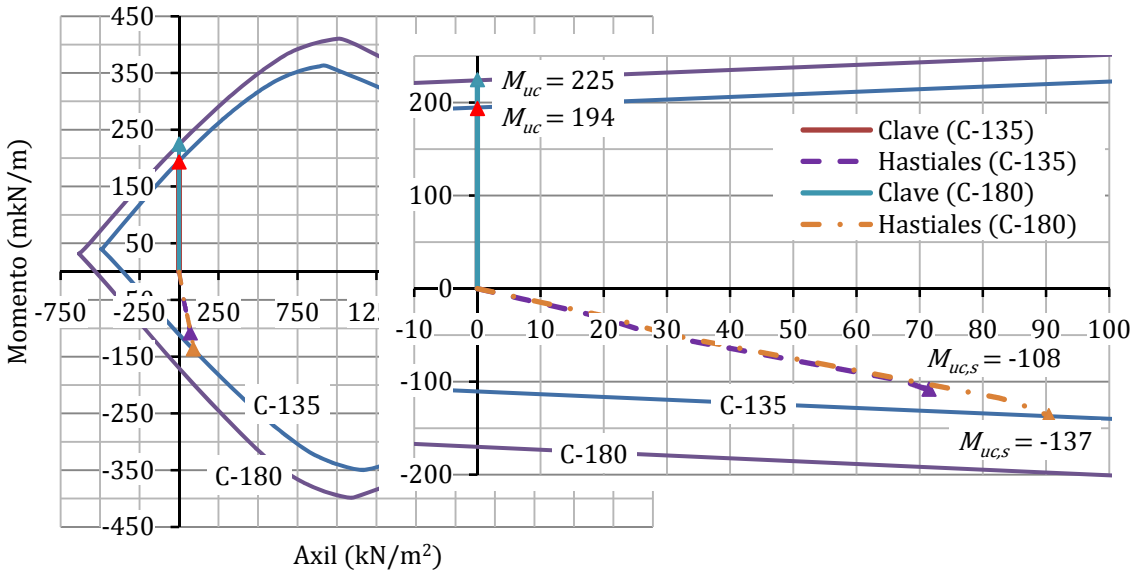

Fig. 12. Diagramas axil – momento últimos y trayectorias obtenidas para las secciones en clave y riñones en la simulación del EA para el tubo 2.80 m C-135 y C-180.

A la luz de los valores señalados en la Fig. 13, se constata la importancia de seguir una estrategia de control exhaustiva de los recubrimientos durante el montaje. En efecto, si el recubrimiento aumenta en 5 mm (11.1%) respecto al valor fijado en el análisis (40 mm), las cargas F_c y F_u se reducen un 7.6% (92 kN/m²) y un 2.1% (140 kN/m²), respectivamente, en relación con los valores obtenidos para 40 mm; si bien, aún se sigue alcanzando la C-135. Asimismo, si el recubrimiento alcanza los 50 mm (un 22.2% más del valor fijado), ya no se logran los requisitos resistentes deseados. En este caso, F_c desciende un 19.3% (83 kN/m²) y F_u un 3.5% (138 kN/m²). Nótese, que en ambos casos, la carga más sensible frente a la variación del recubrimiento es F_c, lo que se debe, principalmente, al peso que tiene este parámetro en la formulación empleada en el Eurocódigo-2 [37] para el cálculo de la separación entre fisuras.

Del mismo modo, se ha probado mediante el modelo ATH que las variaciones de f_{ck} influyen poco tanto en el valor de F_c como en el de F_u. Esto es debido a que el ancho de fisura está gobernado principalmente por parámetros relacionados con la configuración y cuantía de armadura y, la rotura, en este caso, por el valor de la deformación máxima permitida al acero (10.0‰).

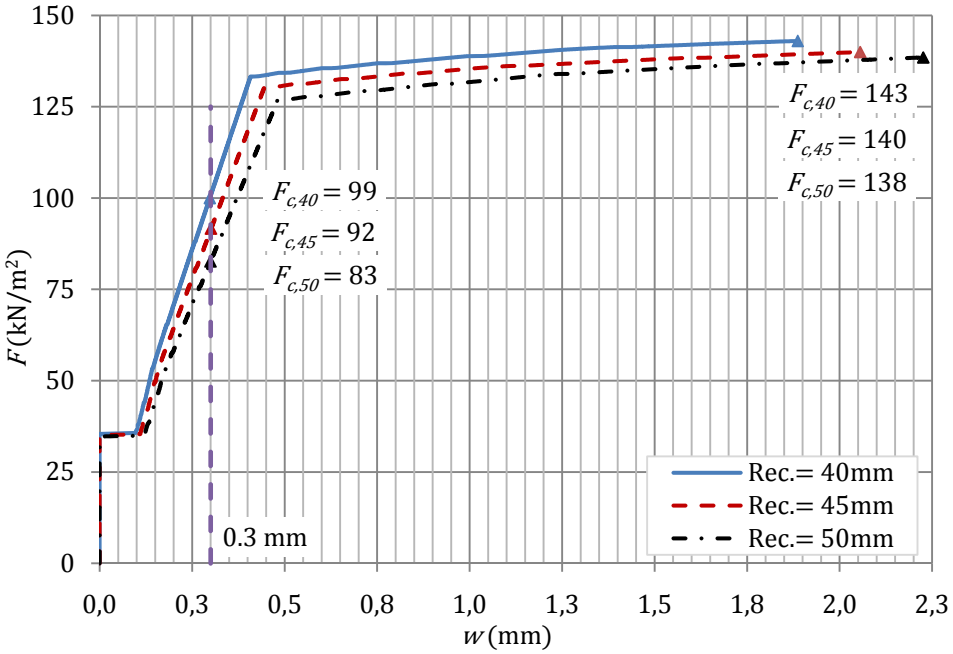

Fig. 13. Curva $F-w$ para el tubo D_n 2.80 m C-135 según el recubrimiento nominal.

3.6.3. Campaña experimental

Los tubos se fabricaron mediante el sistema de la vibrocompresión, obteniéndose acabados y rendimientos excelentes. Este hecho se debe, en gran parte, al estudio previo de la dosificación óptima del hormigón (340 kg/m³ de CEM I 52.5 SR, 855 kg/m³ de arena lavada 0/4, 815 kg/m³ de gravilla y 365 kg/m³ de grava, junto con una relación agua/cemento inferior a 0.43).

Las resistencias características a compresión a los 28 días de edad obtenidas de una muestra total de 37 probetas para la C-135 y 31 para la C-180 fueron de 43.8 N/mm² para la primera y 43.9 N/mm² para la segunda. Por lo tanto, se alcanzaron las resistencias características mínimas establecidas en la UNE 127916.

El refuerzo de los tubos se resolvió con acero B-500S corrugado soldado en forma de espiras circulares. El recubrimiento, tal como se ha comentado, se consideró uno de los parámetros geométricos críticos y se controló exhaustivamente mediante el uso de una densa malla de separadores (ver Fig. 14).

Se fabricaron un total de 435 tubos C-135 y 490 de la C-180 de 2.461 m de longitud con las configuraciones óptimas de armado sugeridas por el modelo ATH. De todos estos, se ensayaron 3 de la C-135 y 4 de la C-180 en el EA (Fig. 1).

Asimismo, debido a la capacidad limitada de carga de las prensas y al elevado coste de estos tubos (se reutilizan después del ensayo), éstos no se sometieron hasta rotura, sino que el ensayo se detuvo cuando se formaba la fisura de ancho 0.3 mm. En dicho instante, se capturó el valor de la carga para posteriormente compararlo con F_c.

En la Tabla 1 se recogen los resultados obtenidos para la carga F_c y se comparan con los valores obtenidos con el modelo ATH.

Fig.14. Estrategia empleada para garantizar los recubrimientos. Cortesía de PREFRAGA.

Tabla 1. Edad (días) y cargas de fisuración controlada (kN/m²) para las probetas ensayadas.

			Campaña		ATH
Clase	Probeta	Edad	F_c	$F_{c,m}$	$F_{c,40}$
C-135	1	10	90.2	90.7	99.0
	2	35	90.7		
	3	21	91.3		
C-180	4	96	120.8	122.2	127.0
	5	24	123.6		
	6	28	122.0		
	7	44	122.5		

Atendiendo los resultados presentados en la Tabla 1 se pone de manifiesto, por una parte, que las cuantías de armadura sugeridas conducen a que se alcancen los valores estipulados de F_c para cada clase resistente. Por otra parte, se desprende que el modelo numérico ATH sobrevalora el valor de ésta respecto a las medias de los resultados experimentales (9.2% para la C-135 y 3.9% para la C-180). Ello puede ser debido a: (1) que los recubrimientos reales son superiores a los 40mm fijados en el análisis; (2) a que no se ha considerado el peso propio en el análisis y (3) a que las condiciones de apoyo consideradas (dos apoyos simples formando 30° respecto el centro del tubo) no coinciden con las condiciones reales. Asimismo, se descarta que esta diferencia se deba a que la edad de ensayo sea distinta a los 28 días considerados en el análisis; pues, según los resultados recogidos en la Tabla 1 este parámetro tiene poca influencia en F_c, incluso para edades de sólo 10 días.

En consecuencia, teniendo en cuenta la multitud de parámetros involucrados en el análisis, se puede afirmar que el modelo se ajusta bien a los resultados experimentales obtenidos y podría ser apto, a falta de una población mayor de ensayos, para abordar la optimización de la configuración y cuantía de armadura para THA como el presentado en este ejemplo.

Se ha contrastado el modelo para otros diámetros y espesores e incluso para THFA y THAFA, llegándose a correlaciones ensayo-modelo satisfactorias [39]. Si bien, aún siguen en marcha varias campañas experimentales que pondrán a disposición más resultados con los que validar el modelo.

3.7. Conclusiones

Este artículo se ha dividido en 3 partes principales, en los cuales se ha tratado y concluido lo siguiente:

- En la primera se ha hecho: (1) un resumen de los principales métodos de diseño de TH, mencionando algunos modelos numéricos ya existentes; (2) una exposición de la situación normativa y (3) se han planteado las carencias detectadas en cuanto a la simulación de THF y THAF así como la necesidad de disponer de una herramienta para el diseño óptimo del refuerzo de estos elementos.
- En la segunda parte se ha hecho un análisis teórico del comportamiento integral de TH sometidos al EA. Se ha visto las principales diferencias en cuanto a la respuesta resistente en función del tipo y configuración de armadura. Este análisis ha servido tanto para enfocar el estudio como para poner de manifiesto cuáles son los principales fenómenos que debe considerar un modelo de análisis no lineal de tubos.
- Por último, se han presentado las bases teóricas y la formulación empleada en el modelo ATH. Asimismo, con el fin de verificar la idoneidad del modelo, se ha propuesto el armado de un tubo de 2.80 m de diámetro y clases resistentes C-135 y C-180 que, posteriormente, se han contrastado en el EA. En la campaña experimental se alcanzaron las clases resistentes deseadas con reducciones del 29.9% (C-135) y del 26.7% (C-180) del armado total y con concordancias modelo-ensayo satisfactorias (error medio del 9.2% para la C-135 y del 3.9% para la C-180). Si bien, estas diferencias se deben, principalmente, a movimientos de las jaulas durante las operaciones de hormigonado, que se han limitado mediante el uso de separadores.

Por otra parte, ATH también simula la respuesta de THF y THAF, si bien, las campañas experimentales siguen en marcha y su difusión está prevista en trabajos futuros. En consecuencia, no se emiten conclusiones en referencia a estos tipos de tubos.

3.8. Agradecimientos

Los autores quieren agradecer a las empresas PRECON, S.A. y PREFRAGA, S.A. por su apoyo económico, material y técnico brindado. Especialmente, a Jaime Armengou (PRECON, S.A.) y a José María Romía (PREFRAGA, S.A.). Asimismo, los autores de este documento también quieren poner de manifiesto su agradecimiento por el apoyo económico recibido vía el Proyecto de Investigación BIA2010-17478: *Procesos constructivos mediante hormigones reforzados con fibras*.

3.9. Bibliografía

1. VIÑOLAS V., AGUADO A., JOSA A. "Evaluación de la sostenibilidad en tuberías de saneamiento". *II Congreso UPC Sostenible 2015*. Barcelona, Spain, 2009.
2. HAKTANIR T., ARI K., ALTUN F., ALTIS C.G., KARAHAN O. "Effects of steel fibers and mineral filler on the water-tightness of concrete pipes". *Cement and Concrete Composites*. 2006, vol. 28, nº 9, p. 811-816.
3. HAKTANIR T., ARI K., ALTUN F., KARAHAN O. "A comparative experimental investigation of concrete, reinforced-concrete and steel-concrete pipes under three-edge-bearing test". *Construction and Building Materials*. 2007, vol. 21, nº 8, p. 1702-1708.
4. DE LA FUENTE A., ARMENGOU "J. Aplicaciones estructurales del HRFA: Tubos de saneamiento, paneles de cerramiento y placas de suelo reforzado". *Aplicaciones estructurales del HRFA*, *Jornada*

Técnica 2007-JT-02, 9 de Octubre de 2007. Barcelona: UPC, ETS Ingenieros de Caminos, Canales y Puertos, Departamento de Ingeniería de la Construcción, 2007.

5. LAMBRETCHS A. "Performance clases for steel fibre reinforced concrete: Be critical". *7th International RILEM Symposium on Fibre Reinforced Concrete*, Chennai, India, 2008.
6. FIGUEIREDO A. "Evaluation of the test method for crushing strength of steel fiber reinforced concrete pipes". *7th International RILEM Symposium on Fibre Reinforced Concrete*, Chennai, India, 2008.
7. THOMAS J., RAMASWAMY A. "Mechanical properties of steel fiber-reinforced concrete". *ASCE Journal of materials in civil engineering*. 2007, Vol. 19, nº 5, p. 385-392.
8. CHIAIA B., FANTILLI A.P., VALLINI P. "Evaluation of crack width in FRC structures and application to tunnel linings". *RILEM Materials and Structures*. 2009, Vol. 42, nº 3, p. 339-351.
9. PARROT J. *Estudio de la sostenibilidad en tuberías de saneamiento. Tesina de Especialidad* (Dir. Antonio Aguado). Barcelona: UPC, 2009.
10. EHE-8. *Instrucción de Hormigón Estructural*. Madrid: Ministerio de Fomento, 2008. 702 p.
11. ACPA. *Concrete pipe handbook*. 8th pr. Vienna, 2005. 238 p.
12. ACPA. *Concrete pipe technology handbook: a presentation of historical and current state-of-the-art design and installation methodology*. 3th pr. Vienna, 2005. 143 p.
13. ASCE *Standard No. 27-00. Standard practice for direct design of precast concrete pipe for jacking in trenchless construction*. Reston, VA: American Society of Civil Engineers, 2000. 51 p.
14. HEGER F.J., LIEPINS A.A., SELIG E.T. "SPIDA: An analysis and design systems for buried concrete pipe". *Advanced in underground pipeline engineering*. Proc., Int. Conf., ASCE 1985. New York, N.Y. p. 143-154.
15. KURDIZIEL J.M., TIMOTHY J.M. "SPIDA method for reinforced concrete pipe design". *Journal of transportation engineering*. 1991, vol. 117, nº 4, p. 371-381.
16. WATKINS R.K., ANDERSON L.R. *Structural mechanics of buried pipes*. 1rst ed. Boca Raton, FL: Taylor & Francis, 1999. 444 p.
17. OLANDER H.C. *Stress analysis of concrete pipe*. Engineering monograph, nº 6. U.S. Department of Interior, Bureau Reclamation, 1950.
18. HEGER F.J., McGRATH T.J. *Design methods for reinforced concrete pipe and box sections*. Simpson Gumpertz & Heger Inc. Report submitted to ACPA, December 1982.
19. HEGER F.J. *A theory for the structural behaviour of reinforced concrete pipes*. PhD Thesis. Massachusetts, USA: Department of Civil and Sanitary Engineering, Massachusetts Institute of Technology, MIT, 1962.
20. McGRATH T.J. "Design of reinforced concrete pipe – a review of traditional and current methods". *The 2nd conference on structural performance of pipes*. Columbus, Ohio, USA, March 14-17, 1993.
21. SARGAND S.M., HAZEN G.A., VAITHIANATHAN E., HURD J.O. "Verification of performance of a concrete pipe". *Transportation research board 73rd Annual Meeting*. Washington, DC, USA, Jan 9-13, 1994.
22. UNE-EN 1916 : 2002. *Concrete pipes and fittings, unreinforced, steel fibre and reinforced*. 2002.
23. ASTM C14-07. *Standard Specification for non-reinforced concrete sewer, storm drain, and culvert pipe*. ASCI 2007.
24. ASTM C76-08a. *Standard specification for reinforced concrete culvert, storm drain, and sewer pipe*. ASCI 2008.
25. HEGER F.J. "Structural design method for precast reinforced concrete pipe". *Transportation research record*. 1982, nº 878, p. 93-100.

26. UNE 127916 : 2004. *Tubos y piezas complementarias de hormigón en masa, de hormigón con fibra de acero y de hormigón armado*. Complemento nacional a la norma UNE-EN 1916 : 2003.

27. ASTM C497-05. *Stardard test methods for concrete pipe, manhole sections or tile*. ASCI 2005.

28. VANDEWALLE L. "Cracking behaviour of concrete beams reinforced with a combination of ordinary reinforcement and steel fibers". *RILEM Material and Structures*. 2000, Vol. 33, p. 560-567.

29. CHIAIA B., FANTILLI A.P., VALLINI P. "Evaluation of minimum reinforcement ratio in FRC members and application to tunnel linings". *RILEM Materials and Structures*. 2006, Vol. 40, nº 6, p. 593-604.

30. DE LA FUENTE A., AGUADO A., MOLINS C. "Modelo numérico para el análisis no lineal de secciones prefabricadas construidas evolutivamente". *Hormigón y Acero*. 2008, Vol. 57, nº 247, p. 69-87.

31. MARÍ A., BAIRÁN J. "Evaluación de los efectos estructurales del deterioro, reparación y refuerzo, mediante análisis no lineal evolutivo". *Hormigón y Acero*. 2009, Vol. 60, nº 254, p. 51-63.

32. THORENFELDT E., TOMASZEWICZ A., JENSEN J.J. "Mechanical properties of high–strength concrete and application in design". *Proceedings of the Symposium Utilization of High Strength Concrete*, Stavanger, Norway, 1987.

33. COLLINS M.P., MITCHELL D. *Prestressed concrete basics*. Ontario, Canada: Canadian Prestressed Institute, 1987. 641 p.

34. BARROS J.A.O., FIGUEIRAS J.A. "Flexural behaviour of SFRC: Testing and modelling". *ASCE Journal of Materials in Civil Enineering*. 1999, Vol. 11, nº 4, p. 331-339.

35. VANDEWALLE L. [et al.] "Test and design methods for steel fibre reinforced concrete. σ-ε design method". *RILEM Materials and Structures*. 2003, vol. 36, p. 560-567.

36. BLANCO A., PUJADAS P., DE LA FUENTE A., AGUADO A. "Análisis comparativo de los modelos constitutivos del hormigón reforzado con fibras". *Hormigón y Acero*. 2010, Vol. 61, nº 256, p. 83-100.

37. EUROCODE 2: *Design of concrete structures–Part 1: General rules and rules for buildings*. European Standard ENV 1992-1-1: 1992, Brussels, 1992.

38. CRISFIELD M.A. *Non-linear finite element analysis of solids and structures Vol. 1: Essentials*. New York: John Wiley & Sons, 1991.

39. DE LA FUENTE A., LARANJEIRA F., AGUADO A., MOLINS, C "Structural applications of SFRC. Numerical model for sewer pipes". *2nd National Congress of precast concrete*. Centro de Congresos do LNEC, Lisboa, Portugal, 2008.

CHAPTER 4

Experimentation and numerical simulation of steel fibre reinforced concrete pipes

4.1. Abstract

The main results concerning on an experimental and a numerical study related to the use of SFRC in pipes are presented in this article. Eighteen pipes with an internal diameter of 600 mm and fibre dosages of 10, 20 and 40 kg/m^3 were manufactured and tested by means the three edge bearing machine. Some technological aspects regarding with the production and the test procedure as well the mechanical behaviour of these pipes were concluded. Likewise, due to the lack of both analytical and numerical models available for designing and the checking of SFRCP, a new numerical parameterized model called Model for the Analysis of Pipes (MAP) was implemented. With this model, the simulation of the resistant behaviour during the test of SFRCP can be performed. In this sense, the results obtained in the experimental campaign were contrasted with those suggested by means MAP reaching very satisfactory correlations between them. Taking it into account, it could be said that the numerical model is a useful tool for the optimal design of the SFRCP reinforcement configuration and fibre dosages. One of the main advantages of the model is avoiding the need of the systematic employment of the three edge bearing test as an indirect design method as it would remain as control method. Consequently, the use of this model would reduce the overall cost of the pipes and would give fibres a boost as a reinforcement solution for this structural typology.

Keywords: Concrete sewerage pipes; Fibres; Crushing test; Cracking; crown.

4.2. Introduction

Steel bar reinforced concrete pipes (SBRCP) and steel fibre reinforced concrete pipes (SFRCP) are well-known alternatives used for the conveyance of water, industrial wastes, sewerage among other applications [1-4]. The addition of fibres to these pipes leads to the improvement of mechanical properties of concrete [5], as well as to economic savings [2]. When steel rebars are also used, they perform the main resistance task [6], whereas the fibres activate a bridging mechanism between the cracks which leads to a reduction of their separation and opening [7]. From an economic point of view, the saving of the traditional reinforcement results in a reduction of assembling operations, labour force and machinery, as well as in a decrease in the risks associated to manufacturing [2].

The use of fibres as reinforcement of concrete pipes (CP) is not a recent practice; in fact, its development began practically two decades ago. Nevertheless, its introduction into the market has been progressive, due to factors such as the risk of cuts during the manipulation tasks, lack of knowledge on design and calculation methods and, finally, the traditional inertia towards change [8].

However, through the years, solutions have been found for most of the problems previously mentioned: application of polishing so as to eliminate imperfections and avoid damages, constitutive equations to consider the tensile strength contribution of fibres in the concrete matrix [9-11] and, furthermore, it has been proved that the addition of fibres improves the mechanical behaviour of the pipe and leads to a global reduction of the costs [2 and 8].

With the purpose of examining technological and simulation aspects in detail, several experimental campaigns have been developed between the University of São Paulo [4 and 12] and the Polytechnic University of Catalonia [2]. As regards the former, the work carried put concerns the procedure to follow to implement the crushing test (CT) in accordance with [13]. In this sense, it was also corroborated that the continuous test is representative of the post-failure behaviour of the SFRCP, as was verified in [3]. Likewise, the influence of measuring in only one of the ends of the pipe or in both ends during the execution of the CT in the results was also analyzed. Simultaneously, the Model for the Analysis of Pipes (MAP) was developed for the simulation of the mechanical response of plain concrete pipes (PCP), SBRCP, and SFRCP. This model aims, on the one hand, at contrasting the experimental results with those derived from the model and, on the other hand, at providing a numerical tool that enables the design of the optimal reinforcement for this type of pipes.

Summarizing, the goal of this article consists in introducing the experimental campaign carried out with pipes with an internal diameter of 600 mm and C_f of 10, 20 and 40 kg/m^3, mentioning the bases of the MAP model, and contrasting the numerical results with the experimental ones in order to assess the suitability of the model as a tool for the optimal design of SFRCP.

4.3. Producing the pipes

For the experimental campaign, a total of 18 SFRCP with a D_i of 600 mm and a h of 72 mm were manufactured, in two different series. The values of C_f used were 10, 20 and 40 kg/m^3, and 3 pipes were manufactured with each of the amounts.

In order to avoid the influence of the temporal variable, the pipes corresponding to each of the two series were manufactured on the same day, using in all cases the usual cement and aggregates at the manufacturing plant where they were produced (see Table 1). DRAMIX® RC-80/60-BN metallic fibres were used. In the 1st series there were some problems during the mixing and pouring, due to the loss of workability triggered by the addition of fibres [14]. These problems were corrected in the 2nd series increasing the water content with the increase of C_f. In this way, an excellent finish level and a higher production speed were achieved.

The fibres were added directly in the conveyor belt and the concrete was compacted by means of the vibrocompression method [2]. The pipes were subsequently transported and stored at the stocking area of the factory until the test date (28 days).

Table 1. Dosages used for manufacturing the SFRCP.

Material	Dosage
River Sand (d_{max} = 1.2 mm)	679 kg/m³
Crushed Sand (d_{max} = 4.8 mm)	340 kg/m³
Granitic Crushed Coarse Aggregate (d_{max} = 9.5)	1067 kg/m³
Cement	355 kg/m³
Water	152 l/m³
Fibres	10, 20 y 40 kg/m³

4.4. Crushing test for SFRCP

4.4.1. Procedure according to UNE-EN 1916:2002

The CT (see Fig. 1) consists in the application of a longitudinal load distributed uniformly over the upper generatrix of the pipe, which is supported on two edges forming an angle with value 2β with regard to the centre of the pipe (O). The procedure to follow for the execution of the CT for SFRCP is specified in [15]:

1. Withstanding load F_c for a minute without cracking, or in other words: without reaching load F_{cr}, F_c being equal or higher than the 67% of load F_n.
2. Leading the pipe to failure, obtaining load F_u (higher than F_n).
3. Unloading and reloading the pipe when the load decreases a 5% of F_u, verifying that a load $F_{min,pos}$ not lower than the 67% of F_n is reached. This must be maintained at least for a minute.

The intention of the cyclical process is verifying that the fibre-concrete anchorage and the post-cracking strength of SFRC are suitable for guaranteeing $F_{min,pos}$, even though it was already proved in [3] that the continuous test leads to representative and reliable results of the resistance response of the pipe.

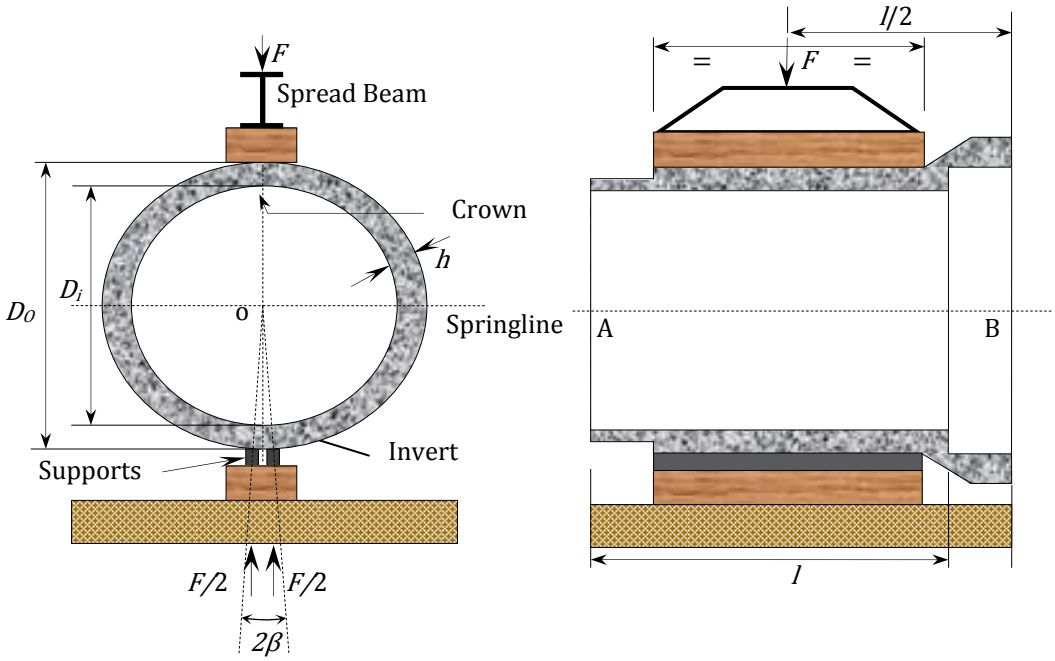

Fig. 1. (a) Cross and (b) longitudinal sections of the test configuration.

4.4.2. Measuring procedure

In order to carry out the tests with enough accuracy, it was necessary to use a device that enables the uninterrupted measurement of v [12]. LVDTs were used: they were stuck to the internal face of the key of the pipe and fixed in the invert. They transferred the data to a computer which processed them to obtain the F–v curves.

For the measurement of v, two configurations were used (1st series and 2nd series). In the 1st series, v was measured in the two edges of the pipe (sections A and B in Fig. 1b), the average value being the resulting displacement adopted; whereas in the 2nd series v was only measured in section A (see Fig. 1b).

4.5. Experimental results

Fig. 2 shows the average of the F–v curves for each C_f obtained in the two series (values of v up to 4 mm for pipes from the 1st series and up to 8 mm for those from the 2nd series). The F-v curves from each individual test are presented and analyzed in the experimental-numerical contrasting section.

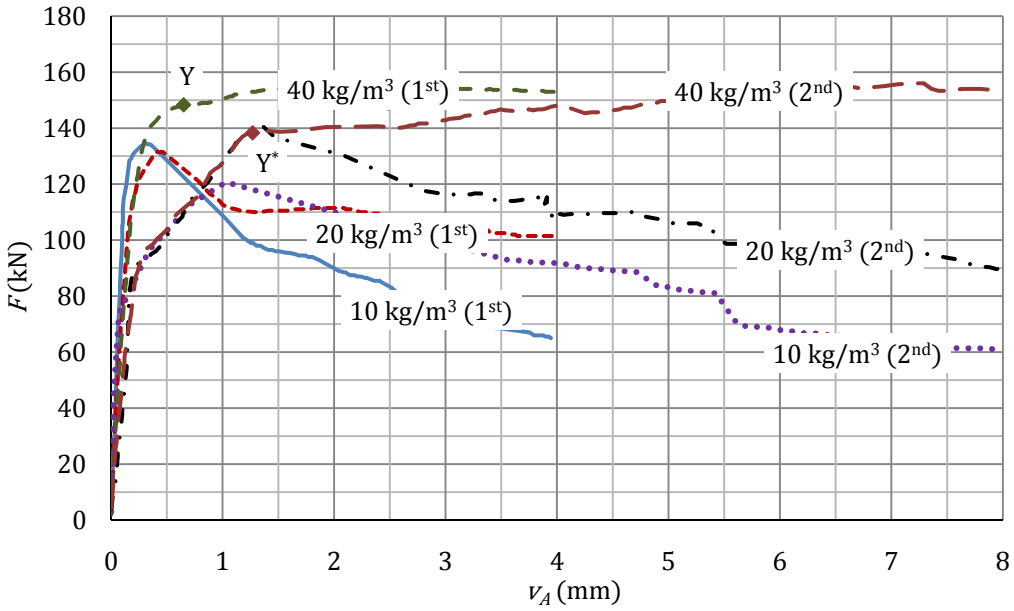

Fig. 2. Average F-v curves obtained for the tested pipes.

As it can be observed, Fig. 2 shows a well-defined softening behaviour pattern in the case of pipes with low amounts of fibres; in other words, the pipe undergoes a loss of resistance capacity with the increase of v once load F_u was reached. On the other hand, the pipes with 40 kg/m³ respond differently, showing hardening when the yielding point is reached (points Y and Y* from Fig. 2 for the pipes with 40 kg/m³ from the 1st and 2nd series, respectively). Consequently, the v required in order to detect the decrease of F which indicates the failure of the element and the post-failure regime are not reached in this sort of pipes.

From Fig. 2 it is also deduced that the pipes in the 1st series show higher stiffness and a longer uncracked stage. This happens because section B (Fig. 1b) is stiffer than section A (Fig. 1b) due to the higher volume of concrete involved and to the higher D_i of the former. Therefore, taking into account that the average value of v is accepted for the pipes of the 1st series, it is reasonable they show higher stiffness in comparison to those from the 2nd series, for which v was only measured in section A.

With respect to this aspect, it was observed that cracking began, in all cases, at the key of section A with values of F_{cr} around 90 kN. On the other hand, in the pipes from the 2nd series, it was observed that the appearance of the first cracks coincided with the change in the slope of the F-v curve. This change was not

detected in the pipes from the 1st series until the springline also cracked, a situation which took place when load F reached average values of 126 kN, 114 kN and 138 kN for the pipes with 10 kg/m³, 20 kg/m³ and 40 kg/m³, respectively. Therefore, it may be assured that if the measurement of v is performed in section A, load F_{cr} can be deduced from the F-v curve at the point where the first slope change takes place. On the other hand, if the measurement is performed as in the 1st series, this procedure would lead to values of F_{cr} on the side of insecurity, requiring a visual inspection in order to detect F_{cr}.

In the case of the pipes with low C_f, instability regions similar to those described in [3] were observed. They were reflected in the F-v curves by means of an increase in the distance between points (see, for instance, the stretch between 1.5 and 3.0 mm of the pipes with 20 kg/m³ from the 2nd series).

Likewise, it was verified that the pipes fulfilled the strength requirements of class C-90 established in [15]. Concretely, for pipes with a D_i of 600 mm it is required to obtain a load F_c of 36 kN/m and a load F_u of 54 kN/m in the CT (90 kN and 135 kN, respectively, taking into account that the length of the pipes was 2500 mm).

Regarding load $F_{min,pos}$, established for C-90 (90 kN), it must be verified that the $F_{max,pos}$ measured in the curve F-v is equal or higher than the former. The value of v for which $F_{max,pos}$ is reached is function of, among other parameters, the diameter of the pipe and the amount and type of reinforcement; in other words, of the global stiffness of the pipe. For this paper it was established that $F_{max,pos}$ is reached for a v of 1.2 mm ($F_{1.2mm}$) and 3 mm (F_{3mm}) for the pipes from the 1st and the 2nd series, respectively [3]. However, this is not the suitable approach in the case of pipes with 40 kg/m³, since they did not show a drop of value F for the displacement regime used in the tests. Consequently, in the case of those pipes only their load F_u is assessed, and it is taken for granted that their post-failure behaviour fits in with the criteria established for class C-90 (the pipes with 20 kg/m³ already fulfil the minimum requirements in post-failure regime).

Table 2 shows the individual and average values of F_{cr}, $F_{1.2mm}$ (1st series), F_{3mm} (2nd series) and F_u obtained experimentally. The results from pipes T3 for the amounts of 10 kg/m³ and 20 kg/m³ from the 1st series were rejected due to some mismatches which occurred during the performance of the test.

Table 2. Individual and average values of F experimentally obtained.

Series	C_f (kg/m³)	F_{cr} (kN)				F_u (kN)				$F_{1.2mm}$ y F_{3mm} (kN)			
		T1	T2	T3	**Average**	T1	T2	T3	**Average**	T1	T2	T3	**Average**
1st	10	96	98	n/a	**97**	149	120	n/a	**135**	107	94	n/a	**101**
	20	96	100	n/a	**98**	140	124	n/a	**132**	118	102	n/a	**110**
	40	93	98	100	**97**	156	163	149	**156**	-	-	-	**-**
2nd	10	100	83	100	**94**	127	132	138	**132**	97	88	98	**94**
	20	98	95	85	**93**	151	145	129	**142**	121	120	108	**116**
	40	80	80	115	**92**	152	140	193	**162**	-	-	-	**-**

Concerning the values gathered in Table 2, it is deduced that the pipes from the 1st series showed loads F_{cr} higher than the 90 kN stipulated for F_c in C-90. Likewise, the pipes from the 2nd series showed average loads of F_{cr} around 94 kN, which were also accepted since no cracking signs were observed during the visual inspection once F_c was reached, not even in pipes T1 and T2 with amounts of 40 kg/m³ from the 2nd series, for which the load F_{cr} was 80 kN.

As regards the response in failure, the values F_u were obtained for displacements close to 0.3 mm for the pipes from the 1st series and close to 1 mm for those from the 2nd series, thus corroborating the stiffer behaviour of the former. It is deduced from Table 2 that, in average value, all the pipes reached the load of 135 kN established for F_u except the pipes reinforced with 20 kg/m³ and 10 kg/m³ of fibres from the 1st series and the 2nd series, respectively. In both cases the average load F_u obtained was of 132 kN (a 2% lower than required). Finally, it is verified that load $F_{min,pos}$ (90 kN) is exceeded by all the pipes except pipe T2 with 10 kg/m³ of fibres from the 2nd series. In any case, the average values of $F_{1.2mm}$ and F_{3mm} are higher

than the $F_{min,pos}$ established for these pipes, proving that the type of fibres and the amounts used are the suitable ones to accomplish the strength requirements.

4.6. Numerical simulation of the crushing test

The numerical simulation of the CT requires a numerical tool capable to consider the nonlinear behaviour of the material and the possibility of modelling the response of SFRC. To this purpose, the Analysis of Evolutive Sections model (AES), described in [16 and 17], was used. This model has already been used satisfactorily as a numerical tool in other applications [18]. On the other hand, the MAP model was developed for the simulation of the CT. Several of the hypotheses accepted in the MAP model were suggested in [19].

By means of the AES model the concrete is discretized into fibre-type elements and the steel bars, into concentrated area elements. It is well known that the addition of fibres modifies the compression behaviour of SFRC depending on the volume used [20]. In this respect, its response to uniaxial compression is described by the expression suggested in [21]. On the other hand, the simulation of its post-cracking behaviour is approached by means of the model gathered in [11], since it has already been successfully used in other works [22 and 23]. The passive steel for the reinforcement is modelled using a trilinear diagram.

For the simulation of the CT at a structural level, the double symmetry of the element (β=0) was taken into account, hence only a quarter of pipe is modelled. Likewise, it is taken for granted that the key and springline sections are the ones which control the response of the pipe. The cracking and yielding phenomena (modelled with the AES subroutine) are concentrated in both sections, whereas in the intermediate sections a linear behaviour of the constituting materials is accepted. The response of the pipe has been divided into three stages: elastic linear stage, elastic stage with cracking at key (see Fig. 1) and elastic stage with cracking at key and springline (see Fig. 1).

The governing equations of the structural problem implemented in MAP were deduced in [19] considering that the bending and axial forces are the determinant ones. In this respect, it is well known that the shear strength of SFRC elements improves noticeably [24], so shear failures are not expected in this type of pipes.

Taking into account the three stages previously described, the curve F-v of the pipe in the CT can be obtained. However, the model guarantees representative results of the CT, provided that no intermediate cracks appear (rigid concrete pipes). This is the pattern observed in the pipes tested for this campaign. Likewise, it has also been observed in SFRCP with D_i of 800 mm [3] and of 1000 mm [2], hence the latter is established as the maximum value of the applicability range of the model for lack of contrasting with larger diameters.

4.7. Simulation of the experimental results with MAP

The model suggested in [21] was used for modelling the compression behaviour of SFRC, fixing a resistance f_{ck} of 50 MPa [4]. On the other hand, the diagram proposed in [11] was used in order to simulate its linear and post-cracking response. However, due to the lack of tests needed [25] in order to be able to determine $f_{R,i}$ for each C_f, the expressions proposed in [26] were used. In this respect, the type of fibres used in this campaign as well as those used in order to calibrate the expressions presented in [26] belong to the type DRAMIX® RC-80/60-BN.

Figs. 3 show the curves F-v obtained experimentally (individual and average values) and numerically for the pipes with C_f of 10, 20 and 40 kg/m^3 from the 2nd series. This series was selected because it was observed that the experimental measurements of v in section A (Fig. 1b) are more representative of the global behaviour of the pipe.

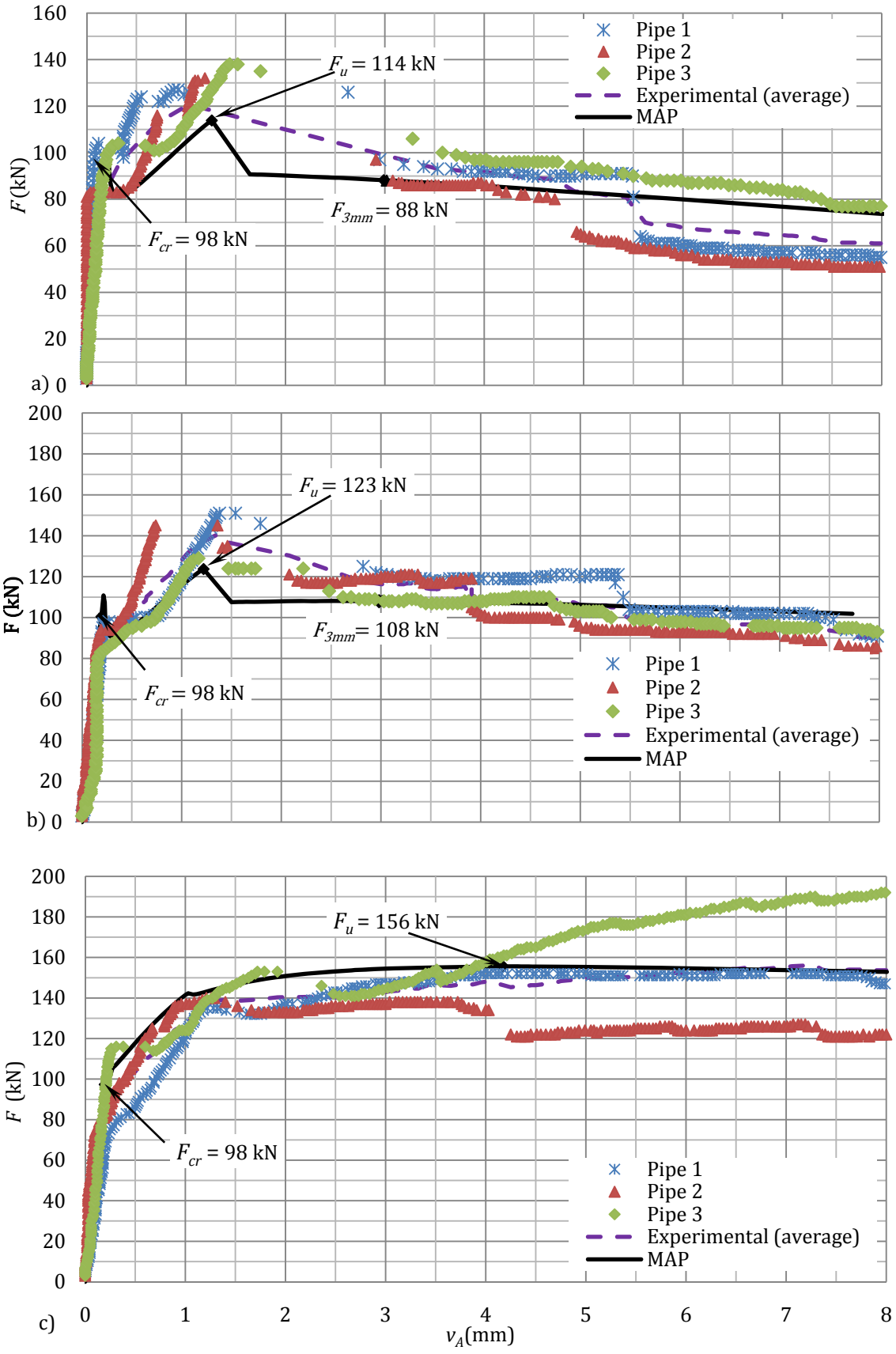

Figure 3. *F-v* curves for the pipes reinforced with (a) 10, (b) 20 y (c) 40 kg/m³ of fibres.

Complementarily, Table 3 gathers the average experimental and numerical values of F_c, F_u and F_{3mm} shown in Figs. 3. The parameter ξ is the relative error with regard to the experimental data. Positive values of ξ indicate that the experimental data exceed the numerical one, and vice versa.

Table 3. Experimental (average) and numerical values of F obtained with the tested pipes.

Fibre dosage (kg/m³)	F_{cr}			F_u			F_{3mm}		
	Exp. (kN)	MAP (kN)	ξ (%)	Exp. (kN)	MAP (kN)	ξ (%)	Exp. (kN)	MAP (kN)	ξ (%)
10	94	98	-4.3	132	114	13.6	94	88	6.4
20	93	98	-5.4	142	123	13.4	116	108	6.9
40	92	98	-6.5	162	156	3.7	-	-	-

From the results presented in Fig. 3a, it can be deduced that the MAP model fits in properly with the experimental results for the amount of 10 kg/m³, particularly both in elastic linear and post-failure stages. In the latter, the numerical results for v higher than 7.5 mm tend toward the experimental maximum values. The values of F_{cr}, F_u and F_{3mm} obtained numerically are 98 kN, 114 kN and 88 kN, respectively. Therefore, since neither F_u nor F_{3mm} reach the minimum values stipulated in [15] for class C-90, it can be stated that according to the model the amount of 10 kg/m³ is not enough to guarantee strength class C-90.

The results from Fig. 3b concerning the dosage of 20 kg/m³ highlight that the simulation by means of the MAP model guarantees values close to the experimental ones. Nonetheless, the model overestimates the load capacity of the pipes for v higher than 5.5 mm. This could indicate that the values $f_{R,i}$ used for the simulation of the behaviour of tensioned SFRC are slightly higher than the real ones for this range of displacements. The values of F_{cr}, F_u and F_{3mm} obtained numerically are: 98 kN, 123 kN and 108 kN, respectively. Consequently, class C-90 will not be reached with 20 kg/m³ either, since the load F_u (123 kN) is lower than the 135 kN required.

Finally, in the case of the pipes with 40 kg/m³ of fibres (Fig. 3c), the numerical model fits in adequately with the experimental results at all stages. In this case, the value of F_{cr} is 98 kN and F_u is 156 kN. Therefore, the model also predicts a strength capacity higher than that specified for a class C-90 pipe of 600 mm [15] with this amount of fibres. In this respect, it is taken for granted that the load F_{3mm} is higher than the 90 kN established for $F_{min,pos}$ (with 20 kg/m³, the average F_{3mm} is already 108 kN). Likewise, the model highlights, in accordance with the experimental results, the existence of hardening once the pipe yields.

From the analysis of the results presented in Table 3 it can be concluded that:

- The load F_{cr} obtained numerically is independent from the amount of fibres. F_{cr} depends exclusively on f_{ct}, D_i and h [2]. On the other hand, the model tends to overestimate F_{cr} with respect to the experimental results between a 4.3% (pipe with 10 kg/m³) and a 6.5% (pipe with 40 kg/m³). This could be due to the incorporation of additional water during the mixing in order to increase the workability of the mixture in the pipes from the 2nd series.
- The model underestimates F_u with regard to the experimental values between a 3.7% (pipe with 40 kg/m³) and a 13.6% (pipe with 10 kg/m³). When F_u is reached, then the reason for the difference obtained could be the constitutive equation used to simulate the post-cracking behaviour of SFRC being too conservative for the levels of v at which F_u is reached. In this respect, in [2] it is verified that the fibres work practically oriented parallel to the flow of stresses when the conventional pipe manufacturing methods are used. Therefore, they work with a high efficiency. An alternative way of considering this fact at the level of calculation would be using the methodology suggested in [27], for example.
- With regard to F_{3mm}, the numerical values obtained are a 6.4% (10 kg/m³) and a 6.9% (20 kg/m³) lower in comparison with the experimental data. This could be due, just as in the case of load F_u, to the underestimation of the parameters involved in the definition of the constitutive equation chosen [11] to model the post-cracking response of SFRC.

Taking into account what has been previously mentioned, it can be assured that the MAP model adjusts satisfactorily to the experimental results, even though a constitutive equation was used in order to model the post-cracking behaviour of SFRC, calibrated from concretes with f_{ck} ranging from 25 to 30 MPa [26] as opposed to the 50 MPa obtained in the concrete used for the pipes in this campaign. Likewise, the constitutive equation does not take into account the effect of the preferential orientation of the fibres within the thickness of the pipe, which in this case is favourable. Consequently, in most of the cases the MAP model tends to underestimate the experimental results, these differences being of a 7.0% in average value and, in any case, not higher than 13.6%. Then, the good correlation obtained can be considered to be a success taking into account the multitude of variables involved in the problem, its uncertainty, and the difficulty of the experimental determination of some of them.

4.8. Conclusions

This article has introduced a work related to the technological aspects and the numerical simulation of SFRCP. It also showed the results obtained in an experimental campaign with 18 SFRC pipes with diameters of 600 mm and amounts of fibres of 10, 20 and 40 kg/m^3. The following conclusions were derived from those results:

- The manufacturing of this type of elements is possible by means of the traditional systems modifying *in situ*, if necessary, the water content of the mixture. The manufacturing time and the labour force are reduced considerably with respect to SBRCP.
- It is confirmed that the continuous test with displacement control by means of LVDTs, as a replacement for cyclical tests, leads to results representative of the strength capacity of this sort of pipes.
- The load F_{cr} observed during the visual inspection is similar regardless of the amount of fibres and the measuring method. The first crack appeared, in all cases, in the internal face of the key (in section A). In the case of the pipes from the 2nd series, the point where the first change in the slope of curve F-v occurs coincides with F_{cr}, exactly as in the numerical simulations.
- The pipes with 40 kg/m^3 show hardening of the curve F-v when global cracking of the pipe (key and springline) occurs. From this fact it is deduced that in these elements the fibres can perform a task similar to that of the traditional bars, even with an improved response to cracking in in-service regime
- The load which is critical in order to fulfil the strength requirements of class C-90 for this type of pipes is F_u.

Moreover, the main bases of the MAP model, developed for the analysis of SFRCP, were introduced. The degree of correlation between experimentation and simulation is considered to be satisfactory, since the model gave results on the side of security with an average relative error of 7.0%. In order to improve the accuracy of the results, it is proposed to adjust the constitutive equation of post-cracked SFRC so that it takes into account the preferential orientation of the fibres.

Consequently, the MAP model can be used as a design method for other diameters (equal or lower than 1000 mm), other thickness and other strength classes, without the need for testing several pipes in order to estimate the optimal dosage of fibres, but only to verify the resulting design. This would mean a significant saving of time and economic resources when there is no established dosage pattern, be it because some geometrical characteristic has been changed, or because it is a strength class uncommon for such a diameter.

Currently, several experimental campaigns are being carried out with the aim of contributing to a larger data bank to contrast and adjust the model.

4.9. Acknowledgements

The authors of this document wish to express their appreciation for the financial support received through the Research Project BIA2010-17478: *Procesos constructivos mediante hormigones reforzados con fibras*.

Likewise, Professor Antonio D. de Figueiredo wishes to thank the support provided by CAPES - Coordenação de Aperfeiçoamento de Pessoal de Nível Superior– for having awarded him the postdoctoral grant that allowed him to participate in this work.

4.10. References

1. Haktanir T, Ari K, Altun F, Karahan O. A comparative experimental investigation of concrete, reinforced-concrete and steel-concrete pipes under three-edge-bearing test. *Construction and Building Materials* 2007; **21**(8): 1702-8. doi:10.1016/j.conbuildmat.2006.05.031.
2. de la Fuente A, Armengou J. Aplicaciones estructurales del HRFA: Tubos de saneamiento, paneles de cerramiento y placas de suelo reforzado. *Aplicaciones estructurales del HRFA*, Jornada Técnica 2007-JT-02, 9 de Octubre de 2007, Barcelona (Spain), UPC, 2007.
3. Figueiredo AD de. Evaluation of the test method for crushing strength of steel fiber reinforced concrete pipes. *7th International RILEM Symposium on Fibre Reinforced Concrete*, Chennai, India, 2008. Fiber Reinforced Concrete: Design and Applications. Babneux - France: RILEM Publications SARL 2008; **1**:989–1000.
4. Figueiredo AD de, Chama Neto PJ. Avaliação de desempenho mecânico de tubos. *Revista DAE* 2008; 178: 34-9.
5. Aa'ad S, Saxer A. Influence of Fiber Geometry on the Flexural Strength Performance of Steel Fiber Reinforced Concrete (SFRC), *Fibre Concrete 2007*, Prague, Czech Republic, 2007.
6. Chiaia B., Fantilli AP, Vallini, P. Evaluation of crack width in FRC structures and application to tunnel linings. *RILEM Materials and Structures* 2009; **42**(3):339-51. doi:10.1617/s11527-008-9385-7.
7. Blanco A, Pujadas P, de la Fuente A, Aguado, A. Análisis comparativo de los modelos constitutivos del hormigón reforzado con fibras. *Hormigón y Acero* 2010; 61(256):83-100.
8. Parrot J. *Estudio de la sostenibilidad en tuberías de saneamiento*, Tesina de especialidad, UPC, Barcelona (Spain). 2009.
9. Hilleborg A, Modéer M, Petersson PE. Analysis of crack formation and crack growth in concrte by means of fracture mechanics and finite elements. *Cement and Concrete Research* 1976; **6**:773-82.
10. Laranjeira, F. Design-oriented constitutive model for steel fiber reinforced concrete. PhD Thesis, UPC, Barcelona (Spain), 2010.
11. Vandewalle, L. *et al*. Test and design methods for steel fibre reinforced concrete: σ-ε design method. Final recommendation. *RILEM Materials and Structures* 2003; **36**(262):560-67. doi:10.1617/14007.
12. Silva JL da, el Debs MK. Influência da bolsa no comportamento estrutural de tubos de concreto armado submetidos à compressão diametral. In: *51º Congresso Brasileiro do Concreto*, 2009, Curitib (Brazil). p.1-13.
13. UNE-EN 1916:2002. *Concrete pipes and fittings, unreinforced, steel fibre and reinforced*. 2002.
14. Moreno E, Fernández M. Mix design of steel fiber reinforced concrete. *Materiales de Construcción* 1997; **47**(247-248):11-26. doi:10.3989/mc.1997.v47.i247-248.
15. UNE 127916. *Tubos y piezas complementarias de hormigón en masa, de hormigón con fibra de acero y de hormigón armado*. Complemento nacional a la norma UNE-EN 1916:2003. 2004.
16. de la Fuente A, Aguado A, Molins C. Modelo numérico para el análisis no lineal de secciones

prefabricadas construidas evolutivamente. *Hormigón y Acero* 2008; **57**(247):69-87.

17. de la Fuente A, Aguado A, Molins C. Diseño óptimo integral de tubos de hormigón. *Hormigón y Acero* 2010; **61**(259). [In press].
18. Klein N, de la Fuente A, Aguado A, Masó D. Hormigón ligero autocompactante con fibras para rehabilitación de forjados. *Materiales de Construcción*. Accepted in 2010 for publication.
19. Pedersen C. *Calculation of FRC pipes based on the fictius crack model*. Department of Structural Engineering. Technical University of Denmark, 1995.
20. Bencardino F, Rizzuti L, Spadea G, Swamy RN. Stress-strain behavior of steel fiber-reinforced concrete in compression. *ASCE Journal of Materials in Civil Enineering* 2008; **20**(3):255-63. doi:10.1061/(ASCE)0899-1561(2008)20:3(255).
21. Barros JAO, Figueiras JA. Flexural behaviour of SFRC: Testing and modelling. *ASCE Journal of Materials in Civil Enineering* 1999; **11**(4):331-9. doi:10.1061/(ASCE)0899-1561(1999)11:4(331).
22. Blanco A. *Durabilidad del Hormigón con Fibras de Acero*. Tesina de especialidad, UPC, Barcelona (Spain). 2008.
23. Pujadas P. *Durabilidad del Hormigón con Fibras de Polipropileno*. Tesina de especialidad, UPC, Barcelona (Spain). 2008.
24. Turmo, J., Banthia, N., Gettu, R., and B. Barragán. Study of the shear behaviour of fibre reinforced concrete beams. *Materiales de Construcción* 2008; **58**(292):5-13. doi:10.3989/mc.2008.40507.
25. Vandewalle L. *et al*. Test and design methods for steel fibre reinforced concrete: Bending test (final recommendation). *RILEM Materials and Structures* 2002; **35**(253):579-82. doi:10.1617/13884.
26. Barros JAO, Cunha VMCF, Ribeiro AF, Antunes JAB. Post-cracking behaviour of steel fibre reinforced concrete. *RILEM Materials and Structures* 2005; **38**(1):47-56. doi:10.1007/BF02480574.
27. Laranjeira F, Molins, C, Aguado, A. Predicting the pullout reponse of inclined hooked steel fibers. Cement *and Concrete Research* 2010; **40**(10):1471-87. doi:10.1016/j.cemconres.2010.05.005.

APPENDIX A: Notation

A: Spigot of the pipe.
B: Socket of the pipe.
C_f: Fibre dosage.
D_i: Internal diameter of the pipe.
D_o: Outside diameter of the pipe.
d_{max}: Maximum diameter of the aggregate.
E_{cm}: Average elongation modulus of the concrete.
F: Applied load.
F_c: Service load (established).
F_{cr}: First cracking load.
F_n: Failure load (established).
$F_{max,pos}$: Maximum post-failure load (simulated).
$F_{min,pos}$: Minimum post-failure load (established).
F_u: Failure load.
$F_{1.2mm}$: Post-failure load for a 1.2 mm vertical displacement of the key (1st series).
$F_{3.0mm}$: Post-failure load for a 3.0 mm vertical displacement of the key (2st series).
f_{ck}: Characteristic compressive concrete strength.
f_{ct}: Tensile concrete strength.
f_{Ri}: Residual flexural concrete strength.
h: Thickness of the concrete wall.
l: Length of the pipe.
O: Centre of the pipe.
v: Vertical displacement of the key.
β: Angle between the supports and the centre of the pipe.
ξ: Relative error of the numerical value.

CHAPTER 5

A new design method for steel fibre reinforced concrete pipes

5.1. Abstract

This article introduces the results from an experimental campaign based on the production and testing of pipes with a diameter of 1000 mm. The results from this campaign, together with other results introduced in previous works, have proved that the hypotheses accepted in the numerical model called Model for the Analysis of Pipes (MAP) are suitable for dealing with the simulation of the mechanical behaviour of this type of pipes. The analysis of the experimental and numerical results leads to the conclusion that the MAP is a suitable tool for the parametric study and the design of this type of pipes. Likewise, this paper also introduces the first procedure, based on the use of the MAP model, to find the minimum amount of fibres necessary to fulfil the strength requirements established in the project.

Keywords: Cracking; Concrete Pipes; Crushing Test; Design; Fibres; Hinge; Ridge; Springline

Albert de la Fuente Antequera; Renata Campos Escariz; Antonio Domingues de Figueiredo; Climent Molins Borrell and Antonio Aguado de Cea

5.2. Introduction

Unreinforced concrete pipes (UCP) and steel-bar reinforced concrete pipes (SBRCP) have been successfully used in rainwater and drainage pipes with internal diameters (D_i) ranging from 300 mm to 3000 mm [1]. On the other hand, plastic pipes (PP) are frequently used for D_i lower than 300 m. This is mainly due to the fact that, in comparison with concrete pipes (CP), PPs are easier to handle and assemble, and this makes them more appealing for this range of small diameters [2].

However, in the last two decades, CP manufacturers have witnessed an intensification of the competition coming from the PP industry [3-5]. This rising competition does not only affect small D_i and low strength classes, but also market segments previously dominated by the sector of CP manufacturers. The main reasons for this change are the improvements introduced by the PP manufacturers at both the material and structural level.

In view of this situation, the CP industry has detected several aspects which can be improved in order to maintain the market share of the D_i and strength classes which has traditionally belonged to it. Namely, it has been proved that the use of steel fibre reinforced concrete (SFRC), partially or totally replacing the steel bars, is a competitive solution from the technical and economic point of view [6-9].

The use of steel fibre reinforced concrete pipes (SFRCP) is a widespread practice; proof of this is the existence of several national and international standards regulating their use (most of these are adaptations of the EN-1916:2002 [10]). However, in spite of the numerous experimental campaigns carried out and published in the scientific literature [5-9], for several reasons their use has not been properly consolidated [7]. Among those reasons, the most important one is the lack of a systematic method for the design of SFRCP. In this respect, the type and the amount (C_f) of fibres for each D_i and strength class has been traditionally selected by means of the crushing test (CT) [11]. This is a reliable method, but not very efficient from the economic point of view, since there exist several D_i, thicknesses (e) and commercial strength classes, and this slows down the technological development of this material.

Therefore, it is evident that there is a need for a methodology that would enable the systematic design of SFRCP for D_i where the SFRC would emerge as a competitive solution with regard to conventional SBRCP. In this respect, only one numerical model capable of analyzing SFRCP with D_i up to 500 mm has been presented [3]. However, according to the CP manufacturers and the results obtained in several experimental campaigns [12-13], it seems that the D_i of 1000 mm is the upper boundary for the use of SFRC.

With the aim of studying the viability of SRFC in CP, the Universitat Politècnica de Catalunya (UPC) and the Univeridade de São Paulo (USP), in conjunction with national companies within the sector of CP manufacturers, have carried out several experimental campaigns [13-14] and developed numerical models for the analysis of SFRCP [12-13]. Among those, the Model for Analysis of Pipes (MAP) introduced in [13] has already been contrasted with experimental results obtained from SFRCP with a D_i of 600 mm [13], obtaining satisfactory correlations.

The main aim of this paper is to introduce the numerical tool (MAP) for which the most recent constitutive equations for the simulation of SFRC have been implemented. It is proved that MAP is appropriate for the analysis of SFRCP and, consequently, for the design of the optimal C_f for SFRCP even with 1000 mm of D_i. The suitability of the MAP for this purpose is verified by contrasting the experimental results obtained from SFRCP with $D_i = 800$ mm and $D_i = 1000$ mm presented in [9] and [14], respectively. Finally, it is concluded that the MAP can be used industrially to generate the design tables for SFRCPs, which would help to systematize and generalize the use of SFRC in this type of elements.

5.3. Steel fiber reinforced concrete pipes subjected to the crushing test (CT)

5.3.1. Test procedure according to EN 1916:2002

The crushing test (see Fig. 1a) is the one traditionally used for the mechanical assessment of CP and SBRCP. It has also been accepted, with several modifications, for the assessment of the mechanical response of SFRCP [10]. The test consists in the application of a longitudinal load uniformly distributed over the upper generatrix of the pipe, which leans on two longitudinal strips. The loading sequence throughout time used with SFRCP is shown in Fig. 1b; what makes it different from that established for CP and SBRFCP is the existence of an unloading-reloading process. Likewise, the pipe has to fulfil the following strength requirements:

1. Maintaining the proof load (F_c) for a minute without undergoing damage noticeable at first sight, that is, without reaching the cracking load (F_{cr}). F_c should be equal or higher than 67 % of the ultimate load (F_n) fixed for the required strength class.
2. Leading the pipe to failure, obtaining a failure load (F_u) higher than F_n.
3. When the load falls at least a 5 % of F_u, the pipe is totally unloaded and then reloaded, verifying that a minimum post-failure load ($F_{min,pos}$) not lower than F_c is reached. $F_{min,pos}$ must be maintained for at least one minute.

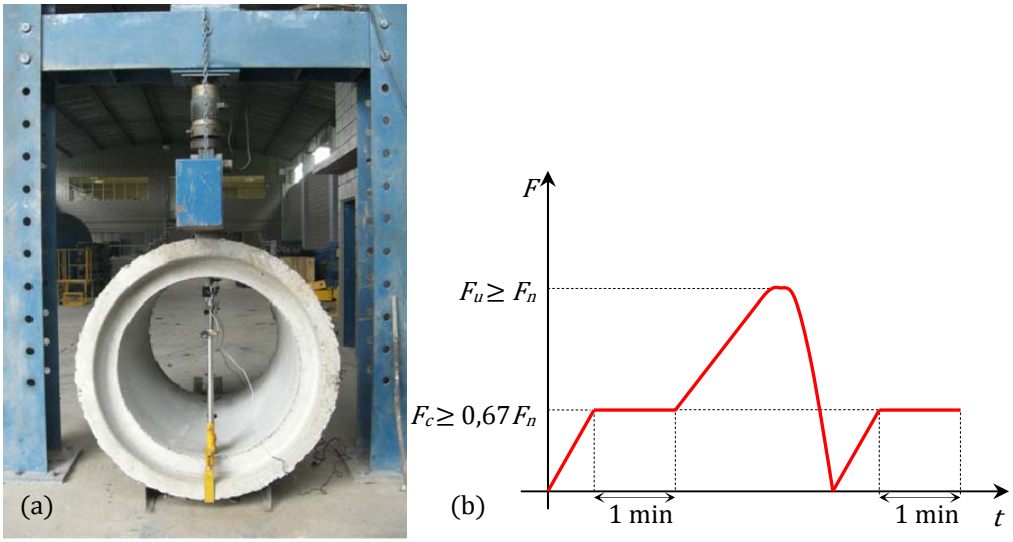

Fig. 1. Crushing test (a) configuration and (b) load pattern.

The cyclical unloading-reloading process aims at verifying that the fibre-concrete anchorage and the residual flexural strength of SFRC ($f_{R,i}$) are the suitable ones in order to guarantee the $F_{min,pos}$ [9]. Nevertheless, in SFRCP with D_i of 800 mm [9] and of 1000 mm [14] it has been proved that the maximum values of the post-failure load ($F_{max,pos}$) obtained by means continuous or cyclical tests do not show significant differences, therefore the first one can be adopted. Thanks to this, the implementation of the CT becomes easier and, consequently, CP manufacturers will not perceive the use of fibres as a difficulty.

5.3.2. Measuring procedure

For the execution of the CT with enough accuracy so as to simulate the loading-unloading-reloading process from Fig. 1b, it is necessary to use devices capable of an uninterrupted measurement of the vertical displacement at the ridge (v) (see Fig. 2). In the campaigns carried out, LVDTs were stuck to the inner face of the pipe ridge and fixed to the invert (see Fig. 1a and Fig. 2). The data recorded were downloaded to a computer and were processed in order to obtain the F–v curves for a subsequent analysis. Additionally, in some specimens the crack width of the ridge (w) was measured for some values of F (see Fig. 2).

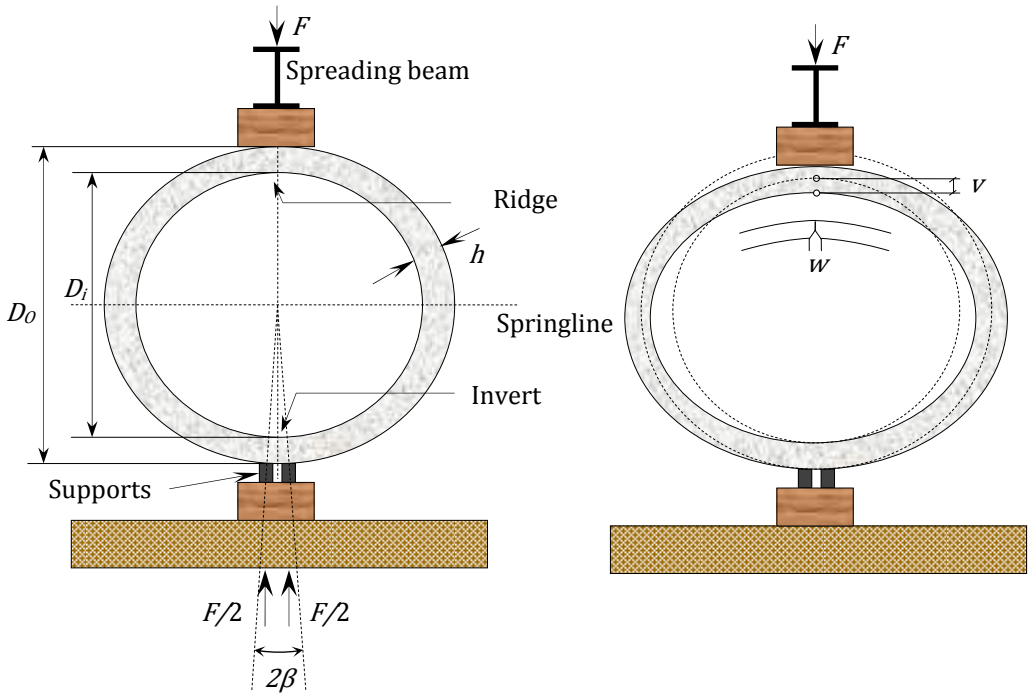

Fig. 2. Main geometrical variables involved in the resistance mechanism.

5.3.3. *Mechanical Behavior*

The mechanical behaviour of a SFRC subjected to the CT depends on its geometry (D_i and h, see Fig. 2) as well as on the type and amount of fibers (C_f) used. In this respect, the responses recorded in the tests coincide with the ones obtained by the numerical simulations carried out [12 and 13] and correspond to three different general patterns, regardless of whether the test is cyclical or continuous (see Fig. 3). In this respect, the integral response of a SFRCP can be described in three stages of behaviour, governed by the stress-strain state of the ridge and haunches sections [13]:

- Stage 1. Linear elastic behaviour of the whole element, which ends when the first crack appears at the ridge once the cracking load has been reached ($F_{r,cr}$). Its value depends on the geometry (D_i and h) and on the flexural strength of the concrete matrix ($f_{ct,fl}$), which is practically independent from C_f [15-16].
- Stage 2. When the first crack appears, the ridge section begins to work in cracking regime, whereas the rest of the sections maintain their linear response. Likewise, due to the loss of stiffness at the ridge and the hyperstaticity of the system, there is a redistribution of moments towards the haunches [17-18]. Initially, the fibres bridging the crack begin to work gradually, thus there is an initial drop of F (snap-through) and a subsequent recovery. For the same pipe, the lower the C_f, the sharper the snap-through, and vice-versa. Stage 2 ends when the cracking load of the haunches is reached ($F_{s,cr}$). In this respect, if the C_f is low in comparison with the dimensions of the pipe (case A from Fig. 3), $F_{s,cr}$ will not reach the $F_{r,cr}$ value, and it will be considered that the response is infracritical [19], coinciding $F_{r,cr}$ with the F_u load of the system. On the other hand, in the case of moderate-high C_f, $F_{s,cr}$ can be higher than $F_{r,cr}$, and thus the response will be supracritical (cases B and C from Fig. 3).
- Stage 3. Just as in stage 2, when $F_{s,cr}$ is reached, there is a snap-through that leads to the post-failure regime. At this stage, two different behaviours can be obtained depending on C_f: softening (cases A and B from Fig. 3) if C_f is low or moderate, or hardening (case C from Fig. 3) if C_f is high with regard to the dimensions of the pipe. Likewise, during this regime $F_{pos,max}$ is reached; this is a value which must be assessed in SFRCP [10]. It must be noted that, in the case of SFRCP with hardening in the post-failure response, the $F_{max,pos}$ load is the highest one in all the test and, therefore, corresponds to the F_u load of the pipe.

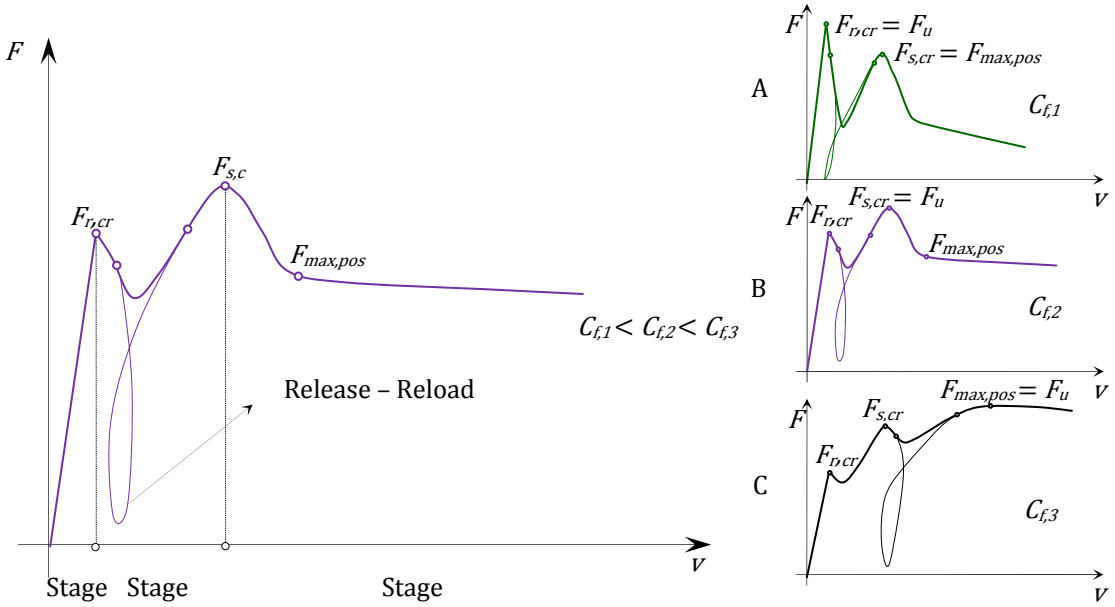

Fig. 3. Typical *F*-v diagrams of SFRCP with a fixed D_f and different C_f submitted to CT.

5.3.4. Numerical simulation of the crushing test

There exist some analytical and numerical models in the literature which enable the simulation of the mechanical response of CP submitted to CT: for SBRCP [12 and 20], for SFRCP [13 and 18] and for SB-SFRCP [12]. In this work the MAP [13] is used. It was developed on the basis of the hypotheses of structural behaviour introduced in [24] for the analysis of UCP and SFRC. The MAP simulates the global response of the pipe considering that the non-linear phenomena (cracking and yielding) occur in the two critical sections (ridge and haunches), whereas the rest of the pipe behaves linearly. This is a non-linear hinge model similar to the one used by other authors for the simulation of beams [21-22] and slabs [23] which can capture the three stages of behaviour previously described (Fig. 3) by incorporating two hinges:

- Stage 1 is simulated considering a linear behaviour throughout the whole element (Fig. 4a).
- Stage 2 is simulated by imposing that the cracking in R activates the non-linear hinge in said section, whereas the rest of the element responds in a linearly (Fig. 4b).
- Stage 3 is simulated by imposing that the cracking in S activates the second non-linear hinge, both hinges being linked by a circumference sector which behaves linearly (Fig. 4c).

This structural behaviour has been observed in UCP and SFRCP with D_f of up to 1000 mm in the various campaigns carried out [5, 7, 9, 13-14]. In all cases, during the loading process four main cracks (see Fig. 5) appeared: firstly, at the ridge (1) and at the invert (2), and, secondly, at the haunches (3 and 3*).

On the other hand, as other authors had done [22-27], the simulation of the cracked sections was carried out by means of a model of layers which takes into account the constitutive equations of SFRC as well as the equilibrium and compatibility equations. In this respect, the simulation of the tensile and the compressive behaviour of SFRC were dealt with the equations proposed in [28] and in [29], respectively (see Fig. 6). Besides, following the recommendations given in [24] for the numerical analysis of pipes, it has been considered that the length of the hinge (s) coincides with the thickness of the pipe (h).

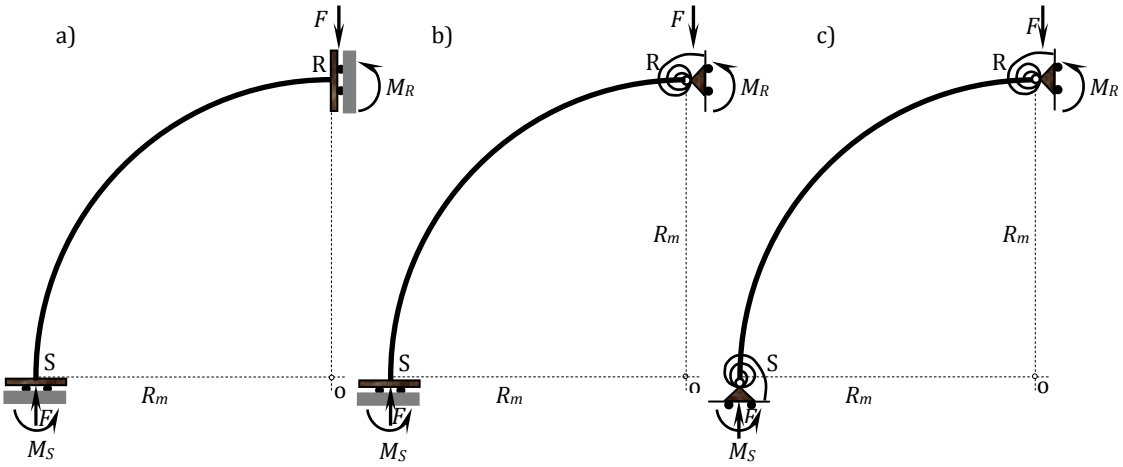

Fig. 4. Structural model in (a) linear regime, (b) linear regime with cracking in R and (c) linear regime with cracking in R and in S.

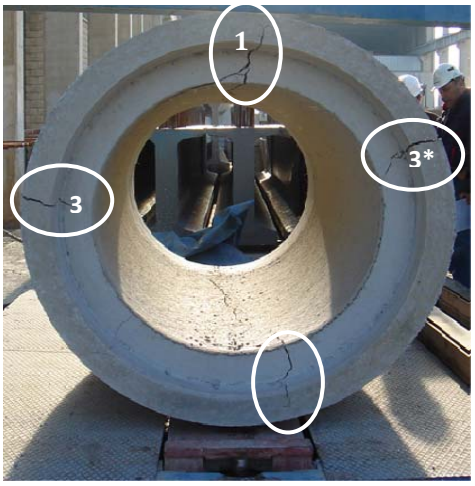

Fig. 5. Failure mechanism with the four non-linear hinges in a pipe with $D_i = 1000$ mm.

5.4. Experimental campaign

Several series of fibre reinforced concrete pipes (FRCP) with D_i of 1000 mm, thickness (h) of 90 mm and length (l) of 1.5 m were produced. Different amounts and types of fibres (plastic and steel) were used with the purpose of verifying aspects like: (1) the possibility of producing FRCP up to that diameter with no need for introducing important modifications in the production systems; (2) comparing the mechanical response in the CT of the different types of FRCP produced, and (3) verifying that it is possible to replace the whole conventional passive reinforcement with moderate amounts of fibres in some of the most commercial strength classes for this diameter. Reference [14] gathers all the details related to the process of manufacturing, the materials and the results from the tests carried out.

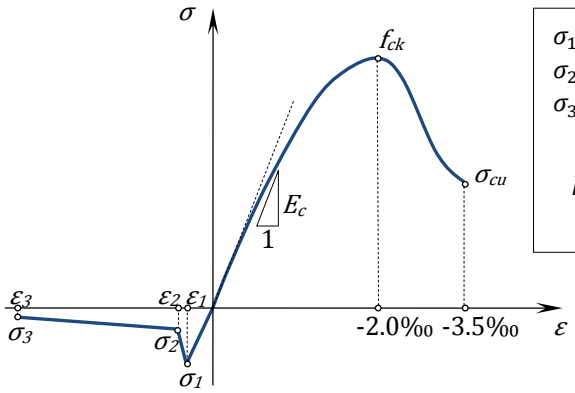

$$\sigma_1 = 0.7 f_{ctm,fl}(1.6 - d) \qquad \varepsilon_1 = \sigma_1 / E_{cm}$$
$$\sigma_2 = 0.45 f_{R,1} k_h \qquad \varepsilon_2 = \varepsilon_1 + 0.01\%$$
$$\sigma_3 = 0.37 f_{R,4} k_h \qquad \varepsilon_3 = 2.5\%$$
$$k_h = 1.0 - 0.6 \frac{h[cm] - 12.5}{47.5} \quad |12.5 \le h < 60|$$

Parameters used to simulate the tension behaviour of SFRC [33]

Fig. 6. Constitutive models used to simulate the mechanical behaviour of SFRC.

The SFRCP manufactured with steel fibres of the type DRAMIX® RC80/60BN (length l_f = 60 mm, diameter d_f = 0.75, Young modulus E_f = 210000 N/mm² and a tensile strength f_{fu} = 1100 N/mm²) are chosen in order to compare results from other pipes (D_i = 600 mm and D_i = 800 mm) produced and tested within other campaigns using the same type of fibres.

Three reference unreinforced concrete pipes (UCP) were manufactured. Moreover, nine SFRCP were produced with the following content of fibres: 20 kg/m³, 25 kg/m³ and 35 kg/m³, three specimens for each (P1, P2 and P3). All twelve pipes were produced by means the vibrocompression method in one single day. This was done in order to avoid the influence of the variability of the concrete time-dependent mechanical properties. Table 1 shows the mix proportion used for the production of the pipes, the water/cement ratio being the average value used in all twelve pipes.

Table 1. Mix proportion of concrete.

Material	(kg/m³)
Portland Cement	320
Crushed Sand	780
Coarse Aggregate	1200
Water/cement ratio*	0.41

On the one hand, the compressive strength tests carried out on cylindrical specimens [14] show that the concrete used fits within the C35/45 class defined in [28]. On the other hand, the pipes were tested at the age of 28 days by the CT (see Fig. 1), following the guidelines given by EN 1916:2002 [10] for the execution of the cyclic test. The displacement v was measured by means of two LVDTs placed at the spigot and the socket of the pipe, respectively, adopting the average value as the reference. Fig. 7 shows the F-v curves obtained in the CT for the SFRCP with D_i of 1000 mm and with (a) 20 kg/m³, (b) 25 kg/m³ and (c) 35 kg/m³. The value of the F load shown in the curves is obtained by dividing the experimental value of F by the length of the pipe (1.5 m) and by its internal diameter (1 m). It should be noted that the snap-through phenomenon associated with the cracking of the ridge and the haunches is not as sharp as the one detected numerically (see Fig. 3). This is due to the fact that the displacement v considered corresponds to the average value among the ones measured in the spigot and the socket of the pipe for the same F load. In this respect, the stiffness of the latter is higher than that of the spigot and, therefore, this instantaneous loss of stiffness is softened with regard to the numerical simulations (the pipe is simulated with a constant D_i). Reference [13] gathers the experimental and numerical results from pipes with D_i = 600 mm, where the phenomenon just described is more evident.

On the basis of the results shown in Fig. 7, it is deduced that:

- The average value of the cracking load $F_{r,cr}$ of the three series of SFRCP is 48 kN/m², and it is practically independent of the C_f. This value is detected in the F-v curves with the first slope change.

- The three series of pipes show a softening-type behaviour similar to that of case B in Fig. 3, $F_{s,cr}$ being the F_u load. However, SFRCP with C_f = 35 kg/m³ show a tendency towards a hardening post-failure response (case C, Fig. 3).

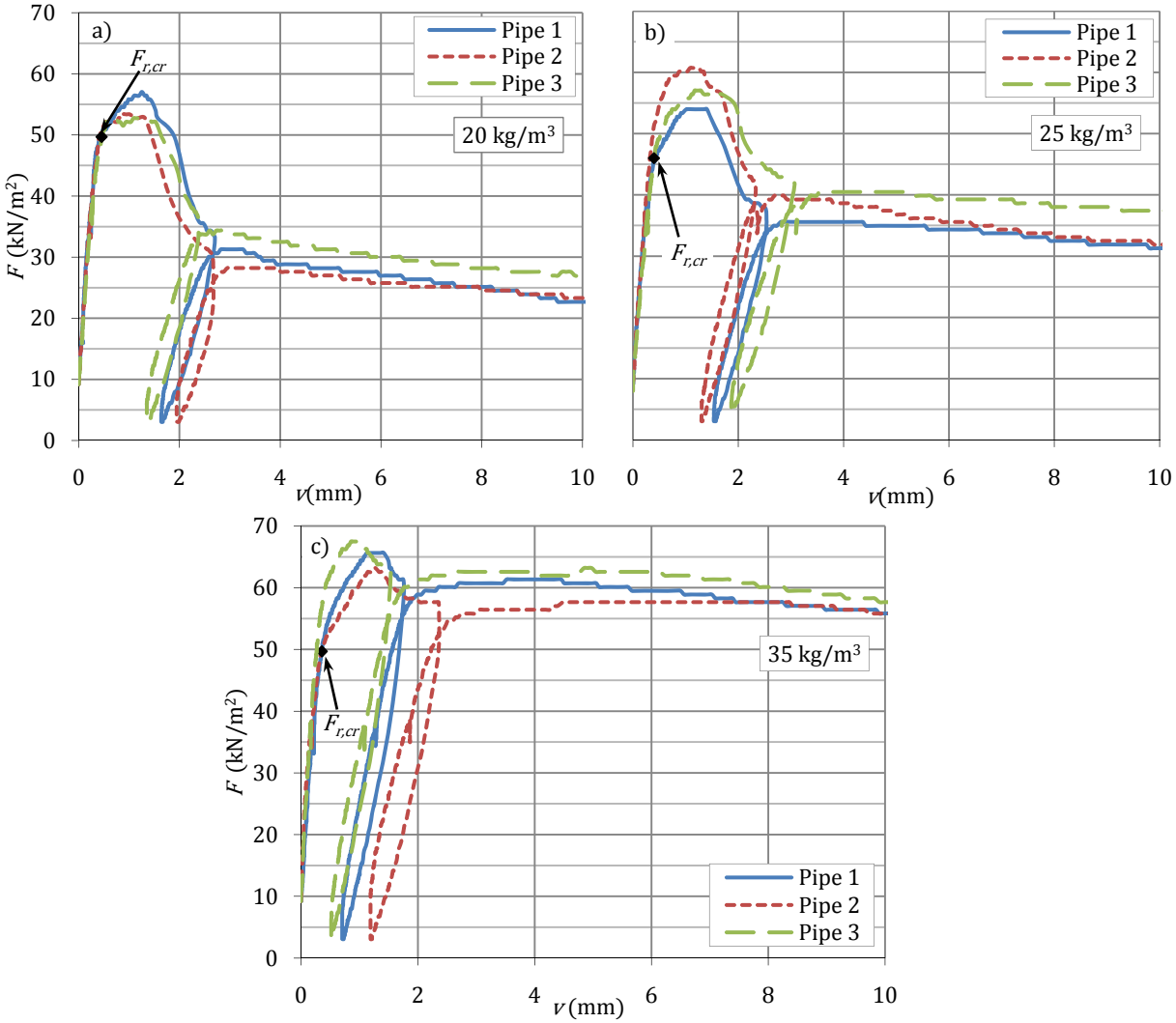

Fig. 7. F-v experimental diagrams for 1000 mm-D_i SFRCP: a) 20 kg/m³, b) 25 kg/m³ and c) 35 kg/m³.

Table 2 gathers the values of F_u and $F_{max,pos}$ reached in all test, as well as their average values (μ_F) and the coefficients of variation ($c_F = \sigma_F/\mu_F$, where σ_F is the standard deviation).

Table 2. Values for F_u and $F_{max,pos}$ obtained in the CT for each pipe.

C_f (kg/m³)	F_u (KN/m²)					$F_{max,pos}$ (KN/m²)				
	P1	P2	P3	μ_{Fu}	c_F (%)	P1	P2	P3	$\mu_{Fmax,pos}$	c_F (%)
0	53	54	48	52	6.2%	-	-	-	-	-
20	59	55	54	56	4.4%	32	29	35	32	9.8%
25	56	63	59	59	5.9%	36	40	41	39	6.9%
35	64	63	66	64	2.9%	62	59	58	60	3.8%

Taking into account the average values of F_u and $F_{max,pos}$ presented in Table 2, it can be stated that, making use of the CT as an indirect design method, a C_f slightly higher than 25 kg/m³ is required in order to reach the C60 strength class (F_c = 40 kN/m² and F_n = 60 kN/m²) defined in [10] without the need to incorporate

conventional steel bars. Likewise, it is highlighted that the coefficients of variation obtained for the different values of C_f are low (an average value of 4.9% and 6.8% for F_u and $F_{max,pos}$, respectively) in comparison to the dispersions produced in the strength response from other elements of SFRC. In this case, this low coefficient of variation can be due to the fact that the cracking regime and the post-failure regime are governed by only two and four main cracks (hinges), respectively. Thus, the influence of both the fibre distribution and the orientation is hardly reduced. There is still a lack of information concerning the influence of the industrial processes associated with the manufacturing of SFRCP on the content, distribution and orientation of the fibres within the pipe. However, some ongoing research lines [30-31] could shed some light on the doubts in relation to these aspects.

Fig. 8 shows the experimental F_u-C_f and $F_{max,pos}$-C_f diagrams for the SFRCP with D_i of 1000 mm. It can be observed that the individual experimental results fit properly with a linear tendency ($R^2 = 0.706$ for F_u and $R^2 = 0.961$ for $F_{max,pos}$) for the range of C_f between 20 – 35 kg/m^3. At a design level, a relevant application of these curves consists of estimating the value of C_f from which the response with hardening (type C described in Fig. 3) would appear. For this particular pipe ($D_i = 1000$ mm and $e = 90$ mm), the intersection point of the experimental diagrams F_u-C_f and $F_{max,pos}$-C_f (see Fig. 8) provides a minimum value of $C_f = 39$ kg/m^3.

5.5. Numerical simulation

The numerical model MAP [13] was used to simulate the response of the SFRCP with diameters of 600 mm [13], of 800 mm [9] and of 1000 mm subjected to CT. All SFRCP were built using the same type of fibre, described in the previous section.

In order to define the post-cracking behaviour of SFRC, Eqs. 1 and 2 suggested in [26] were used to obtain the residual flexural strength of SFRC ($f_{R,i}$) associated with each C_f. These equations were experimentally adjusted using the same type of fibres used in the tested pipes analyzed in this work. Therefore, on the basis of the estimated values of $f_{R,i}$ for each C_f, the σ-ε diagrams [28] were deduced in MAP to simulate the tensile behaviour of SFRC (see Fig. 6).

$$f_{R,1} = 0.0945 C_f + 0.702 \quad (1)$$

$$f_{R,4} = 0.926 f_{R,1} \quad (2)$$

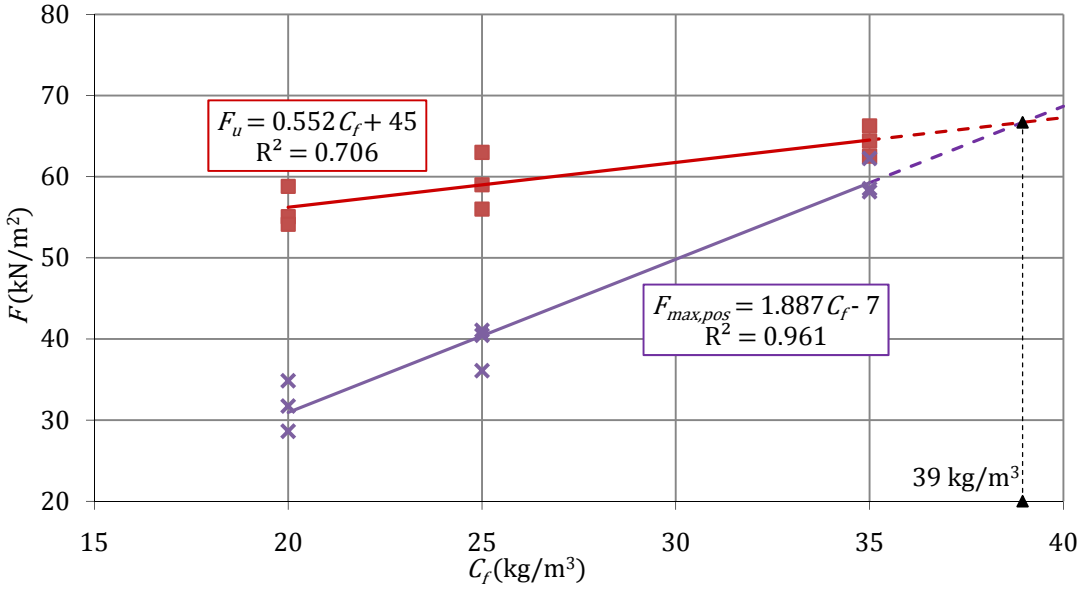

Fig. 8. F-C_f experimental diagrams.

The average values of F_u and $F_{max,pos}$ obtained in the tests and by using MAP are presented in Table 3, where ξ stands for the relative error of the numerical value with regard to the experimental one. Positive values of the latter indicate that the experimental value is higher than the numerical one, and vice versa. Likewise, Table 3 details the type of behaviour obtained by means of the numerical model for each pipe, taking into account the classification introduced in Fig. 3.

Table 1. Experimental and numerical results.

Geometry	C_f (kg/m³)	Concrete Strength Class [33]	CODE	F_u (kN/m²)			$F_{max,pos}$ (kN/m²)			Type of Response
				Experim.	MAP	ξ(%)	Experim.	MAP	ξ(%)	
D_i = 600 mm e = 72 mm	10	C50/60	600/72-10	56	48	14.3%	40	37	7.5%	B
	20		600/72-20	60	52	13.3%	49	46	6.1%	B
	40		600/72-40	69	66	4.3%	69	66	4.3%	C
D_i = 800 mm e = 92 mm	10	C40/50	800/92-10	76	75	1.9%	41	38	7.3%	A
	20		800/92-20	87	82	5.7%	63	57	9.5%	B
	25		800/92-25	92	88	4.3%	77	66	14.3%	B
	30		800/92-30	92	91	1.1%	81	75	7.4%	B
	35		800/92-35	97	96	1.0%	89	85	4.5%	B
	40		800/92-40	95	100	-5.3%	88	92	-4.5%	B
D_i = 1000 mm e = 90 mm	0	C35/45	1000/90-0	52	51	1.1%	-	9	-	A
	20		1000/90-20	56	51	8.4%	32	33	-3.1%	B
	25		1000/90-25	59	53	10.7%	39	39	0.0%	B
	35		1000/90-35	64	58	9.5%	60	53	11.7%	B

The numerical simulations highlight that the mechanical response of the pipes from the series 600/72-10, 800/92-10, 1000/90-0 and 1000/90-20 (D_i/h-C_f) in the CT correspond to a behaviour of the type A from Fig. 3 ($F_{r,cr} = F_u$). The remaining pipes show a type B behaviour ($F_{s,cr} = F_u$), except the pipes from the series 600/72-40 which show a type C behaviour. For the latter series, a quasi-perfect plastic behaviour was obtained after the detection of the failure load F_u (with values of $F_{max,pos}$ slightly higher than $F_{s,cr}$) both in the experimental tests and in the numerical simulation.

Further conclusions from the results shown in Table 3 are:

- The maximum value of the error ξ detected for F_u is 14.3% (600/72-10), whereas the minimum value is -5.3% (800/92-40), the average value being 5.4%. Consequently, in this study MAP tends to underestimate the F_u load of the system, possibly due to the fact that the Eqs. 1 and 2 used for the calculation of the $f_{R,i}$ lead to safe results.
- The maximum value of the error ξ obtained in $F_{max,pos}$ is 14.3% (800/92-25), and the minimum value is -4.5% (800/92-40). In this case, the average value of ξ is 5.2%, which leads to the conclusion that MAP also tends to underestimate the $F_{max,pos}$ load.

Taking into account the values of ξ obtained, it can be stated that the correlation between the experimental and the numerical values is acceptable for design purposes for D_i equal or lower than 1000 mm.

5.6. Using MAP as a tool for the design of SFRCP

The design of the reinforcement of a SFRCP by means of the CT, fixing the geometry (D_i and h) and the strength class of the pipe, can be a time consuming and economically expensive process, depending on the experience of the manufacturers. If the same type of pipe has been already produced by the manufacturer, an initial value of C_f is known, and consequently the process of trial and error requires less testing. This will be true as long as the nature and the properties of the aggregates as well as the type of fibres are maintained with regard to previous experiments. Nevertheless, in most cases the manufacturers do not

have former experience, since the possible commercial combinations of D_i, h and strength classes are numerous and, in consequence, a high number of tests could be needed to guarantee an optimal value of C_f. Apart from all that, there is also the fact that, up to now, no national regulation has established values for the amounts of C_f in SFRCP.

In order to improve this current framework, the MAP is proposed as a tool so as to make it easier for the manufacturers to design these elements. The strategy consists in using the MAP to obtain a reliable initial value of C_f (by means of the F_u-C_f and $F_{max,pos}$-C_f curves) for the D_i, h, type of fibres and strength class the manufacturers must work with. In this way, the initial uncertainty regarding the value of C_f is considerably reduced and, therefore, so does the number of tests necessary in order to adjust its optimal value.

As an example of how can this process implemented, the results obtained with the MAP for the pipes 600/72, 800/92 and 1000/90 (see Table 3) will be used to adjust the F_u-C_f and $F_{max,pos}$-C_f curves which will provide the values of C_f necessary to reach the strength classes C60 (F_c = 40 kN/m² and F_n = 60 kN/m²) and C90 (F_c = 60 kN/m² and F_n = 90 kN/m²). These classes are widely used in those diameters for the transportation of drainage and rainwater.

Figs. 9a, 9b and 9c show the previously mentioned curves for the SFRCP with geometry 600/72, 800/92 and 1000/90, respectively. In the case of pipe 600/72 (Fig. 9a) class C60, the procedure has been graphically illustrated.

The results gathered in Figs. 9a, 9b and 9c corroborate that the linear tendency fits perfectly the individual numerical values, showing R^2 coefficients higher than 0.98 in all cases. This is due to the fact that the relations $f_{R,1}$-C_f and $f_{R,4}$-C_f are linear, and the compression behaviour of concrete is also linear for the range of displacements v (lower than 10 mm) which has been fixed. On the other hand, it should be noted that the relation F_u-C_f for pipe 1000/90 (Fig. 9c) has a horizontal segment (values of C_f for which the response is of the type A, $F_{r,cr} = F_u$) and a sloping one (values of C_f for which the response is of the type B, $F_{s,cr} = F_u$).

Once the relations F_u-C_f and $F_{max,pos}$-C_f have been obtained for each geometry, they can be used for the deduction of the minimum values of C_f necessary in order to reach the stipulated loads (F_c and F_n) in each of the strength classes defined by the EN 1916:2002 [10]. For the analysis, a maximum value of C_f = 60 kg/m³ has been considered for technical and economic reasons.

Table 4. Minimum C_f necessary to reach the strength classes C60 and C90 for each of the SFRCP geometries.

SFRCP geometry	Strength Class	$C_{f,Fu}$	$C_{f,Fmax,pos}$
600/72	C60	31	13
	C90	>60	34
800/92	C60	0	11
	C90	28	22
1000/90	C60	38	25
	C90	>60	42

The analysis of the individual results from Table 4 leads to conclude that:

- For a type 600/72 pipe, 31 kg/m³ of fibres would be enough to reach the class C60, whereas class C90 requires a fiber content larger than 60 kg/m³, unless the value of h were increased or a cage of conventional reinforcement were additionally introduced.
- For a type 800/92 pipe, only 11 kg/m³ of fibres would be needed in order to fulfil the minimum post-failure load requirement ($F_c = F_{min,pos}$ = 40 kN/m²) established for class C60, whereas the F_n load (60 kN/m²) can be withstood even by an UCP. However, in the case of class C90, the F_n load (90 kN/m²) is the most restrictive one and 28 kg/m³ are needed in order to meet such a requirement.
- For a type 1000/90 pipe, an amount of fibres of at least 38 kg/m³ is needed to reach the F_n load (60 kN/m²) required in class C60, the most restrictive condition. Likewise, more than 60 kg/m³ would be needed to reach class C90. This is due to the fact that the value of h used (90 mm) is low in comparison

with the diameter of the pipe (1000 mm). In this respect, it has been proved (experimentally [7] and numerically by means of the MAP) that 25 kg/m³ of fibres would be enough in order to reach class C90 if a thickness of h = 120 mm (pipe 1000/120) were used.

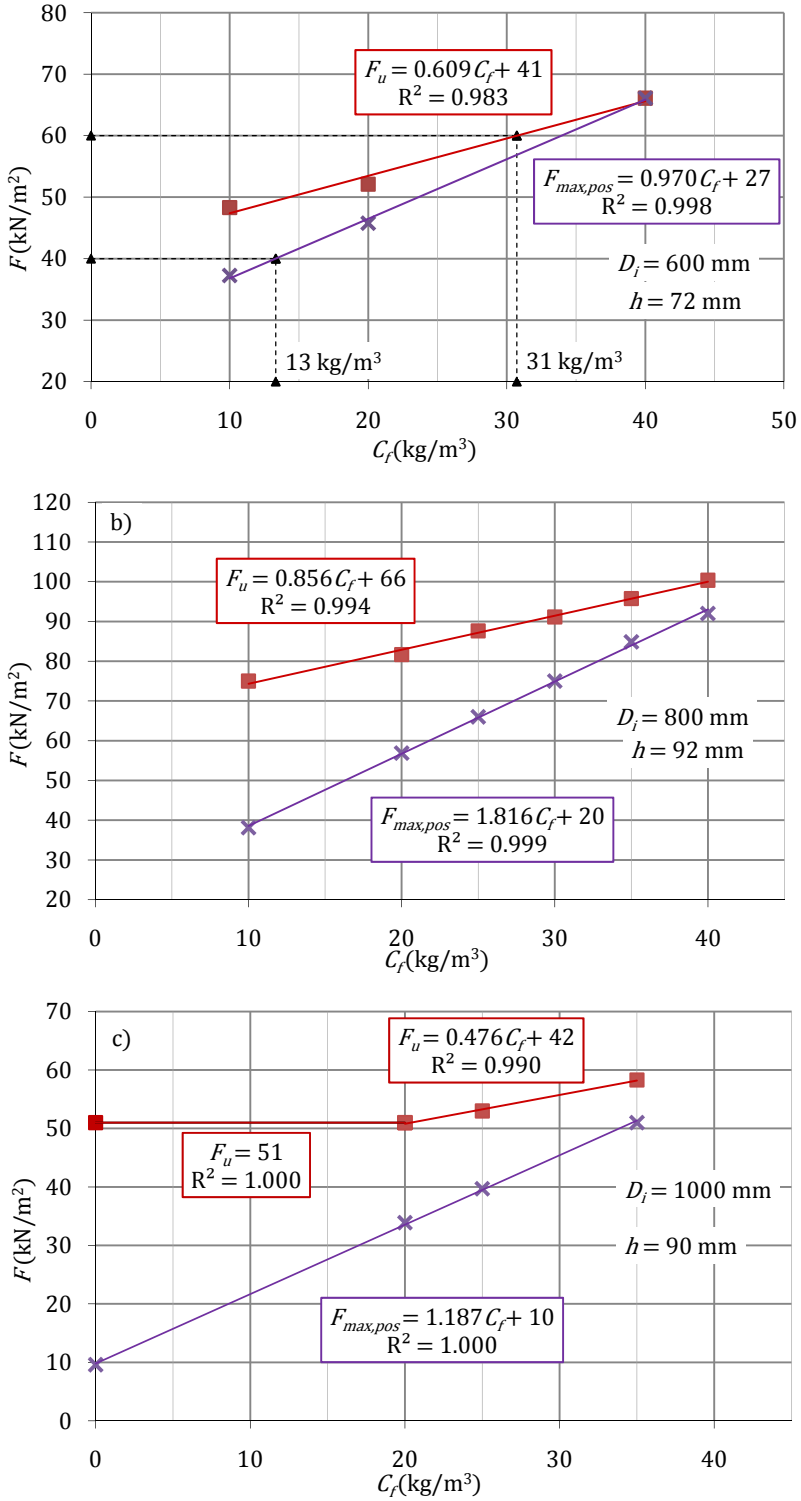

Fig. 9. F_u-C_f and $F_{max,pos}$-C_f diagrams obtained for: a) D_i = 600 mm, b) D_i = 800 mm and c) D_i = 1000 mm SFRCP.

This systematic procedure could be carried out with SFRCP with D_i up to 1000 mm and with any established h and strength class (maintaining some maximum values of C_f). In this way, the designers would have an initial design value of C_f at their disposal for each case. The study presented here dealt with a fixed type of fibres; however, the MAP and the procedure introduced are also valid for other types of fibres, as long as their tensile behaviour can be simulated with diagrams similar to those used in this study.

5.7. Conclusions

The MAP model simulates satisfactorily the mechanical response of SFRCP subjected to the CT. In the case of the pipes analysed in this paper, it tends to slightly underestimate their strength capacity compared with those obtained experimentally. Still, the average error for the F_u load and the $F_{max,pos}$ load is 5.4% and 5.2% respectively, and, in any case, on the side of safety.

The F_u-C_f and $F_{max,pos}$-C_f curves obtained by using MAP fit very well simple straight tendencies, thus simplifying the process of designing SFRCP for a particular strength class. Through these expressions, good estimations of the values of C_f corresponding to each strength class can be obtained.

Summarizing, the results obtained illustrate that both the numerical model and the methodology introduced in this paper are useful for designing SFRCP, helping thus to spread the use of SFRC in CP.

Currently, several experimental campaigns related to the use of concrete with fibres in CP are being developed. They aim at: (1) getting to know the structural response of concrete pipes reinforced with other types and amounts of fibres different from the ones used in this work, and (2) creating a large data base which would make it possible to validate the model for other types of concretes and geometries. Likewise, the MAP is expected to be updated with new constitutive equations [30-31] which can take into account the manufacturing procedure, the type of fibres and other relevant parameters as regards the simulation of the post-cracking behaviour of FRC.

5.8. Acknowledgements

The authors of this document wish to show their gratitude for the economic support received through the Research Project BIA2010-17478: *Construction processes by means of fiber reinforced concretes*.

Likewise, Prof. Antonio D. de Figueiredo wishes to thank the CAPES *Coordenação de Aperfeiçoamento de Pessoal de Nível Superior* for their support in awarding him the postdoctoral scholarship developed at the UPC, which made possible his participation in this research work.

Finally, Renata C. Escariz is grateful to the Fundação de Amparo à Pesquisa do Estado de São Paulo (FAPESP) for their support in awarding her the postgraduate scholarship.

5.9. References

1. Ministerio de Fomento 2009. Sewerage and drainage pipelines technical guideline. Ed. CEDEX, 2009. 635 p. [In Spanish].
2. Viñolas B. Applications and advances of the MIVES methodology in multicriteria decision analysis. PhD thesis, Universitat Politècnica de Catalunya, UPC, Barcelona (Spain), 2011.
3. Pedersen EJ. Fiber reinforced concrete pipes. UNICON beton I/S. December 1992.
4. Parrot, J. Sustainability research in sewerage pipes. Minor Thesis, Universitat Politècnica de Catalunya, UPC, Barcelona (Spain), 2008.

5. Figueiredo AD, Chama Neto PJ. Mechanical performance evaluation of pipes. Revista DAE 2008;**178**:34-9.

6. Haktanir T, Ari K, Altun F, Karahan O. A comparative experimental investigation of concrete, reinforced-concrete and steel-concrete pipes under three-edge-bearing test. *Const build mat* 2007;**21**(8):1702-08.

7. de la Fuente A, Armengou J. Structural applications of FRC: Concrete pipes, sandwich panels and earth retaining panels. *Technical Symposium 2007-JT-02,* Universistat Politècnica de Catalunya, UPC, Barcelona (Spain), 2007.

8. Fraay ALA, Venstermans J, Nemegeer D. Berekening van staalvezelbetonbuizen. *Civiele Techniek* 1983;**38**(1). [In Flemish].

9. Figueiredo A. Evaluation of the test method for crushing strength of steel fibre reinforced concrete pipes. *7th International RILEM Symposium on Fibre Reinforced Concrete*, Chennai (India), 2008.

10. EN 1916:2002. Concrete pipes and fittings, unreinforced, steel fibre and reinforced. 2002.

11. ACPA. Concrete pipe handbook. 8th pr. Vienna, VA; 2005.

12. de la Fuente A, Aguado A, Molins C. Diseño óptimo integral de tubos de hormigón. *Hormig y Acero* 2010. [In press].

13. de la Fuente A, Figueiredo A, Aguado A, Molins C, Chama Neto PJ. Experimentation and numerical simulation of steel fibre reinforced concrete pipes. *Mater Construct* 2010. [In press].

14. Campos R. Comparative analysis of the mechanical performance of polypropylene and steel fibre reinforced concrete pipes. Projeto FASESP 2009/03982-3. Technical Report. Universidade São Paulo, Sao Paulo (Brasil), 2010. [In Portuguese].

15. As'ad S, Saxer A. Influence of Fiber Geometry on the Flexural Strength Performance of Steel Fiber Reinforced Concrete (SFRC), *Fibre Concrete* 2007, Prague (Czech Republic), 2007.

16. Laranjeira F. Design-oriented constitutive model for steel fiber reinforced concrete. PhD thesis, Universitat Politènica de Catalunya, UPC, Barcelona (Spain), 2010.

17. Heger FJ. A theory for the structural behaviour of reinforced concrete pipes, PhD thesis, Massachusetts Institute of Technology, MIT, Massachusetts (USA), 1962.

18. Pedersen EJ. Calculation of FRC pipes based on the fictious crack model. Technical University of Denmark, 1995.

19. Chiaia B, Fantilli AP, Vallini P. Evaluation of minimum reinforcement ratio in FRC members and application to tunnel linings. *Mater Struct* 2009;**42**(3):339-51.

20. Silva JL, El Debs MK, Beck AT. Reliability evaluation of reinforced concrete pipes in crack opening limit state. Revista DAE 2008;**1**(4):314-30.

21. Ulfkjaer J, Krenk S, Brinker R. Analytical model for fictitious crack propagation in concrete beam. ASCE *J. Eng Mech* 1995;**121**(1):7-15.

22. Vandewalle L. *et al*. Test and design methods for steel fiber reinforced concrete. Design of steel fibre reinforced using σ-w method: principles and applications. *Mater Struct* 2002;**35**(249):262-78.

23. Forbes J. Fictitious crack propagation in fiber-reinforced concrete beams. *ASCE J. Eng Mech* 2001;**127**(3):272-80.

24. Pedersen EJ. The moment-rotation relationship with implementation of stress-crack width relationships. Department of Structural Engineering. Technical University of Denmark, 1995.

25. Kooiman AG. Modelling steel fibre reinforced concrete for structural design. PhD thesis, Delft University of Technology, TU Delft, Delft (The Netherlands), 2000.

26. Barros JAO, Cunha VMCF, Ribeiro AF, Antunes JAB. Post-cracking behaviour of steel fibre reinforced concrete. *Mater Struct* 2005;**38**(1):47-56.

27. de la Fuente A, Aguado A, Molins C. Numerical model for the non linear analysis of precast and sequentially constructed sections. *Hormig y Acero* 2008;**57**(247):69-87. [in Spanish].

28. Vandewalle L. *et al*. Test and design methods for steel fibre reinforced concrete. σ-ε design method. Mater Struct 2003;**36**:560-7.

29. Barros JAO, Figueiras JA. Flexural behaviour of SFRC: Testing and modelling. *ASCE J Mater Civil Eng* 1999;**11**(4):331-9.

30. Laranjeira F, Grünewald S, Walraven J, Blom C, Molins C, Aguado A. Characterization of the orientation profile of steel fibre reinforced concrete. RILEM Mater and Struct 2010. [In press].

31. Laranjeira F, Molins C, Aguado A. Predicting the pullout response of inclined hooked steel fibers. Cem Concr Res 2010;**40**(10):1471-87.

CAPÍTULO 6

Conclusiones y perspectivas futuras

6.1. Conclusiones generales

El empleo de fibras con carácter estructural como complemento o incluso como alternativa a los sistemas tradicionales de refuerzo del hormigón (armaduras pasivas y/o activas), es una estrategia que está demostrando conducir a resultados atractivos desde el punto de vista técnico y económico para numerosas tipologías estructurales. Bajo esta perspectiva, la presente Tesis Doctoral tiene un carácter generalista y en la misma se han tratado aspectos relacionados con el análisis de la viabilidad del uso de fibras en varios elementos de interés como aspectos asociados al análisis estructural y el diseño de éstos teniendo en cuenta la particularidad del empleo de fibras. Entre estas aplicaciones, el grueso del trabajo se centra principalmente en las tuberías de hormigón; si bien, también se incluyen los avances logrados en paneles de hormigón para muros de tierra armada y en dovelas de hormigón prefabricado.

Del conjunto de trabajos realizados, publicados o en proceso de revisión, que conforman la presente tesis doctoral, se derivan las siguientes conclusiones de carácter general.

Análisis de secciones

El modelo numérico desarrollado para abordar el análisis de secciones Análisis de Secciones Evolutivas (AES, del inglés Analysis of Evolutionary Sections) ha resultado ser una herramienta potente, versátil y adaptable a diferentes tipos de secciones (compuestas por varios hormigones y/o mixtas y con la posibilidad de simular el refuerzo con armaduras activas y/o pasivas e incluso fibras). Parte de dicha herramienta es fruto de los trabajos llevados a cabo en el marco de la Tesina de Especialidad presentada y

defendida por el mismo autor de esta Tesis Doctoral. Si bien, de cara a dotar de mayor generalidad y potencia de cálculo al modelo numérico, se han realizado varias ampliaciones. De entre éstas, la más relevante ha consistido en la implementación de ecuaciones constitutivas que permiten tener en cuenta el comportamiento post-fisuración del HRF (ver Anejo D).

En esta línea, hay que resaltar que al no estar aún contempladas las fibras con una visión estructural en muchas de las normativas de estructuras de hormigón, son escasas las experiencias reales en las que se han empleado fibras como material de refuerzo del hormigón, teniendo en cuenta su contribución estructural y que hayan sido publicadas en la literatura técnica. Esta es una de las principales motivaciones que han conducido a empresas internacionales, como CEMEX por ejemplo, a interesarse por el modelo AES y a incorporar una versión simplificada de éste en su propia página web. Asimismo, se está desarrollando una versión docente que será empleada por los alumnos de grado y de máster de la Escuela de Caminos Canales y Puertos de Barcelona a partir del curso 2011-2012.

Tubos de hormigón armado

El modelo llamado Análisis de Tubos de Hormigón (ATH) desarrollado también en el marco de la presente Tesis Doctoral para el análisis estructural de tubos de hormigón armado, ha resultado ser una herramienta muy atractiva para el diseño óptimo de este tipo de elementos frente a los métodos tradicionales disponibles. El modelo ATH permite la simulación del ensayo de aplastamiento de tubos de hormigón armado de cualquier diámetro y configuración de refuerzo e incorpora el modelo AES como herramienta para el análisis de secciones.

Con el modelo ATH es posible diseñar la estrategia de armado óptima para alcanzar los requisitos estructurales fijados en proyecto. En definitiva, con el planteamiento de diseño propuesto en esta Tesis Doctoral se supera la práctica más extendida y consistente en el uso de tablas de diseño (función de la geometría del tubo y de la clase resistente deseada) junto con el ensayo de aplastamiento como método de control de la resistencia del tubo. En ocasiones, dichas tablas de armado sugieren configuraciones de armado con opción a mejora, sobretodo en diámetros de la gama comercial alta.

La validación del modelo ATH se ha llevado a cabo contrastado resultados experimentales recogidos en los registros de control de calidad de diferentes empresas nacionales (PRECON, S.A. y PREFRAGA) para distintas geometrías y configuraciones de armadura, obteniéndose correlaciones satisfactorias. Ello ha motivado posteriores estudios de optimización en tubos de gran diámetro para los cuales o bien no existe configuración de armadura tabulada o bien se han empleado hasta la fecha cuantías muy superiores a las estrictamente necesarias. Concretamente, con el modelo ATH se ha diseñado la configuración de armado para los tubos de 2800 mm clase C-135 y C-180 de la red de saneamiento de 2300 m de longitud para el polígono Arco Sur (Zaragoza), lográndose reducciones de hasta un 30% de la armadura inicialmente propuesta en proyecto. Todos los tubos se han fabricado en la empresa PREFRAGA y los resultados del ensayo de tres aristas pusieron de manifiesto que el modelo ATH propone configuraciones de refuerzo del lado de la seguridad, con diferencias entre los resultados experimentales y los numéricos que no superan el 10% de error relativo, concluyendo por lo tanto que se trataba de cuantías de refuerzo próximas al óptimo estructural y económico.

En consecuencia, se deriva que el modelo es una herramienta adecuada para el diseño óptimo de tubos de hormigón armado y que puede substituir y/o complementar el método tradicional basado en el uso de tablas de diseño.

Tubos de hormigón armado con fibras

En paralelo con los avances relacionados con la simulación y la experimentación de tubos de hormigón armado, también se ha ahondado en el uso de fibras estructurales para el refuerzo del hormigón frente a las tracciones. Actualmente, algunas normativas específicas de tubos de hormigón ya incluyen las fibras como material de refuerzo, si bien, no se proponen cuantías mínimas para cada uno de los diámetros y clases resistentes comerciales. Consecuentemente, los proyectistas deben acudir a métodos indirectos de diseño prueba y error que, a la postre, pueden conducir a un encarecimiento del producto final y a un rechazo del uso de fibras en esta aplicación.

Para hacer frente a esta situación, en esta Tesis Doctoral se ha presentado la primera metodología para el dimensionamiento de tubos de HRF basada en el uso Model for the Analysis of Pipes (MAP); un modelo

implementado para simular la respuesta de tubos de HRF en el ensayo de tres aristas y que incluye también la subrutina AES. El modelo se ha contrastado con una amplia campaña experimental de tubos, desarrollada conjuntamente con la Universidad de Sao Paulo, consistente en la fabricación y ensayo de un total de 85 tubos de diámetro de entre 600 mm y 1000 mm con distintas cuantías de fibras, obteniéndose coeficientes de correlación excelentes entre los valores numéricos y los experimentales. Las conclusiones principales obtenidas en esta parte del trabajado han sido que:

- Es posible emplear fibras sin que ello conduzca a alteraciones significativas en las dosificaciones y en los métodos de fabricación.
- Es posible la eliminación total del armado en forma de barras por fibras manteniendo e incluso mejorando la respuesta en régimen fisurado y de rotura (en tubos de hasta 1000 mm de diámetro).
- La metodología de diseño conduce a cuantías de fibras muy cercanas al valor óptimo tanto estructural como económico, tal como corroboran los resultados experimentales.

En consecuencia, se puede afirmar que fruto de los trabajos realizados en el marco de esta Tesis Doctoral se ha conseguido plantear un enfoque de diseño de tubos de hormigón armado (con fibras y/o barras de acero) alternativo al método indirecto clásico. Su idoneidad y validez se ha contrastado con diversas campañas experimentales e, incluso, ya se ha aplicado en obras reales de envergadura con ahorros económicos importantes asociados al refuerzo del hormigón. En definitiva, todo indica que esta metodología puede conducir a importantes ventajas técnicas y económicas, así como a un impulso al uso de fibras en el refuerzo de tubos de hormigón.

6.2. Conclusiones específicas

En respuesta a los objetivos específicos fijados en el Capítulo 1, se presentan los diversos avances alcanzados en cada una de las líneas de investigación tratadas en esta Tesis Doctoral.

Desarrollo de un modelo de análisis de secciones

- El modelo AES, desarrollado para el análisis de secciones, permite simular la respuesta en el tiempo y hasta rotura de secciones compuestas por varios hormigones y mixtas de hormigón y acero. Asimismo, permite considerar su construcción evolutiva así como la posibilidad de emplear refuerzo activo y/o pasivo.
- Para la simulación del comportamiento en régimen post-fisuración de secciones de HRF se han implementado diversas ecuaciones constitutivas. Entre éstas, se han incorporado en el modelo AES las recogidas en los principales códigos normativos europeos (ver Anejo D).
- El modelo se ha contrastado con resultados experimentales recogidos en la bibliografía obteniéndose correlaciones satisfactorias con los resultados numéricos en régimen de respuesta lineal, fisurada y en rotura.
- El modelo se ha implementado de forma modular, de modo que puede ser ampliado con nuevos modelos de comportamiento del material y, más importante aún, se puede incorporar como subrutina de cálculo seccional en modelos generales de barras.

Avances en tuberías de hormigón armado convencionales

- Se han recopilado los registros de resultados obtenidos en el ensayo de tres aristas de tubos de hormigón armado convencional llevados a cabo por dos empresas nacionales de fabricación de tubos. Tras el análisis de los mismos, así como de los métodos de diseño empleados en cada caso, se ha concluido que en ocasiones el refuerzo está sobredimensionado, que hay margen de mejora en la mayoría de los casos y que es posible optimizar el armado de estos elementos.
- La idoneidad de las hipótesis de comportamiento de los materiales y de la respuesta estructural implementadas en el modelo ATH se han verificado contrastando los resultados experimentales para diversos diámetros y configuraciones de armado, obteniendo buenas correlaciones entre éstos y los resultados numéricos.

- El modelo ATH se ha empleado como herramienta para el diseño del refuerzo de tubos de 2800 mm de diámetro clase C-135 y C-180 destinados a una obra real. Se ha obtenido una configuración de refuerzo consistente en 20.3 cm^2/m en la cara interna del tubo y 10.7 cm^2/m en la cara externa para el tubo clase C-135 y de 22.5 cm^2/ml y de 18.0 cm^2/m, respectivamente, para el tubo clase C-180. Estas densidades de armadura suponen un ahorro del 29.9% (C-135) y de un 26.7% (C-180) de la cuantía de acero respecto a la solución empleada hasta la fecha para cada clase resistente.
- El plan de control de calidad de dichos tubos de 2800 mm de diámetro, armados con la configuración de refuerzo propuesta en base al modelo ATH, incluía el ensayo de 10 tubos (3 clase C-135 y 7 C-135). Los resultados experimentales han puesto de manifiesto que el modelo ATH propone cuantías de armado que están del lado de la seguridad, si bien las diferencias entre los resultados experimentales y los numéricos son de un 9.2% y de un 3.9% para los tubos clase C-135 y los clase C-180, respectivamente, concluyéndose que el modelo es adecuado para el diseño del refuerzo de tubos de hasta este rango de diámetros.
- Teniendo en cuenta las excelentes correlaciones obtenidas entre los resultados experimentales y los resultados numéricos obtenidos mediante el modelo ATH, se propone éste último como herramienta para el diseño óptimo de tubos de hormigón. En definitiva, con el modelo ATH se pueden reestructurar y rediseñar las tablas de armado utilizadas hasta la fecha teniendo en cuenta: (1) los parámetros mecánicos de los hormigones y del acero empleados en cada planta, (2) los recubrimientos de la armadura realmente empleados, y (3), las condiciones de apoyo de la prensa empleada en cada laboratorio de control interno. Todo ello permitiría adecuar el diseño de los tubos a los requerimientos mecánicos particulares para cada proyecto, optimizar los materiales empleados para cada diámetro y clase resistente, y, por último, reducir el número de ensayos necesarios para obtener el armado óptimo para cada configuración geométrica (diámetro y espesor) y para cada clase resistente. Todo ello conduciría a importantes ahorros económicos y a un salto cualitativo en el ámbito tecnológico de las tuberías de hormigón armado.

Avances en tuberías de hormigón armado con fibras estructurales

- El modelo MAP permite simular la respuesta de tubos de hormigón reforzado con fibras de hasta 1000 mm de diámetro sometidos al ensayo de tres aristas e incluye el modelo AES como subrutina de cálculo seccional. La hipótesis principal admitida en el modelo MAP consiste en considerar que la respuesta no lineal del tubo se puede describir mediante dos rótulas plásticas, que concentran los fenómenos no lineales, conectadas a través de un cuadrante de circunferencia que responde de forma lineal frente las acciones impuestas.
- Se han llevado a cabo varias campañas experimentales conjuntamente con la Universidad de Sao Paulo (Brasil) asociadas a la fabricación y al ensayo de tubos de 600 mm, 800 mm y 1000 mm de HRF con cuantías que oscilan entre los 10 kg/m^3 y los 40 kg/m^3. Las principales conclusiones obtenidas en estas campañas son: (1) que es posible el empleo de fibras sin que ello conduzca a cambios importantes ni en las fórmulas de dosificación del hormigón habitualmente empleadas ni en los sistemas de producción de los tubos; (2) que el ensayo de tres aristas realizado de forma continua conduce a resultados representativos del comportamiento post-rotura del tubo, y, (3), que es posible substituir totalmente el armado convencional por cuantías de fibras moderadas en los diámetros de la gama baja – media (hasta 1000 mm).
- Los resultados numéricos obtenidos con el modelo MAP, para los distintos diámetros ensayados y las distintas cuantías de fibras empleadas, han concordado de forma excelente con los resultados experimentales en todos los regímenes de carga. En este sentido, los resultados numéricos obtenidos están del lado de la seguridad, habiéndose obtenido un error medio del 5.4% para la carga de rotura y un 5.2% para la carga de pos-rotura estipulada para cada clase resistente.
- Teniendo en cuenta que ninguna de las actuales normativas nacionales de tubos de hormigón, que ya permite el uso de fibras como refuerzo, sugiere cuantías mínimas para los diámetros y clases resistentes comerciales, se propone una metodología de diseño basada en el uso del modelo MAP. Se trata de una alternativa muy atractiva en contraposición a la práctica profundamente arraigada y centrada en el uso sistemático del ensayo de tres aristas como método indirecto de diseño. La metodología propuesta consiste, principalmente, en obtener las relaciones carga última y carga post-

fisuración en función de la cuantía de fibras para una geometría fijada (diámetro y espesor). Con estas curvas, que en la mayoría de las ocasiones responden a tendencias sensiblemente lineales, puede obtenerse la cuantía de fibras óptima para garantizar los requisitos fijados en la clase resistente objetivo. Mediante esta estrategia se parte ya con un valor inicial de diseño para la cuantía de fibras (óptimo desde el punto de vista numérico), que posteriormente se corroborará en el ensayo de tres aristas. En definitiva, se trata de un método altamente útil, sobre todo cuando se pretende trabajar con geometrías y clases resistentes de las que no se tiene experiencia previa. En estas circunstancias, la cuantía óptima sugerida por el método propuesto permitirá reducir drásticamente el número de tanteos (probetas testadas en el ensayo de tres aristas) hasta hallar el óptimo estructural.

6.3. Perspectivas de futuro

En esta Tesis Doctoral se ha logrado realizar un avance considerable en el ámbito tecnológico de las tuberías de hormigón. Ello ha sido posible gracias también al apoyo y trabajo conjunto tanto con empresas de prefabricados del hormigón (PRECON S.A. como PREFRAGA) como con Universidades (Universidad de Sao Paulo), lo cual hace ser optimista y pensar que las propuestas realizadas tienen una alta probabilidad final de implementación. Si bien, aún quedan puntos en los que es necesario ahondar de cara a garantizar una perfecta implantación de dichas mejoras e, incluso, trabajar sobre otras que no se han tratado en este documento.

- Se ha considerado que los tubos de hormigón con fibras son un medio continuo y homogéneo, sin embargo, debido al proceso de hormigonado, vibrado y compactación del tubo, se producen concentraciones diferenciales de fibras, incluso en una misma sección de tubo. Estas acciones sobre el hormigón en estado fresco conducen a una distribución no homogénea del refuerzo, y por tanto, la hipótesis de homogeneidad considerada en el cálculo no se cumpliría de modo estricto. Asimismo, las fibras tienden a una orientación preferente debido al efecto pared (mayor cuanto menor es la relación entre el espesor de pared del tubo y la longitud de la fibra). Todos estos factores pueden alterar el comportamiento resistente del tubo y pueden justificar las sensibles diferencias entre los resultados experimentales y los resultados numéricos obtenidos con el modelo MAP, pues ninguno de ambos fenómenos se ha tenido en cuenta en la simulación del comportamiento mecánico del HRF. En este sentido, recientemente, en el mismo Departamento de Ingeniería de la Construcción de la UPC, se ha desarrollado una nueva ecuación constitutiva que permite simular la respuesta mecánica del HRF incorporando aspectos como: el método de hormigonado y las acciones en estado fresco. En definitiva, aspectos que posteriormente influyen sobre la orientación final de las fibras en estado endurecido. Así pues, resultaría altamente interesante implementar dicha ecuación constitutiva en el modelo AES y simular el comportamiento mecánico de los tubos atendiendo a que, en realidad, existe un fuerte efecto pared durante las operaciones de fabricación del tubo y que fuerzan una orientación preferente de las fibras.
- Las fibras estructurales empleadas en este trabajo han presentado un excelente rendimiento. No obstante, independientemente del diámetro del tubo, cuando se pretende alcanzar clases resistentes elevadas utilizando únicamente fibras como refuerzo, es necesario emplear altas cuantías, resultando económicamente poco atractivo. Para hacer frente a estos casos y poder generalizar el empleo de fibras para todos los diámetros y clases resistentes, se propone recurrir a la sinergia que se produce cuando se emplean fibras y armadura pasiva tradicional: las fibras cosen las fisuras, aumentan el número de éstas y reducen su ancho, y, por otra parte, las barras de acero garantizan la capacidad estructural del elemento en estados de pre-rotura y de rotura. El uso conjunto de ambos tipos de refuerzo permitiría reducir la cuantía total de acero dispuesto respecto las soluciones tradicionales. Para abordar el análisis de viabilidad de dicha alternativa, se requiere hacer un estudio paramétrico profundo de las principales variables involucradas, para lo cual se puede emplear el modelo ATH desarrollado en esta tesis doctoral.
- Actualizar las cuantías de refuerzo propuestas en las tablas de diseño para tubos de hormigón armado tradicionales en base al modelo ATH. Al mismo tiempo, proponer una tabla con las cuantías mínimas de fibras necesarias, para los diámetros y clases resistentes en los que su uso es viable,

empleando la metodología propuesta en base al modelo MAP para tubos de HRF. Para esto último sería necesario también fijar unas características geométricas y mecánicas mínimas de las fibras.

APPENDIX A

Innovations on components and testing for precast panels to be used in reinforced earth retaining walls

A.1. Abstract

The present article introduces three innovations related to precast concrete panels to be used in reinforced earth-retaining wall systems. These innovations concern the anchor system of the panel, the set-up of the pull-out test to assess the effectiveness of the anchors and the use of fibres as reinforcement. The viability of all this innovations has been proved by an experimental research program. Results show the advantages of these innovations in terms of performance and of production process.

Keywords: Anchors; FRC; Precast panels; Pull–out test; Earth retaining walls.

A.2. Introduction

Reinforced earth retaining wall systems have proved their performance as a cost effective construction technique in a variety of applications (bridge abutments, mine dump walls, storage silos, haul road overpasses, containment dykes, dams, blast barriers, landscaping, among others).

The modern methods of soil reinforcement for retaining wall construction were pioneered by the French architect and engineer H. Vidal in the early 1960s. His research led to the invention and development of Reinforced Earth®, a system in which steel strips are used as the soil reinforcement element [see 1 and 2].

Since the constitution of Reinforced Earth® several other proprietary and nonproprietary systems have been developed and used, see [3] for a partial summary of some of the current systems by proprietary name, reinforcement type, and anchor system.

Research and developments have taken several directions including: the use of galvanised steel mesh reinforcement, geosynthetic reinforcement, earth compacting systems, experimental contrasting methods and external appearance for improving its aesthetics [4]. However, the knowledge generated about the anchor of the panels has not been published due to the market strategies followed by manufacturers. Fig. 1 shows one of the most commonly used anchor system in Spain that appeared in the market in the lasts decades.

Cracking of precast panels may occur during the demolding, transport and storage tasks, as well as during the service life of the panels [4]. In that sense, some kind of reinforcement has to be provided in order to control the crack width. Up to date, the use of steel rebars has been the traditional option so as to resist these tensile stresses. However, new trends have appeared as alternatives to the traditional reinforcement. The structural fibres, both metallic and synthetic, might be one of the most important examples. Several remarkable applications related to the use of fibre reinforced concrete (FRC) have been reported in the international literature [see 5-7 for a summary of different applications]. However, only a few examples related to the application of FRC in earth retaining structures have been previously published [7 and 8].

The main advantages offered by the use of fibres on these elements are:

- The control of the width of the superficial microcracks generated by the restrained shrinkage [9 and 10].
- The bridging effect of fibres in the cracks around the failure surface of the fastening elements. This phenomenon improves the internal behaviour to resist the punching shear action [11-13].
- A great capacity of energy absorption and deformability as well, to resist both static [14] and dynamic loads [15].
- The possibility of a partial or even a total substitution the steel rebars [16].

The mains goals of this article are: (1) study and also compare a new anchor system with the one traditionally used in Spain. (2) present a new test set-up to measure the pull-out response of the anchorage and (3) present and discuss the results of an experimental campaign which involves several variables like the concrete cover of the anchor and different types and configurations of reinforcement (rebars and steel or polypropylene fibres).

A.3. Anchor system

The connection between the strip and the precast panel could be solved with a U-shape anchor, hereinafter RE (see Fig. 1). Its use requires interposed steel plates with a double joint holding the strips as illustrated in Fig. 2.

Fig. 1. U-shape anchor system.

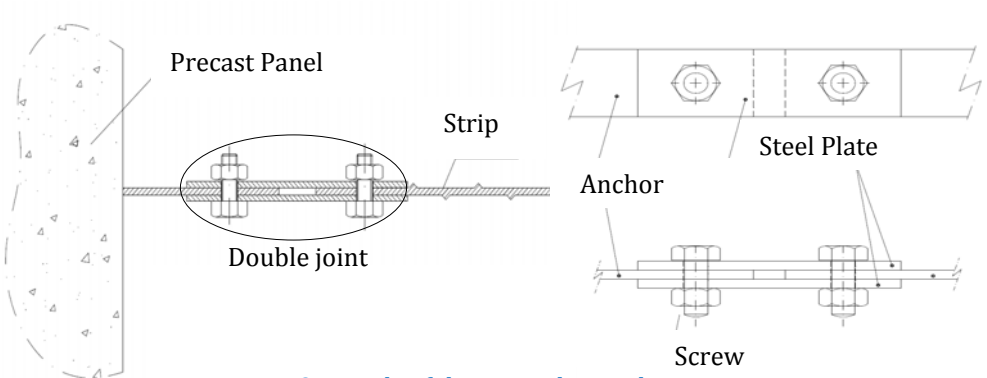

Fig. 2. Details of the RE anchor and its connection.

On the other hand, a pear-shape anchor (PS) (see Fig. 3) is being used by various precast panels manufacturers as an alternative to the traditional one. The new alternative presents the following related advantages in contrast with the RE anchor: (1) it requires a single pin for fastening the metal strip, which means time and cost reduction regarding the production of the panel; (2) the reduction of the number of joints leads to a decrease of the vulnerability facing the local forces originated as a consequence of incorrect manufacturing and accidental eccentricities (as it is presented in the results section).

Many different parameters may influence the structural response of the PS anchor; mainly: the inclination (φ) of the concrete failure surface, the concrete cover (c) and the maximum width of pear (s = 9.0 cm) (see Fig. 3). The average value of the angle φ ranges between 25° and 30° at failure for steel mesh reinforced slabs subjected to concentrated loads [17]. The improvement of the shear capacity and also the dowel action provided at FRC leads to an increase of φ [18 and 19]. Moreover, the experimental results show that c significantly affects the structural response of the anchor system. In that sense, the less concrete cover the greater volume of concrete involved in the failure conical surface.

In the research herein presented, the strip was not considered as a variable because it was the same that is commonly used in the standard solution.

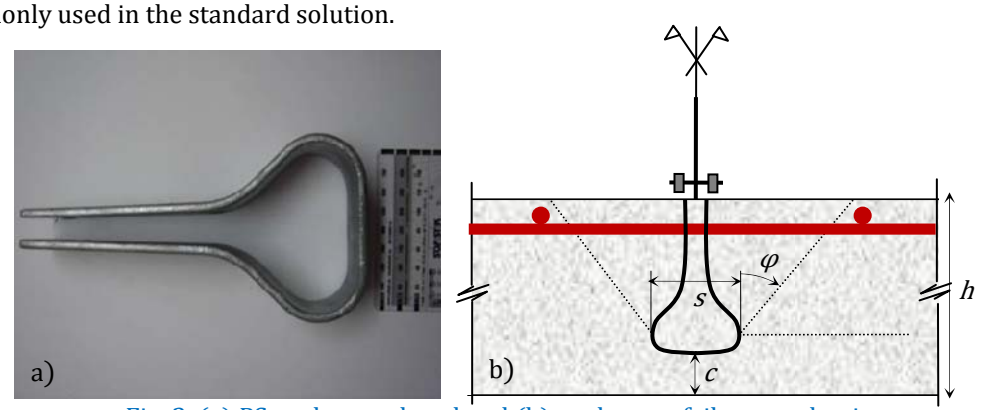

Fig. 3. (a) PS anchor analyzed and (b) anchorage failure mechanism.

A.4. New test proposal

There are several test set-ups for assessing the capacity and performance of this kind of anchors. Fig. 4 shows the one used by the Eduardo Torroja Institute of Construction Science (IETcc) in Spain. This set-up is well adapted to the equipments that are normally found in large laboratories. However, it requires large panels, thus the test preparation involves heavy weights. Panels can be either square or circular. The three point reaction frame (Fig. 4) has the advantage of providing experimental results with a low scattering.

Fig. 2. Anchor pullout test set-up from IETcc.

A new test configuration is proposed in this work. It consists of a square steel reaction frame (see Fig. 5) which can be easily transported (55.0 cm and 45 cm of external an internal length, respectively). The square specimens are supported on its four sides and have an external length of 55 cm. In consequence, the use of such reduced dimensions (approximately 3 times less in comparison with the traditional specimens used in IETcc) leads to: (1) a lighter and easier to manipulate specimen (requires 2 people at maximum, see Fig. 6), and (2) a reduction of the bending moments which can distort the desired pull-out boundary conditions.

The traditional RE anchor generates a wider contact area with the concrete specimen in comparison to the one proposed herein because its embedded length is significantly larger. In this sense, the mobilisation of a wider concrete volume implies: (1) larger dimensions of the panels to avoid distortions produced by the boundaries, and (2) lower average stresses when the RE anchor is subjected to identical pull-out force in respect with the PS anchor, causing a reduction of its structural efficiency. In consequence, the second one is more efficient from a structural point of view. This, however, does not imply that the failure load reached must be higher than the one obtained with the RE anchor since the dimensions of the latter are larger.

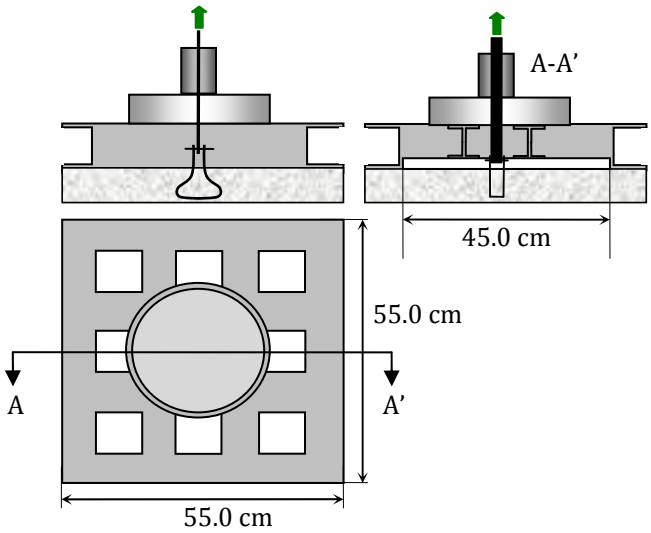

Fig. 5. Test configuration.

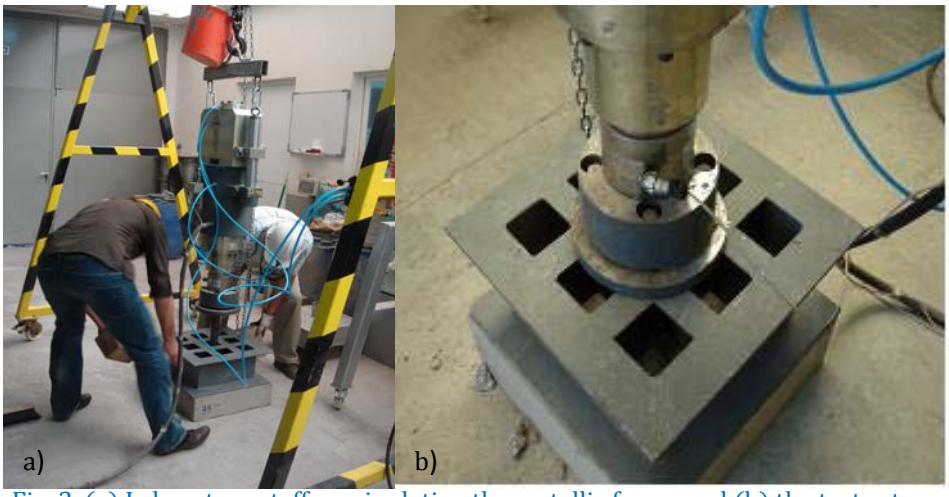

Fig. 3. (a) Laboratory staff manipulating the metallic frame and (b) the test set-up.

A.5. Experimental program

An experimental program was carried out aiming to: (1) prove the suitability of the PS anchor studied, (2) adjust and up-date the new test set-up described in section 3, and (3) to assess the contribution of the fibres in the structural response.

Several variables/cases were analyzed with the purpose of gaining knowledge regarding the general behaviour of the element during all the stages of the test:

- Relative position of the anchor element within the thickness of the specimen (cover c in Fig. 3).
- Type of fibre used in the mix. To that purpose, hooked-end steel fibres (S) and rolling polypropylene macrofibres fibres (P) have been applied taking into account their structural contribution (Table 1) gathers the main parameters of the fibre used in this experimental campaign).
- The use of a steel mesh or combined with fibres.

Table 1. Main parameters of the fibres used in the experimental campaign.

Property	**Steel Fibres** (S)	**Polypropylene Fibres** (P)
Length (l)	60 mm	45 mm
Equivalent diameter (d)	0.75 mm	0.95 mm
Aspect ratio (l/d)	80	47
Tensile strength (f_{max})	1050 MPa	400 MPa
Young modulus (E_f)	210 GPa	9 GPa

The experimental program involved the production of 33 specimens prepared with the dimensions indicated in Fig. 7 and based on the concrete mixtures presented in Table 2. The mixtures were designed according to those commonly used in the precast plant. This way of proceeding leads to satisfactory results in terms of the manufacturing process and is normally better accepted by the staff. However, it was necessary to introduce slight variations of the water content to improve the workability of the mixture when steel fibres were added.

It must be pointed out that no significant adjustment in the equipment was required. Notwithstanding, when working with a massive industrial production, it is convenient to have a fibre dispenser in order to accelerate the fibre weighing and pouring operations. The mixing times were similar both for the conventional concrete as well as for the FRC. No difficulties were observed during the mixing, even with the mixer at full capacity. Slump cone test [20] results were always over 20 cm, which confirms that a reasonable workability was achieved for carrying out the pouring and vibrating operations with the concrete mixtures defined in Table 2. The occluded air [21] of these mixtures was around 1.5%.

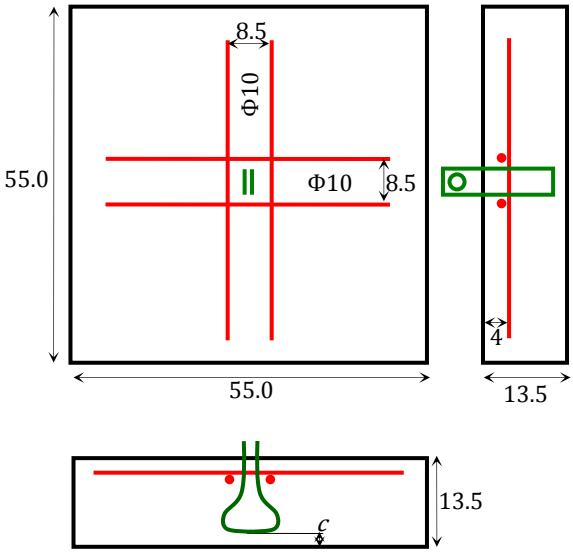

Fig. 7. Dimensions (in cm) of the specimens.

Table 2. Concrete mixtures for the panels in kg/m³.

Material	Mixture		
	M1	M2	M3
Cement I-52,5R	350	350	350
Sand 0/4 (in mm)	880	800	800
Gravel 4/20 (in mm)	1.000	1.080	1.080
Water	160	160	160
Steel Fibers	-	25	-
Polypropylene Fibers	-	-	5
Admixture Viscocrete 20HE	0,86	0,86	0,86

For each mixture, a set of 6 samples were prepared to determine the compressive strength in cylindrical specimens with a diameter of 15 cm and a height of 30 cm according to [22]. Compression tests were performed 22 hours after mixing the concrete in order to confirm if the minimum strength of 15 MPa required for demoulding the panels was reached. The average results obtained were 22.0 MPa, 17.4 MPa and 18.1 MPa for the plain concrete, SFRC and PFRC, respectively. Likewise, 12 cylindrical (15 cm of height and 15 cm of diameter) cores were extracted (6 for SRFC and 6 for PFRC) from the precast panels in order to characterize the tensile behaviour of the two FRC used in this experimental campaign. For this purpose, the Barcelona test [23] (see Fig. 8a) was performed since its use is already spreading in other applications [24] and it is presumed to present less scatter in comparison with other sort of tests [25]. The average results obtained are presented in Fig. 8b.

The results presented in Fig. 8b show that the SFRC cores reached an average maximum load (P_{max}) close to a 10% higher than the PFRC cores. Moreover, the energy dissipation in tension was 21% over the value obtained for the PFRC cores. Nevertheless, this value is a lower bound of that percentage because when drilling cores of SFRC specimens some fibres lose their hooked end.

Table 3 summarizes the different panels that were produced and the codification used (3 specimens per panel code). These codes respond to each one of the different variables considered:

- *Type of anchor*: RE for the traditional one and P for the PS anchor.

- *Type of reinforcement*. U for the unreinforced panels, B for those reinforced with the steel mesh (two in each direction, see Fig. 7), P for panels reinforced with plastic fibres and S for panels reinforced with steel fibres. Hybrid configurations of reinforcement are indicated by their initials.
- *Cover*. C: 3 and 4 cm covers were considered.

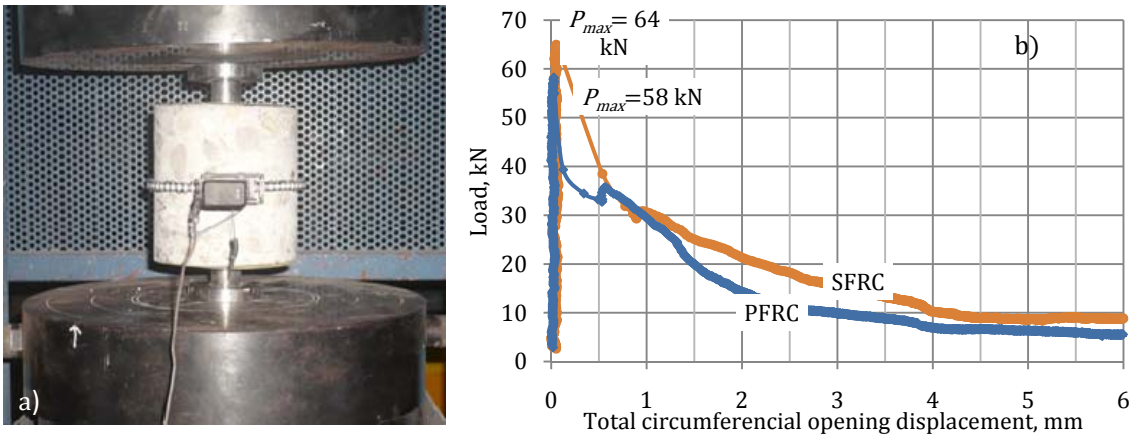

Fig. 8. (a) Barcelona test set-up and (b) average results obtained.

Table 3. Reinforcement configurations and specimen codes.

Anchorage	Mixture	Reinforcement	Cover (cm)	Code
RE	M1	-	4	REU
	M1	4Ø10		REB
PS	M1	-	4	PUC4
	M1	4Ø10		PBC4
	M3	5 kg/m³ of polypropylene fibres		PPC4
	M1	-	3	PUC3
	M1	4Ø10		PBC3
	M3	5 kg/m³ of polypropylene fibres		PPC3
	M2	25 kg/m³ of steel fibres		PSC3
	M3	5 kg/m³ of polypropylene fibres + 4Ø10		PBPC3
	M2	25 kg/m³ of steel fibres + 4Ø10		PBSC3

A.6. Results

Table 4 presents the results obtained for the average maximum load (F_{max}) achieved during the pull – out test and the average compressive strength of concrete (f_{cm}) at the testing age.

It can be observed that FRC presented slightly lower f_{cm} in respect to the plain concrete. However, these differences did not affect the behaviour of the panel, which is mainly influenced by the anchor characteristics and the reinforcement properties.

Failure of the panels was either brittle or ductile depending on the reinforcement configuration. In all cases, the minimum pull – out load established for these structural elements [26-27] was reached.

The second specimen of the PBPC3 series presented an unusual failure caused by an incorrect strip – anchorage connection. This inaccurate union led to increasing local stress concentration that caused the premature strip failure (see Fig. 9). This result was rejected.

Testing equipment allowed continuous data acquisition of the applied pull-out load (F) and the vertical displacement (δ). With that device, the maximum load achieved and the post-failure behaviour were measured. However, the values of displacement included the previous adjustment of the fastening elements during the first loading stage (0.2-0.5 mm). In some cases, this causes a slight overestimation of the final displacement and thus the system ductility. Notwithstanding, a suitable evaluation of the ductility could be made in order to quantify the influence of the reinforcement on the overall structural response.

Fig. 9. Failure of the strip due to an inappropriate connection.

Table 4. Test results. Average values for each series.

Code	Age (Days)	f_{cm} (MPa)	F_{max} (KN)
REU	6	35.1	67.6
REB	6	35.0	74.5
PUC4	3	30.1	60.5
PBC4	3	30.3	64.1
PPC4	4	31.2	62.7
PUC3	3	33.5	63.2
PBC3	4	34.1	69.1
PPC3	4	31.3	65.1
PSC3	5	30.0	70.4
PBPC3	4	32.3	74.1
PBSC3	5	30.2	84.3

A.6.1. Influence of the anchor type

To assess the influence of the anchor type, the results of REU and PUC4 were compared (Fig. 10). In spite of having different anchors, a concrete cover of 4 cm and the absence of reinforcement were preserved in both. Diagrams of Fig. 10 shows that the traditional RE anchor reached a maximum load F_{max} (67.6 kN) higher than the PS anchor (60.5 kN) which represents a 10.5% increase of its capacity. Both exceeded the minimum load established by the regulations. After reaching the maximum load, the series PUC4 did not present any residual strength, forming a conic failure surface (see Fig. 11). On the contrary, the RE system guaranteed an average 20% post-failure load.

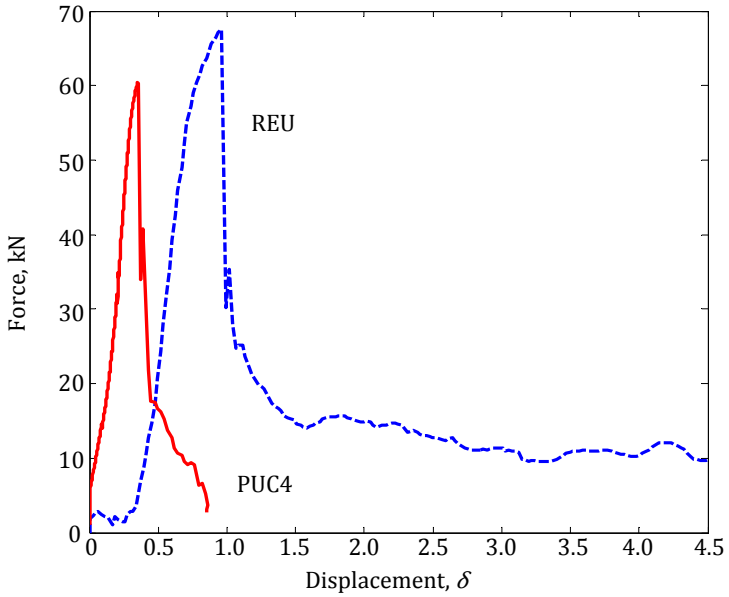

Fig. 11. F–δ diagrams for the series REU and PUC4. Focus on the influence of the anchors.

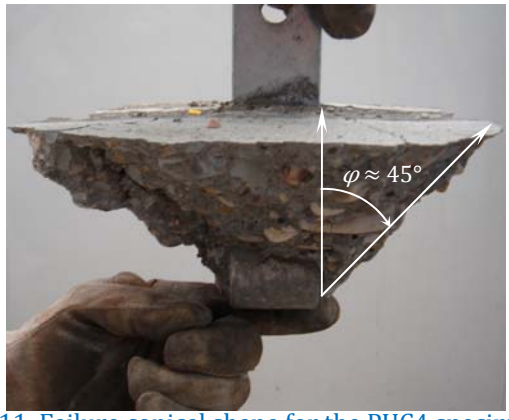

Fig. 11. Failure conical shape for the PUC4 specimens.

A.5.2. Influence of concrete cover

The concrete cover of the anchorage was an important variable that influenced the pull – out maximum load. Fig. 12 shows the average results of the series PUC3 and PUC4 (same anchorage and different covers).

As expected, the specimen with less cover and deeper embedment showed higher capacity: 63.2 kN for the series PUC3 and 60.5 kN for PUC4 (Table 4). Thus, according to the results obtained, reductions of the concrete cover around 1 cm led to an increase of 4.5% of F_{max}.

A first approach to justify this behaviour could be done by means of the parameters represented in Fig. 3. Considering a value of 45° for φ in failure state (see Fig. 11 and [28]), a height (h) and a width of the base of the anchor (s), it is analytically confirmed that the lateral area of the failure conical surface (S_L) increases with the reduction of c [see Eq. 1]. Therefore, the concrete volume involved in the fracture mechanism is higher and also the number of fibres bridging the cracks.

$$S_L = 2\pi \left(s + \frac{h-c}{tan\varphi}\right) \frac{h-c}{sin\varphi} \quad (1)$$

Some guidelines and design equations related with this phenomenon can be found in [29].

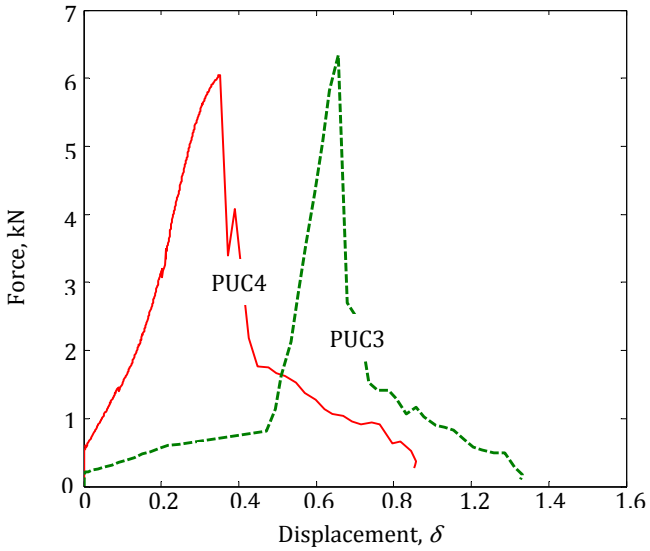

Fig. 13. F–δ diagrams for the series PUC4 and PUC3. Focus on the concrete cover influence.

A.6.3. Influence of the use of rebars

It was observed that the panel failure, both for the RE and for the PS anchor, was brittle for unreinforced panels (REU, PUC4 and PUC3).This is not fundamental for the minimum *pull-out* strength required since the values established in the rules [26-27] were fulfilled in all tested specimens. However, according to the final position of the panel on the earth-retaining wall, bending forces may appear in combination with the pull-out load. As a consequence of that, reinforcement must be used. For that purpose, steel rebars have been used up to date.

The response of the panel facing the pull-out action changes if steel rebars are added. To show the structural behaviour of the steel bar reinforced panel series, two different diagrams are plotted in order to eliminate the influences of the concrete cover and the type of anchorage on the final results. The curves obtained for series REU and REB are illustrated in Fig. 13a. On the other hand, the results for series PUC4 and PBC4 are gathered in Fig. 13b.

For the series REB (74.5 kN), an average 10.2% increase on F_{max} was obtained with respect to the REU (67.6 kN) specimens. Regarding the pear - shape pull-out load, an increase of 6.0% was obtained for the series PBC4 (64.1 kN) in contrast to the 60.5 kN reached by the PUC4 series. This increase of F_{max} was due to the bridging effect developed by the reinforcement mesh across the fracture surface.

A.5.4. Influence of fibres

As mentioned in the introduction, the use of fibres is expected to partially or totally substitute the steel rebars according to their contribution on the global resistance. However, in order to verify the suitability of this change, the correct structural bending response must be verified through another type of test that was not carried out in this experimental program.

Fig. 14a presents the results obtained for the series PBC4 and PPC4, whereas Fig. 14b shows the series PBC3, PPC3 and PSC3. The purpose of these diagrams is to evaluate the influence of the fibres for a fixed cover.

Results show that the average maximum load value F_{max} (Table 4) of the series PPC4 (62.7 kN) and PPC3 (65.1 kN) differ by 2.2% and 5.8% with respect to the reference series PBC4 (64.1 kN) and PBC3 (69.1 kN), respectively. Therefore, in the case of total substitution of the steel mesh reinforcement by the plastic

fibres, the results show that the amount of 5 Kg/m^3 of polypropylene fibres could be enough to guarantee similar values of F_{max}.

In case of steel fibres, the effect of the substitution is more evident since an increase of 1.9% in the series PSC3 (70.4 kN) is obtained in contrast to the reference series PBC3 (69.1 kN).

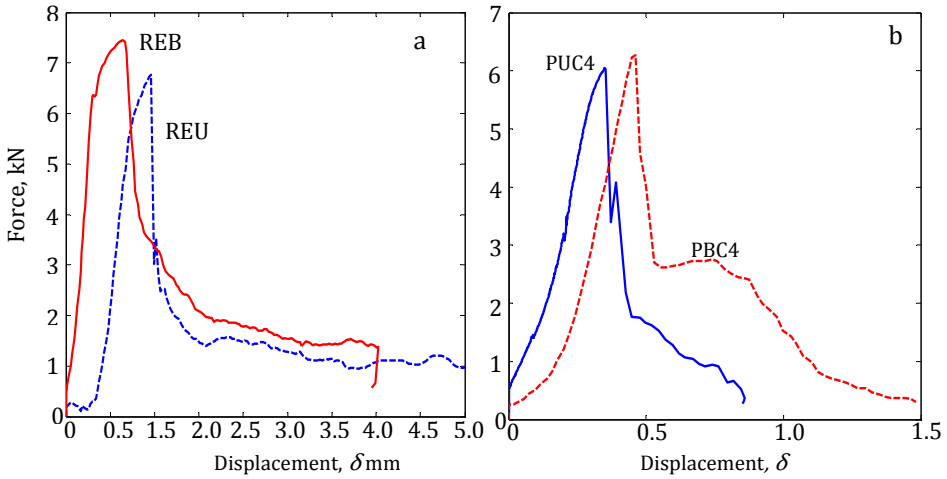

Fig. 13. F–δ diagrams (a) for the series REU and REB and (b) for the series PUC4 and PBC4. Focus on the influence of the passive reinforcement.

Unlike the specimens reinforced with the steel mesh, the fibres are randomly distributed throughout the whole concrete and are able to provide bridging effect across the whole failure surface. Precisely, increases of 3.0% for the series PPC3 (compared with PUC3) and 11.4% for the series PSC3 (compared with PUC3) have been obtained. In that sense, it must be pointed out that the contribution of the steel fibers is almost four times greater in respect to the plastic fibres used in this experimental campaign.

As a result, the steel rebar reinforcement substitution for fibres is technically possible, provided that the amount and both the geometrical and mechanical properties of the fibres used are equivalent to those applied in this experimental program.

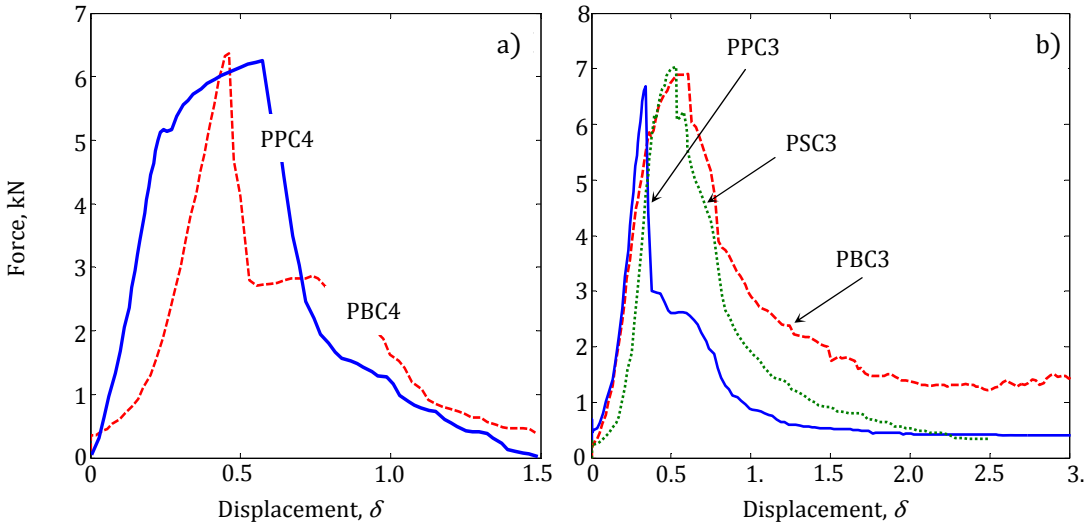

Fig. 14. F–δ diagrams: (a) series PBC4 and PPC4, and (b) series PBC3, PPC3 and PSC3. Focus on the influence of the fibres.

A.6.5. Influence of the hybrid reinforcement

The possibility of mix reinforcements is also technically viable. It would be applied in cases where the bending forces are important and the total substitution of the bar reinforcement by fibres is not feasible, either because of structural or economical reasons. In this sort of situation, both types of reinforcement provide crack width control and also increase the ultimate capacity.

Fig. 15 shows the results obtained in PBPC3 and PBSC3 compared to those obtained in the REB. According to Fig. 15, the panels made with hybrid reinforcement and the proposed anchor led to the highest pull-out loads. Specifically, the F_{max} reached was of 74.1 kN in the series PBPC3, around a 0.5% less than the REB (74.5 kN) series. In contrast to that, the PBSC3 (84.3 kN) series showed an increase of 10.5% with respect to the REB series. Furthermore, as a consequence of the structural contribution provided by the fibres, both series (PBPC3 and PBSC3) confirmed significant higher energy absorption in comparison with the REB series.

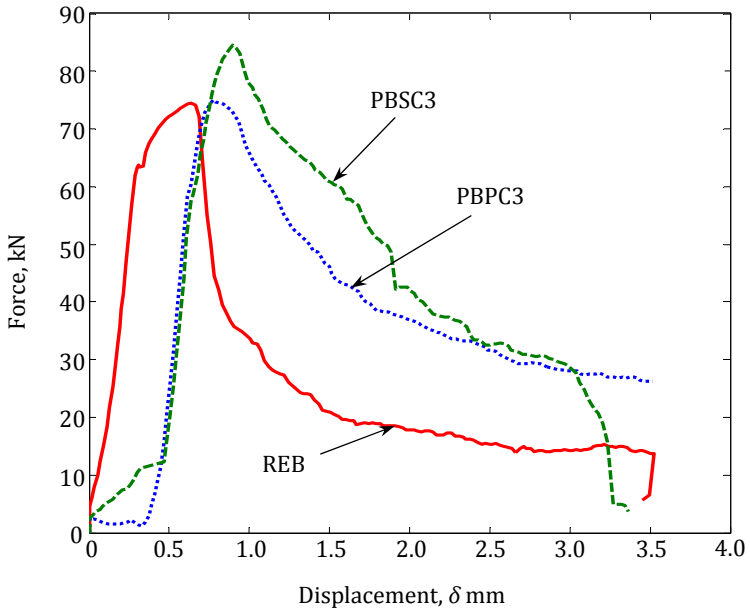

Fig. 15. F–δ diagrams: REB, PBPC3 and PBSC3 series, focusing on the hybrid reinforcement.

A.7. Conclusions

Three innovations within the field of precast panels to be used in reinforced earth retaining walls have been presented in this work: (1) an anchor with a different geometry from the one of the most commonly used up to date in Spain (RE); (2) a new test configuration to check its capacity and (3) structural fibres have been incorporated to replace partially or completely the steel rebars and also to reduce the production time and final costs.

In order to develop and verify the suitability of these changes, an experimental program with a total amount of 33 specimens was performed to analyze the main parameters that influence its structural behaviour (the type and the amount of the reinforcement, the concrete cover and the anchor type). The most significant outcomes are:

- The PS anchor proposed leads to a reduction of the construction tasks. It requires half the amount of joints and fastening elements in comparison to the traditional solution (RE). As a result, the possibility of local failure by the effect of the poor performance of the connection is reduced.

- The proposed anchor leads to a lower pull-out load in comparison with the RE anchor. However, the minimum values established in the regulations are reached with a higher structural efficiency.
- The new test configuration reproduces the desired boundary conditions. In addition, both the equipment and the specimens are small; therefore the tests could be easily carried out in the laboratories facilities of the precast plants. However, the test set-up is still being improved and might need some adjustment in order to be standardized. In particular, the sizes of the panel and the steel frame should be studied to determine the suitable dimensions to ensure that there are no interactions between the failure surface and the support zones that could affect the final results.
- The inclusion of fibres in the concrete mixture is possible once the dosages and the process associated with the manufacturing of the panels are taken into account. It was observed that the fibres could remain exposed at the extrados of the panels (non visible area) after the vibrating operations. It does not represent a problem regarding durability conditions. However, it is necessary to focus on this aspect to avoid damages during the manipulation of the pieces.
- Panels from series PPC4 and PPC3 (reinforced with 5 kg/m^3 of plastic fibres) showed 2.2% and 5.8% lower pull-out force than those obtained with series PBC4 and PBC3, respectively. In contrast, the specimens of the series PSC3 (reinforced with 25kg/m^3 of steel fibres) showed 1.9% higher loads with respect to the PBC3 series.
- The hybrid reinforcement (fibres plus bars) is also possible. In that case, the use of both plastic and steel fibres is a suitable alternative. This combination is particularly interesting when the bending forces are relevant and the total substitution is not justified economically or technically.

A new experimental campaign is being planned since the conclusions are based on the results obtained with 33 specimens. In this sense, a certain scatter has been found in the results, especially in both the maximum displacements and the energy absorption. Furthermore, a statistical analysis and a detailed study on the phenomena involved in the fracture mechanism should be done in order to confirm the abovementioned conclusions.

A.8. Acknowledgements

The authors wish to acknowledge PRECON, S.A. for the financial support and resources both physical and human which has made available to carry out this work, especially Juan José Rojo.

A.9. References

1. Vidal HC. Constructional Works. U.S. Patent No 3686873; 1972.
2. Vidal HC. Stabilized earth structures. U.S. Patent No 4116010; 1978.
3. Elias V, Christofer BR, Berg RR. Mechanically stabilized earth and reinforced soil slopes. Design & Construction Guidelines. FHWA Report N°FHWA-NHI-00-043; 2001.
4. Ling H, Leshchinsky D, Tatsuoka F. Reinforced Soil Engineering: Advances in Research and Practice. NY: Marcel Dekker; 2003.
5. Li VC. Large volume, high-performance applications of fibres in civil engineering. J of app polymer science 2002. Vol. 83, John Willey & Sons, p. 660-686.
6. Walraven J. High performance fibre reinforced concrete: progress in knowledge and design codes. Mater Struct 2009;42(9):1247-60.
7. di Prisco M. FRC: Structural applications and standards. Mater Struct 2009;42(9):1169-71.
8. di Prisco M, Plizzari G, Vandewalle L. Fibre reinforced concrete: new design perspectives. Mater Struct 2009;42(9):1261-81.
9. Grzybowski M, Shah SP. Shrinkage cracking of fibre reinforced concrete. ACI Mat J 1990;87(2):138-48.

10. Nanni A, Ludwing DA, McGillis MT. Plastic shrinkage cracking of restrained fibre-reinforced concrete. Transp Res Record No. 1382, Part 2: Developments in concrete technology; 1993.

11. Shaaban AM, Gesund H. Punching shear strength of steel fibre reinforced concrete flat plates. ACI Struct J 1994;91(4):406-14.

12. Swamy RN, Ali AR. Punching shear behavior of reinforced slab-column connections made with steel fibre concrete. ACI J Proceedings 1982;79(5):392-406.

13. Ding Y, Kusterle W. Comparative study of steel fibre-reinforced concrete and steel mesh-reinforced concrete at early ages in panel tests. Cem. Concr. Res. 1999;29(11):1827-34.

14. Elavenil S, Knight GMS. Behaviour of steel fibre reinforced concrete beams and plates under static load. J Res Sci Comput Eng 2007;4(3):11-28.

15. Gopalaratnam VS, Shah SP. Properties of steel fibre reinforced concrete subjected to impact loading. ACI J Proc 1986; 83(1):117-26.

16. de la Fuente A, Aguado A, Molins C. Integral optimum design of concrete pipes. Hormig y Acero 2010; 61(259).

17. CEB (1993): *CEB-FIP Model Code 1990*. Bulletin d'Information 213/214, Lausane, Switzerland; 1993. p. 437.

18. Swamy RN, Bahía HM. Influence of fibre reinforcement on the dowel resistance to shear. ACI J 1979;76(2):327-56.

19. di Prisco M, Caruso ML, Piattu S. On fibre role in dowel action. Studi e Recerche No. 15:151-94. Politecnico di Milano; 1994.

20. BS EN 12350-2:2000. Testing fresh concrete - Part 2: Slump Test.

21. ASTM C231-09a. Standard test method for air content of freshly mixed concrete by the pressure method; 2009.

22. ASTM C39/C39M-09a. Standard test method for compressive strength of cylindrical concrete specimens; 2009.

23. UNE 83515. Fibre reinforced concrete. Determination of cracking strength, ductility and residual tensile strength. Barcelona Test; 2010.

24. Molins C, Aguado A, Marí AR. Quality control test for SRFC to be used in precast segments. Tunn Undergr Space Technol 2006;21(3):423-4.

25. Molins C, Aguado A, Saludes S, Double punch test to control the energy dissipation in tension of FRC (Barcelona Test). Mater Struct 2009;42(4):415-25.

26. Norme NFP 94-220-0. Ouvrages en sols rapportés renforcés par armatures ou nappes peu extensibles et souples - Justification du dimensionnement; 1998.

27. Norme NFP 94-220-2. Ouvrages en sols rapportés renforcés par armatures ou nappes peu extensibles et souples - Renforcement par des armatures métalliques en treillis - Justification du dimensionnement ; 1998.

28. CPH (Ministerio de Fomento). *EHE 2008*: Instrucción del Hormigón Estructural; 2008.

29. DD CEN/TS 1992-4-1:2009. Design of fastenings for use in concrete. General; 2009.

APPENDIX B

Experiences in Barcelona with the use of fibres in segmental linings

B.1. Abstract

This paper presents the most outstanding experiences regarding the use of fibres as the main reinforcement in precast segmental linings in the metropolitan area of Barcelona. It is known that the addition of structural fibres improves, on the one hand, the mechanical behaviour of the structure during its construction, especially in cases such as the thrust of the jacks, and on the other hand it leads to a reduction of the global costs by reducing the conventional passive reinforcement. The aim of this paper consists in presenting three real experiences that are representative of the application of FRC in urban tunnels and a design methodology to take into account the structural contribution of the fibres. Two particular cases of the application of this design method are presented. In the first case, the use of 25 kg/m^3 of fibers has led to a reduction of 70% of the conventional reinforcement initially proposed in the project. In the second one, which was planned to employ fibers but without considering its structural contribution, the parametric study reflected the possibility of reducing up to a 38% of the rebars adding 25 kg/m^3 of steel fibres in the concrete mixture. In light of good results, construction companies in Spain have become aware of the advantages of using fibers in these structures and have carried out experimental stretches. This attitude has also been influenced by the approval of the new Spanish Code, which includes the FRC as a construction material with design purposes.

Keywords: SFRC; Precast segments; TBM; Design; Non linear analysis; Cracking.

B.2. Introduction

Fibre reinforced concrete (FRC) is a composite material that has proved to be a competitive material in many types structures [1-4]. In particular, there are many advantages when using FRC in the manufacturing of segmental linings of tunnels built by means of a Tunnel Boring Machine (TBM) [5-8]. In this field, the use of steel fibre reinforced concrete (SFRC) improves the mechanical behaviour of concrete enhancing: (1) thoughness; (2) resistence to fire; (3) resistance to fatigue and (4) its response facing impacts and concentrated loads that can be occur in stages prior to the placement of the segments (curing, transport and handling), during its assembling (thrust of the jacks) and during service stage (contact between joints).

Likewise, the use of SFRC may lead to the total or a partial removal of rebars, improving the production efficiency and ensuring economic competitiveness with regards to the traditional solution. There are many studies both experimental [9] and numerical [7-8 and 10-14] in which the advantages associated to the use of SFRC in precast segments are proved as well as the use of steel bar reinforced concrete (RC) and SFRC in the same precast concrete segment (RC-SFRC, hereinafter).

In the last 8 years, the construction of more than 120 km of tunnel has started in the metropolitan area of Barcelona (Spain), some of which are still under construction. The internal diameter (D_i) of these tunnels ranges from 6.00 m to 10.9 m, with aspect ratios ($\lambda = D_i/h$) of even 31 as in the Can Zam stretch of the Line 9 Subway of Barcelona. Basically, the applications were either related to railways, metro lines or for hydraulic conduits.

The use of SFRC began at several stretches of Line 9 Subway of Barcelona (started in 2003). Nevertheless, the structural contribution of the fibres was not considered in the design due to the lack of regulations in the Spanish Code regarding the use of FRC. Conversely, they were considered to improve the toughness and enhance the cracking control during handling and assembling operations, while rebars kept the main resistant function. In this sense, the most advanced regulations currently available when these first applications were carried out in Barcelona did take already into account the structural contribution of the fibers, but they were too recent [15-17]. Nowadays, the Spanish regulation [18] includes SFRC as a material with a structural responsibility.

Subsequently to the beginning of the construction of the Line 9 Subway of Barcelona, several experimental applications of SFRC precast segments were performed in various stretches. In these cases, 60 kg/m^3 of steel fibers were used to replace the steel rebars. However, two groups of stirrups similar to the ones used in the analysis of the Line 1 Subway of Valencia (Venezuela) [7] were maintained in order to confine the concrete.

Currently, some experiences concerning precast concrete segments reinforced only with fibres have been done (see Table 1), but the great majority of them are related to values of λ generally smaller than those used in the Line 9 Subway of Barcelona. Examples of these applications are: a tunnel for the transportation of water in Ecuador [19], Gold Coast and South East Queensland in Australia [20], Heating Tunnel from the Island Amager to Copenhagen in Denmark [21], Line 4 Subway of Sao Paulo [22], CLEM Jones Tunnel in Brisbane [23], Hobson Bay Sewer Tunnel in New Zealand [24] and Bright Water Sewer System Seattle Tacoma in USA [25].

The challenge in the recent experiences carried out in the metropolitan area of Barcelona was to analyze the feasibility of exceeding the diameters previously reached. Thus, the purpose of this article is, on the one hand, to present these experiences. On the other hand, this article also aims at showing the design methodology used for the optimization of the amount of fibres (C_f) in SFRC and RC-SFRC precast segments.

Table 1. International experiences on the use of fibers in tunnels

Project	D_i (m)	h (m)	λ	Nº of segments	Year
Heathrow Baggage Handling Tunnel (UK)	4.5	0.15	30.0	7+key	1993
Heathrow Express Tunnel (UK)	5.7	0.22	25.8	5+key	1994
2nd Heinenoord Tunnel Rotterdam (ND)	7.6	0.35	21.7	7+key	1999
Oënzberg (SW)	11.4	0.40	28.5	7+key	2003
Channel Tunnel Rail Link (UK)	7.2	0.35	20.4	9+key	2004
Line 9 Subway of Barcelona. Can Zam stretch (SP)	10.9	0.35	31.1	7+key	2003
Heathrow Express Extension to T5 (UK)	5.7	0.22	25.8	9+key	2005
Line 9 Subway of Barcelona. Stretch I (Spain)	8.4	0.32	26.3	6+key	2006
San Vicente Tunnel (USA)	3.6	0.18	20.3	5+key	2006
Beacon Hill Station and Tunnels (USA)	5.7	0.30	19.1	6+key	2009
Line 4 of the Underground of Sao Paulo (BR)	8.4	0.35	24.1	7+key+invert	2009
Clem Jones Tunnel (AUS)	11.4	0.40	28.5	8+key	2010

B.3. Pionner experience in the metropolitan area of Barcelona

The first pilot test for the application of SFRC in precast segments was carried out in the year 2004, in the Can Zam stretch of the Line 9 Subway. It must be highlighted that the execution and the working conditions in this first experience were highly adverse: descending stretch and water leaks with a temperature of up to 60°C. The solution adopted in this case was a ring with a $D_i = 10.9$ m, divided by an intermediate slab separating two independent levels (one for each traffic direction). The thickness of the segment was 0.35 m, and a FRC with 60 kg/m^3 of steel fibers dosage was used. A total of thirty rings were constructed; three of them were instrumented in order to carry out a loading test for simulating the soil pressure in the field conditions by means of jacks [26].

In Fig. 1a the instrumented specimen is presented. Notice, that the conventional reinforcement was limited to the stirrups (a similar solution was developed by [7]). Likewise, Fig. 1b shows the flat-bed press placed in the extrados of the segment to perform the loading test.

As previously mentioned, the working conditions were adverse. As a matter of fact, some splitting cracks and local failures appeared. Fig. 2a shows the crack pattern generated during the assembling of the segments. This cracking was due to the high eccentricity of the load transmitted by the jacks in the descending part of the stretch [8 and 27]. Fig. 2b also shows the existence of water leaks. Nonetheless, there was no concrete detachment thanks to the presence of fibres bridging the cracks.

Even considering the problems already mentioned, which also took place in the stretches with traditional reinforcement, the results from the loading test were satisfactory [26]. In spite of the success achieved, the solution was not generalized in the whole tunnel for several reasons, many of them bearing no relation to the technical reasons.

On the basis of the results obtained in this pilot application and the international experiences related with the use of SFRC in precast segments (see Table 1), new ones were proposed in the metropolitan area of Barcelona: FontSanta–Trinitat Tunnel and Terrassa Tunnel. In the first case, 10 optimized RC-SFRC rings were placed, while in the second case a RC-SFRC precast segmental lining was used in the whole tunnel.

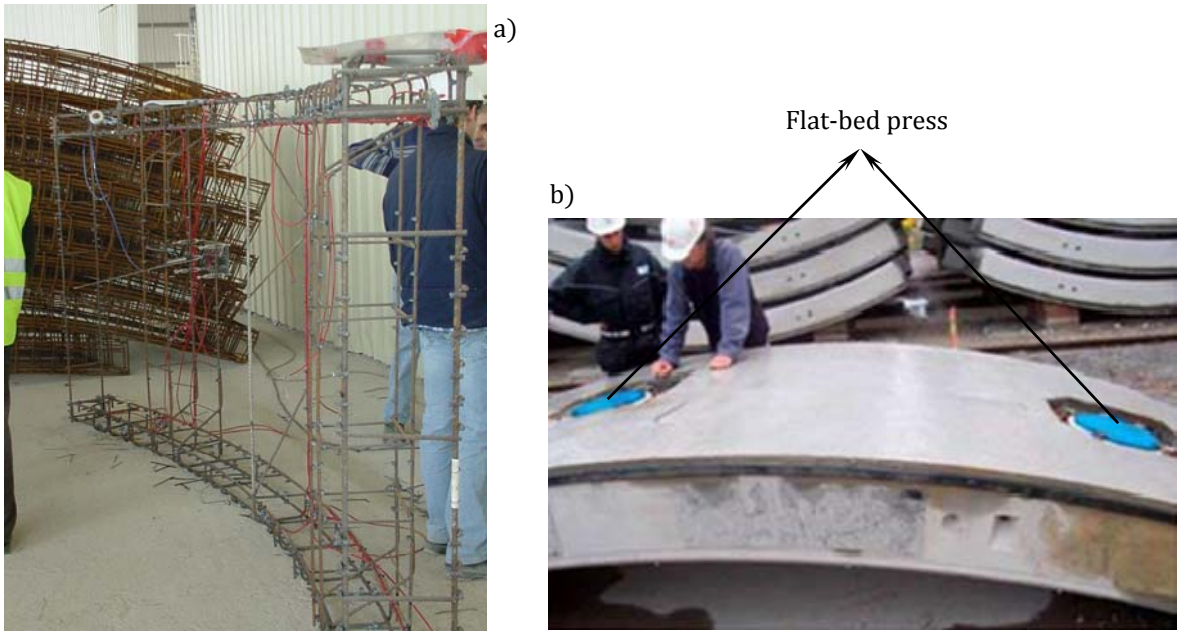

Fig. 1. Load test of the RC-SFRC precast segments: a) instrumented specimen and b) flat-bed press configuration.

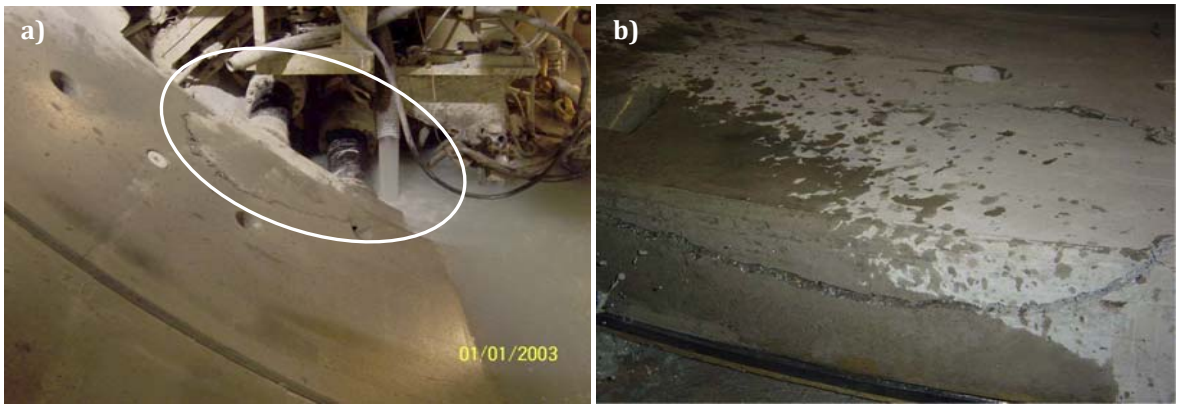

Fig. 1. (a) Assembling operations: (a) crack pattern due to the thrust of the jacks and (b) presence of water leaks.

B.4. Numerical model for the nonlinear analysis of sections

B.4.1. Introduction

The cross sectional behaviour of the precast segments was simulated by means the model called Analysis of Evolutive Sections (AES) presented in [28]. The structural feasibility of the application of fibers in the studied rings, as well as the optimization of its reinforcement, was dealt with AES. With this aim, the moment-curvature (M_k-χ) and the interaction (N_u-M_u) diagrams were used to provide the necessary information about the mechanical behaviour both in SLS and in ULS for each control cross-section of the segment.

B.4.2. Sectional analysis model

Modeling of the materials

The concrete is dicretized in layers with constant thickness, whereas steel rebars are simulated as concentrated-area elements. Subsequently, the suitable constitutive model is assigned to each element in order to integrate the stresses resulting from a given deformation plane (ε_o, χ) (see Fig. 3a).

The addition of steel fibres modifies the behaviour of SFRC depending on the volume of fibers used [29]. Its response under uniaxial compression is described with the expression suggested by [30]. On the other hand, the simulation of its post-cracking behaviour is solved by means of the model type σ_c-ε_c suggested in [16]. This is an internationally accepted model (see Fig. 3b) which has already been used in several numerical-experimental contrasting applications obtaining excellent results [31-32].

The crack width (w) is evaluated differently depending on the type of reinforcement of the section: for RC sections the formulation proposed in [33] is used, whereas in the case of SFRC-RC sections an extension of the previous formulation [34] is used.

The steel for rebars is simulated with the bilinear diagram presented in Fig. 3c.

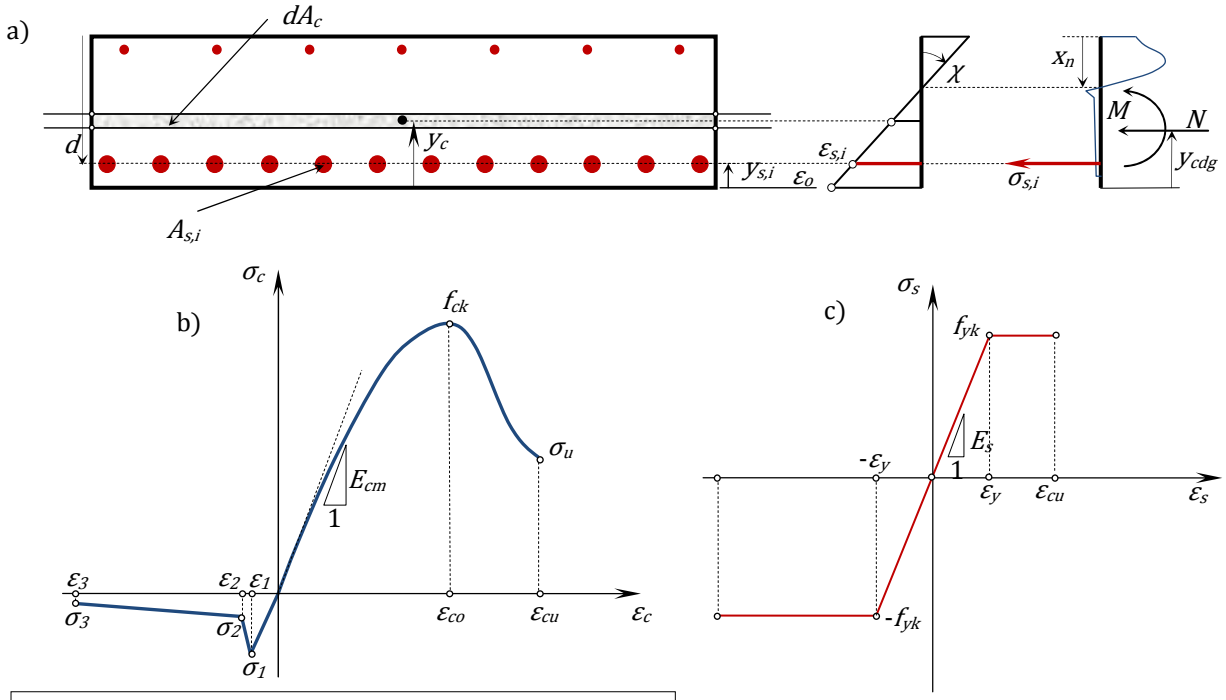

$\sigma_1 = 0.7 f_{ctm,fl}(1.6 - d)$ $\quad \varepsilon_1 = \sigma_1 / E_{cm}$

$\sigma_2 = 0.45 f_{R,1} k_h$ $\quad \varepsilon_2 = \varepsilon_1 + 0.1‰$

$\sigma_3 = 0.37 f_{R,4} k_h$ $\quad \varepsilon_3 = 25‰$

$$k_h = 1.0 - 0.6 \frac{h[cm] - 12.5}{47.5} \quad |12.5 \leq h < 60|$$

Parameters proposed by [16]

Fig. 3. (a) Sectional discretization; (b) SFRC and (c) steel bar constitutive equations.

Basic hypotheses

The following hypotheses have been considered: (1) perfect bond between the materials; (2) sections remain plane before the application of the external forces or after imposing fixed strains and (3) shear strains are negligible, therefore, these were not taken into account.

Equilibrium and compatibility

Once the suitable constitutive equations have been assigned to each of the materials, a Newton–Raphson iterative method [3] is used to solve the nonlinear equation system resulting from the considering the equilibrium conditions (Eqs. 1 and 2) and compatibility (Eq. 3).

$$N = \int_{A_c} \sigma_c(\varepsilon_c).dA_c + \sum_{i=1}^{n_s} \sigma_{s,i}(\varepsilon_s).A_{s,i} \quad (1)$$

$$M + Ny_{cdg} = \int_{A_c} \sigma_c(\varepsilon_c).y_c.dA_c + \sum_{i=1}^{n_b} \sigma_{s,i}(\varepsilon_s).y_{s,i}\,A_{s,i} \quad (2)$$

$$\varepsilon_c(y_c) = \varepsilon_o + y_c.\chi \quad (3)$$

B.5. Examples of application

B.5.1. FONTSANTA-TRINITAT Tunnel

Project Overview

It consists of a tunnel for the transportation of desalinated water from the Llobregat River toward the Ter River. For this purpose, a main station was built in Fontsanta (Sant Just d'Esvern, Barcelona), which pumps the water toward the Distributing Station of Trinidad (Barcelona) by means a concrete pipe with an internal diameter of 1800 mm. The flow is 2.0 m^3/s in the first stage, but it is expected to reach up to 3.6 m^3/s in the future.

The tunnel was excavated under the Collserola Mountain (Barcelona) simultaneously from two opposite fronts (Riera de Sant Just and La Trinidad) using two double-shielded TBMs [36] with an internal diameter of 6.0 m. Likewise, three service galleries were built to facilitate intermediate access, ventilation and emergency exits.

The layout gets across heterogeneous soil with several different geological formations. The predominant materials are schist and phyllite (35% of the length), slate and quartzite slate (15%), being the latter ones the worst concerning its geotechnical quality. On the contrary, the rest of the formations are rocks with medium-high quality (granodiorite, hornfels, porphyr, quartzite and metamorphic rocks).

Taking into account the geotechnical characteristics of the ground and the excavation method used, a universal ring (see Fig. 4) with an internal diameter of 5.2 m consisting of 5 +1 precast segments with a thickness of 0.25 m and a width of 1.40 m was designed. Two different concrete strength classes were used in order to adequately face the different levels of compression which could be reached during the service life of the structure. In that sense, a concrete C30/37 (see [16]) was used in for the precast segments (PS-30) in those stretches where the presence of the phreatic level was not expected. On the contrary, a C50/60 concrete (PS-50) was chosen to resist the high compressive stresses attributable to the poor quality of the rock mass as well as the presence of the phreatic level expectable in a few stretches according to the geotechnical analyzes.

The design stages considered in the analysis were: (1) curing operations, (2) storage, (3) transport, (4) assembling tasks and (5) the soil pressure during service stage. Concerning the analysis of stage 5, the calculation was performed by means of a 3D-FEM developed with the commercial code FLAC3D [37]. The tunnel construction method, the concrete rings as well as the grouting process were simulated taking into account the soil-structure interaction and the possible presence of water.

The length of the shield (11.2 m) was considered proportional to the length of the ring (1.4 m) in the 3-D FEM model. Likewise, the model dimensions are 140.0 m in the axial direction of the tunnel and 64.0 m in the other two directions (see Fig. 5), considering a uniformly distributed load to simulate the rest of the soil up to covers of 205 m and 325 m. The model has been discretized in the direction of the tunnel in elements with a length of 1.4 m, corresponding to the length of each of the rings.

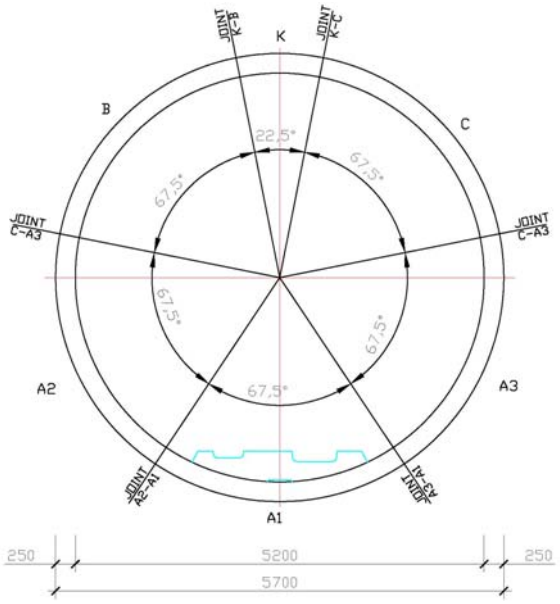

Fig. 4. Main measures (in mm) of the transversal section of the FontSanta-Trinitat tunnel.

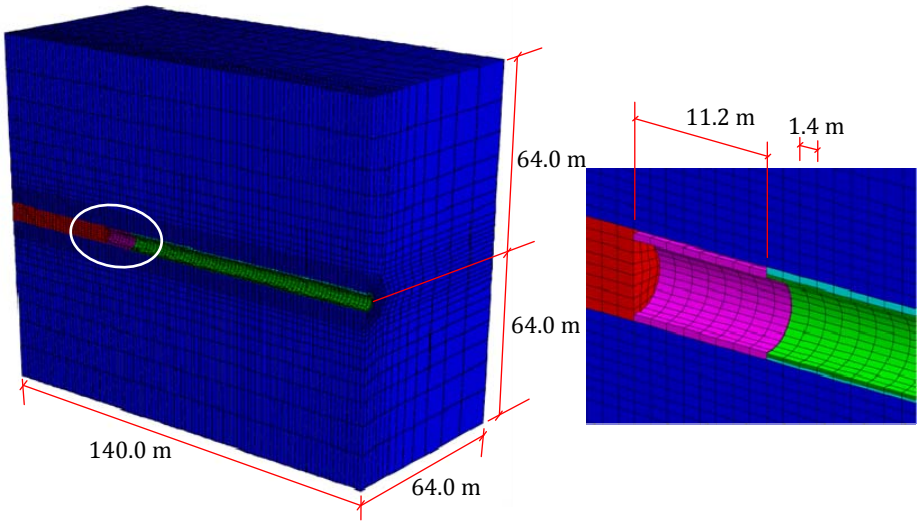

Fig. 5. FE mesh used to simulate the excavation process and the in-service state behaviour of FontSanta-Trinitat Tunnel.

Specifically, the two worst scenarios were analyzed: (1) slates formation (specific weight $\gamma_r = 27.5$ kN/m^3, cohesion $c_r = 556.10^{-3}$ N/mm^2, friction angle $\Phi_r = 33.8°$, Young modulus $E_r = 2277$ N/mm^2, Poisson ratio $\nu_r = 0.25$) with 205 m of soil cover and with no water presence for the PS-30 and (2) porphyr dike formation ($\gamma_r = 26.8$ kN/m^3, $c_r = 1162.10^{-3}$ N/mm^2, $\Phi_r = 43.6°$, $E_r = 2636$ N/mm^2, $\nu_r = 0.30$) with a cover of 325 m and considering a water column with a height of 120 m for the PS-50 precast segment. In any case soil stress relaxation has been considered. Likewise, an earth pressure coefficient (K_o) of 1.5 has been taken into account in both simulations.

The characteristic and design values of the axial and bending forces obtained in the five stages (see Table 2) are low in relation with the dimensions of the cross section of the segment. However, a minimum amount of reinforcement consisting of 10Φ10 (see Fig. 6a) and 10Φ12 (see Fig. 6b) for SL-30 and for SL-50, respectively, was placed to avoid the brittle failure. Taking these factors into account, it was decided

that the reinforcement could be optimized by using a RC-SFRC configuration, with the aim of reaching the benefits previously mentioned.

Table 2. Characteristic and design values for the forces at each of the stages.

Stage		N_k (kN)	M_k (mkN)	N_d (kN)	M_d (mkN)
Curing (1)		0	11	0	21
Storage (2)		0	10	0	20
Transport (3)		0	11	0	21
Handling (4)		0	11	0	21
Service (5)	SL-30	1059	9	1588	13
	SL-50	3070	8	4604	11

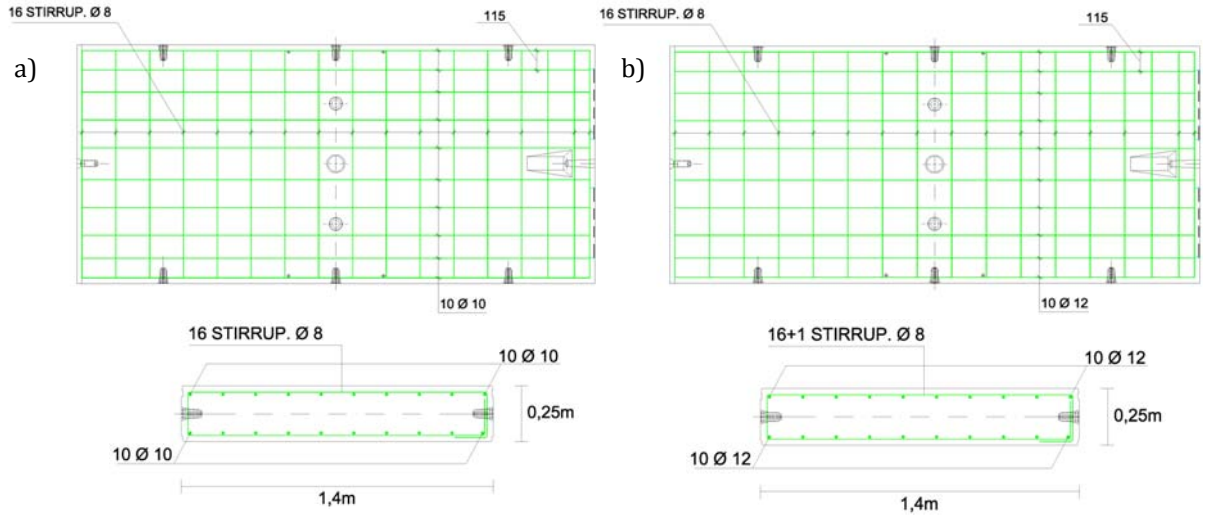

Fig. 6. Longitudinal and transversal conventional reinforcement cages used for: (a) precast segment PS-30 and (b) precast segment PS-50.

Since this was a pilot experience, ten rings with the new RC-SFRC proposed below were manufactured. They were placed in a stretch where the installation conditions and the service structural requirements were representative of the average characteristics of the tunnel.

Design accounting for the structural contribution of fibers

The results obtained with the model AES showed that that neither bottom nor upper fibers of the concrete section analyzed (see Figs. 6b and 6c) reach the characteristic flexural strength ($f_{ctk,fl}$) in any of the transitory stages (stages 1 to 4), while in service (stage 5) is totally compressed. Therefore the section was not expected to crack.

Bearing in mind this fact, the strategy proposed in this document to design the new RC-SFRC precast segment consists in obtaining the minimum content of reinforcement (steel rebars plus fibres) that assure a ductile failure for the hypothetical situation of reaching the cracking bending force M_{cr} in any of the transitory stages. Thus, it was established that M_{cr} should be strictly equal to M_u (see Eq. 4 and Fig. 7). This approach was proposed for RC sections in [38] and successfully used in [7 and 13-14] for the optimal design of RC-SFRC segments.

To accomplish this goal, it is necessary to solve the Eq. 4. For RC sections, this equation is linear and can be solved analytically. Otherwise, a nonlinear system is obtained when Eqs. 1-4 are combined for SFRC or RC-SFRC sections, and then the numerical model AES previously introduced has to be used to solve it.

$$M_{cr} = M_u \quad (4)$$

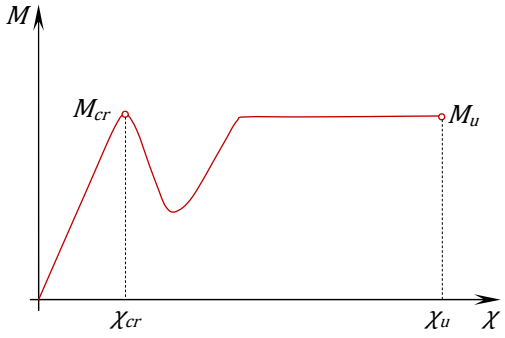

Fig. 7. M-χ diagram for an optimized RC-SFRC section with ductile failure.

In the same way proposed in [7] for the RC-SFRC precast segments of the Line 1 Subway of Valencia (Venezuela), two groups of stirrups where maintained along the two longer sides in order to confine the concrete in this zone. This reinforcement configuration could reduce the splitting cracks that may occur due to the compressive stresses expected during the thrust of the jacks and in the radial joints in-service conditions. With the aim of comparison, in Fig. 8a the reinforcement cage initially projected for the segment PS-50 is showed, while in Fig. 8b the steel stirrups maintained for the RC-SFRC solution are also showed. It can be noted that the optimized solution proposed (Fig. 8b) presents a considerable reduction of the conventional reinforcement (70%) with regard to the initial one (Fig. 8a).

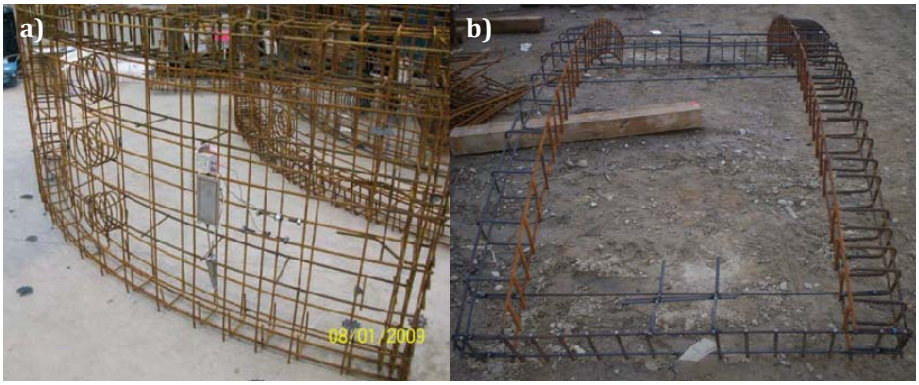

Fig. 8. Reinforcement cages for the precast segments: (a) PS-50 and (b) optimized RC-SFRC segment.

Fig. 9 gathers the RC-SFRC cross section of the segment used for the numerical modelling. The optimum value of C_f was determined using the AES model so as to fulfil Eq. 4. In this respect, the value of M_{cr} for the segment PS-50 (74 mkN) is higher than the one obtained for the segment PS-30 (49 mkN), due to the higher $f_{ctk,fl}$ of the former. Thus, it was decided optimize the value of C_f for the precast segment SL-50 (concrete strength class C-50/60) and use the same reinforcement configuration for the PS-30 (concrete strength class C-30/37) so as to systematize the construction procedures.

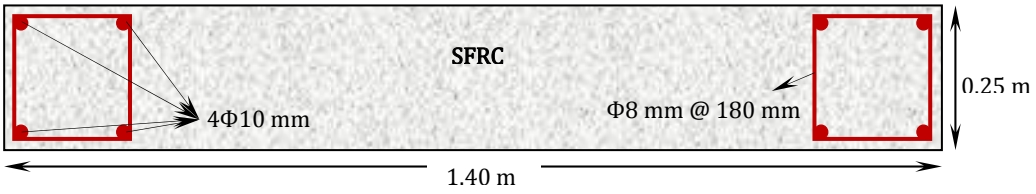

Fig. 9. Steel stirrups used for the RC-SFRC precast segment.

The simulation of post-cracking behaviour of SFRC was dealt with the constitutive equation suggested by the [16] (see Fig. 3b). However, at this stage of the design process neither data of the fibre content which was going to be used in the concrete nor results from characterization tests of SFRC tension behaviour were available. Alternatively, Eqs. 5 and 6 proposed by [39] were used for the calculation of the residual flexural strength ($f_{R,i}$) of SFRC as a function of C_f. These expressions were calibrated on basis of the results

obtained in bending tests of prismatic beams of SFRC with same hooked-end steel fibres used in the optimized RC-SFRC precast segments analyzed in this work (length l_f = 60 mm, diameter d_f = 0.75, Young modulus E_f = 210000 N/mm² and a failure tensile strength f_{fu} = 1100 N/mm²).

$$f_{R,1} = 0.0945C_f + 0.702 \quad (5)$$

$$f_{R,4} = 0.0926f_{R,1} \quad (6)$$

For this study, the values of C_f adopted range between 0 kg/m³ and 40 kg/m³. The latter value is motivated by economic criteria. Table 3 gathers the numerical values of the parameters used to simulate the post-cracking behaviour of SFRC.

Table 3. Values of σ_i and ε_i used to simulate the post-cracked behaviour of SFRC (C50/60).

C_f (Kg/m³)	$f_{R,1}$ (N/mm²)	$f_{R,4}$ (N/mm²)	σ_1* (N/mm²)	ε_1 (mm/m)	σ_2 (N/mm²)	ε_2 (mm/m)	σ_3 (N/mm²)	ε_3 (mm/m)
0	0.702	0.650	4.844	0.131	0.266	0.231	0.203	25.000
10	1.647	1.525	4.844	0.131	0.624	0.231	0.475	25.000
20	2.592	2.400	4.844	0.131	0.982	0.231	0.748	25.000
30	3.537	3.275	4.844	0.131	1.340	0.231	1.021	25.000
40	4.482	4.150	4.844	0.131	1.698	0.231	1.293	25.000

* σ_1 was evaluated by means de expression $\sigma_1 = 0.52 f_{ctm,fl}(1.6\text{-}d)$ proposed by [39] due to the high values obtained with the one suggested by [16].

The mechanical behaviour of the steel rebars has been simulated by considering a bilinear diagram (see Fig. 3c), as well as a value of 500 N/mm² for f_{yk} and 210000 N/mm² for E_s.

Fig. 10 shows the M-χ diagrams (N_k = 0) numerically obtained for the RC-SFRC precast segment reinforced with different values of C_f and the steel stirrups presented in Fig. 9.

The results presented in Fig. 10 confirm the requirement of using a C_f higher than 20 kg/m³ to fulfil Eq. 4. Particularly, by representing the relation M_u-C_f (see Fig. 11), it can be deduced the optimum value for C_f is closely to 25 kg/m³.

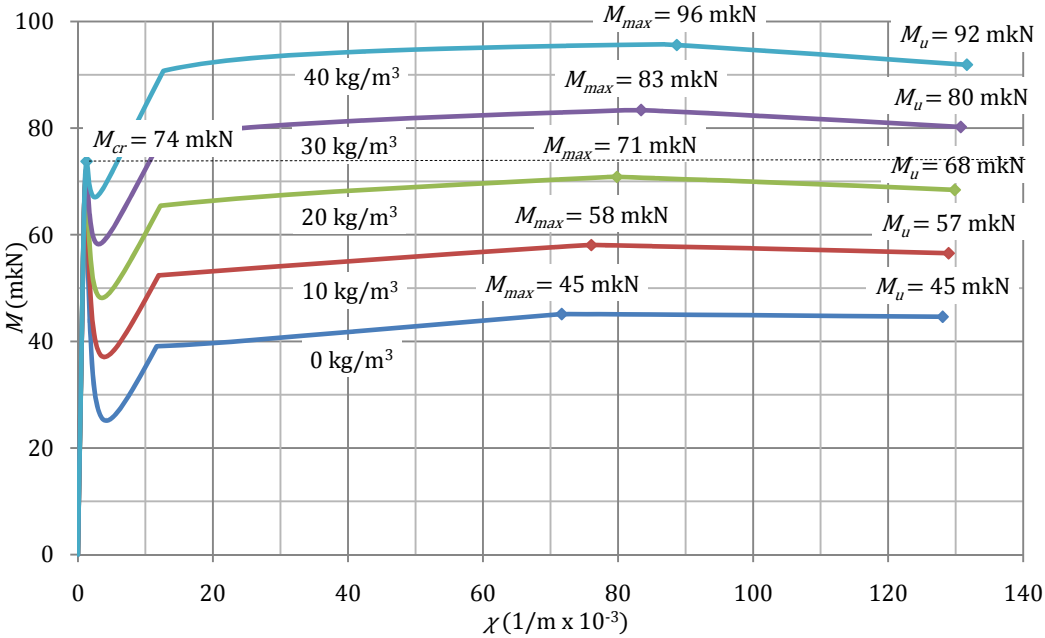

Fig. 10. M-χ diagrams for the C50/60 concrete strength class RC-SFRC precast segment with different amounts of steel fibres.

It must be remarked that this is the optimum value for C_f obtained considering the bending forces (M) and the compression forces (N) presented in Table 2. In this sense, in order to confirm the correctness of this value for the rest of load types, the influence of C_f in the behaviour of the precast segment under concentrated loads (thrust of the jacks and serviceability stresses in the joints) must be analyzed. Up to date, several numerical studies [5-8; 21 and 27] and some experimental experiences [9] that confirm the excellent response of the fibres in these load cases, have been presented in the international literature. Nevertheless, a systematical methodology has not been proposed yet to find the optimum value of C_f considering all the possible load states due to the numerous variables that take part in the study. There is, however, a generally accepted design method that consists in a numerical evaluation of the optimum value of C_f by means of a structural analysis considering the forces (N, M) and verifying numerically and/or experimentally that the segmental lining behaves also properly under concentrated loads.

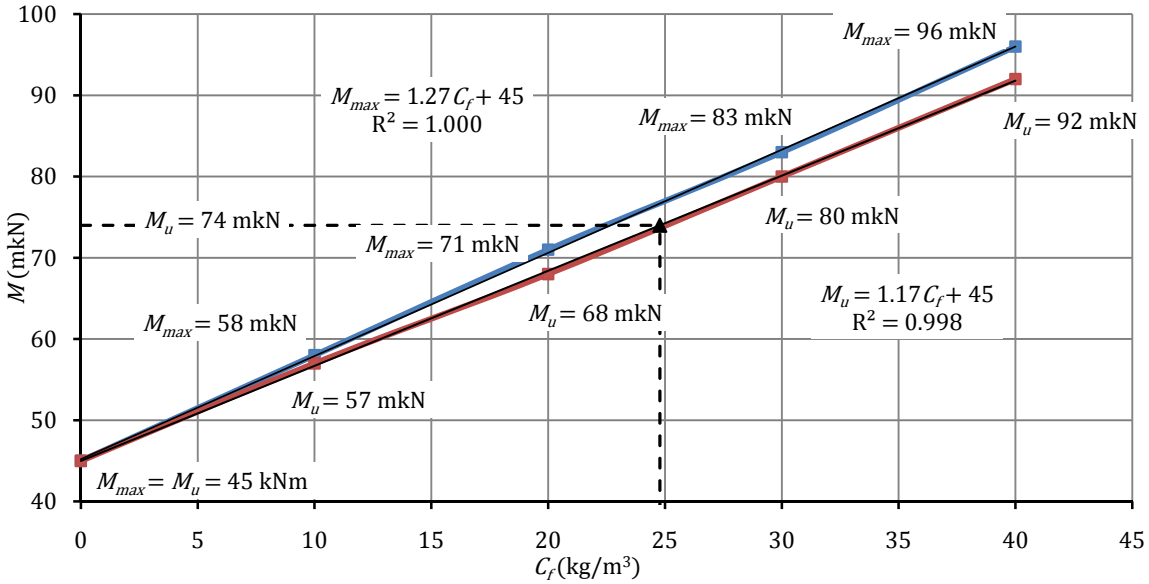

Fig. 11. Increase of M_{max} and M_u with the amount of fibres C_f.

Considering the above mentioned and the results obtained in the numerical analysis, it was decided to manufacture ten rings with an amount of 25 kg/m³ of steel fibres together with the reinforcement cage proposed in Fig. 8b and Fig. 9. It has to be mentioned that none of the rings presented cracks during the assembling operations neither service loads. This fact confirms that the value of 25 kg/m³ previously deduced numerically could be the desired optimum value of C_f for the geometrical and mechanical boundary conditions simulated fixed in this analysis case.

B.5.2. TERRASSA Tunnel

Project Overview

This case consists in two parallel rail tunnels built in the urban area of Terrassa as the extension of the Ferrocarriles de la Generalitat de Catalunya (FGC). Both tunnels are drilled successively being the total length of each one of 4510 m. The tunnels consist of rings (see Fig. 12) with an internal diameter of 6.0 m and formed by 6+1 RC-SFRC precast concrete C30/37 segments with a width of 1.5 m and a thickness of 0.30 m.

Both tunnels were excavated by means of a TBM with a diameter section of 6.90 m. The existing gap between the segmental lining ring and the drilled soil was 15 cm wide and it was filled with grout.

The analyzed stretch passes through a soil formed by quaternary clay, with a 24.5 m cover and with the presence of the phreatic level 9.5 m above the tunnel crown. In this sense, the numerical simulation of the soil–structure interaction was also carried out with the commercial code FLAC3D [37]. For that purpose, a mesh of 150.0 m wide, 27.5 m high and 40.0 m deep with respect to the horizontal axis of the tunnels was

generated (see Fig. 13). The elements width in the direction of the tunnel equals the width of the precast segment (1.5 m). Concerning the material properties, the following parameters were considered: $\gamma_r = 21.5$ kN/m^3, $c_r = 30.10^{-3}$ N/mm^2, $\Phi_r = 25.0°$, $E_r = 84$ N/mm^2, $\nu_r = 0.30$. Likewise, a coefficient $K_o = 1.3$ was adopted to take into account the possibility of finding overconsolidated soils (according to the geotechnical reports).

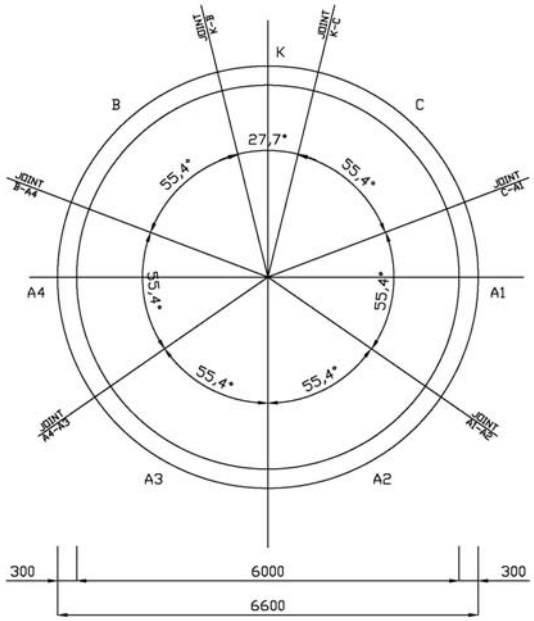

Fig. 12. Main measures (in m) of the transversal section of the Terrassa Tunnel.

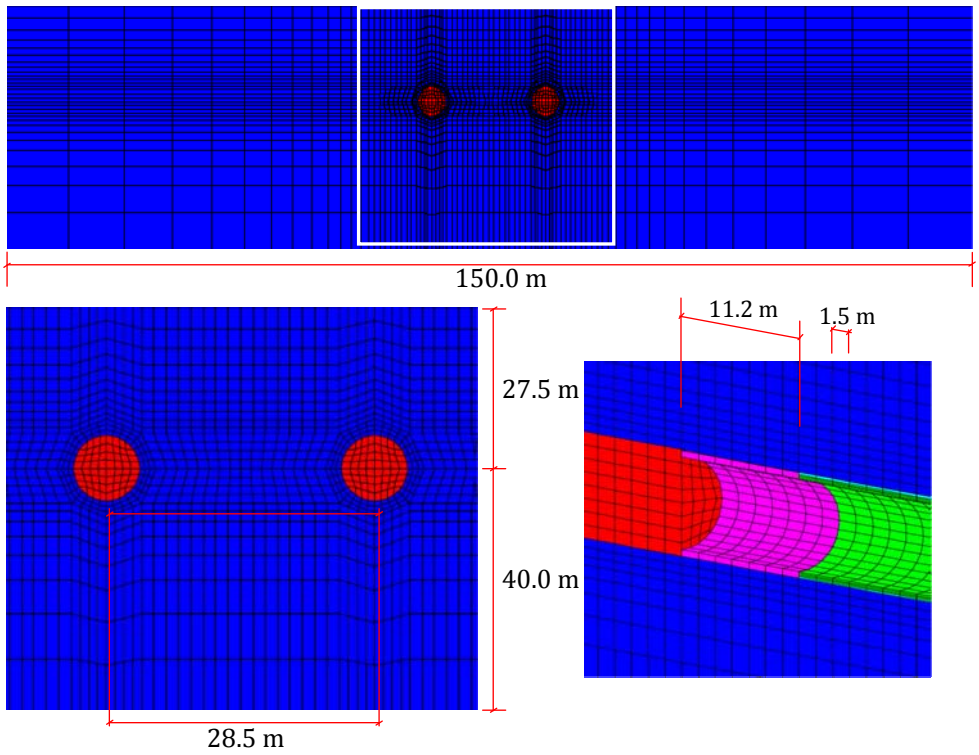

Fig. 13. FE mesh used to simulate the excavation process and the in-service state behaviour for the Terrassa Tunnel.

Table 4 presents the characteristic and design values of N and M obtained for the transitory stages (curing, storage, transport and handling) and the service stage (5), being the latter the most adverse in terms of the design of the reinforcement.

In order to resist the forces presented in Table 4, an initial RC-SFRC precast segment with 15Φ12 in each side (see Fig. 14) plus 25 kg/m³ of fibres was proposed in the project, though the structural contribution of the fibres were not taken into account. The purpose of the fibres in this case was to improve the behaviour under the high expected concentrated loads (thrust of jacks and compressive stresses in the radial joints).

Table 4. Characteristic and design values for the forces at each of the stages.

Stage	N_k (kN)	M_k (mkN)	N_d (kN)	M_d (mkN)
Curing (1)	0	13	0	19
Storage (2)	0	21	0	42
Transport (3)	0	21	0	42
Handling (4)	15	55	29	110
Service (5)	2806	361	4209	542

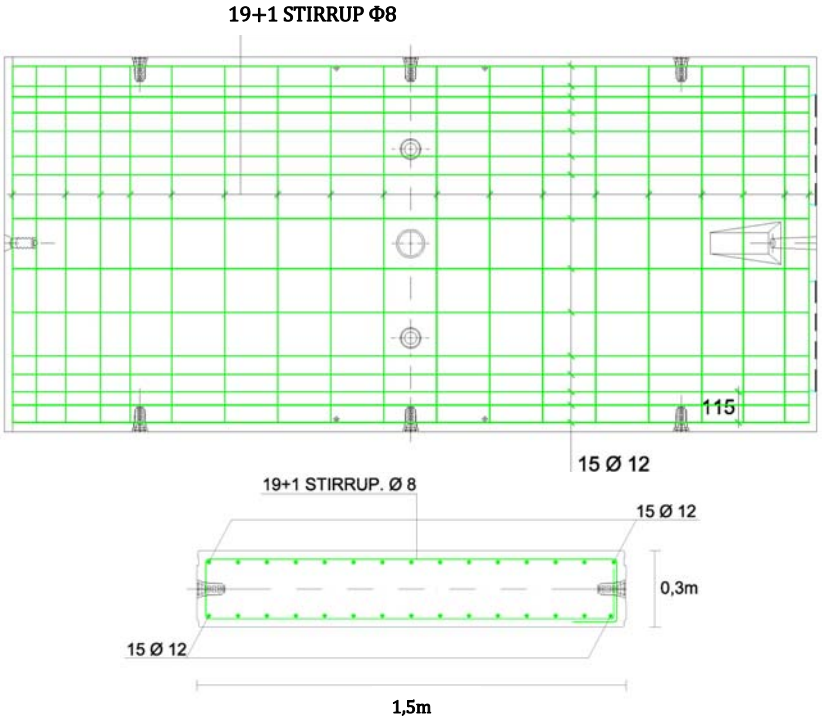

Fig. 14. Steel rebar reinforcement configuration of the segment initially proposed in the project.

Design accounting for the structural contribution of fibers

Similarly to the first case analyzed, a steel rebar reinforcement cage consisting of 11Φ12 and stirrups Φ8 each 25 cm was established (see Fig. 15) to subsequently iterate with different C_f (0, 15, 25 and 30 kg/m³) until the design condition was fulfilled.

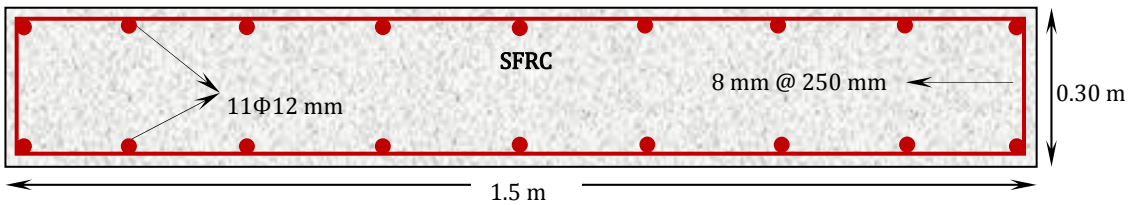

Fig. 15. Optimum RC-SFRC precast segment proposed.

In this case, the service stage (5) leads to the most unfavourable stress-strain conditions. The precast segment is subjected to a high axial load N_d with a concomitant M_d which cracks the section. Thus, the amount of reinforcement resulting from imposing Eq. 4 would be insufficient and, therefore, would not be on the side of safety. Hence, the classical criterion of optimum in ULS design was used, which consists in fixing N_d and impose Eq. 7. Likewise, once the optimum value of C_f was obtained, it was verified that w_k was lower than the $w_{max} = 0.3$ mm established in the basis of the project.

$$M_u = M_d \tag{7}$$

Once again, since no previous experimental data about SFRC for the different values of C_f was available, Eqs. 5 and 6 were used with the aim of defining the parameters (see Table 5) of the constitutive equation chosen (see Fig. 3b) for simulating the post-cracking behaviour of SFRC class C30/37.

Table 5. Values of σ_i and ε_i used to simulate the post-cracked behaviour of SFRC (C30/37).

C_f (Kg/m³)	$f_{r,1}$ (N/mm²)	$f_{r,4}$ (N/mm²)	σ_1* (N/mm²)	ε_1 (mm/m)	σ_2 (N/mm²)	ε_2 (mm/m)	σ_3 (N/mm²)	ε_3 (mm/m)
0	0.702	0.650	3.245	0.101	0.246	0.201	0.187	25.000
15	2.120	1.963	3.245	0.101	0.743	0.201	0.566	25.000
25	3.065	2.838	3.245	0.101	1.074	0.201	0.818	25.000
30	3.537	3.275	3.245	0.101	1.240	0.201	0.944	25.000

* σ_1 was evaluated by means de expression $\sigma_1 = 0.52 f_{ctm,fl}(1.6\text{-}d)$ proposed by [39] due to the high values obtained with the one suggested by [16].

The response of the steel rebars was dealt with the diagram of Fig. 3c, assigning $f_{yk} = 500$ N/mm² and $E_s = 210000$ N/mm².

Fig. 16 shows the N_u-M_u interaction diagram for the section with the RC-SFRC precast segment defined in Fig. 15 with values of C_f ranging between 0 and 30 kg/m³.

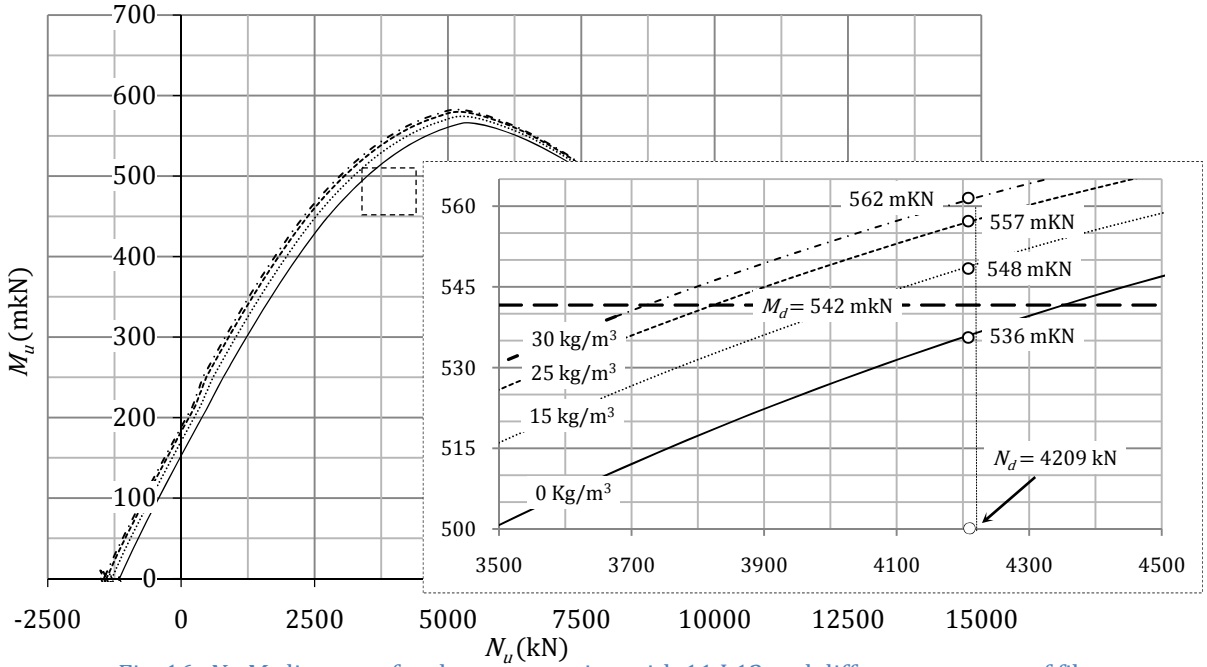

Fig. 16. N_u-M_u diagrams for the cross section with 11Φ12 and different amounts of fibers.

On the basis of the results gathered in Fig. 16, it is observed that with a C_f of 15 kg/m³, the M_d of 542 mkN (see Table 4) is already exceeded. Likewise, it should be noted that the maximum increase of M_u does not exceed 5% (RC-SFRC with $C_f = 30$ kg/m³) with regard to the RC precast segment ($C_f = 0$ kg/m³) if $N_d =$

4209 kN. In other words, in this case the rebars perform the main resistance function in failure, whereas the fibers play a more important role in the crack width control.

Fig. 17 shows the M_u-C_f and $M_{0.3mm}$-C_f curves numerically obtained by fixing N_d = 2806 kN, highlighting that: (1) both curves can be excellently well approximated with straight tendencies; (2) ULS is the most unfavourable state, however just a minimum of 7 kg/m³ is required in order to verify Eq. 7; and (3) the growth rate of $M_{0.3mm}$ (1.22 mkN/kg/m³) is a 42% higher than that of M_u (0.86 mkN/kg/m³), proving the higher effectiveness of the fiber for loads in the SLS in comparison with ULS.

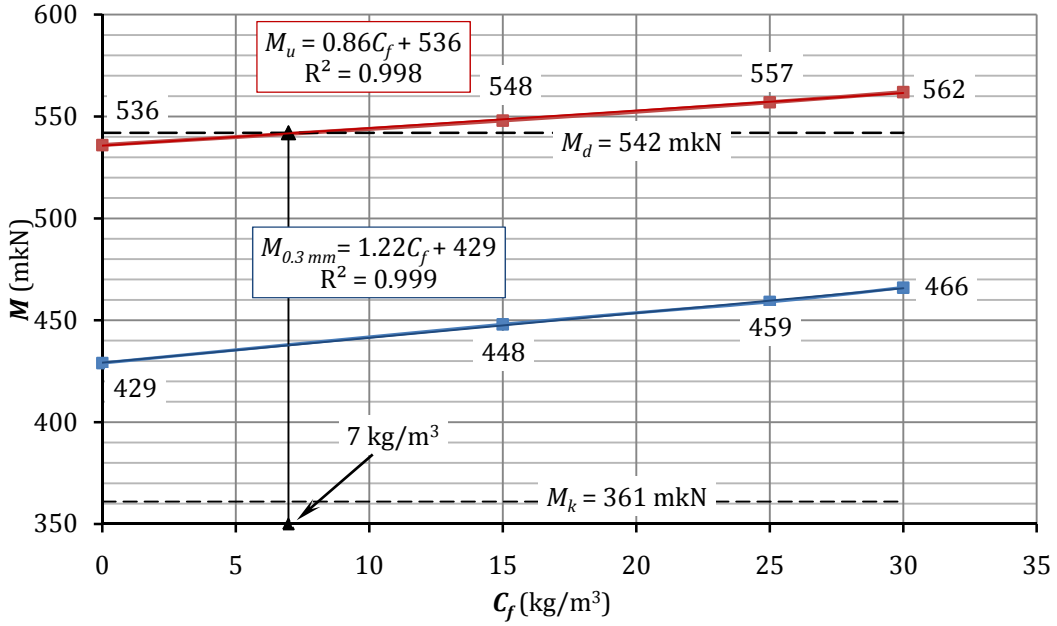

Fig. 17. Evolution of the $M_{w=0.3mm}$ and M_u with C_f

Finally, it was suggested the use of the same C_f of 25 kg/m³ established in the project together with the steel rebar cage presented in Fig. 15 (which represents a reduction around the 38% of the conventional reinforcement comparing with the initial solution gathered in Fig. 14), in opposition to the optimum value of 7 kg/m³ obtained numerically. This decision was made for several reasons: (1) it is unusual to work with such low values of C_f and (2) that the previous experiences indicate that a minimum amount of 20 kg/m³ is required for the control of the possible cracking due to the effect of concentrated loads.

B.6. Conclusions

A summary that includes the main worldwide applications of SFRC in precast segmental linings as well as a design methodology for the optimization of the reinforcement taking into account the structural contribution of the fibres have been presented.

To highlight both the advantages of using fibres and the suitability of the design methodology described, two real experiences carried out in Barcelona in which SFRC has been used in the tunnel segments have been presented. The reached conclusions are:

- The use of both fibres and a minimum amount of steel rebars is an ideal alternative to enhance the behaviour of the segments to the thrust of the jacks and avoid cracking during this operation.
- When the design forces are relatively low in comparison with the segment cross-section dimension, the use of fibres can lead to a significant reduction (up to 70%) of the steel rebars, remaining the concrete confining stirrups as the only passive reinforcement.

- In cases when design forces are moderate, the required amount of fibres to resist them can be economically unfeasible as the case of Terrassa Tunnel. Alternatively, the combined solution of fibres and rebars can be used. With this the fibres work from the onset of cracking, controlling its width and spacing, while the rebars take on the main resistant function.

One experimental stretch consisting of ten RC-SFRC precast pilot rings with an optimum reinforcement configuration (two edge stirrups Φ8 mm @ 180 mm + 25 kg/m^3 of steel fibres) has been carried out in the FontSanta Trinitat tunnel. Likewise, the RC-SFRC precast segment proposed for the Terrassa Tunnel (11Φ12 in each side + 1 stirrup Φ8 mm @ 250 mm + 25 kg/m^3 of steel fibres) has been presented. However, the RC-SFRC precast segmental lining initially designed in the project (for which the contribution of the steel fibres was not considered) was finally used. The obtained results were excellent at a production level (reducing times and risks during the manufacture) as well as in efficiency rates (decreasing significantly the problems related to impact and the thrust of jacks) thanks to the use of fibres.

These satisfying results have motivated the appearance of new tunnelling projects in which the use of fibres is being taken into account as a reinforcement material for concrete.

B.6. Acknowledgments

The authors of this paper want to acknowledge the economical support provided in order to develop the study of the FontSanta-Trinitat Tunnel (FCC Construcción, S.A., OHL, S.A., and COPISA, S.A.) and the Terrassa Tunnel (FCC Construcción, S.A., OHL, S.A., and COPISA, S.A.). Likewise, this work has been possible thanks to the economical support received of the Research Project BIA2010-17478: Procesos constructivos mediante hormigones reforzados con fibras.

B.7. References

1. di Prisco, M., Toniolo, G., 2000. Structural applications of steel fibre reinforced concrete. In: Proceedings of International Workshop, Milan (Italy), April 4, 2000 (CTE Publ., Milan (Italy)).
2. di Prisco, M., Plizzari, G., Vandewalle, L., 2009. Fibre reinforced concrete: New design perspectives. RILEM Materials and Structures **42** (9), 1169-1171.
3. Walraven, J., 2009. High performance fibre reinforced concrete: progress in knowledge and design codes. RILEM Materials Structures **42** (9), 1247-1260.
4. de la Fuente, A., Aguado, A., Molins, C., Armengou, J., 2010a. Innovations on components and testing for precast panels to be used in reinforced earth retaining walls. Construction and Building Materials. [In Press].
5. Waal, R.G.A. de., 1999. Steel fibre reinforced tunnel segments for the application in shield driven tunnel linings. ISBN 90-407-1965-9, Delft (The Netherlands).
6. Blom, C.B.M., 2002. Design philosophy of concrete linings in soft soils. ISBN 90-407-2366-4, Delft (The Netherlands).
7. Plizzari, G.A., Tiberti, G., 2006. Steel fibres as reinforcement for precast tunnel segments. Tunnelling and Underground Space Technology **21** (3-4) pp. 438-439. Special Issue: Safety in Underground Space (CD-ROM Proceedings of the ITA-AITES 2006 World Tunnel Congress and 32nd ITA General Assembly).
8. Burguers, R., Walraven, J., Plizzari, G.A., Tiberti, G., 2007. Structural behavior of SFRC tunnel segments during TBM operations. In: World Tunnel Congress ITA-AITES 2007, Prague (Czech Republic), pp. 1461-1467.

9. Caratelli A, Meda A, Rinaldi Z, Romualdi P., 2010. Structural behavior of precast tunnel segments in fiber reinforced concrete. Tunnelling and Underground Space Technology. [In Press].
10. Plizzari, G.A., Cominoli, L., 2005. Numerical simulations of SFRC precast tunnel segments. In: World Tunnel Congress ITA-AITES 2005, Istambul (Turkey), May 7-12, pp. 1105-1111.
11. Tiberti, G., Plizzari, G.A., Walraven, J., Blom, CBM. 2008. Concrete tunnel segments with combined traditional and fiber reinforcement. Tailor Made Concrete Structures, 2008, Chapter 37. Walraven & Stoelhorst (eds.) 2008 Taylor & Francis Group, London, ISBN 978-0-415-47535-8.
12. Tiberti, G., Plizzari, G.A., 2008. Final concrete linings with optimized reinforcement. In: World Tunnel Congress ITA-AITES 2008, Agra (India), September 22-24, pp. 922-932.
13. Chiaia, B. Fantilli, A.P. Vallini, P. 2009a. Combining fiber-reinforced concrete with traditional reinforcement in tunnel linings. Engineering Structures **31** (7), 1600-1606.
14. Chiaia, B., Fantilli, A.P., Vallini, P., 2009b. Evaluation of minimum reinforcement ratio in FRC members and application to tunnel linings. RILEM Materials and Structures **42** (3), 339-351.
15. DBV – Recommendation (German Concrete Association). 1992. Design principles of steel fibre reinforced concrete for tunnelling works, pp. 19-29.
16. RILEM TC 162-TDF, 2003. Test and design methods for steel fibre reinforced concrete. σ-ε design method: Final recommendation. RILEM Materials and Structures **36** (262), 560-567.
17. CNR DT 204/2006. 2006. Guidelines for the Design, Construction and Production Control of Fibre Reinforced Concrete Structures, Italian National Research Council - CNR.
18. CPH 2008. EHE-08: Instrucción del Hormigón Estructural.
19. Vandewalle, M., 2005. Tunnelling is an art. Ed. by N.V. BEKAERT, S.A., Zwevegem (Belgium). 400 pp.
20. Angerer, W., Chappell, M., 2008. Design of steel fibre reinforced segmental lining for the gold coast desalination tunnels. In: 13th Australian Tunneling Conference, Melbourne (Australia), May 4-7, pp. 263-470.
21. Kasper, T., Edvardsen, C., Wittneben, G., Neumann, D., 2008. Lining design for the district heating tunnel in Copenhagen with steel fibre reinforced concrete segments. Tunnelling and Underground Space Technology **23** (5), 574-587.
22. Telles, R.C.A., de Figueiredo, A.D., 2006. The possibility of using new technologies in precast concrete segments for TBM-excavated tunnels. Concreto e Construção **33** (41), 30-35. [In Portuguese].
23. Sandy, A., 2008. Clem Jones Tunnel joins up ahead of schedule. In: Queensland Newspapers (12-08-2008).
24. MACCAFERRI 2009. Hobson Bay Sewer Tunnel. Case History. Technical Report 1, October 2009.
25. Jones, J., 2009. Steel and synthetic fiber in tunnels and mine, Technical Report. BASF 2009.
26. Molins, C., Marí, A.R., García, T., 2009. On-site stress tests of lining segments for Barcelona's underground tunnel. Scientific journal HBM measurement. Report in: Applied Measurement. ISSN 1614-9912.
27. Cavalaro, S.H.P., 2009. Aspectos tecnológicos de túneles construidos con tuneladora y dovelas prefabricadas de hormigón. PhD Thesis, UPC, Barcelona (Spain).
28. de la Fuente, A., Aguado, A., Molins, C., 2008. Numerical model for the nonlinear analysis of precast and sequentially constructed sections. Hormigón & Acero **57** (247), 69-87. [In Spanish].
29. Bencardino, F., Rizzuti, L., Spadea, G., Swamy, R.N., 2008. Stress-strain behavior of steel fiber-reinforced concrete in compression. ASCE Journal of Materials in Civil Enineering **20** (3), 255-263.
30. Barros, J.A.O., Figueiras, J.A., 1999. Flexural behaviour of SFRC: Testing and modeling. ASCE Journal of Materials in Civil Engineering **11** (4), 331-339.

31. Blanco, A., Pujadas, P., de la Fuente, A., Aguado, A., 2010. Comparative analysis of constitutive models of fibre reinforced concrete. Hormigón & Acero **61** (256), 83-100. [In Spanish].

32. de la Fuente, A., de Figueiredo, A.D., Aguado, A., Molins, C., Chama Neto, P.J., 2010b. Experimentation and numerical simulation of steel fibre reinforced concrete pipes. Materiales de Construcción. [In press].

33. ENV 1992-1-1/2005. Eurocode 2: Design of concrete structures – Part 1-1: General rules and rules for buildings. CEN.

34. Vandewalle, L., 2000. Cracking behaviour of concrete beams reinforced with a combination of ordinary reinforcement and steel fibers. RILEM Materials and Structures **33** (3), 164-170.

35. Yang, W.Y., Wenwu, C., Chung, T.S., Morris, J., 2005. Applied numerical methods using Matlab. John Wiley & Sons Inc., Hoboken, New Jersey (USA).

36. Nguyen, D.T., 2006. TBM and lining – essential interfaces. Master Thesis. Politecnico di Torino (Italy).

37. Itasca Consulting Group Inc. 2006. FLAC-3D Manual: Fast Lagrangian Analysis of Continua in 3 Dimensions. Version 3.10. Itasca Consulting Group Inc., Minnesota (USA).

38. Levi, F., 1985. On minimum reinforcement in concrete structures. ASCE Journal Structural Engineering **111** (12), 2791-2796.

39. Barros, J.A.O., Cunha, V.M.C.F., Ribeiro, A.F., Antunes, J.A.B., 2005. Post-cracking behaviour of steel fibre reinforced concrete. RILEM Materials and Structures **38** (1), 47-56.

Nomenclature

A_c: Total concrete area.
$A_{s,i}$: Area of the i-th steel bar.
dA_c: Differential of concrete area.
C_f: Amount of steel fibres.
c_r: Cohesion of the soil.
D_i: Internal diameter of the tunnel.
d: Effective depth of the tensioned steel rebars.
d_f: Diameter of the fibre.
E_{cm}: Average Young modulus of concrete.
E_f: Young modulus of the fibre.
E_r: Young modulus of the soil.
E_s: Young modulus of steel.
f_c: Compressive strength of the concrete.
f_{cm}: Average compressive strength of concrete.
f_{ck}: Characteristic compressive strength of the concrete
$f_{ctm,fl}$: Average flexural strength of the concrete.
$f_{ctk,fl}$: Characteristic flexural strength of the concrete.
f_{fu}: Failure tensile strength of the steel fibre.
$f_{R,i}$: I-th post-cracking residual flexural strength of SFRC.
f_{yk}: Characteristic yielding strength of steel.
h: Height of the cross section of the segment.
K_o: Coefficient of lateral earth pressure.
k_h: Size factor.
l_f: Length of the fibre.
M: Applied external bending moment.
M_{cr}: Cracking bending moment.
M_d: Design bending moment.
M_k: Characteristic bending moment.
M_{max}: Maximum bending moment.
$M_{0.3mm}$: Bending moment associated with a crack width of 0.3 mm.
M_u: Ultimate bending moment.
N: Applied external axial force.
N_d: Design axial force.

N_K:	Characteristic axial force.
N_u:	Ultimate axial force.
n_s:	Number of steel bars.
x_n:	Depth of the neutral axis.
y_c:	Ordinate of the gravity centre of the concrete area element.
y_{cdg}:	Ordinate of the gravity centre of the section.
$y_{s,i}$:	Ordinate of the *i*-th steel bar.
w:	Crack width.
w_{max}:	Maximum crack width.
w_K:	Characteristic value of the crack width.
Φ:	Steel bar diameter.
Φ_f:	Friction angle of the soil.
γ_f:	Specific weight of the soil.
ε_c:	Concrete strain.
ε_{co}:	Strain for the maximum compressive stress of the concrete.
ε_o:	Strain of the bottom fibre.
ε_{cu}:	Maximum strain of the compressed concrete.
ε_i:	*I*-th post-cracking tension strain of the SFRC.
ε_s:	Strain of the steel.
$\varepsilon_{s,i}$:	Strain of the *i*-th steel bar.
ε_y:	Yielding strain of the steel.
λ:	Aspect ratio of tunnel (D_i/h).
ν_f:	Poisson ratio of the soil.
σ_c:	Concrete stress.
σ_i:	*I*-th post-cracking tension strength of the SFRC.
σ_u:	Compressive stress of concrete at maximum strain.
σ_s:	Stress of the steel.
$\sigma_{s,i}$:	Stress of the *i*-th steel bar.
χ:	Sectional curvature.
χ_{cr}:	Cracking sectional curvature.
χ_u:	Ultimate sectional curvature.

APPENDIX C

Lightweight self-compacting concrete reinforced with fibres for slab rehabilitation

C.1. Abstract

The slabs of certain buildings in Barcelona and its surroundings are formed by unidirectional beams, with a ceramic arch in between. The filling material placed between the arch and the upper floor is usually broken pottery or construction waste. Therefore, these structures often present problems such as displacement and detachment of the tiles arranged over it due to the lack of stiffness of the filling material. This situation poses a risk to the user and could also cause durability problems. Therefore, in order to rehabilitate these structures, a lightweight self-compacting concrete reinforced with fibres (HLACF, from Spanish *hormigón ligero autocompactante con fibras*) has been designed to be used as filling material, with the purpose of improving the stiffness of the structure.

This paper presents a structural analysis of a standard structure and also the results obtained in the experimental campaign performed for the design of the HLACF. As a result, the concrete designed has a density of 1,665 kg/m^3, a slump flow of 605 mm and a compressive strength of 22.3 MPa, at 28 days. These results are in agreement with the requirements. The segregation problems commonly found in this type of concrete have been overcome.

Key words: Viscosity modifier admixture, lightweight concrete, self-compacting concrete, fibres, rehabilitation

C.2. Introduction

The buildings in the area which expanded from the citadel of Barcelona were designed by Ildelfons Cerdà. The common structural solution adopted for the slabs of these buildings consists of unidirectional beams, with a ceramic arch in between, as shown in Fig. 1. A filling material is placed between the arch and the upper floor, which is often formed by broken pottery or construction waste [1-2]. The basic function of the filling material is to provide flatness at the upper side of the slab and to guarantee a monolithic structure, even though reinforcement is commonly not present over the beams.

Fig. 1. Typical bottom view of the slabs studied.

In this configuration, when a load is placed over a beam, the transversal distribution of the load is deficient. This is a consequence of the low transversal stiffness, which creates movement and detachment of the tiles arranged over the slab. Therefore, the durability of the structure is compromised because it facilitates the entrance of aggressive agents from the cleaning products. In addition, the movement of the tiles provokes imperfections on the floor that could lead to injury of the user, especially of elderly people, who may have disabilities of movement or vision.

With the passing of time or the changing of the function of the buildings, rehabilitation is required. For the situation presented in this paper, several factors should be observed, such as: the necessity of producing monolithic structures, maintaining the structure weight or adapting the casting of the filling material to urban reality, bearing in mind the reduction of time of public highway occupation.

To address these conditions, it is proper to think about a lightweight self-compacting concrete reinforced with fibres (HLACF, from Spanish *hormigón ligero autocompactante con fibras*). The lightweight feature meets the need of maintaining the structure weight and even allows increasing the thickness of some elements. The self-compactability facilitates the construction process and reduces the time of casting, and fibres provide stiffness and better mechanical characteristics. The rehabilitation solution consists of removing the supra-structure that does not develop any mechanical function (tiles and filling material), while maintaining the ceramic arch and the beams. Subsequently, the filling with HLACF would be carried out. After that, the restitution of the tiles would take place.

The production of the HLACF is considered a challenge because the contrasting properties are inherent to the configuration proposed. A clear example of that is the use of lightweight aggregates, which could promote segregation with their floatation on a self-compacting mortar. Although the technical literature makes ample references to some types of SCC, like lightweight SCC or SCC with fibres, and it also contains information on the potential problems [3], there are scarce references when it comes to the proposed material. Experimentation with lightweight self-compacting concrete with steel fibres has been developed [4], but the mechanical results are insufficient when contrasted to the performance required in the present situation.

The first purpose of this paper is to determine the order of magnitude of the mechanical characteristics required by the HLACF at a sectional level. And the second one is to demonstrate the viability of this concrete from an experimental point of view. In forthcoming papers, the industrial viability will be analysed since it has already been verified.

To address these matters, a structural analysis for a standard structure is firstly developed with the objective of defining the basic requirements. Later, the results obtained in the concrete experimental campaign will be presented and analysed. The aim of the strategy is to offer an integrated vision of the engineering problems. This is important in order to solve them satisfactorily and increase the industrial acceptance of the results. The HLACF presented in this paper has been patented and licensed by the PROMSA Company [5].

C.3. Structural verification

C.3.1. Structural scheme and applied loads

For this initial calculation, the structure dimensions that were adopted were slightly higher than the real ones, as the main purpose was only to determine the order of magnitude of the concrete requirements. For this, a rectangular slab of 5 x 10 metres is considered, in which the direction of the beams is parallel to the short side of the slab, and the distance between each beam is of 1 m, as shown in Fig. 2. To verify the limit states, 4 sections were chosen (indicated with the letter S). The numbers indicate the height of the section in cm.

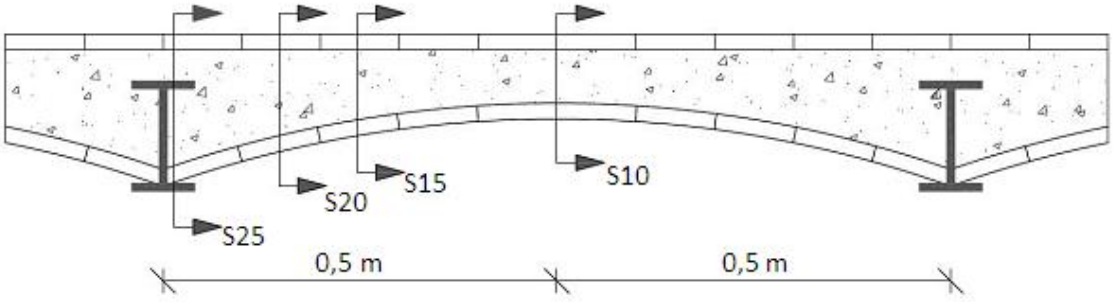

Fig. 2. Sections taken as representatives of the arch behavior.

With the purpose of calculating the internal forces, it has been considered that the slab is simply supported in the four perimeter edges. This configuration leads to the highest bending moments in the centre of the slab and also to the maximum displacements. This numerical treatment of the boundary conditions is important to determine the orders of magnitude. But it is also reasonably realistic as these slabs do not present continuity and there is no reinforcement between the slab and the structural wall that might guarantee the connection or stiffness. On the other hand, the steel beams were considered embedded in the lateral wall.

The resistant section considered is only the HLACF, which – in the absence of bar reinforcement – behaves in the same way in the presence of bending forces of both positive and negative sign. It is important to highlight that the transversal section is formed in the bottom side with the ceramic arch and in the top with the tiles (floor), so that the strength is slightly higher. However, this possible increase is not taken into account for a couple of reasons: due to the difficulty to model this situation and because its contact and irregular position may lead to think that all these elements work in a monolithic way.

To verify the limit states, the actions and combinations proposed by the *SE-AE Acciones en la Edificación* [6] have been taken as valid. More specifically, it has been considered that the buildings belong to the residential category type (A), subcategory A2. Therefore, considering the suggestions proposed in this code, the uniform load q_p is 3 kN/m² and the concentrated overload q_c is 2 kN/m². These actions are properly combined, together with the weight of the structure and the supra-structure in order to obtain the internal forces used to design the concrete reinforcement.

C.3.2. Materials and analysis method

The analysis carried out is supported by the experimental campaign presented later. During this campaign both steel and synthetic structural fibres were used. However, for the structural analysis initially made, only synthetic fibres were considered because they generally present a tensile residual strength smaller than that of the steel fibres. In this numerical study, Strux 90/40 fibres were considered since contrasting results were available [7]. The compressive strength considered was 25 MPa and the specific weight was 18 kN/m^3.

The modelling of the compressive and the tensile behaviour of HLACF is simulated using a curve considering the softening behaviour of concrete in compression [8] and the constitutive law suggested by the TDF-162 Committee [9], respectively. In Table 1 the parameter values of stress and strain (σ_i and ε_i, respectively) used for the definition of the constitutive curve of HLACF in tension are presented [7]. The relative values and the fibres content of 2.28 and 4.55 kg/m^3 are real, while the other fibre contents were linearly extrapolated. As a first approximation, this approach is valid and justified for moderated amounts of steel fibres [10]. These values have been considered valid for representing the behaviour of concrete at sectional level.

Table 1. Parameter values of the constitutive equation (σ_i and ε_i are stress and strain, respectively).

Fibres (kg/m^3)	f_{ck} (MPa)	σ_1 (MPa)	σ_2 (MPa)	σ_3 (MPa)	ε_1 (mm/m)	ε_2 (mm/m)	ε_3 (mm/m)
2,28	25	2,75	0,50	0,31	0,0859	0,186	25,000
4,55	25	2,75	0,69	0,49	0,0859	0,186	25,000
5,5	25	2,75	0,77	0,56	0,0859	0,186	25,000
6,5	25	2,75	0,85	0,63	0,0859	0,186	25,000
7,5	25	2,75	0,94	0,71	0,0859	0,186	25,000

The design strategy adopted for the reinforcement was initiated with the calculation of the unfavourable internal forces under the combinations derived from the hypothesis of loads, and considering the linearity of the structural response. In order to do this, the software SAP2000 v.11.0 non-linear version was used to model the slab through 2D elements; and the metallic beams, through beam elements.

With the internal forces values obtained from previous analyses, the model *Análisis Evolutivo de Secciones (AES)* [11-12] is used to simulate the behavior of the 4 control sections. When the global behavior of these sections is known, an iteration is carried out with several fibre contents until all the design bending moments are compatible with the dimentions and the reinforcement of the control sections.

C.3.3. Results and discussion

Structural level

Through the structural analysis using the finite elements method (FEM), it is verified that the structure presents a predominant unidirectional behaviour. It is demonstrated that the bending moments M_{yy} are negligible in practically the whole central zone of the slab, as shown in Fig. 3. Indeed, the bending moments are concentrated on the area of contact between beam and concrete for reasons of compatibility of movement and local effects. At the same time, at this area, the concrete presents a higher height. For this reason, its strength response is also higher. Thus, it is verified that the predominant behaviour is unidirectional in the direction x, as shown in Fig. 4. Therefore, the structural analysis will be carried out considering this direction.

The design bending moments (M_d) from the sections considered as representative (see Fig. 2) are taken to verify the ULS. These bending moments are shown in Table 2. Due to the structural continuity in the beam-concrete contact area (S25), negative bending moments are generated (compression on the bottom side of the slab) in the centre zone between two beams. These moments decrease until the sign is changed

(tensile on the bottom side of the slab). Indeed, the bending moments in the beam-concrete area of contact (S25) are approximately 10 times higher than the ones in the centre section (S10).

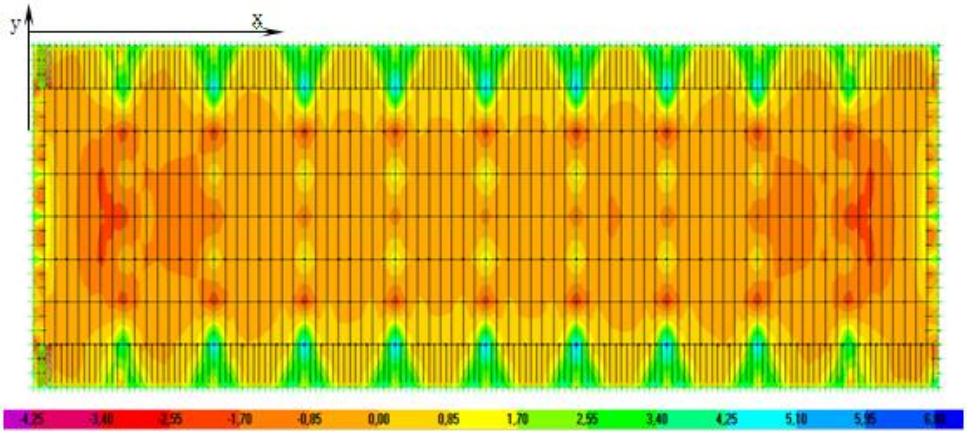

Fig. 3. Bending moments in the *y* direction (M_{yy})

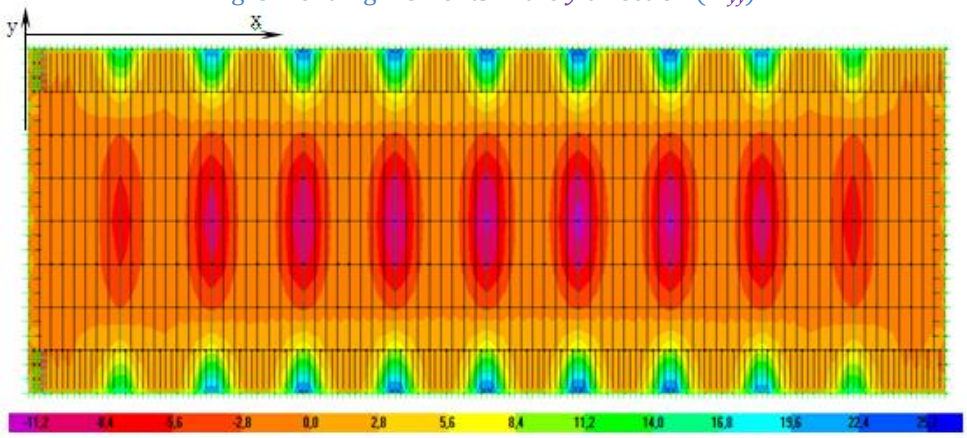

Fig. 4. Bending moments in the *x* direction (M_{xx})

Table 1. Design bending moments M_d (absolute value) for the control sections (mkN/m).

S25	S20	S15	S10
23,0	14,3	8,0	2,0

Another parameter that should be controlled is the maximum displacement of the structure. Controlling this variable to a reasonable extent would prevent the movement and detachment of the tiles, and the consequent repercussions at the esthetical and functional levels. The calculation shows that the maximum displacement is of 0.8 mm in the most unfavourable hypothesis (self weight + uniform overload + centred overload). This value is sufficiently small to guarantee that in real structures, with distances smaller than 1 metre between beams, the tiles would not suffer any displacement or detachment.

Sectional level

The numerical model AES [11-12] provides failure bending moments M_u for distinct h heights and different amounts of ρ fibres. The height values adopted vary from 10 to 25 cm (height of the control sections presented in Fig. 2) and the fibre content between 2.28 and 7.5 kg/m^3, which were considered technically and economically viable. The results show that M_u increases in a parabolic way with ρ, according to the Eq. 1, where ξ_1 depends on the fibre content (ρ), considering a specific fibre type and concrete.

$$M_u = \xi_1 h^2 = 10^{-3}(3.53\rho + 11.04)h^2 \quad (1)$$

Therefore, using Eq. 1 and considering the design loads presented in Table 3, it is possible to calculate the minimum fibre densities necessary to meet structural requirements.

Table 3. Calculation of the minimum fibre content ρ_{min} using Eq. 1.

Section	h (cm)	M_d (mkN/m)	$\rho_{mín}$ (kg/m^3)
S25	25	22,3	7,0
S20	20	14,3	6,8
S15	15	8,0	6,9
S10	10	2,0	2,5

According to the obtained results shown in Table 3, it is verified that the reinforcement design is governed by the sectional behaviour in the beam-concrete contact area, where the highest bending moments are developed (negative flexion). Thus, the minimum fibre content ρ_{min} that should be used is of 7.0 kg/m^3, because, for smaller distances between beams, the bending moments and the fibre content needed to address the respective requirements will also be lower.

It is important to highlight that this initial structural analysis was carried out in order to determine the order of magnitude of the variables involved in the design of the structural elements and the concrete. In fact, the values adopted for the calculation are higher than the usual ones for real structures. Indeed, with the purpose of verifying the viability of the material, the established requirements are: a slump flow diameter of 600 $\pm$ 50 mm at the fresh state, a density lower than 1,700 kg/m^3 at the hardened state and a minimum compressive strength of 20 MPa, at 28 days.

C.4. Experimental campaign

Once the order of magnitude of the concrete requirements was established, an experimental campaign was performed to analyse the viability of the HLACF.

C.4.1. Materials and mix design

The selected materials for the experimental campaign are:

- As coarse aggregates: lightweight aggregates of expanded clay from two different plants of the same brand. One has a spherical form and the other, a more oval one. Besides, two ranges of size distribution were used, 3-10 mm and 6-16 mm, which correspond to the densities of (550 $\pm$ 50) kg/m^3 and (325 $\pm$ 50) kg/m^3, respectively. These aggregates had been added to the mixture on a dry condition, without previous saturation.
- 0-4 mm sand and 4-10 mm gravel have been used as natural aggregates. They are both crushed and limestone aggregates. Limestone filler has also been used as mineral admixture to improve the workability and the self-compactability.
- Two types of fibres have been used: steel fibres with a length of 30 mm and a diameter of 0.67 mm, with formed ends; and waved synthetic fibres (polyester) with a length of 30 mm and a thickness of 1.2 mm. For the application considered, both types of fibres can be used because they will be protected by the concrete.
- The other materials are: Portland cement CEM II/A-L 42.5 R, the chemical admixtures are a plasticizer and a superplasticizer of polycarboxylate base. This last admixture has been proved to be efficient on the control of segregation when a concrete with component materials of very different densities is produced [13]. Finally, a viscosity modifier admixture is also used to guarantee the reduction of concrete segregation.

Table 4 shows the dosage of the component materials used to produce the studied concretes. Three series can be observed: series 1 has the purpose of evaluating the influence of the filler content, while series 2

seeks to investigate the effect of a modified granular skeleton. What is more, the influence of the viscosity modifier admixture and the fibres are also analysed. Series 3 has the objective of examining the changes produced when lightweight aggregates of different sources are used. For this reason, the mix proportions P_7 and P_8 are the same, but produced with different aggregates. The results from this last evaluation have demanded an increase in fluidity, and for that reason, the filler content has been raised in P_9.

Table 4. Studied proportions (kg/m³), where P_i is mix proportions 1, 2, etc.

Materials (kg/m³)	**Series 1**			**Series 2**				**Series 3**	
	P_1	**P_2**	**P_3**	**P_4**	**P_5**	**P_6**	**P_7**	**P_8**	**P_9**
Sand 0-4 mm	774	774	774	500	500	500	500	500	500
Gravel 4-10 mm	206	206	206	80	80	80	80	80	80
Lightweight aggregate 3-10 mm	228	228	228	85	85	85	85	85	85
Lightweight aggregate 6-16 mm	-	-	-	90	90	90	90	90	85
Cement	450	405	360	450	450	450	450	450	450
Limestone filler	-	45	90	75	75	75	75	75	100
Steel fibres	40	40	40	40	40	-	-	-	-
Synthetic fibres	-	-	-	-	-	6	6	6	6
Water (l/m³)	188	188	188	183	203	203	203	203	203
Plasticizer	2,7	2,7	2,7	2,7	2,7	2,7	2,7	2,7	2,7
Superplasticizer	8,73	8,73	8,73	8,73	8,73	8,73	8,73	8,73	8,73
Viscosity modifier	-	-	-	-	1	1	0,85	0,85	0,85
Total	1897	1897	1897	1514	1535	1501	1501	1501	1521

The granular skeletons proposed occupy approximately 70 % (granular skeleton A, series 1) and 63 % (granular skeleton B, series 2 and 3) of the concrete volume. The coarse aggregates occupy around 45 % of the total volume. Generally, the volume of the coarse aggregates in SCC is lower [14]. However, for the HLACF it is important to raise the volume of coarse aggregates because these are responsible for reducing the density of the concrete. Table 4 shows that the fresh density of the concretes from mix proportions P_4 to P_9 is clearly below the specified value. This fact enables the full exploration of the possibilities of this new concrete.

C.4.2. Production

For each dosage studied, a 100 litres of concrete was produced, enough for the characterization in fresh and hardened state. The mix was produced in a vertical axis mixer of 250 litres of maximum capacity. The addition of component materials was manual and in a reverse order of grain size, starting with dry coarse aggregates and fine aggregates, and following with the cement and the limestone filler. A dry mixture was first produced (30 seconds) to homogenize and after that, the fibres were added with the mixer moving. In the concretes where the viscosity modifier admixture was used, it was added at the dry state. Before adding water (1 minute mixture) 2 litres were separated to be added along with the plasticizer (1 minute mixture) and the superplasticizer (4 minutes mixture). Its purpose is to improve the dispersion of these chemical admixtures.

C.4.3. Concrete characterization

Table 5 presents the tests to characterize the concrete in fresh and in hardened state and also the reference standards.

Table 5. Performed tests and reference standards.

Fresh state		Hardened state	
Density	UNE-EN 12350-6:2006 [15]	Density	UNE-EN 12390-7:2001 [19]
Slump flow	UNE 83361:2007 [16]	Compressive strength	UNE 12390-3:2003 [20]
Slump flow with the Japanese ring	UNE 83362:2007 [17]	Tensile strength	UNE 83515:2007 [21]
Incorporated air	UNE-EN 12350-2:2006 [18]	-	-

C.5. Results

C.5.1. Results obtained

Fig. 5 presents the results at the fresh state. Axis *x* shows the evaluated variables at each series and the mix proportions in which the viscosity modifier admixture was used. Axis *y* shows the results of the slump flow (with and without the Japanese ring; in mm) and the percentage of incorporated air. This last property was not evaluated for concretes from P_1, P_2 and P_3 because the measuring equipment was unavailable at the time. For the other mix proportions studied, the results are high, as a consequence of the addition of lightweight aggregates at the dry state. In this Fig.5, and also in Fig. 6, the letters VMA and LWA mean viscosity modifier admixture and lightweight aggregate, respectively.

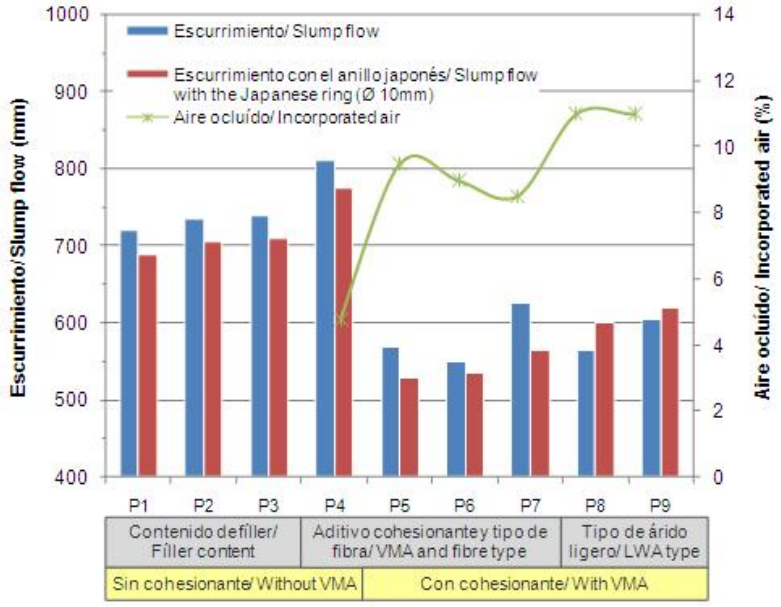

Figure 5. Results at the fresh state.

Fig. 6 shows the results of the compressive strength contrasted with the density at the hardened state (axis *y*). In axis *x*, the variables evaluated at each series are presented and, as well as the mix proportions in which the granular skeletons A and B were used.

Fig. 7 gives the results of the tensile strength obtained by the Barcelona test (UNE 83515: 08). The results are not given for proportions P_1 to P_4 because for these proportions the determination of tensile strength was made by the Brazilian test (UNE 83306: 1985). In axis *x* of this figure, the circumferential deformation is presented (in mm) while the tensile strength obtained for the respective deformation is given in axis *y*, also called residual strength [22].

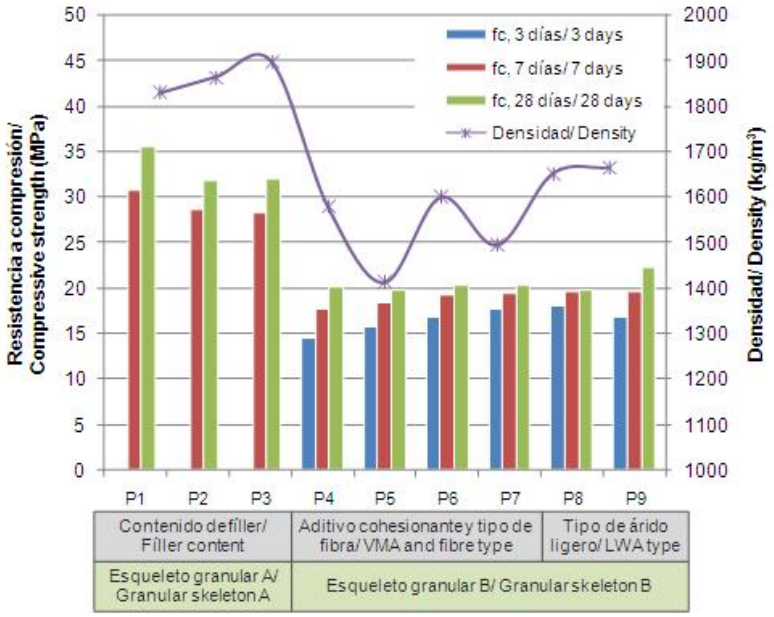

Fig. 6. Results at the hardened state, compressive strength and density.

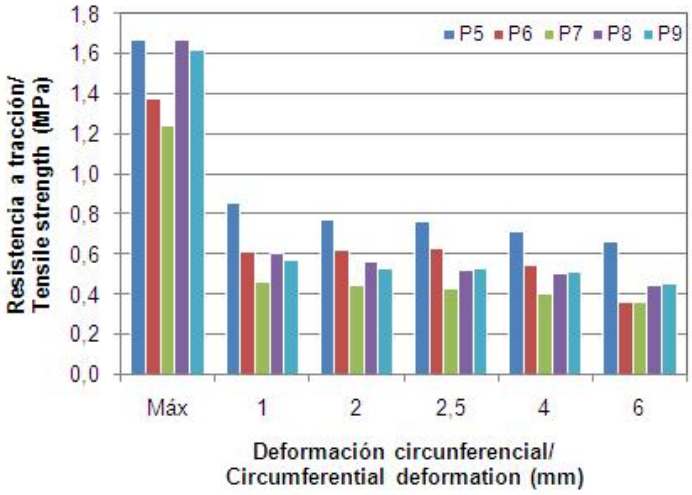

Fig. 7. Results at the hardened state, tensile strength.

Fig. 7 shows that the concrete with steel fibres (P_5) presents residual tensile strengths higher than those of concretes with polyester fibres. This behaviour is due to the anchorage system of the steel fibres, which is more efficient than that of synthetic fibres. Other studies have already revealed that the residual strength is under the influence of the anchorage system. It has been observed that concretes produced with steel fibres present higher residual strength when the ends of the fibre are formed, and lower strength when the ends are flattened. Likewise, both steel-fibres types provide a higher strength than the one given by waved plastic fibres [23].

Table 6 shows the density results at fresh and hardened state, at the age of 24 hours. It is possible to observe that the density at the hardened state is higher than the density at the fresh state in 7 of the 9 studied concretes. This increase may be due to the fact that the container used to determine the volume and the mass of the concrete at the fresh state had a larger capacity than that of the mould of a specimen (used for the determination at the hardened state). Moreover, to release part of the occluded air and

increase the compactness, energy was applied to the specimen moulds with a few hits at the time of casting.

Table 6. Results of density (kg/m³).

Tests	Series 1			Series 2				Series 3	
	P_1	P_2	P_3	P_4	P_5	P_6	P_7	P_8	P_9
Fresh state	1743	1652	1683	1590	1469	1575	1386	1500	1525
Hardened state	1830	1864	1897	1579	1413	1600	1494	1652	1665

C.5.2. Result analysis by variables

To analyse the influence of the *limestone filler content*, the mix proportions P_1, P_2 and P_3 were tested. Although these concretes present high fluidity at the fresh state (a slump flow over 700 mm), they also show a tendency for segregation, and the lightweight aggregates are likely to float in the mass of concrete. Nevertheless, a small increase in the diameter of the slump flow was verified as the filler was added to the concretes (less than 5 % in each situation). This trend is kept in the slump flow tests with the Japanese ring. On the other hand, a small reduction in the strength value was simultaneously observed.

The reason for this behaviour is centred in the specific surface of the filler, which is smaller than that of the cement. When the filler content is increased, the amount of water available in the mixture also increases. Consequently, the workability improves and the strength decreases (around 11 % at 28 days) as a result of the higher water/cement ratio (it goes from 0.42 in the P_1 to 0.52 in the P_3). The strength decrease could be much higher considering the variation observed in the water/cement ratio. Nevertheless, the filler packing effect counterbalances the situation and is favourable to the concrete strength. It is also responsible for the density increase (see table 6 and figure 6).

These first series pointed out the necessity of using a viscosity modifier admixture in order to avoid segregation. That would also allow the incorporation of a lightweight aggregate with larger grains, which would provide lower density.

In the above-mentioned Fig. 5 it is possible to observe that the *incorporation of a viscosity modifier admixture* (in mix proportions P_5 to P_9) reduces significantly the results of the slump flow test (around 20 %). Considering the scope of values (from 0.85 to 1 kg/m³), it seems that the saturation point of the admixture is reached as significant variations in results are not observed. The adoption of a lower admixture content (0.85 < admixture content < 1 kg/m³) would lead to intermediary results of slump flow among the ones obtained for concretes from P_1 to P_4 and P_5 to P_9. It can be observed that mix proportions P_6 and P_7 differ only in the amount of viscosity modifier admixture.

The effect of the viscosity modifier admixture can also be verified in the appearance of segregation and blockage in the Japanese ring. Fig. 8 shows the slump flow test with the Japanese ring for concretes P_4 and P_5, where both mix proportions have the same granular skeleton, but only mix proportion P_5 presents the admixture in its composition. It can be observed that the concrete from P_4 presents segregation, bleeding and great blockage inside the Japanese ring. The same behaviour cannot be seen in the concrete from P_5, because it is homogeneous and is not blocked by the ring bars. Nevertheless, the concrete from P_5 needs a higher amount of water because the viscosity modifier admixture is a powder of great fineness.

At the hardened state, the effect of the viscosity modifier admixture is lower, as can be seen in the Fig. 6 previously presented. An indication of it is the compressive strength at 28 days, which is very similar for all the concretes studied. However, it is important to highlight the vital importance of the viscosity modifier admixture in the production of the HLACF, especially at the fresh state, because the properties which were initially in conflict became compatible.

The results obtained for the concretes from P_1 to P_3 lead to the incorporation of the viscosity modifier admixture and to changes on the *granular skeleton*, which was made starting from mix proportion P_4 with

the intention of reducing concrete density. The changes performed consist of the reduction of natural aggregates and 3-10 mm (550 kg/m^3) lightweight aggregate content, with the incorporation of 6-16 mm (325 kg/m^3) lightweight aggregate and limestone filler, without substituting cement. As a final result, the total amount of aggregates was reduced a 37.5 % in mass, and a 7.0 % in volume.

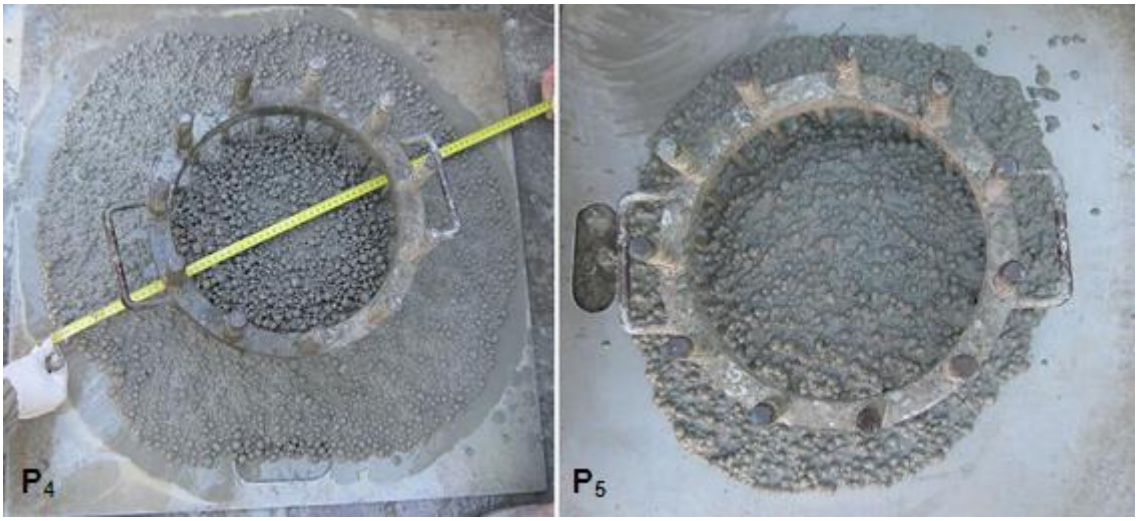

Fig. 8. Slump flow test with the Japanese ring, concretes P_4 and P_5.

At the fresh state, an increase in the concrete fluidity can be observed as a result of the measures adopted in the modification of the granular skeleton, such as the filler incorporation and the reduction on the 0-4 mm sand content. The tendency to segregation is confirmed in the concrete from P_4, which points out the need for improving the cohesion, as can be seen in Fig. 8 (P_4).

At the hardened state, significant reductions on density are observed and as a consequence, compressive strength also decreases. The values of density around 1,800 kg/m^3 obtained on the first series (P_1 to P_3) are reduced to values around 1,600 kg/m^3. The compressive strength decreases to values around 20 MPa at 28 days.

The influence of the ***type of fibre*** is verified through the concretes from mix proportions P_5 and P_6. The change from steel fibres (P_5) to synthetic fibres (P_6) produces a small reduction on fluidity (3.5 %). This can be a consequence not only of the material (the higher roughness of polyester fibres) but also of the fibre aspect ratio, which is higher for the synthetic fibres. However, the results of the slump flow test with the Japanese ring show higher reduction of diameters for concretes with steel fibres, which indicates a higher blockage. This could be the result of the higher stiffness of the steel fibres when compared to the synthetic ones.

At the hardened state, the effect of the fibre type is reflected not on the compressive strength, but on the tensile strength. The results show that the compressive strength is a little bit higher for concrete with synthetic fibres (only a 2.5 %). However, when it comes to tensile strength, the differences are more evident as the concrete with steel fibres presents a maximum tensile strength an 18 % higher than that of the concrete with polyester fibres.

The residual tensile strengths are also higher for concretes with steel fibres (see Fig. 7). This property is very important for the structure. The reason for this behaviour is centred not so much on the material strength of each fibre (steel fibres present a tensile strength around 1,000 MPa, while the tensile strength of polyester fibres is between 400 and 800 MPa), because the fibres do not break. Thus, the main cause may be the efficiency of the anchorage system and the bounding of the fibres to the concrete matrix, which is favourable in this case to the steel fibres.

The coarse lightweight aggregate used had to be changed in the middle of the experimental campaign because its origin was also changed. The implication of this fact was the modification in the form of the

grains (from a spherical to an oval form with an increase in the superficial porosity), as can be seen in Fig. 9. Therefore, it became necessary to investigate the influences of the *lightweight aggregate form of the grains* on the concrete. This explains why concretes from P_7 and P_8 present the exact same proportions of component materials: the difference between the two concretes lies on the use of lightweight aggregates from different origins.

Fig. 9. Lightweight aggregates from different origins.

The changes on the characteristics of aggregates influence the behavior of concrete at the fresh state. The slump flow diameter decreases approximately a 10% when the aggregate is changed, which is a significant value for an SCC. At the hardened state, the compressive strength does not change much regardless of the type of aggregate. On the other hand, the tensile strength is around a 35 % higher in the concrete from P_8. It may be due to the oval form of the grains that produce greater interlocking than the spherical grains.

Some adjustments were made in the concrete from P_8 in order to increase the fluidity and enable the use of the concrete for the required application. Thus, the component material proportions of concrete P_9 were modified: the amount of filler was increased and the 6-16 mm lightweight aggregate content was decreased. This measure resulted favourable and the fluidity lost when the lightweight aggregate was changed (P_8 with respect to P_7) was recovered in great part. Fig. 10 shows the slump flow test with the Japanese ring and the edge of the concrete. It is possible to observe a good mass distribution and a lack of segregation or bleeding.

Fig. 10. Slump flow test with the Japanese ring and the edge of concrete, concrete P_9.

At the hardened state, a small increase in the compressive strength was observed, as a consequence of the improvements in the matrix compactness provided by the higher content of limestone filler. In these last

series, no segregation or bleeding was verified, but the concrete proved itself homogeneous, with a good distribution of the lightweight aggregates and the fibres. For this reason, this mix proportion was tested at industrial scale and it had been properly pumped, presenting good results.

C.6. Conclusions and recommendations

The most relevant conclusion obtained is that it is possible to produce a lightweight self-compacting concrete reinforced with fibres (concrete P_9) to respond to the requirements established for a rehabilitation concrete, from different points of view: technical and structural, environmental and social. The technical literature consulted did not include any material with the characteristics reported in this paper, so that made it possible to patent this concrete. The main variable for the achieved success was the use of a viscosity modifier admixture, because otherwise the concrete mixture would present segregation.

Also, it is important to highlight the significance of the structural and sectional study performed, which made it possible to delimit rigorously the main structural variables. This non-linear study considers the guidelines presented in annex 14 of the EHE 08 [24] about the structural vision of concrete reinforced with fibres, which opens a new way for this type of concrete.

Finally, it should be mentioned that industrial pumping tests had already been performed with the concrete studied. The tests were a success and the material had proved itself viable for application. The next step that is being considered is the application of the concrete to the rehabilitation of a real structure.

C.7. Acknowledgments

No experimental investigation is possible without the collaboration of laboratory technicians. For this reason we would like to thank the collaboration of the technicians from the PROMSA laboratory, as well as the company itself for the trust received throughout the years, during the realization of different investigation projects.

C.8. References

1. RASELL CALAMINA, J. La construcció en l'arquitectura de Barcelona a finals del segle XVIII. Doctoral *thesis directed by Pere Hereu.* Barcelona: UPC, 1996.
2. PARICIO CASADEMUNT, A. Analisi del sistema constructiu a base de murs de carrega, utilitzats en la formació de l' Eixample de Barcelona. *Doctoral thesis directed by Fructuoso Maña.* Departament de Construccions Arquitectòniques I. Barcelona: UPC, 1999.
3. HAIST, M. y MÜLLER, H. S. Optimization of the pumpability of self-compacting lightweight concrete. *The Second North American Conference on the Design and Use of Self-Consolidating Concrete.* Chicago: s.n., 2005.
4. TASDEMIR, M. A., ATAHAN, H. N., GOKALP, I. y YERLIKAYA, M. Comparison of workability and mechanical properties of normal and lightweight SCCS with and without steel fibers. *The Third North American Conference on the Design and Use of Self-Consolidating Concrete.* Chicago: s.n., 2008.
5. AGUADO, A. MASÓ, D. KLEIN, N. S. Hormigón autocompactante ligero con fibras estructurales para rehabilitación de forjados de edifícios. Patent application nº P 2009 02445.
6. B.O.E., 23/10/2007. Documento básico SE-AE Acciones en la edificación. 2007.

7. PUJADAS, P. Durabilidad del Hormigón con Fibras de Polipropileno. *Dissertation (Tutors: Aguado de Cea, A., Vandewalle, M.).* Barcelona: UPC, 2008.

8. COLLINS, M. P. y MITCHELL, D. Prestressed Concrete Basics. Ontário: Canadian Prestressed Institute, 1987.

9. RILEM. Tests and Design Methods for Steel Fibre Reinforced Concrete. s.l.: Materials and Structures, 2003. Vol. 36, 262, pages 560-567.

10. BARROS, J. A. O., CUNHA, V. M. C. F.; RIBEIRO, A. F.; ANTUNES, J.A. B. Post-cracking behavior of steel fibre reinforced concrete. *Materials and Structures.* 2005. Vol. 38, pages 47-56.

11. DE LA FUENTE, A. Análisis no lineal y comportamiento en servicio y rotura de secciones construidas evolutivamente sometidas a flexocompresión recta. *Dissertation (Tutors: Aguado de Cea, A., Molins Borrell, C.,).* Barcelona: UPC, 2007.

12. DE LA FUENTE, A., AGUADO, A. y MOLINS, C. Modelo no lineal para el análisis de secciones prefabricadas construidas evolutivamente. *Hormigón y Acero.* 2008. Vol. 57, 247, pages 69-87.

13. REVUELTA, D. BARONA, A. NAVARRO, D. Measurement of properties and of the resistance to segregation in heavyweight, self-compacting barite concrete. *Materiales de construcción.* 2009. Vol. 59, 295, pages 31-44.

14. DOMONE, P. L. Self-compacting concrete: an analysis of 11 years of case studies. s.l.: Cement and Concrete Composites 28, 2006. pages 197-2008.

15. AENOR, Asociación Española de Normalización y Certificación. UNE-EN 12350-6 - Ensayos de hormigón fresco. Parte 6: Determinación de la densidad. Madrid: s.n., 2006.

16. —. UNE 83361 - Hormigón autocompactante – Caracterización de la fluidez – Ensayo del escurrimiento. Madrid: s.n., 2007.

17. —. UNE 83362 - Hormigón autocompactante – Caracterización de la fluidez en presencia de barras – Ensayo del escurrimiento con el anillo japonés. Madrid: s.n., 2007.

18. —. UNE-EN 12350-2 - Ensayos de hormigón fresco. Parte 2: Determinación del contenido de aire del hormigón fresco. Métodos de presión. Madrid: s.n., 2006.

19. —. UNE-EN 12390-7 - Ensayos de hormigón endurecido, parte 7: densidad del hormigón endurecido. Madrid: s.n., 2001.

20. —. UNE-EN 12390-3 - Ensayos de hormigón endurecido. Parte 3. Determinación de la resistencia a compresión de probetas. Madrid: s.n., 2003.

21. —. UNE 83515 – Hormigones con fibras. Determinación de la resistencia a fisuración, tenacidad y resistencia residual a tracción. Ensayo Barcelona. Madrid: s.n., 2008.

22. MOLINS, C., AGUADO A. y SALUDES S. Double Punch Test to control the tensile properties of FRC (Barcelona test). *Rev. Materials and Structures (RILEM).* Vol. 42, nº 4, May 2009 pages 415-425.

23. TURMO, J. BANTHIA, N. GETTU, R. BARRAGÁN, B. Study of the shear behaviour of fibre reinforced concrete beams. *Materiales de construcción.* Vol. 58, 292, pages 5-13.

24. Comisión Permanente del Hormigón. Instrucción del hormigón estructural EHE-08. Ministerio de Fomento. December, 2008.

APPENDIX D

Análisis comparativo de los modelos constitutivos del hormigón reforzado con fibras

D.1. Resumen

La aparición de normas específicas para el empleo del Hormigón Reforzado con Fibras es, sin lugar a duda, una herramienta clave que proporciona al proyectista un mayor margen de confianza como solución estructural. Actualmente existen numerosas directrices y recomendaciones normativas que definen las bases de cálculo de este material, lo que a su vez supone una gran oportunidad para extender su uso. Por ello, en este artículo, se ha realizado un análisis detallado de los principales modelos normativos a nivel europeo (DBV, RILEM, CNR-DT 204 y EHE) y se han contrastado los resultados de una campaña experimental con los resultados numéricos que con sendas ecuaciones constitutivas se obtienen.

Key words: Hormigón; Fibras; Ecuaciones constitutivas; Normativas; Diseño.

D.2. Introduction

El Hormigón Reforzado con Fibras (en adelante: HRF), constituye una de las innovaciones más relevantes en el campo de los hormigones especiales. El HRF debe ser entendido como un hormigón que incluye en su composición fibras cortas y discretas, distribuidas aleatoriamente en su masa. Una vez el hormigón ha fisurado, la pérdida de adherencia y el arrancamiento (*pull-out*) de las fibras disipa una mayor energía, lo que conduce a un importante incremento de la tenacidad [1]. Actualmente, son cada vez más las aplicaciones en las cuales se emplea esta tecnología con una clara responsabilidad estructural como se recoge en [2] y [3]. Sin embargo, el camino por recorrer para un amplio uso del HRF como material estructural es importante y largo [4] pues existen aspectos que dificultan el uso de las fibras como refuerzo del hormigón, entre los que destacan: la estimación económica de las ventajas del uso de las fibras y la falta de experiencia [5].

En este sentido cabe destacar la importante labor de los investigadores y, en especial, de la Instrucción de Hormigón Estructural (EHE-08 [6]), atenta siempre a contemplar la tecnología del hormigón desde posiciones avanzadas. Mediante la incorporación a la EHE-08 del Anejo 14 relativo al empleo de fibras con finalidad estructural, se pone fin al vacío normativo existente hasta el momento en el ámbito español como se indica en [7]. Dicho anejo tiene un papel primordial en la extensión de la aplicación de este hormigón a otros ámbitos de la construcción, y proporciona un mayor margen de confianza al proyectista para emplearlo en el diseño de sus soluciones [8].

En aras a optimizar el diseño estructural, resulta imprescindible disponer de modelos sólidos y racionales que reflejen de forma fidedigna el comportamiento fenomenológico del material como se apunta en [9]. Sin embargo, actualmente no existe una única ecuación constitutiva que caracterice adecuadamente el comportamiento del HRF ([10] y [11]), sino que existen numerosos modelos y enfoques recogidos en normativas y artículos de referencia.

D.2. Razón de ser y objetivos

Ante las diferencias de criterio en la implantación de la ecuación constitutiva, cabe plantearse cuáles son las causas que provocan estas heterogeneidades y evaluar los modelos propuestos en las distintas normativas. Por este motivo, el presente documento persigue el doble objetivo de:

- Realizar una revisión de los principales trabajos técnicos, directrices y recomendaciones normativas para la definición de las ecuaciones constitutivas que actualmente se emplean para caracterizar el HRF.
- Evaluar y comparar qué modelos ajustan mejor los resultados experimentales recogidos en [12] y [13], analizando la idoneidad de los mismos para cada caso de estudio.

Con ello se pretende contribuir al conocimiento del HRF en el campo estructural y ayudar a extender su uso.

D.3. Estado del arte: modelos constitutivos del HRF

D.3.1. Criterios para su obtención.

A diferencia de lo que ocurre a tracción, el comportamiento a compresión del HRF no dista de la respuesta del hormigón convencional [14]. Es por ello que uno de los retos más importantes es el de desarrollar un modelo de ecuación constitutiva que permita caracterizar adecuadamente el comportamiento a tracción de dicho material. El diseño de secciones con HRF se basa en el método tradicional de análisis de secciones para el hormigón armado (HA) presentado en la Fig. 1a. La única diferencia reside en que el modelo tensión-deformación (σ-ε) usado en el diseño del HRF considera la aportación a tracción debido al efecto puente (*bridging effect*) de las fibras [10] como se ilustra en el esquema de la Fig. 1b.

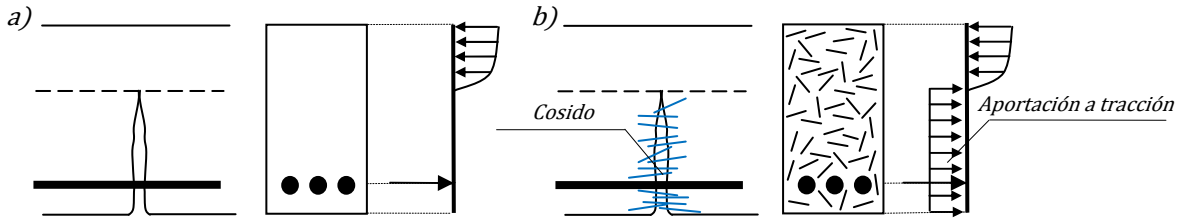

Fig. 1. Distribución de tensiones para una sección: a) de HA y b) HRF con armadura. [5].

En la literatura técnica se han recogido, hasta el momento, numerosos modelos tanto de índole experimental como de carácter meramente teórico. Dichos modelos se pueden obtener adoptando criterios y procedimientos diversos. A continuación se presentan las bases conceptuales sobre las que estos modelos se han desarrollado.

Modelos tensión-ancho de fisura (σ-w) / Modelos tensión-deformación (σ-ε)

La descripción del comportamiento a tracción del hormigón reforzado con fibras puede realizarse, entre otras, mediante la relación σ-w [15] relacionado con el concepto del modelo de la fisura ficticia (*fictitious crack model*) o la relación σ-ε ([10], [11] y [16]), ambas representadas esquemáticamente en la Fig. 2.

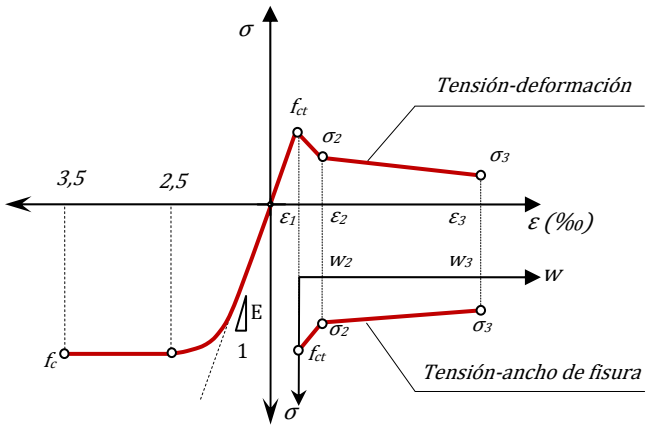

Fig. 2. Diagrama constitutivo del comportamiento a compresión y a tracción.

El diagrama σ-ε permite la definición del comportamiento a tracción del material en los mismos términos que el de compresión, conduciendo a un único diagrama para la representación del comportamiento del HRF. Asimismo, este tipo de diagrama resulta de especial interés por su compatibilidad con el del acero, permitiendo aplicar una metodología encaminada hacia la visión conjunta del material (HRF) como hormigón estructural.

Por este motivo, se introduce el concepto de longitud característica (l_{cs}) que permite establecer una relación entre el ancho de fisura y la deformación del material $w=f(\varepsilon, l_{cs})$ ([17] y [18]). Existen numerosas propuestas para tratar de evaluar dicha longitud recogidas en [19], [20] y [21], sin embargo la clara dependencia tanto de las condiciones de ensayo como de la geometría del elemento ensayado dificultan enormemente su determinación [1]. Una descripción más detallada sobre este concepto puede encontrarse en Hillerborg [22].

Análisis inverso / Análisis directo

El empleo del análisis inverso y el análisis directo no es sólo exclusivo de la caracterización del comportamiento a tracción del HFR. Se acude a estos procedimientos también, por ejemplo, cuando se quiere abordar la caracterización de la respuesta adherente y de anclaje de una barra de acero o de una fibra embebidas en el hormigón ([23] y [24]).

En la Fig. 3 se presenta un diagrama de flujos en el que se esquematizan los planteamientos inverso y directo que se explican a continuación.

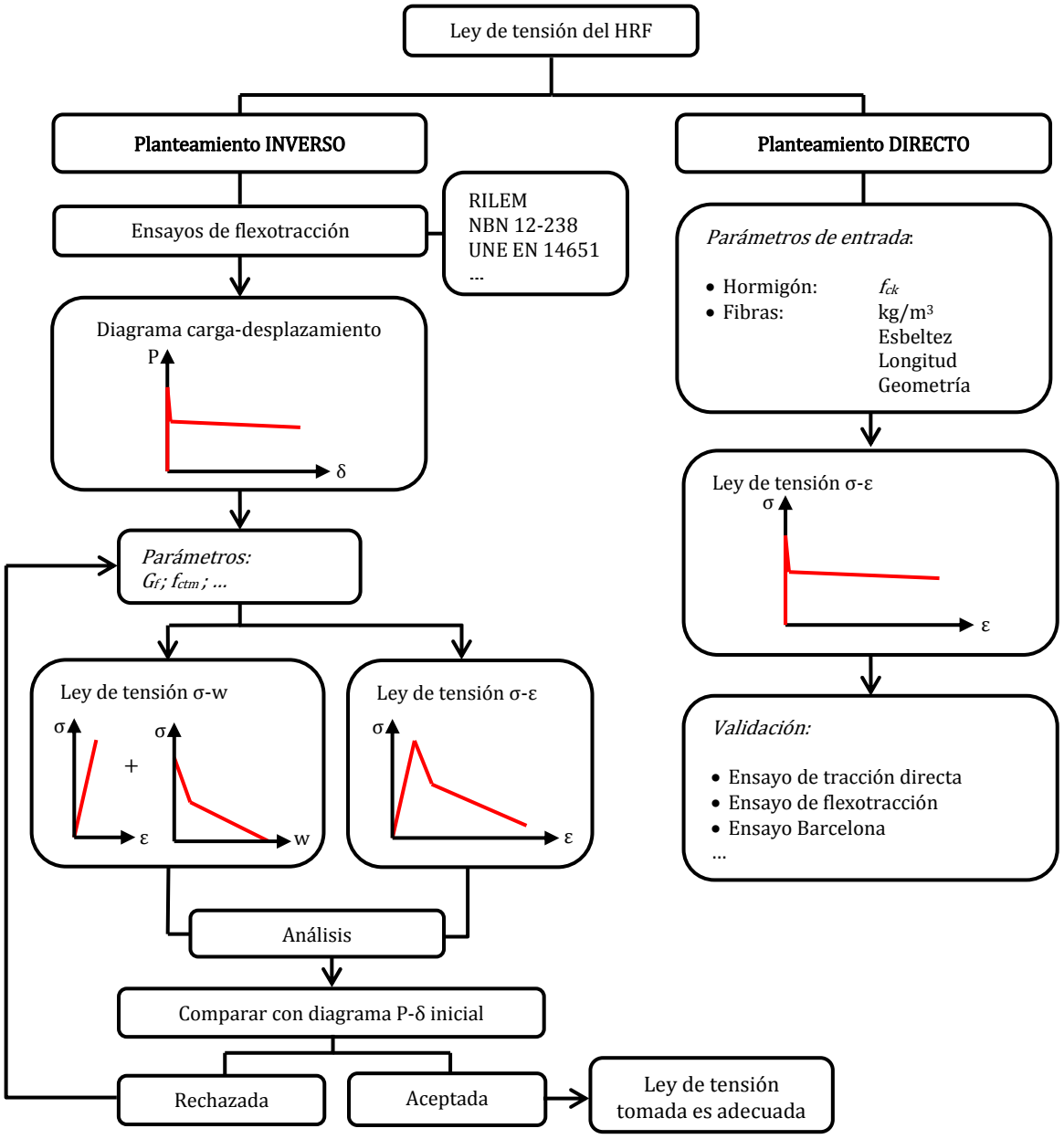

Fig. 3. Procedimientos para la obtención de un modelo constitutivo del HRF. [16]

El *análisis directo* para el análisis de secciones y/o estructuras de HRF se basa en fijar la forma de una ecuación constitutiva (tipo σ-ε o σ-w) para simular la respuesta a tracción del HRF, ya sea alguna de las recogidas en los códigos o referencias internacionales (RILEM [25], EHE [6]...), o alguna de las propuestas por otros investigadores y recogidas en bibliografía especializada ([10], [1] y [26]). Los parámetros constitutivos de cada una de éstas pueden obtenerse experimentalmente [RILEM, EHE...] o se pueden fijar a partir de ciertas propiedades de las fibras empleadas, del hormigón utilizado y del procedimiento de fabricación y hormigonado elegido [15]. Fijada la ecuación constitutiva y el resto de variables e hipótesis necesarias para simular el comportamiento a nivel seccional, se ejecuta el algoritmo de cálculo ([27], [28] y [29]) y se obtienen la respuesta tenso-deformacional de los materiales constituyentes de la sección. A

nivel estructural, se puede integrar la respuesta de cada sección para obtener el comportamiento global de la misma. En el caso de disponer de resultados experimentales del elemento estudiado, se pueden comparar con los obtenidos numéricamente. Dicha comparación y el grado de ajuste, proporcionará una estimación de cuán adecuada es la forma de la ecuación constitutiva empleada para la simulación del comportamiento a tracción del HRF así como de los parámetros que la definen.

En el *análisis indirecto* la estrategia parte de los resultados experimentales (ver Fig. 3) de la sección y/o estructura cuyo comportamiento se quiere simular numéricamente, y se ajustan los valores de una ecuación constitutiva, cuya forma puede haberse predefinido. Concretamente, el planteamiento consiste en obtener los parámetros que definen la ecuación constitutiva del HRF traccionado, variándolos de forma que la respuesta de la estructura obtenida numéricamente se ajuste a la obtenida experimentalmente [30]. En este proceso se pueden aplicar métodos de cálculo simplificados u otros más sofisticados, como el método de los elementos finitos. El proceso de fisuración puede ser representado a través de la teoría de la fisura difusa (*smeared crack approach*) o por la teoría de la fisura discreta (*discrete crack approach*). El primero asume fisuras distribuidas en el elemento mediante el concepto tensión-deformación, σ-ε, ([31] y [32]) y el segundo utiliza una ubicación predefinida de la fisura y se basa en la relación tensión-ancho de fisura, σ-w ([10] y [19]).

Ecuación continua / Ecuación definida por tramos

Hasta la fecha la gran mayoría de ecuaciones constitutivas propuestas son ecuaciones definidas por tramos. Sin embargo, para la obtención de una ecuación constitutiva parametrizada, que represente de forma fidedigna el comportamiento a tracción uniaxial del HRF, se requiere de muchos puntos. Es por ello que cada vez más se tiende a investigar modelos continuos [30]. Entre éstos cabe destacar el modelo con cuatro funciones exponenciales (*four-e*), con el que sus autores [31] definen el comportamiento pre-fisuración y post-fisuración del hormigón reforzado con fibras de acero (HRFA) con una única ecuación mediante seis parámetros.

Conviene enfatizar la tendencia de muchas normativas, entre las que se encuentran la norma española [5] que a pesar de valerse de modelos definidos por partes (o tramos), proponen un mayor número de inputs con el objetivo de obtener resultados más precisos.

D.3.2. Ecuaciones constitutivas propuestas en la literatura técnica

Las estructuras de HRF pueden calcularse con un análisis plástico que permita aprovechar la mayor capacidad de redistribución de esfuerzos proporcionada por la contribución de las fibras. No obstante, no existe aún un modelo constitutivo relativo al comportamiento a tracción del HRF que se imponga sobre los demás. Este hecho ha conducido a la aparición de numerosas propuestas, recogidas en la literatura técnica, algunas de las cuales se presentan a continuación.

El diagrama de la Fig. 4a [33] fue uno de los primeros estudios de diagrama σ-ε para el HRFA. En este estudio los autores consideran cuantías pequeñas de fibras y asumen que en la zona de pre-fisuración del hormigón el efecto de las fibras es despreciable [34]. El modelo representado en la Fig. 4b [35] está formado por tres etapas, siendo la primera de tipo parabólico; la zona intermedia se incluyó para estimar mejor la resistencia post-pico.

Dupont [36] desarrolla un diagrama de tensión deformación (Fig. 5a) de dos niveles basado en las mismas suposiciones que el del modelo trilineal de la RILEM [25] o la DBV [37] (que se verá posteriormente). Este modelo no presenta la desventaja del modelo trilineal, ya que se modela mediante dos niveles (o escalones) de tensión definidos por las deformaciones ε_2 (2,5‰) y ε_3 (15‰) de modo que el comportamiento post-fisuración sea independiente de la resistencia a tracción (f_{ct}). Dicho modelo justifica la aproximación en dos niveles en base a la necesidad de las fibras a deformarse previamente a actuar "cosiendo" las fisuras.

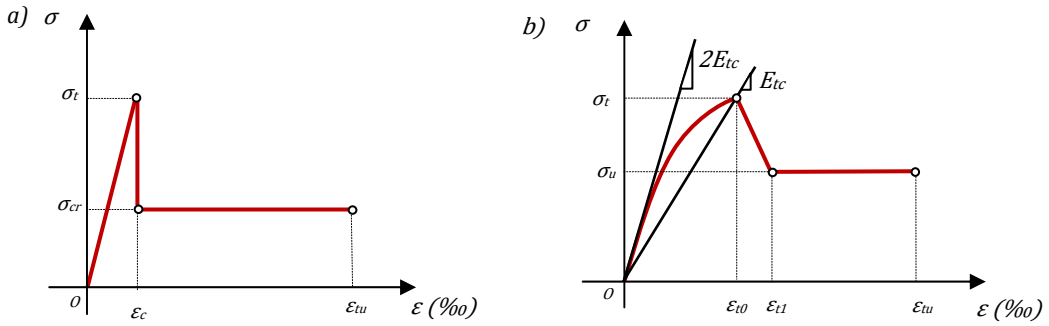

Fig. 4. Ecuaciones constitutivas (σ-ε) para caracterizar el comportamiento a tracción del HRF. [33].

Con el objetivo de simplificar el modelo constitutivo y predecir el comportamiento para deformaciones mayores, en [10] se propone un diagrama constitutivo σ-ε compuesto de dos fases (Fig. 5b). La primera depende exclusivamente de la cuantía en peso de fibras (v_p) y de la resistencia a tracción de la matriz (f_{ctk}). En la segunda, la caída de tensión a σ_2 viene gobernada por una ecuación hiperbólica garantizando una pérdida de tensión en función de un parámetro de forma que refleja la influencia del tipo de fibra en la rama de *softening*.

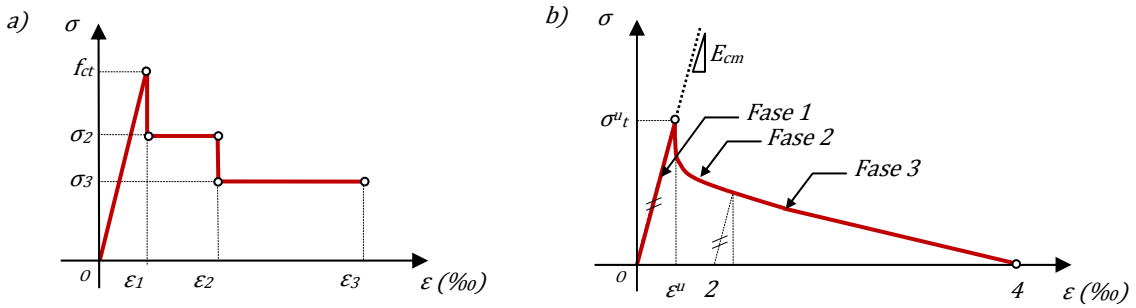

Fig. 5. Ecuaciones constitutivas (σ-ε) para caracterizar el comportamiento a tracción del HRF. [36] y [10].

Por otra parte, en [26] se propone un modelo bilineal σ-w, representado en la Fig. 6, que asume un primer tramo de reblandecimiento (*softening)* y considera en el tramo final el efecto de las fibras. Este último tramo se define con las tensiones para dos anchos de fisura determinados (0,3 mm y 1,8 mm). El modelo bilineal presentado en [26] sobreestima el inicio de la colaboración de las fibras [38], representado por la intersección de la primera y la segunda rama post-pico. Por este motivo, el comportamiento post-fisuración se representa mejor si se asume un modelo trilineal σ-w como el que presenta Colombo [38], de acuerdo con la Fig. 6, que puede entenderse como una modificación del bilineal anteriormente citado.

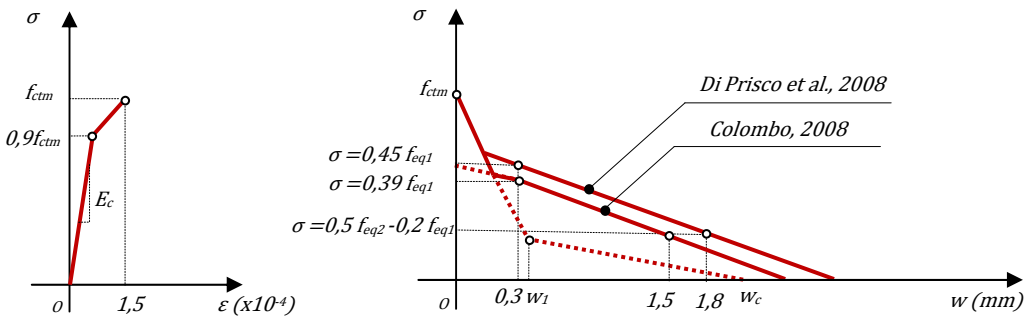

Fig. 6. Ecuaciones constitutivas (σ-w) a tracción del HRF. [38].

D.4. Modelos constitutivos normativos

La identificación del modelo constitutivo a tracción representa uno de los pasos fundamentales en el diseño de estructuras de HRF. Durante los últimos 15 años se han desarrollado numerosas recomendaciones técnicas con el fin de facilitar el diseño de este tipo de estructuras y extender su uso ([39] y [40]). La variedad de ecuaciones constitutivas existentes hace patente la falta de un único modelo aceptado de forma general. Ante esta situación, cabe plantearse la necesidad de un análisis y valoración de cada uno de los modelos con el fin de evaluar su idoneidad.

En la Tabla 1 se presentan los modelos constitutivos propuestos por las normativas europeas citadas que han sido agrupados según su diagrama (rectangular, bilineal y trilineal), indicando los parámetros que definen los modelos. Así mismo se representa esquemáticamente el ensayo requerido para obtener los valores de dichos parámetros. Una vez presentados los modelos constitutivos se realiza un análisis de las similitudes y diferencias entre ellos, valorando los puntos a favor y en contra de las hipótesis y consideraciones realizadas en cada uno de ellos.

Por otro lado, en la Tabla 2 se presentan los conceptos que se tratarán a continuación para cada uno de los modelos constitutivos presentados en las normas DBV (alemana), RILEM, CNR-DT 204 (italiana), el Model Code y la EHE (española) siguiendo un criterio cronológico de aparición. En la misma se señalan los factores que tienen en cuenta cada una de ellas. Esta tabla se referencia con posterioridad en el análisis pormenorizado de cada normativa.

D.4.1. Norma alemana: DBV-Merkblatt Stahlfaserbeton (1992/2001)

La *German Concrete Society* fue la propulsora en 1992 de la primera normativa que se valía de una ecuación σ-ε para el diseño de HRFA [9] (específica para fibras metálicas). Dicha normativa se creó en su momento con el propósito de disponer de un diagrama para el diseño estructural de túneles (DBV, 1992 [41]). En el año 2001, se publicó la nueva normativa (DBV, 2001 [37]), vigente en actualidad, en la que se propone la utilización de un modelo trilineal para Estados Límite de Servicio (ELS) con posibilidad de emplear un diagrama bilineal (e incluso rectangular) para Estados Límite Últimos (ELU), representados en la Fig. 7.

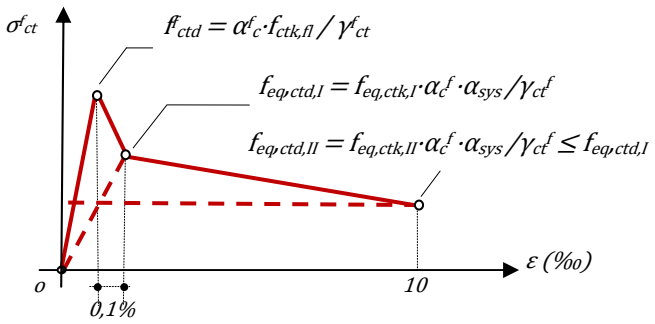

Fig. 7. Diagramas propuestos por la norma alemana, DBV.

Ambos diagramas, definidos por las resistencias a flexotracción equivalentes, se deducen de los resultados sobre probetas bajo la configuración de flexión a cuatro puntos ("*4-point bending test*"). La tensión pico (f^f_{ctd}) del modelo trilineal propuesto se obtiene a partir de las cargas máximas obtenidas en el ensayo dentro de un rango de flecha de 0,100 mm. Sin embargo esta tensión, obtenida mediante un ensayo a flexión, sobrestima la resistencia a tracción real del hormigón, por este motivo, algunos autores [16] proponen emplear un ensayo a tracción directa para su determinación.

El modelo alemán obtiene las resistencias a tracción equivalentes a partir de las resistencias a flexotracción equivalentes. Los factores que rigen esa relación son 0,45 y 0,37, representando una reducción respecto a la distribución elástica-lineal de las tensiones consideradas: $f_{eq,ctk,I}$=0,45$f_{eqk,I}$ y $f_{eq,ctk,II}$=0,37$f_{eqk,II}$ (ver Tabla 1).

Tabla 1. Modelos constitutivos de diversas normativas.

Diagrama	Parámetros	Ensayo	
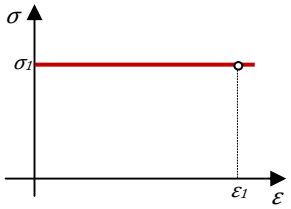	$\sigma_1 = f_{ctRd} = 0{,}33 f_{R,3,d}$ $\varepsilon_1 = \varepsilon_u$=[20‰ flexión;10‰ tracción]	3-point bending test. UNE EN 14651 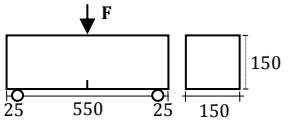	EHE
	$\sigma_1 = f_{Ftu} = f_{eq2}/3$ $\varepsilon_1 = \varepsilon_u$= [20‰ reblandecimiento ; 10‰ endurecimiento]	4-point bending test UNI 11039 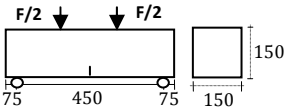	CNR-DT 204
	$\sigma_1 = f_{eq,ctd,II} = f_{eq,ctk,II} \cdot \alpha_c^f \cdot \alpha_{sys} / \gamma_{ct}^f \leq f_{eq,ctd,I}$ $\varepsilon_1 = \varepsilon_u = 10‰$	4-point bending test NBN B 15-238 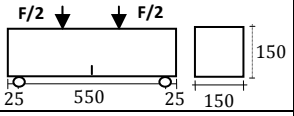	DBV
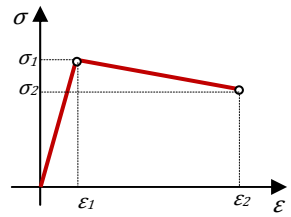	$\sigma_1 = f_{eq,ctd,I} = f_{eq,ctk,I} \cdot \alpha_c^f \cdot \alpha_{sys} / \gamma_{ct}^f$ $\sigma_2 = f_{eq,ctd,II} = f_{eq,ctk,II} \cdot \alpha_c^f \cdot \alpha_{sys} / \gamma_{ct}^f \leq f_{eq,ctd,I}$ $\varepsilon_2 = \varepsilon_u = 10‰$	4-point bending test NBN B 15-238 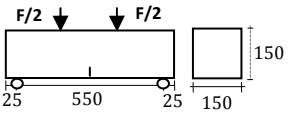	DBV
	$\sigma_1 = f_{Fts} = 0{,}45 f_{eq1}$ $\sigma_2 = f_{Ftu} = k[f_{Fts} - (w_u/w_{i2})(f_{Fts} - 0{,}5 f_{eq2} + 0{,}2 f_{eq1})]$ k=[0,7 tracción pura, 1 resto de casos] $\varepsilon_2 = \varepsilon_u$= [20‰ reblandecimiento; 10‰ endurecimiento]	4-point bending test. UNI 11039 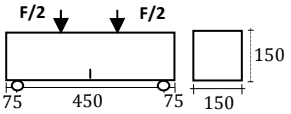	CNR-DT 204
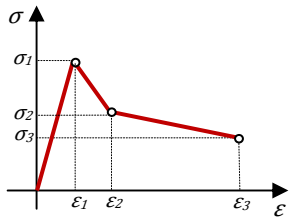	$\sigma_1 = f^f_{ctd} = \alpha^f_c \cdot f_{ctk,fl} / \gamma^f_{ct}$ $\sigma_2 = f_{eq,ctd,I} = f_{eq,ctk,I} \cdot \alpha_c^f \cdot \alpha_{sys} / \gamma_{ct}^f$ $\sigma_3 = f_{eq,ctd,II} = f_{eq,ctk,II} \cdot \alpha_c^f \cdot \alpha_{sys} / \gamma_{ct}^f \leq f_{eq,ctd,I}$ $\varepsilon_1 = \sigma_1 / E_{HRF}$ $\varepsilon_2 = \varepsilon_1 + 0{,}1‰$ $\varepsilon_3 = \varepsilon_u = 10‰$	4-point bending test NBN B 15-238 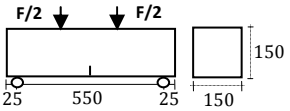	DBV
	$\sigma_1 = 0{,}7\ f_{ctm,fl}\ (1{,}6\text{-d})$ $\sigma_2 = 0{,}45 \cdot \kappa_h \cdot f_{R,1}$ $\sigma_3 = 0{,}37 \cdot \kappa_h \cdot f_{R,4}$ $\varepsilon_1 = \sigma_1 / E_{HRF}$ $\varepsilon_2 = \varepsilon_1 + 0{,}1‰$ $\varepsilon_3 = \varepsilon_u = 25‰$	3-point bending test RILEM TEST 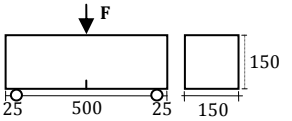	RILEM
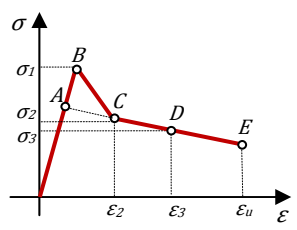	$\sigma_1 = f_{ct,d} = 0{,}6\ f_{ct,fl,d}$ $\sigma_2 = f_{ctR1,d} = 0{,}45 f_{R,1,d}$ $\sigma_3 = f_{ctR3,d} = k_1(0{,}5 f_{R,3,d} - 0{,}2\ f_{R,1,d})$ $\varepsilon_2 = 0{,}1 + 1000 \cdot f_{ct,d} / E_{c,0}$ $\varepsilon_3 = 2{,}5 / l_{cs}$ (l_{cs}: long.crítica) ε_u=[20‰ flexión; 10‰ tracción]	3-point bending test. UNE EN 14651 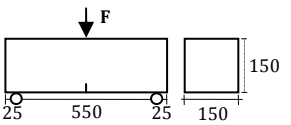	EHE

Entre los aspectos a destacar de la propuesta de la DBV cabe mencionar la consideración de la dispersión en el comportamiento post-pico, coeficientes parciales de seguridad y el efecto de cargas sostenidas (coeficiente de cansancio) con reducciones que pueden alcanzar hasta un 25% en hormigones ligeros y hasta un 15% en hormigones normales. Dicho modelo también introduce el concepto del efecto tamaño o coeficiente de forma (α_{sys}) que tiene en cuenta el efecto del canto sobre el comportamiento a flexotracción de la sección, penalizando sensiblemente (hasta un 20%) las secciones de mayor canto.

Tabla 2. Cuadro resumen de los modelos constitutivos.

	DBV	RILEM	CNR-DT 204	FIB MODEL –CODE	EHE
Tensión-deformación (ε)/ Tensión-ancho de fisura (w)	ε	ε	ε/w	ε/w	ε
Análisis directo (AD) /Análisis indirecto (AI)	AI	AI	AI	AI	AI
Ecuación Continua (EC) / Ecuación Discontinua (ED)	ED	ED	ED	ED	ED
Trabaja con resistencias residuales		●			●
Trabaja con resistencias equivalentes	●		●	●	
Distinción de la deformación última			●	●	●
Deformación ultima (‰)	10	25	20/10	20/10	20/10
Reducciones respecto a la distribución elástica-lineal de las tensiones	●	●			●
Aplicación de la longitud característica en la obtención de la deformación			●	●	●
Considera coeficientes de seguridad	●		●	●	●
Considera efecto tamaño	●	●			
Considera efecto de cargas sostenidas	●				
Considera la cuantía de fibras					
Norma específica para fibras de acero	●	●			
Considera aportación de las fibras en la separación entre fisuras		●	●	●	

La deformación última, en la revisión de 2001, aumenta significativamente hasta ε_u=10‰ respecto a la antigua propuesta (1992), ε_u=5‰. Aunque dicho valor resulta razonable para elementos con armadura mixta, pues la armadura convencional limita dicha deformación, es cuestionable para elementos sometidos a flexión únicamente reforzados con fibras donde se pueden alcanzar deformaciones mayores.

El modelo presenta también ciertas inconsistencias en su propuesta de diagrama trilineal para ELS al no definir adecuadamente el comportamiento inicial tras la post-fisuración, vinculado a la resistencia a tracción elástica del material [36]. Ésta, sin embargo, es una propiedad intrínseca al hormigón sin fisurar y completamente independiente de la resistencia post-fisuración siendo esta última función, únicamente del tipo y dosificación de fibras.

D.4.2. RILEM: RILEM TC 162-TDF (2003)

La primera propuesta de ecuación constitutiva de la RILEM [42] consistía en un diagrama σ-ε trilineal en el que se caracterizaba el comportamiento post-fisuración del HRFA, como en el caso de la DBV, mediante la resistencia a flexotracción equivalente. La diferencia principal radicaba en que RILEM se valía del ensayo a flexión de 3 puntos ("*3-point bending test*") y no consideraba el efecto tamaño en el comportamiento post-fisuración. Tras numerosas investigaciones llevadas a cabo en el proyecto Brite Euram [43], se concluyó que, la relación tensión-deformación propuesta hasta el momento, se podía

mejorar, por lo que se propuso un nuevo diagrama trilineal recogido en [25] para hormigón reforzado con fibras metálicas (tal y como se recoge en la Tabla 2).

A priori, resulta evidente la similitud de este modelo con el propuesto por la DBV, sin embargo existen diferencias que es necesario destacar. El cambio más significativo de esta nueva ecuación constitutiva es que no tiene en cuenta la resistencia a flexotracción equivalente ($f_{eq,i}$), sino que utiliza resistencias a flexotracción residuales ($f_{R,i}$). Hay que señalar que el empleo de $f_{eq,i}$ frente a $f_{R,i}$ conduce a resultados con mayor índice de fiabilidad, pues el aparato teórico empleado para el cálculo de f_{eq} es más realista, aunque de aplicación más tediosa [11]. No obstante, las diferencias obtenidas son pequeñas y el empleo de ambos conceptos arroja resultados suficientemente precisos desde el punto de vista del diseño estructural. Cabe destacar el alto valor de la tensión pico (σ_1) que se obtiene con la formulación propuesta por la RILEM en comparación con el resto de normativas (como se verá más delante).

El valor de la deformación última (ε_u) propuesta por la RILEM aumenta (respecto al 10‰ considerado tanto en la versión RILEM del 2000, como en la revisión de DBV del 2001, ver tabla 2) hasta un 25‰ como resultado de considerar una altura de la fibra neutra de 140 mm por encima del punto en el que se mide la CMOD y asumiendo una longitud característica igual a dicha distancia. Para un CMOD de 3,5mm, se obtiene una deformación de (3,5/140)=25‰.

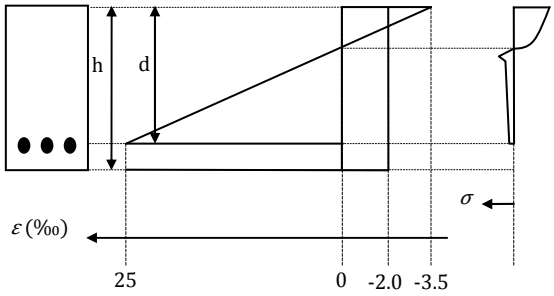

Fig. 8. Distribución tensión-deformación en sección transversal (RILEM, 2003).

Asimismo las tensiones asociadas a $f_{R,1}$ y $f_{R,4}$ deben afectarse adecuadamente por el coeficiente de forma (κ_h), siendo éste mucho menor que el propuesto por la DBV tal y como se desprende de la comparación realizada en la Fig. 9.

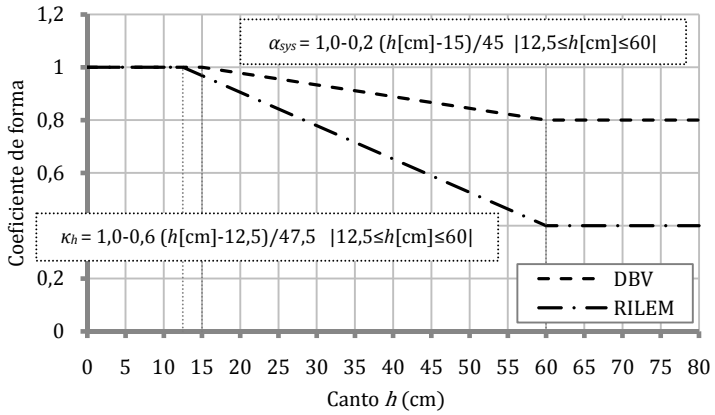

Fig. 9. Comparación del factor tamaño aplicado en la norma DVB y en la RILEM.

D.4.3. Norma italiana: CNR-DT 204 (2006)

El Comité Nacional de Investigación Italiano publicó en 2006 unas recomendaciones para el diseño, ejecución y control de las estructuras de HRF (CNR-DT 204/2006 [43]). Este documento propone dos relaciones para el comportamiento a tracción del HRF: el modelo elástico-lineal y el modelo rígido-plástico

(ver Fig. 10). Dichos modelos son presentados en la CNR-DT 204 en dos versiones: como una relación tensión-deformación y una relación tensión-ancho de fisura.

El modelo rígido-plástico se utiliza para cálculo en rotura mientras que el elástico-lineal es aplicable tanto en rotura como en servicio. Ambos modelos permiten representar materiales con comportamientos de reblandecimiento (*softening*) y endurecimiento (*hardening*). En la Fig. 10 se esquematiza una sección transversal con las distribuciones de tensiones correspondientes a cada modelo: elástico-lineal y rígido-plástico. Se observa en el modelo elástico-lineal cómo admite materiales con comportamiento de endurecimiento y reblandecimiento.

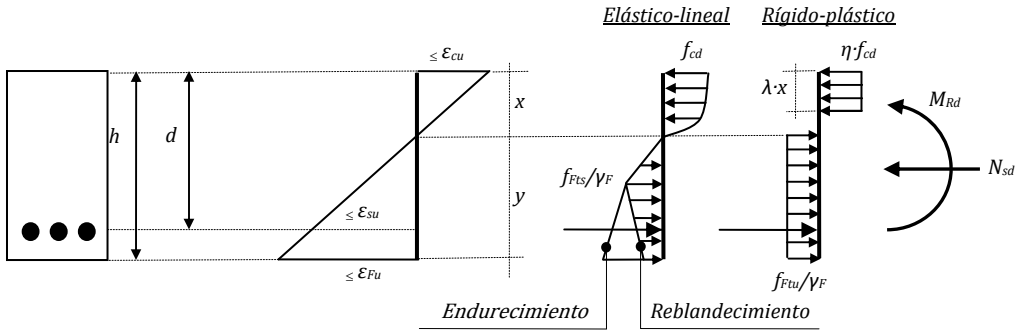

Fig. 10. Modelos elástico lineal y rígido plástico propuestos en la norma italiana CNR-DT-204.

Los modelos emplean el concepto de resistencias a flexión equivalentes para caracterizar los diagramas y se definen por medio de ensayos a flexión de 4 puntos (UNI 11039 [45]) o ensayos de tracción uniaxial (UNI 11188 [46]). Las resistencias a flexión equivalentes que se utilizan para definir la ecuación constitutiva se obtienen a partir de la media de las resistencias obtenidas en los ensayos para unos intervalos de ancho de fisura determinados, lo que supone un planteamiento conservador.

La forma de evaluar la deformación del elemento varía según se trate de un material con comportamiento de endurecimiento o de reblandecimiento. En el primer caso, al producirse múltiples fisuras, la deformación se calcula a través del valor medio de ancho de fisura. En el segundo caso, con la aparición de una única fisura, la deformación se asocia al valor último de ancho de fisura.

La equivalencia entre deformación última (ε_u) y ancho de fisura último (w_u) se realiza por medio de una longitud característica que resulta del valor mínimo entre la distancia media entre fisuras y la altura del eje neutro. Para el caso de materiales con reblandecimiento, la máxima deformación a tracción, ε_{Fu}, es de un 20‰. El valor último de ancho de fisura, w_u, debe cumplir la limitación: $w_u = \varepsilon_u \cdot l_{cs} \leq 3$ mm. En el caso de materiales con comportamiento de endurecimiento, la deformación máxima a tracción, ε_{Fu}, es igual al 10‰.

Ambos diagramas resultan sencillos por su rapidez de aplicación y prácticos para el diseño en rotura, sin embargo la precisión del modelo (en este caso el elástico-lineal) en un análisis más sensible, como ELS puede no reproducir determinados fenómenos como el *snap-through* de la forma más adecuada.

D.4.4. FIB Model Code (2007)

El modelo constitutivo incluido en el FIB Model Code [47] corresponde al presentado en la norma italiana CNR-DT 204, motivo por el cual no se repite su valoración en este apartado.

D.4.5. Norma Española: EHE (2008)

La norma española [6] recoge recomendaciones específicas para el uso del HRF, sin especificar tipo de fibra siempre que se trate de fibras estructurales. En dicha norma se presentan dos diagramas tensión-deformación: un diagrama rectangular y un diagrama multilineal, cuya aplicación dependerá de la situación a tratar.

En el caso de cálculo en rotura (ELU) se aplica de manera general el diagrama rectangular y para casos particulares que requieran más precisión el diagrama simplificado bilineal (definidos por los puntos A-C-D-E del diagrama multilineal). En casos como el de pequeñas deformaciones en servicio (ELS) se aplica el diagrama multilineal (definido por A-B-C-D-E), similar al propuesto por la norma alemana. Este diagrama con la resistencia adicional que proporciona el pico A-B-C permite una mejor aproximación y mayor precisión. Los parámetros que definen ambos diagramas son las resistencias a flexión residuales obtenidas a partir de un ensayo a flexión según la Norma Europea (EN 14651, 2005 [48]).

Un aspecto a destacar del modelo multilineal es la definición de la caída de tensión en el comportamiento post-fisuración por medio de una resistencia a flexotracción que no corresponde al valor de deformación última como en otros modelos. En este caso se asocia a un punto intermedio correspondiente a un ancho de fisura de 2,5 mm y se cuantifica por medio de una longitud característica l_{cs} (mínimo entre la distancia media entre fisuras y la altura de la fibra neutra).

Además, la norma española distingue valores distintos de deformación última en función de la solicitación de la sección: 20‰ para flexión y 10‰ para tracción, de manera análoga a la situación existente para diagrama tensión-deformación en compresión (-3,5‰ para flexión y -2‰ para compresión simple).

Comparando estos modelos con los existentes en otras normas y recomendaciones se observa que el modelo rectangular sigue la misma filosofía que el modelo rígido plástico de la norma italiana y el modelo multilineal es similar a los modelos trilineales de la norma alemana y RILEM. En cierto modo se puede decir que la norma española, a pesar de no aportar avances significativos, presenta la ventaja de haber adoptado los conceptos principales de las recomendaciones anteriormente mencionadas [5].

D.5. Programa experimental

De acuerdo con los objetivos planteados, se han contrastado los resultados de una campaña experimental con las ecuaciones constitutivas anteriormente analizadas. Dicha campaña se ha llevado a cabo en el Laboratorio de Tecnología de Estructuras de la Escuela Técnica Superior de Ingenieros de Caminos, Canales y Puertos de Barcelona entre Febrero y Mayo de 2008, como parte de los trabajos presentados en [12] y [13].

En la campaña experimental se han ensayado elementos con dimensiones de 3 metros de longitud, 1 metro de ancho y 0,20 metros de canto. Las losas presentan una armadura mixta, es decir, disponen de un armado convencional y las fibras. El armado convencional consta de 7 barras de diámetro 16 mm en sentido longitudinal y de barras de diámetro 8 mm cada 20 cm en sentido transversal (no soldadas) y de calidad B 500S. El recubrimiento del hormigón en el armado longitudinal es de 55 mm para las losas con fibras de acero y de 60 mm para las losas con fibras de polipropileno. Un mayor detalle de la campaña experimental puede encontrarse en [12] y [13].

Las fibras empleadas en el armado son de dos tipos: acero y polipropileno. La dosificación en que han sido aplicadas es de 40 kg/m^3 y 4,55 kg/m^3 respectivamente, correspondiendo ambas cuantías a un 0,50% del volumen. En las Tablas 3 y 4 se presentan las propiedades del hormigón y de las fibras respectivamente.

Los ensayos de caracterización de flexotracción del hormigón se realizaron mediante probetas prismáticas (15 x 15 x 60 cm) según la norma EN14651 (en la Tabla 5 se presenta un resumen de los resultados obtenidos). En la Fig. 11 se observa el diferente comportamiento del material según el tipo de fibras añadidas. En el caso de las fibras de polipropileno se observa un comportamiento de reblandecimiento ("*softening*") tras la fisuración, y para el caso de las fibras de acero se observa el fenómeno de endurecimiento ("*hardening*").

Las losas se cargaron según la configuración de un ensayo a flexión de 4 puntos de acuerdo con el esquema presentado en la Fig. 12.

Tabla 3. Propiedades del hormigón.

PROPIEDADES	
Clase resistente	C25/30
Cemento aplicado	CEM III A42.5N
Relación a/c	0,55
Tamaño máximo del árido	16 mm
Volumen superplastificante	1,5%
Tiempo de mezcla	5 min

Tabla 4. Propiedades de las fibras.

PROPIEDADES	Acero	Polipropileno
Longitud (l)	60 mm	55 mm
Diámetro equivalente (d)	0,75 mm	0,80 mm
Esbeltez (l/d)	80	70
Resistencia a tracción	1050 MPa	300MPa
Módulo de elasticidad	210 GPa	3 GPa
Dosificación (0,50% vol)	40 kg/m³	4,55 kg/m³

Tabla 5. Resultados de los ensayos a flexotracción.

RESULTADOS ENSAYOS DE CARACTERIZACIÓN					
$CMOD_i$ (mm)	δ_i (mm)	Acero		Polipropileno	
		f_{Ri} (MPa)	F_{Ri} (kN)	f_{Ri} (MPa)	F_{Ri} (kN)
0,05	0,08	f_L=3,12	F_L=9,86	f_L=3,51	F_L=11,12
0,5	0,46	f_{R1}=3,93	F_{R1}=12,41	f_{R1}=1,15	F_{R1}=3,63
1,5	1,32	f_{R2}=4,49	F_{R2}=14,20	f_{R2}=0,95	F_{R2}=3,02
2,5	2,17	f_{R3}=4,56	F_{R3}=14,42	f_{R3}=0,94	F_{R3}=2,98
3,5	3,00	f_{R4}=4,62	F_{R4}=14,61	f_{R4}=0,97	F_{R4}=3,06

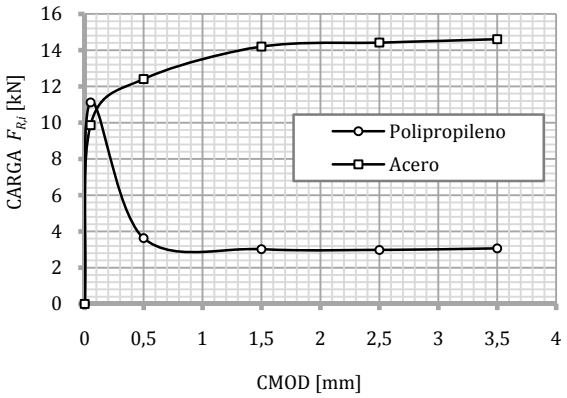

Fig. 11. Comportamiento del HRF.

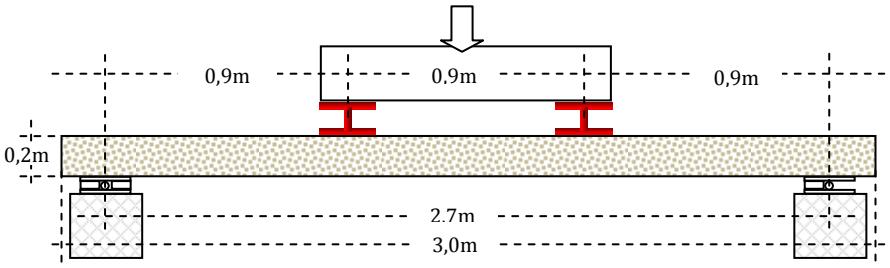

Fig. 12. Configuración de los ensayos.

A partir de los datos obtenidos en el laboratorio, se realiza un estudio de las diversas ecuaciones constitutivas con el objetivo de evaluar cuáles se ajustan mejor a los resultados experimentales. Para realizar dicho estudio se ha empleado un modelo numérico de análisis seccional AESS [28] que consiste en un conjunto de subrutinas programadas en código Matlab®. Dicho modelo permite reproducir numéricamente los ensayos anteriormente descritos y obtener la curva carga-desplazamiento para cada una de las ecuaciones constitutivas estudiadas. En dicho estudio no se han considerado coeficientes de seguridad para la mayoración de acciones ni para la minoración de los materiales en ninguno de los modelos constitutivos.

Tal y como se ha presentado en la Tabla 1, los modelos propuestos por en la DBV y CNR-DT se valen del ensayo a flexión de 4 puntos. Al no disponer de dichos ensayos, se han utilizado los resultados de los ensayos a flexión de 3 puntos que se realizaron para caracterizar el HRF.

D.6. Resultados

D.6.1. Influencia de la armadura en la respuesta del elemento

La combinación de fibras y armadura convencional se presenta como una solución estructural y económicamente competitiva en el diseño de estructuras. En estas configuraciones híbridas (barras de acero y fibras), el armado tradicional aporta en gran medida la capacidad resistente, sin embargo, gracias a la contribución estructural de las fibras, las cuantías de armado convencional necesarias pueden ser significativamente reducidas [29].

Concretamente, para el caso de los elementos descritos en este artículo, la presencia de armadura convencional influye notablemente en la respuesta estructural de las losas. Dicho armado gobierna el comportamiento a flexión de los elementos ensayados, si bien la adición de fibras estructurales proporciona una mayor ductilidad y capacidad resistente, tanto en servicio como en rotura [49]. En la Fig. 13 se presentan las gráficas carga-desplazamiento obtenidas experimentalmente bajo la configuración descrita con anterioridad en el apartado 5 para tres configuraciones de armado: armadura convencional (sin fibras), armadura mixta con 0,5% de fibras de polipropileno y armadura mixta con 0,5% fibras de acero.

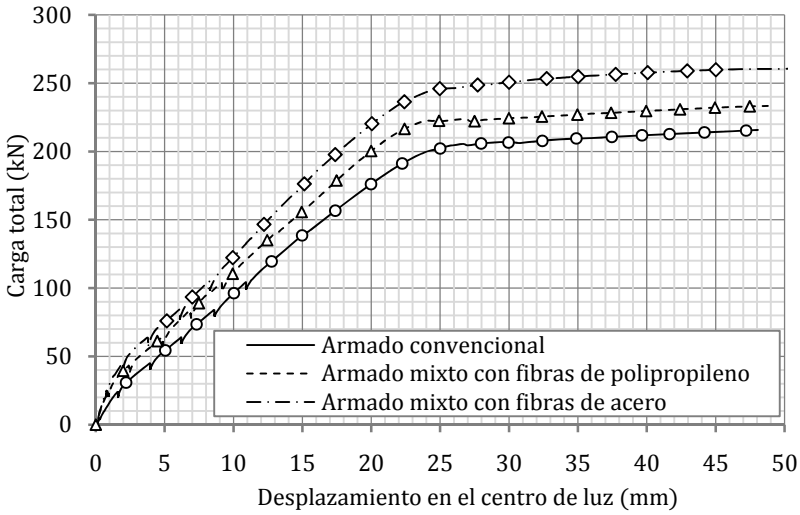

Fig. 13. Diferencia en la respuesta del elemento según el tipo de armado.

En la Fig. 13 se observa el incremento de resistencia que supone la adición de fibras de polipropileno (4,55 kg/m³ en este caso) y fibras de acero (40 kg/m³ en este caso), un mayor detalle puede verse en la tabla 6 donde se presenta los valores obtenidos experimentalmente para las flechas de 10, 20 y 40mm.

Tabla 6. Valores de carga para flechas de 10mm, 20mm y 40mm (en kN) obtenidos experimentalmente.

Configuración de armado	Valor de la carga		
	Flecha = 10 mm	Flecha = 20 mm	Flecha = 40 mm
Armado convencional	97,2	177,6	212,2
7 Φ16 + fibras polipropileno	111,0	200,0	229,5
7Φ16 + fibras de acero	123,4	220,3	257,7

D.6.2. Fibras de acero

En las siguientes figuras se presentan los diagramas de las ecuaciones constitutivas estudiadas para las fibras de acero descritas anteriormente, las curvas carga-desplazamiento obtenidas con dichos modelos y la obtenida experimentalmente. En la Figs. 14, 15 y 16 se presentan los resultados para los modelos trilineales, bilineales y rectangulares respectivamente.

En la Fig. 14a se observa cómo el modelo propuesto por la RILEM adopta unos valores de tensión de fisuración y comportamiento post-pico sensiblemente superiores a los del resto de modelos trilineales. Esta diferencia se traduce en una sobreestimación de la respuesta estructural del elemento que se pone de manifiesto en la curva carga-desplazamiento de la Fig. 14b. La DBV, en cambio, presenta valores de resistencias residuales muy inferiores a la RILEM y la EHE resultando en un comportamiento más conservador en la fase de rotura. Con el modelo de la EHE se obtienen unos resultados sobreestimados para pequeñas deformaciones pero que se sitúan del lado de la seguridad en rotura.

Los modelos representados en la Fig. 14a son modelos diseñados para reproducir con mayor acierto y precisión el comportamiento elástico-lineal previo a la fisuración, mediante la consideración de un efecto pico (ver Fig. 14a). Esta hipótesis de los modelos multilineales, a diferencia de los modelos simplificados, permite recoger el cambio de rigidez del material al fisurar. Dicho fenómeno se observa en la Fig. 14b para desplazamientos inferiores a 4 mm.

En la Fig. 15, de nuevo es el modelo de la DBV el que presenta unos valores de resistencia residual más bajos y aunque ajusta de forma satisfactoria la respuesta del elemento en la Fig. 15b para fase de servicio, en rotura la subestima notablemente. Los modelos de la CNR-DT y la EHE presentan un valor de tensión de fisuración igual, sin embargo las resistencias residuales son menores en el caso de la EHE, tal como se observa en la Fig. 15a. Esta diferencia en las resistencias residuales se aprecia posteriormente en la curva carga-flecha de la Fig. 15b, donde la EHE permanece del lado de la seguridad en fase de rotura y la CNR-DT se sitúa ligeramente del lado de la inseguridad.

En la Fig. 16 la CNR-DT presenta un valor de resistencia residual ligeramente superior al de la EHE en la Fig. 16a y los resultados que proporcionan de carga-desplazamiento se ajustan satisfactoriamente a la curva experimental. El modelo de la DBV, sin embargo, considera un valor de resistencia residual cuatro veces menor al valor de los anteriores. Consecuentemente, esta hipótesis se traduce en una predicción del comportamiento más conservadora que el resto, tal como se observa en la Fig. 16b.

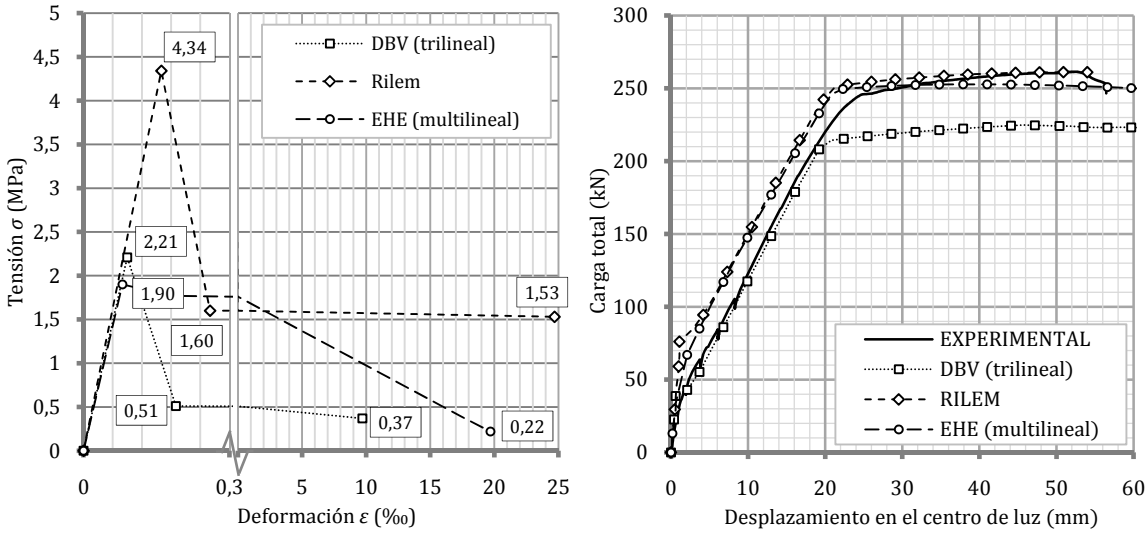

Fig. 14. Diagramas de los modelos multilineales (a)[1] y curvas carga-desplazamiento obtenidas (b).

[1] :Cambio de escala en el eje de abscisas

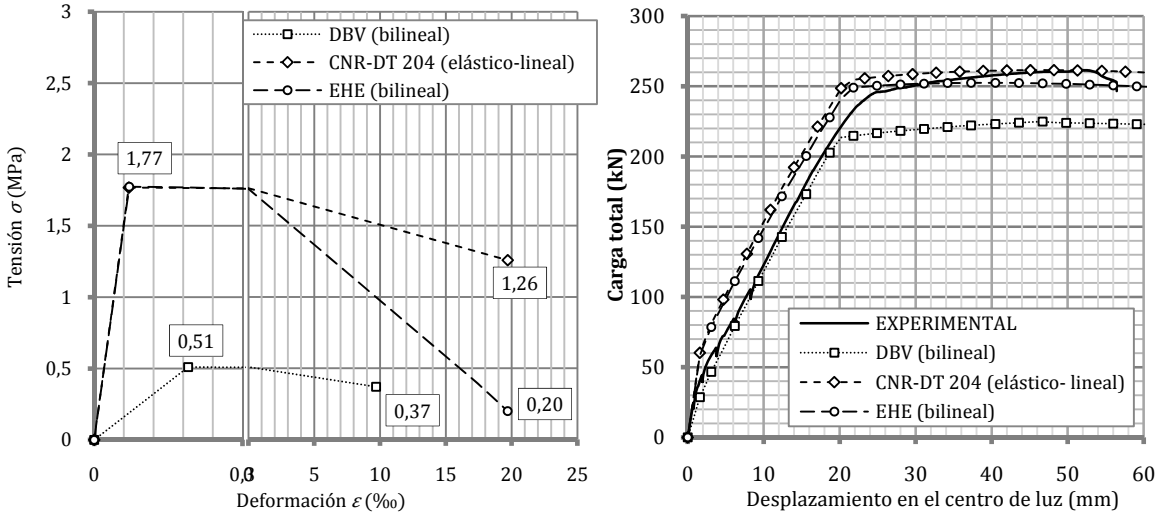

Fig. 15. Diagramas de los modelos bilineales (a) y curvas carga-desplazamiento obtenidas (b).

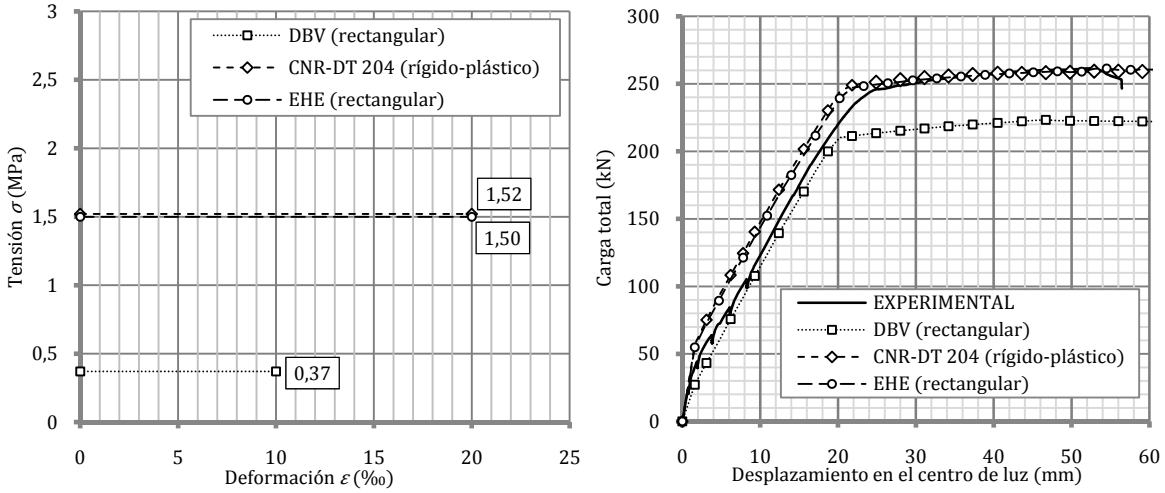

Fig. 16. Diagramas de los modelos rectangulares (a) y curvas carga-desplazamiento obtenidas (b).

En la Tabla 7 se presentan los valores de carga para flechas de 10 mm, 20 mm y 40 mm derivados de la curva carga-desplazamiento (Figs. 14b, 15b y 16b). Estos valores reflejan la tendencia de cada modelo constitutivo descrito anteriormente. En los valores para una flecha de 40 mm se aprecia qué modelos se sitúan del lado de la seguridad para grandes deformaciones.

Tabla 7. Valores de carga para flechas de 10mm, 20mm y 40mm (en kN). Fibras de acero.

Modelos		Flecha = 10 mm	Flecha = 20 mm	Flecha = 40 mm
Datos Experimentales		123,4	220,3	257,7
DBV	Trilineal	118,4	211,1	223,1
	Bilineal	118,1	212,0	223,0
	Rectangular	114,6	208,7	220,9
RILEM	Trilineal	150,2	243,5	259,8
CNR-DT 204	Elástico-lineal	153,2	246,7	261,1
	Rígido-plástico	147,1	242,0	257,7
EHE	Multilineal	148,5	239,3	257,7
	Bilineal	148,3	239,2	252,4
	Rectangular	143,5	237,3	257,0

A partir de los datos de la Tabla 7 se obtiene que para desplazamientos pequeños de 10 mm y 20 mm, los modelos que mejor se ajustan a los resultados experimentales son los presentados por la DBV. En este

sentido, los modelos trilineal y bilineal presentan una diferencia respecto a los datos experimentales de aproximadamente un 4%, sin embargo, el modelo rectangular experimenta una variación de un 7,1% en el caso de 10 mm y de 5,3% en el caso de 20 mm. La predicción de dichos modelos se sitúa en todo momento del lado de la seguridad.

Para un desplazamiento de 10 mm los modelos propuestos por la RILEM, la CNR-DT y la EHE sobreestiman el comportamiento entorno a un 20%, siendo el máximo un 24,2% del modelo elástico-lineal de la CNR-DT 204. En el caso de la flecha de 20 mm, la sobreestimación de estos modelos se reduce hasta la mitad, siendo un 10,5% para la RILEM, en torno a un 10% para la CNR-DT 204 y alrededor de un 8% para la EHE.

Para desplazamientos mayores, 40 mm, los modelos de la RILEM, la CNR-DT 204 y la EHE presentan una variación muy pequeña respecto a los valores experimentales. Dicha diferencia, en todos los casos es inferior a un 2%, no obstante, los modelos de la RILEM y el elástico-lineal de la norma italiana se sitúan del lado de la inseguridad. Los modelos de la DBV infravaloran la respuesta del elemento en torno al 13,5-14%.

Los resultados reflejan que para pequeñas deformaciones el modelo propuesto por la DBV se ajusta mejor a los resultados experimentales que el resto de modelos, sin embargo subestima sensiblemente la respuesta para deformaciones mayores. De hecho, este modelo reproduce un comportamiento muy similar a losas idénticas a las descritas armadas únicamente con barras de acero [12]. La causa de la sobreestimación de resultados con el modelo RILEM reside en la utilización de valores elevados en los parámetros que definen la fase post-fisuración de la ley constitutiva, tal y como apuntan algunos autores [10]. Con el objetivo de mejorar el modelo se han publicado recientemente nuevos valores para dichos parámetros [11].

D.6.3. Fibras de polipropileno

Del conjunto de las distintas normativas estudiadas, DBV y RILEM hacen referencia únicamente a las fibras de acero, sin embargo las normas italiana (CNR-DT 204) y española (EHE) presentan un planteamiento general para todo tipo de fibras. Si bien hay que tener presente que la base fundamental del conocimiento es para fibras de acero, lo que se refleja, en cierta medida en dichas normativas. A continuación se presentan los resultados obtenidos para las losas con fibras de polipropileno.

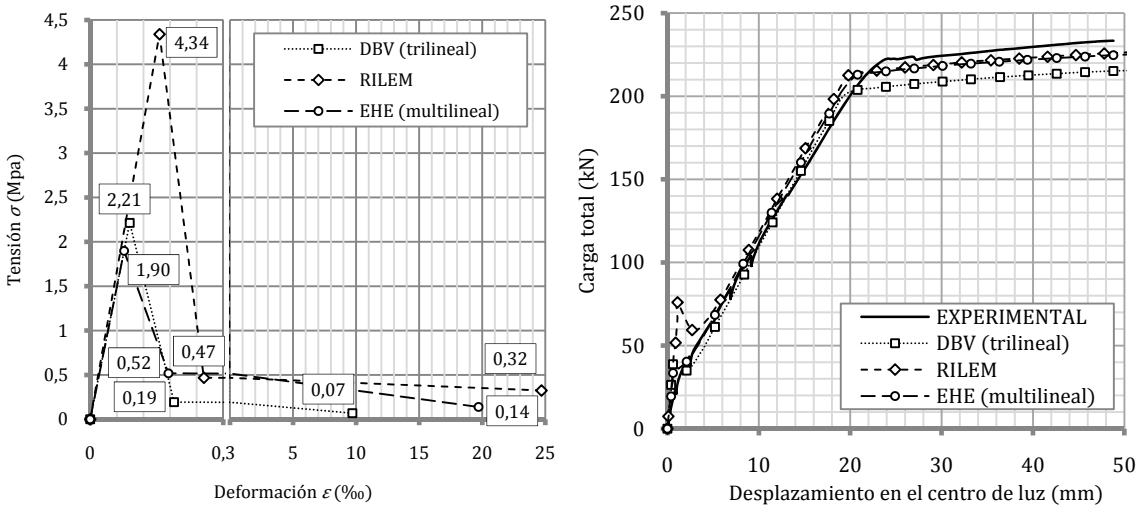

Fig. 17. Diagramas de los modelos multilineales (a)[2] y curvas carga-desplazamiento obtenidas (b).

[2] : Cambio de escala en el eje de abscisas

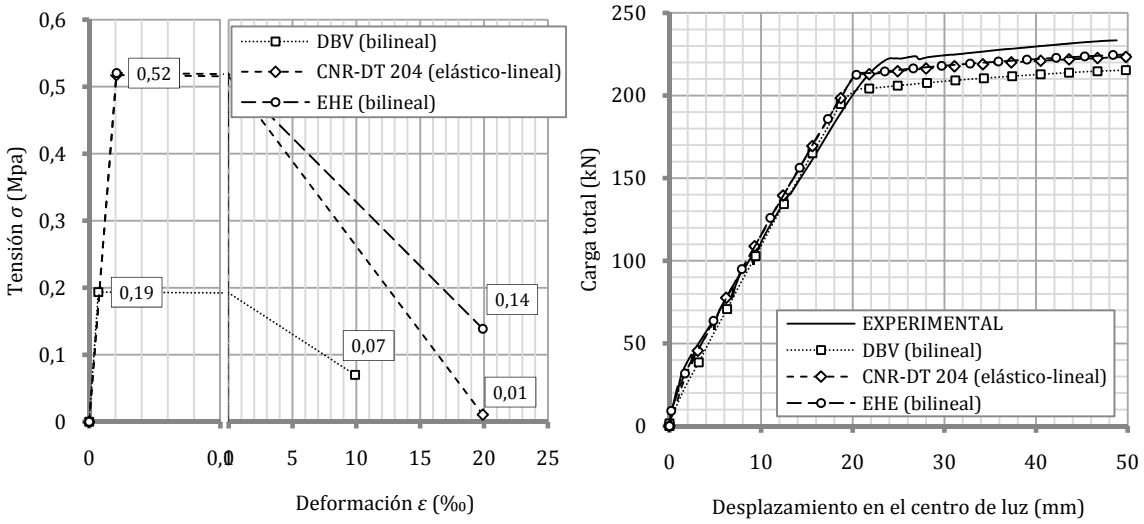

Fig. 18. Diagramas de los modelos bilineales (a) y curvas carga-desplazamiento obtenidas (b).

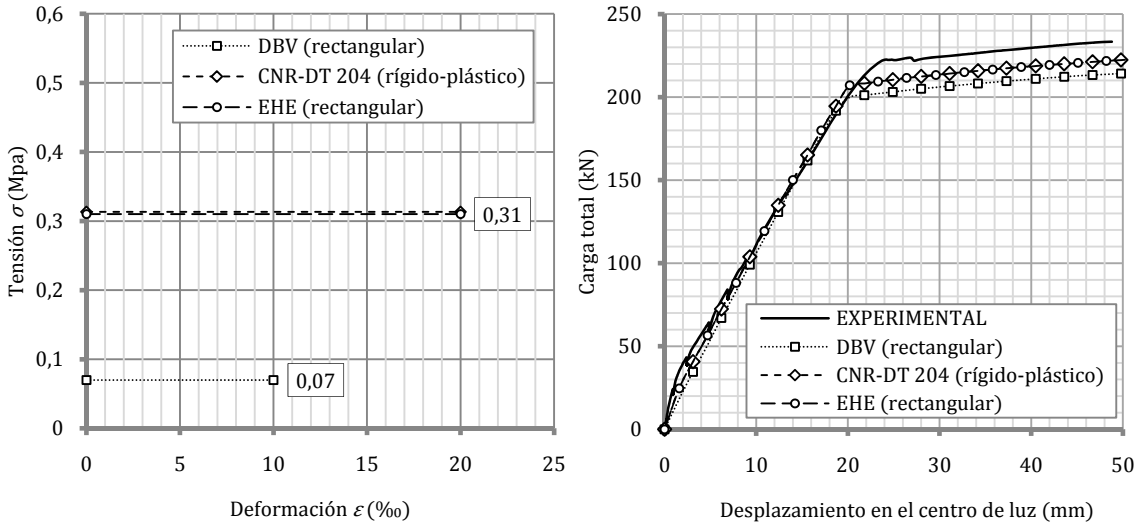

Fig. 19. Diagramas de los modelos rectangulares (a) y curvas carga-desplazamiento obtenidas (b).

Modelos más elaborados, como el multilineal completo de la EHE, trilineal de la DBV o el propuesto por la RILEM (representados en la Fig. 17) tratan de recoger de forma más fidedigna el comportamiento fenomenológico del HRF, atribuyéndole una mayor responsabilidad estructural. Estos modelos reproducen el comportamiento elástico-lineal hasta fisuración (ver Fig. 17b) y recogen el comportamiento del efecto pico, consecuentemente se trata de modelos reservados, *a priori*, para aplicaciones que requieren de un cálculo más ajustado como un cálculo no lineal o casos en los que se requiera trabajar en dominios de pequeñas deformaciones (ELS). El valor de la tensión pico (o de fisuración) propuesto por la RILEM es excesivamente optimista y proporciona valores muy altos.

Los modelos simplificados como el modelo rectangular o bilineal de la EHE y DBV o los propuestos por la CNR-DT 204 (Fig. 18) resultan de especial interés, por su sencillez y rápida aplicación, para el cálculo en ELU en el que el análisis en rotura es primordial. Nótese (Figs. 18b y 19b) que a diferencia de los multilineales o trilineales (Fig. 17b), éstos no reproducen la fase elástica-lineal previa a la fisuración de la losa, reproduciendo el proceso de carga con la rigidez fisurada desde origen.

Nótese que los modelos simplificados son muy conservadores, en comparación con los multilineales o trilineales, subestimando la resistencia residual del material, sin embargo, como veremos a continuación, conducen a resultados más que satisfactorios.

En la Tabla 8 se presentan los valores de carga para flechas de 10 mm, 20 mm y 40 mm correspondientes a la curva carga-desplazamiento (Figs. 17b, 18b y 19b). Estos valores muestran la tendencia de cada modelo constitutivo estudiado.

Tabla 8. Valores de carga para flechas de 10mm, 20mm y 40mm (en kN). Fibras de polipropileno.

Modelos		Flecha = 10 mm	Flecha = 20 mm	Flecha = 40 mm
	Experimental	111,0	200,0	229,5
DBV	Trilineal	109,3	201,7	212,7
	Bilineal	109,0	201,6	212,6
	Rectangular	106,0	198,7	210,7
RILEM	Trilineal	118,3	212,8	223,3
CNR-DT 204	Elástico-lineal	115,4	209,9	220,9
	Rígido-plástico	110,5	205,3	218,6
EHE	Trilineal	115,8	208,4	222,0
	Bilineal	115,6	209,5	222,0
	Rectangular	110,4	205,3	218,5

Para ELS (flecha de 10), los modelos bilineal y multilineal de la EHE y RILEM sobrestiman los valores en referencia con los obtenidos experimentalmente en torno a un 4,3% y 6,5% respectivamente. En cambio, los modelos rectangulares y los propuestos por la DBV infravaloran dichos resultados.

En este sentido, resulta evidente la clara influencia de los coeficientes que afectan a las resistencias residuales ($f_{R,i}$) en las ecuaciones constitutivas propuestas por la EHE y la RILEM. Dichos coeficientes, según se concluye de los resultados obtenidos, son excesivamente optimistas para hormigones reforzados con fibras de polipropileno (incluso para fibras de acero, como se apunta en [10]). Por el contrario, la aproximación indirecta propuesta por la DBV es la que mejor ajusta los valores experimentales obtenidos en la campaña para pequeñas deformaciones (errores relativos de 1,5-1,8%). A diferencia de las normas anteriormente citadas, la DBV se vale de las resistencias equivalentes (f_{eq}) para la definición de la ecuación constitutiva sin afectarlas con ningún coeficiente.

El modelo rectangular de la EHE, en el que la contribución a tracción de las fibras considerada es significativamente menor, infravalora en un 0,5% la carga obtenida experimentalmente para la flecha de 10 mm, mientras que el modelo rectangular de la DBV lo hace en un 4,5%.

Para deformaciones intermedias entre servicio y rotura (flecha de 20mm) sigue siendo la DBV la que proporciona los valores más próximos a los obtenidos experimentalmente con errores relativos entre 0,65-0,85%. Observamos cómo todos los modelos, exceptuando el rectangular de la DBV, sobrevaloran los tomados como referencia, pero nunca con errores superiores al 6,5% (obtenido con la RILEM).

Para estados próximos a rotura (flechas de 40 mm), el comportamiento de la losa está principalmente gobernado por la armadura convencional y su brazo mecánico existente, todos los modelos utilizados quedan del lado de la seguridad. La DBV presenta un error relativo de un 7,0-8,0%, la RILEM de 2,7%, y tanto la CNR-DT 204 como la EHE de entre un 3,0-4,0%.

D.7. Conclusiones

La aparición de nuevas normativas o recomendaciones técnicas relativas al empleo de fibras con finalidad estructural supone una oportunidad para el sector de emplear el HRF como solución estructural. Las normas y códigos de referencia, con objeto de recoger el comportamiento fenomenológico del HRF a tracción, proponen distintas ecuaciones constitutivas, de las que en este artículo se han estudiado las más relevantes a nivel europeo.

Con el fin de ilustrar la capacidad de cada modelo para predecir el comportamiento estructural del HRF se ha presentado un ejemplo sobre el que se ha realizado un estudio comparativo detallado del que se pueden concluir los siguientes puntos:

- La base conceptual sobre la que se sustentan las normativas son los estudios y trabajos realizados para fibras de acero. Ello no impide su utilización para hormigones reforzados con fibras plásticas. Fruto de tal circunstancia, los resultados aquí presentados muestran que las ecuaciones constitutivas más elaboradas de la EHE y RILEM (trilineales y bilineales), son relativamente optimistas para el cálculo en servicio de secciones de HRF con fibras de polipropileno. Dichas ecuaciones conducen a valores que sobrestiman los resultados experimentales (no así la DBV).
- Los modelos recogidos en la DBV (que presenta un planteamiento distinto al resto de modelos) infravaloran el comportamiento del material, situándose en todos los casos (ya sea modelo trilineal, bilineal o rectangular) del lado de la seguridad. En el caso particular de deformaciones mayores próximas a rotura, los modelos de la DBV son los que presentan mayores diferencias con los datos experimentales, tanto en fibras de acero como de polipropileno.
- El modelo con el que se obtiene un mayor error en servicio respecto a los resultados experimentales es el trilineal de la RILEM, mientras que en rotura es el modelo que mejor aproxima los valores recogidos en el laboratorio.
- La norma CNR-DT 204 presenta el modelo elástico-lineal y rígido-plástico, siendo con este último con el que se ha obtenido un resultado más próximo a los datos experimentales para los dos tipos de fibras estudiados.
- Atendiendo a los resultados obtenidos en el caso práctico estudiado, los modelos recogidos en la EHE presentan una buena predicción del comportamiento del elemento de forma general para ambos tipos de fibra. A pesar de que los modelos de la DBV reproducen de forma fidedigna la respuesta en pequeñas deformaciones (mejor que los modelos de la EHE), para deformaciones mayores se obtienen unos valores sensiblemente inferiores a los datos experimentales.

Puede concluirse por tanto, que existe en la actualidad una importante base normativa sobre la que asentar e impulsar la tecnología del HRF. A pesar de los distintos planteamientos propuestos por las normativas a la hora de abordar el comportamiento a tracción del HRF, debe destacarse el esfuerzo de las normativas más recientes de recopilar y asimilar la experiencia adquirida a través de las primeras normas y recomendaciones. Merece mención especial el acierto de la Comisión Permanente del Hormigón (CPH) en la redacción del Anejo 14 de la EHE, que ha asentado las bases de un marco de unicidad técnica, coherente y armonizada con lo establecido a nivel europeo.

D.8. Agradecimientos

Los autores desean agradecer los constructivos comentarios de Pedro Serna y Marco di Prisco que han ayudado a la mejora del artículo. Asimismo se agradece a las empresas Bekaert y Grace, y en particular a Ann Lambechts y Gerhard Vitt, su acertada colaboración y disposición a compartir sus conocimientos y experiencia con nosotros.

D.9. Referencias

1. Barros, J. A. O.; Figueiras, J. A. *Flexural behavior of SFRC: testing and modeling*, Journal of Materials in Civil Engineering, November 1999, pp. 331-339.
2. Lambrechts, A. *Self compacting steel fibre concrete, and its use in segmental linings,* Aplicaciones estructurales de hormigón con fibras (Jornada Técnica), Dpto. de Ingeniería de la Construcción, UPC, 2007, pp. 53-68. www.bmbupc.org
3. Serna, P. *Recientes ejemplos estructurales de aplicación de hormigón con fibras*, Aplicaciones estructurales de hormigón con fibras (Jornada Técnica), Dpto. de Ingeniería de la Construcción, UPC, 2007, pp. 33-48. www.bmbupc.org

4. Naaman A.E.; Reinhardt H.W. *Fiber reinforced concrete: Current needs for structural implementation*, Proceedings of US-European workshop on Advanced Fiber Reinforced Concrete, Plizzari GA, di Prisco M (eds.), Italy, 2004.

5. Serna, P.; Arango, S.; Ribeiro, T.; Núñez, A.M.; Garcia-Taengua, E. *Structural cast-in-place FRC: technology, control criteria and recent applications in Spain*. Materials and Structures, Accepted 11 June 2009 (DOI: 10.1617/s11527-009-9540-9).

6. Comisión Permanente del Hormigón Ministerio de Fomento. *EHE-08 Instrucción del Hormigón Estructural*, 2008.

7. Aguado, A.; Laranjeira, F. *Presentación del Anejo de Hormigón con Fibras de la EHE y ecuación constitutiva del Hormigón Reforzado con Fibras*, Aplicaciones estructurales de hormigón con fibras (Jornada Técnica), Dpto. de Ingeniería de la Construcción, UPC, 2007, pp. 1-32. www.bmbupc.org

8. di Prisco, M.; Plizzari, G.; Vandewalle L. *Fibre reinforced concrete: new design perspectives*, Materials and Structures, Accepted 11 June 2009 (DOI: 10.1617/s11527-009-9529-4).

9. Kooiman, A. *Modelling Steel Fibre Reinforced Concrete for Structural Design*, PhD Thesis, Delft University of Technology, Delft, 2000.

10. Tlemat, H.; Pilakoutas, K.; Neocleous, K. *Modelling of SFRC using inverse finite element analysis*, Materials and Structures, vol. 39, nº4, 2006, pp. 221-233.

11. Barros, J. A. O.; Cunha, V.M.C.F.; Ribeiro, A.F.; Antunes, J.A.B**.** *Post-cracking behaviour of steel fibre reinforced concrete*, Materials and Structures Journal, vol. 38, 2005, pp. 47-56.

12. Blanco, A. *Durabilidad del hormigón reforzado con fibras de acero*, Tesina de especialidad (Dir. A. Aguado de Cea y M. Vandewalle), UPC, Barcelona, 2008. www.bmbupc.org

13. Pujadas, P. *Durabilidad del hormigón reforzado con fibras de polipropileno*, Tesina de especialidad (Dir. A. Aguado de Cea y M. Vandewalle), UPC, Barcelona, 2008. www.bmbupc.org

14. Bencardino, F.; Rizzuti, L.; Spadea, G.; Swamy R.N. *Stress-Strain Behavior of Steel Fiber-Reinforced Concrete in Compression*, Journal of Materials in Civil Engineering, March 2008, pp. 255-263.

15. Löfgren, I.; Stang, H.; Forbes Olesen, J. *Fracture Properties of FRC Determined through Inverse Analysis of Wedge Splitting and Three-Point Bending Tests*, Journal of Advanced Concrete Technology, vol. 3, nº 3, October 2005, pp. 423-434.

16. Laranjeira, F.; Aguado, A.; Molins, C. *Constitutive equations of fiber reinforced concrete*, Proceedings of the ECCOMAS Thematic Conference on Computational Methods in Tunneling (EURO: TUN 2007), Vienna, 2007.

17. Bischoff, P. H. *Tension stiffening and cracking of steel fiber-reinforced concrete*, Journal of Materials in Civil Engineering, March 2003, pp. 174-182.

18. Fernandes, A. *Modelos de fenda discreta na simulação do comportamento em flexão de betão reforçado com fibras de aço*, PhD Thesis, Universidade do Minho, Guimarães, 2004.

19. Bazant, Z.P.; Oh, B.H. *Crack band theory for fracture of concrete*, Materials and Structures, vol. 16, 1983, pp. 155-177.

20. Hu, X.; Wittmann, F. H. *Experimental method to determine extension of fracture-process zone*, Journal of Materials in Civil Engineering, ASCE, 2(1), 1990, pp. 15–23.

21. Foote, R.; Mai, Y. W.; Cotterell, B. *Process size and crack growth measurements in fibre cements. Fibre reinforced concrete properties and applications*, American Concrete Institute, Detroit, 1987, pp. 55–70.

22. Hillerborg, A. *Analysis of fracture by means of the fictitious crack model, particularly for fibre reinforced concrete*. International Journal of Cement Composites, vol. 2(4), 1980, pp. 177–184.

23. Banholzer, B.; Brameshuber, W.; Jung, W. *Analytical evaluation of pull-out tests-The direct problem*, Cement and Concrete Composites, vol. 27, 2005, pp. 93-101.

24. Banholzer, B.; Brameshuber, W.; Jung, W. *Analytical evaluation of pull-out tests-The inverse problem*, Cement and Concrete Composites, vol. 28, 2006, pp. 564-571.

25. *RILEM TC 162-TDF Test and design methods for steel fibre reinforced concrete - σ-ε design method: Final Recommendation*, Materials and Structures, vol. 36, October 2003, pp. 560-567.

26. di Prisco, M.; Ferrara, L.; Colombo, M.; Mauri, M. *On the identification of SFRC constitutive law in uniaxial tension*. Proceedings of Sixth RILEM Symposium on Fibre-Reinforced Concretes BEFIB 2004, 2004, pp. 827-836.

27. Cunha, V.M.C.F.; Barros, J.A.O.; Sena-Cruz, J. *Modelling the influence of age of steel fibre self-compacting reinforced concrete on its compressive behaviour*, Materials and Structures, vol. 41, 2008, pp. 465-478.

28. de la Fuente, A. *Modelo numérico para el análisis no lineal de secciones prefabricadas construidas evolutivamente,* Hormigón y Acero, vol. 57, nº 247, 2008, pp. 69-87.

29. Chiaia, B.; Fantilli, A.P.; Vallini, P. *Evaluation of crack width in FRC structures and application to tunnel linings*, Materials and Structures, vol. 42, 2009, pp. 339-351.

30. Laranjeira, F. *Constitutive model of fiber reinforced concrete*, Project of Doctoral Thesis, (Dir. A. Aguado de Cea and C. Molins), UPC, Barcelona, 2007.

31. Barr, B.I.G.; Lee, M.K. *A four-exponential model to describe the behaviour of fibre reinforced concrete,* Materials and Structures, vol. 37, 2004, pp. 464-471.

32. Sousa, J. A. O.; Gettu, R. *Inverse analysis of notched-beam test data for obtaining tensile stress-crack opening relation of fiber reinforced concrete*, Proceedings of the Sixth RILEM Symposium on Fibre-Reinforced Concretes BEFIB 2004, 2004, pp. 809-818.

33. Lim, T.Y.; Paramsivam, P; Lee, S.L. *Bending Behaviour of Steel-Fiber Concrete Beams*, ACI Journal, vol.84, 1987, pp. 286-298.

34. Elsaigh, W.A., Robberts, J.M. and Kearsley, E.P. *Modelling non-linear behaviour of steel fibre reinforced concrete*, Proceedings of Sixth RILEM Symposium on Fibre-Reinforced Concretes BEFIB 2004, 2004, pp. 837-846.

35. Lok, T.S.; Xiao, L. *Tensile behaviour and moment-curvature relationship of steel fibre reinforced concrete*, Magazine of Concrete Research, vol. 50, nº 4, 1998, pp. 359-368.

36. Dupont, D. *Modelling and experimental validation of the constitutive law (σ-ε) and cracking behaviour of steel fibre reinforced concrete*, PhD Thesis, Katholieke Universiteit Leuven, 2003.

37. *DBV Merkblatt Stahlfaserbeton, Deutsche Beton Vereins, 2001.*

38. Dozio D. *SFRC structures: Identification of the uniaxial tension characteristic constitutive law*, PhD Thesis, Politecnico de Milano, 2008.

39. *Soranakom*, C. Mobasher, B. *Flexural design of fiber-reinforced concrete*, ACI Materials Journal, vol. 105, nº 5, 2009, pp. 461-469

40. [40] *Walraven*, J.C. *High performance fiber reinforced concrete: progress in knowledge and design codes*, Materials and Structures, Accepted 11 June 2009 (DOI: 10.1617/s11527-009-9538-3).

41. *DBV Technologie des Stahlfaser-betons und Stahlfaserpritzbetons*, Deutsche Beton Vereins. 1992.

42. *RILEM TC 162-TDF Test and design methods for steel fibre reinforced concrete*, Materials and Structures, vol. 33, March 2000, pp. 75-81.

43. BRITE EURAM PROJECT BRPR-CT98-0813, *Test and design methods for steel fibre reinforced concrete*, project funded by the European Community under the Industrial & Materials Technologies Programme (Brite-Euram II), 2002.

44. *CNR-DT 204 Istruzioni per la Progettazione, l'Esecuzione ed il Controllo di Strutture Fibrorinforzato*, Consiglio Nazionale delle Riserche, Italia, 2006.

45. *UNI 11039 Calcestruzzo rinforzato con fibre d'acciaio; (1a) Parte I: Definizioni, classificazione e designazione; (1b) Parte II: Metodo di prova per la determinazione della resistenza di prima fessurazione e degle indici di duttilità*, 2003.

46. UNI 11188 *Elementi strutturali in calcestruzzo rinforzato con fibre d'acciaio: progettazione esecuzione e controllo*, 2004.

47. *FIB Model Code 2007 "Fibre Reinforced Concrete"*, Draft version. Joint Paper by Horst Falkner (Germany), Marco di Prisco and Giovanni Plizzari (Italy).

48. *EN 14651 Test method for metallic fibrered concrete - Measuring the flexural tensile strength (limit of proportionality (LOP), residual)*, 2005.

49. Chiaia,B.; Fantilli, A.P.; Vallini, P. *Evaluation of minimum reinforcement ratio in FRC members and application to tunnel linings,* Materials and Structures, vol. 40, 2007, pp. 593-604.